

Out of the Dark, into the Light?

Influence of Wildfire and Thermokarst on Greenhouse Gas Fluxes from Boreal Peat Landscapes
near the southern Limit of Permafrost

by

Christopher Schulze

A thesis submitted in partial fulfillment of the requirements for the degree of

Doctor of Philosophy

in

Water and Land Resources

Department of Renewable Resources

University of Alberta

© Christopher Schulze, 2024

Abstract

Wildfire and permafrost thaw have been common disturbances in the boreal zone for millennia and are now intensified by warming due to human-made climate change. The Taiga Plains ecozone in northwestern Canada is warming at a faster rate than other regions. In this ecozone, permafrost is found at relatively low latitudes due to the vast abundance of peatlands, whose large, frozen carbon (C) and nitrogen (N) stocks are vulnerable to warming. Ecosystems and atmosphere exchange C and N as greenhouse gas (GHG) fluxes such as carbon dioxide (CO₂), methane (CH₄), and nitrous oxide (N₂O), which are altered, directly by warming and indirectly by wildfire and permafrost thaw. This may lead to further warming by an increase in net radiative GHG forcing, resulting in positive climate feedback.

I examined the effects of wildfire and permafrost thaw on the GHG balance in three field studies covering three peatland complexes at the southern limit of permafrost across the Taiga Plains at two spatial and temporal scales: a) by monthly static chamber flux measurements from plots affected by wildfire or permafrost thaw (chapter 2), b) by continuous eddy covariance measurements at the landscape scale including different permafrost extents (chapter 3) and different years of wildfire (chapter 4).

Previously often neglected, the GHG N₂O was the focus of chapter 2, where I compared the GHG exchange from soil plots affected by different stages of thermokarst (=permafrost thaw) and wildfire disturbance to the ones of intact permafrost plateaus. I found uptake of N₂O by peat plateaus which decreases post-fire but increased post-thaw, the latter driven by N₂O soil gas concentrations below-ambient, warmer soil temperatures and higher soil moisture contents. From a net radiative GHG forcing point of view, changes in N₂O were minor compared to alterations

in soil respiration and CH₄, determined by the monthly chamber-based flux measurements over one growing season. To quantify differences in CO₂ and CH₄ with a higher temporal resolution, I then investigated multi-year and high-frequency eddy covariance datasets.

In chapter 3, I contrasted two peatland complexes with different extents of permafrost, sporadic (<50% permafrost) and discontinuous (>50% permafrost), and their fluxes of CO₂ and CH₄ as well as resulting balances of C and net radiative GHG forcing. The net uptake of CO₂ and the release of CH₄ was higher at the sporadic permafrost site due to the higher abundance of permafrost-free wetlands in the landscape. Consequently, thaw-induced shrinking of permafrost extent will thus lead to increases in peatland C uptake driven by CO₂ along with increases in net radiative GHG forcing driven by CH₄.

In chapter 4, I investigated the effects of wildfire on the CO₂ exchange post-fire. CO₂ release was large from a recently burned permafrost peatland, accumulating up to half of the C combustion losses. However, the massive CO₂ losses were not sustained into the decade after the wildfire due to the recovery of the peatland vegetation. However, old C may be reintroduced to the atmosphere, as the active layer rapidly deepens towards the end of the growing season in the years after fire compared to unburned sites.

My doctoral research adds knowledge to our limited understanding of the magnitude and direction of change of GHG fluxes of permafrost peatlands in a warmer world. Here, I quantify future climate feedback resulting from thawing permafrost and wildfires increasing in severity and frequency. My findings suggest that the two disturbances are not only similar in their aerial extent across the Taiga Plains, but also in their effects on increased net radiative GHG forcing,

leading to further warming by both, CO₂ release following wildfire and CH₄ following permafrost thaw.

Preface

Contributions of authors

All research presented in this doctoral thesis includes the contributions of multiple co-authors, so that each chapter is a collaborative effort of several scientists aiming to submit each chapter to peer-reviewed journals. All co-authors were thus involved in the writing. Below, the author order convention is used so that the first author represents the lead author, and the last author is the Principal Investigator of the corresponding study. For all chapters, I designed the study together with my supervisors, Dr. David Olefeldt and Dr. Oliver Sonnentag. I had a lead on fieldwork, data analysis, and manuscript writing. Other author contributions that are not my own are given below.

Chapter 2: Schulze, C., Sonnentag, O., Voigt, C., Thompson, L., van Delden, L., Heffernan, L., Hernandez-Ramirez, G., Kuhn, M., Lin, S., & Olefeldt, D. (2023). Nitrous Oxide Fluxes in Permafrost Peatlands Remain Negligible After Wildfire and Thermokarst Disturbance. *Journal of Geophysical Research: Biogeosciences*, 128(4), e2022JG007322.

<https://doi.org/10.1029/2022JG007322>. This chapter was published, and I have confirmed that I have the right to include it as stated in my publisher agreement, the publisher's re-use policy, or by obtaining the publisher's permission.

Contributions that are not my own: Guillermo Hernandez Ramirez, Sisi Lin, and the research group of Christina Biasi (University of Eastern Finland) including Maija Marushchak and Lona van Delden processed the gas samples including all laboratory work on the gas chromatographs. PRS probes were analyzed by Western AG. Carolina Voigt and Gabriel Hould Gosselin did all the field work at Scotty Creek.

Chapter 3: Schulze, C., Olefeldt, D., Kljun, N., Chasmer, L., Detto, M., Gosselin, G. H., Helbig, M., Hopkinson, C., & Sonnentag, O.: Permafrost extent controls landscape-scale fluxes of greenhouse gases in boreal peatlands in northwestern Canada. A version of this is in preparation for submission to *Global Change Biology*.

Contributions that are not my own: Oliver Sonnentag, Gabriel Hould Gosselin, and Haley Alcock did all the data curation including post-processing of the eddy covariance data for this chapter. The footprint models were run by Natascha Kljun, while Laura Chasmer and Chris Hopkinson generated the landcover maps. Figure 3.1 was edited by Rémi Lord-Quintric.

Chapter 4: Schulze, C., Sonnentag, O., Emmerton, C., Harris, L., Alcock, H., Marouelli, K., Gosselin, G. H., & Olefeldt, D.: Large Losses of Carbon Dioxide and Carbon from Burned Permafrost Peatlands in the First Years after Wildfire. A version of this is in preparation for submission to *Geophysical Research Letters*.

Contributions that are not my own: Kate Marouelli did all field and laboratory work regarding the carbon combustion losses during wildfire. Haley Alcock did the flux calculations in eddypro and post-processing of the eddy covariance datasets.

Dedication

Reader discretion is advised –

the following page contains coarse language that some readers may find offensive:



“So, Chris, you want to do environmental research. But let me warn you: humans do not really care much about anything that they cannot eat, drink, or f...”.

In loving memory of my late Opa (grandfather) Ludwig Beck, who expressed his thoughts in his way, when I shared my plan to enter a PhD program in Canada on how climate change affects our Earth’s ecosystems. In the awareness that such words do not belong in a doctoral thesis, I want to emphasize the fact that he had a lot more wisdom to share with me before he slept away peacefully on the exact day that the second chapter of this thesis got published.

Indigenous people of North America have expressed it in a more sophisticated way:

“Only after the last tree has been cut down / Only after the last river has been poisoned / Only after the last fish has been caught / Then will you find that money cannot be eaten.”

To the readers of this thesis, I wish that you do care and to all of us I wish that we understand the wisdom of my Opa and the wisdom of Indigenous people and act accordingly before it is too late.

Acknowledgements

I want to express my deep gratitude to all my family, friends, colleagues, research funding agencies, visitors, soccer mates, mentors and supervisors, Dr. David Olefeldt and Dr. Oliver Sonnentag, and supervisory committee member Dr. Guillermo Hernandez who all made this Canadian journey a wonderful experience. The many happy and difficult moments we shared together will remain and mean a lot to me during a demanding time in which Covid-19 forced us to social distancing, online video conferences, and loneliness. To me, the pandemic was a test of character for all of us that believe in science and a blueprint for future climate change scenarios in which one must put own needs and interests behind the interests of the bigger mass. In the future, we will find out together whether we are shaped for the challenges we will face due to climate change. It might help us to listen to music, warnings, and wisdom of the Indigenous People of Canada whose lands are subject to massive changes addressed in this thesis.

In Deutschland möchte ich meiner gesamten Familie, meiner Frau Kathrina, unserer Tochter Pari, meinem Bruder Maximilian und seiner Frau Lara und ihrem Sohn Ferdinand, meiner Mutter Sabine und Ehemann Robert, meinem Vater Thomas und seiner Frau Elke, meinen Großeltern Renate, Ludwig, Elisabeth und Hans-Jürgen für all die bedingungslose Unterstützung und Geduld mit mir danken. Ebenso will ich mich bei meinem Freund Gernot für seine beiden Besuche bei mir in Kanada und die Anregung zur Rückkehr nach Deutschland bedanken, die maßgeblich zu meiner Entscheidungsfindung hinsichtlich meiner zukünftigen Karriere beigetragen haben.

Table of Contents

Abstract.....	ii
Preface.....	v
Dedication.....	vi
Acknowledgements.....	vii
Table of Contents.....	viii
List of Tables.....	xi
List of Figures.....	xii
List of Abbreviations and Symbology.....	xvii
1. Introduction.....	1
1.1 Carbon and Nitrogen Cycling in Northern Peatlands under a warming Climate.....	1
1.2 Boreal Peatlands underlain by Permafrost in the Taiga Plains.....	4
1.3 Out of the Dark, into the Light.....	7
1.3.1 Landcover Change in the Taiga Plains – from forested Plateaus to treeless Wetlands.....	7
1.3.2 Changes in Carbon and Nitrogen Cycling - from Frozen-solid in the Ground to Gaseous Release to the Atmosphere.....	9
1.4 Objectives.....	12
2. Nitrous Oxide Fluxes in Permafrost Peatlands remain negligible after Wildfire and Thermokarst Disturbance.....	14
2.1 Introduction.....	15
2.2 Materials and Methods.....	18
2.2.1 Study Sites and Sampling Design.....	18
2.2.2 Greenhouse Gas Flux Measurements.....	20
2.2.3 Environmental and Soil Data.....	22
2.2.4 Porewater Chemistry.....	23
2.2.5 Soil Gas Concentration Profiles.....	23
2.2.6 Statistical Analyses.....	24
2.3 Results.....	25
2.3.1 Environmental Conditions.....	25
2.3.2 Porewater Nutrient Concentrations and Supply Rates.....	26
2.3.3 Soil Gas Concentrations.....	27

2.3.4	Greenhouse Gas Fluxes.....	30
2.3.5	N ₂ O Fluxes from Peatlands Ponds.....	32
2.3.6	Impact of Wildfire and Permafrost Thaw on the Net Radiative Balance	34
2.4	Discussion.....	35
2.4.1	Greenhouse Gas Balance of Peat Plateaus.....	35
2.4.2	Greenhouse Gas Balance of Burned Peat Plateaus	36
2.4.3	Greenhouse Gas Balance of Thermokarst Bogs	38
2.4.4	Greenhouse Gas Balance of Peatland Ponds	39
2.4.5	Implications of Climate Change on the Net Radiative Balance	40
2.5	Conclusion	42
3.	Permafrost extent controls landscape-scale fluxes of greenhouse gases in boreal peatlands in northwestern Canada.....	56
3.1	Introduction.....	57
3.2	Materials and methods	62
3.2.1	Study Sites	62
3.2.2	Eddy Covariance Measurements.....	64
3.2.3	Supporting Measurements	64
3.2.4	Data Processing.....	65
3.2.5	Landcover Classification and Footprint Modeling	68
3.2.6	Statistical Analyses	69
3.3	Results.....	70
3.3.1	Landscape Composition and Flux Footprints	70
3.3.2	Seasonal Patterns of Fluxes of CH ₄ and CO ₂	71
3.3.3	Diurnal Patterns of Fluxes of CH ₄ and CO ₂	74
3.3.4	Relationships between Environmental Variables and Fluxes of CH ₄ and CO ₂	76
3.3.5	Carbon Balance and Net Radiative Greenhouse Gas Forcing	77
3.4	Discussion.....	79
3.4.1	CH ₄	79
3.4.2	GPP and ER	81
3.4.3	NEE.....	83
3.4.4	Net Ecosystem Carbon Balance and Net Radiative Greenhouse Gas Forcing	85

3.5	Conclusion	87
4.	Large Losses of Carbon Dioxide and Carbon from Burned Permafrost Peatlands in the First Years after Wildfire	88
4.1	Introduction	89
4.2	Materials and methods	92
4.2.1	Study Sites	92
4.2.2	Eddy Covariance Measurements.....	94
4.2.3	Net Annual CO ₂ Fluxes	95
4.2.4	Static Chamber Soil Respiration.....	96
4.2.5	Depth to Frost Table Position	96
4.2.6	Estimation of Combustion C Losses.....	97
4.2.7	Net CO ₂ Balance over 20 Years after Fire.....	98
4.3	Results.....	99
4.3.1	Eddy Covariance CO ₂ Fluxes	99
4.3.1	Soil Respiration.....	101
4.3.2	Soil Thermal Regime	102
4.3.3	Wildfire Carbon Losses	102
4.3.4	Net CO ₂ Balance over 20 Years after Fire.....	103
4.4	Discussion.....	105
4.5	Conclusion	111
5.	Summary, conclusions, and directions for future research.....	112
5.1	Summary of Findings.....	112
5.2	Directions for future Research	115
	References.....	117
	Appendices.....	160

List of Tables

Table 1.1: Overview of peatland complexes, disturbances, flux measurement methods, and GHGs by chapter	13
Table 2.1: Peatland Stage Properties and Growing Season Environmental Characteristics	25
Table 2.2: Peatland pond characteristics	33
Table 3.1: Comparison of characteristics for Scotty Creek and Smith Creek study sites, including land cover, leaf area index, and climate	71
Table 4.1: Combustion carbon losses during the wildfire at 2019 Burn.	103
Table A2.1: Overview of sampling occasions, activities (marked with 'X', GHG = greenhouse gas, PRS = plant root simulators©) and locations including peatland stages: B19 = 2019 Burn, B07 = 2007 Burn, P = Peat Plateau, PE = Plateau Edge, YB = Young Bog, and MB = Mature Bog.	163
Table A2.2: Two-way ANOVA results, comparing porewater nutrient concentrations and supply rates among sites (Lutose, Smith Creek), and among peatland stages (Peat Plateau, Plateau Edge, Young Bog, Mature Bog).	164
Table A2.3: One-way ANOVA results, comparing porewater nutrient concentrations and supply rates among peatland stages (2019 Burn, 2007 Burn, Peat Plateau, Plateau Edge, Young Bog, Mature Bog), or among disturbances (Intact, Thermokarst, Wildfire).	165
Table A2.4: Two-way ANOVA results, comparing collar average N ₂ O, CH ₄ and CO ₂ fluxes among sites (Lutose, Smith Creek), and among peatland stages (Peat Plateau, Plateau Edge, Young Bog, Mature Bog).	166
Table A2.5: One-way ANOVA results, comparing collar average N ₂ O, CH ₄ , and CO ₂ fluxes among peatland stages (2019 Burn, 2007 Burn, Peat Plateau, Plateau Edge, Young Bog, Mature Bog), or among disturbances (Intact, Thermokarst, Wildfire).	166
Table A4.1: Overview of installed instruments for meteorological and soil measurements at the two sites 2019 Burn and 2007 Burn.	172

List of Figures

- Figure 1.1:** Map of study region portraying the Taiga Plains ecozone (Marshall et al., 1999), permafrost zonation based on Obu et al. (2019) and the distribution of histel soils, i.e., peat soils affected by permafrost (Hugelius et al., 2013). The three study sites Lutose (59.50°N, 117.20°W), Scotty Creek (61.30°N, 121.30°W), and Smith Creek (63.15°N, 123.25°W) are peatland complexes underlain by permafrost. Photos are drone images taken by David Olefeldt and show all five measurement locations that are all included in Chapter 2. Blue background of drone images hints at Chapter 3 which investigated Scotty Creek as part of the sporadic permafrost zone and Smith Creek as part of the discontinuous permafrost zone with a higher extent of peat plateaus in the landscape. Red background of images indicates that Lutose was the only peatland complex that had recent wildfire disturbance (2019 and 2007) and is specifically investigated in Chapter 4. 7
- Figure 1.2:** (a) Conceptual figure portraying permafrost peatlands characteristic for the Taiga Plains indicating intact permafrost peatlands and both disturbances wildfire and thermokarst (=permafrost thaw) and resulting changes in oxic and anoxic conditions: brown line = peat/ground surface, blue line = water table, black line = frost table. (b, c) Images taken on the ground representing (b) burned and (c) thawed peatlands. (d, e, f) Images taken by drones. Photo Courtesy for (d, e, f): David Olefeldt (University of Alberta)..... 12
- Figure 2.1:** (a) Map of study region including permafrost zones (Obu et al., 2019) and distribution of histel soils, i.e., peat soils affected by permafrost (Hugelius et al., 2013) within the Taiga Plains ecozone (Marshall et al., 1999). (b) Peatland disturbances in relation to peatland stages; adapted from Estop-Aragonés et al. (2018). The stars in different colors represent the sampled peatland stages: each peatland stage had a minimum of four replicate collars per site, and the burned stages had eight collars each. Photos of the (c) 2019 Burn at Lutose, and (d) the Smith Creek thermokarst transect with the four corresponding peatland stages indicated. 20
- Figure 2.2:** Porewater concentrations and supply rates of (a, b) nitrate (NO_3^-), (c, d) ammonium (NH_4^+), and (e) phosphate (PO_4^{3-}) and (f) phosphorus (P) across all peatland stages, i.e., 2019 Burn (B19), 2007 Burn (B07), Peat Plateau (P), Plateau Edge (PE), Young Bog (YB), and Mature Bog (MB) at Lutose and Smith Creek. Measurements were collected over the 2019 growing season. Note the logarithmic scale of all y-axes..... 27
- Figure 2.3:** Soil gas concentrations of (a) nitrous oxide (N_2O), (b) methane (CH_4), and (c) carbon dioxide (CO_2) for Peat Plateau, Plateau Edge, Young Bog, and Mature Bog depth profiles from three peatland sites (Lutose, Scotty Creek, and Smith Creek). Measurements were done at the end of the growing season, in September 2018 at Scotty Creek and in August 2019 at Lutose and Smith Creek. Water table position is shown for every soil profile, indicated to be above or below the gas sampling depths (2, 5, 10, and 20 cm). Note the logarithmic scale for the CH_4 and CO_2 soil gas concentrations. 29
- Figure 2.4:** Fluxes and temperature dependency of (a, b) nitrous oxide (N_2O), (c, d) methane (CH_4), and (e, f) soil respiration (CO_2) from peatland stages, that is, 2019 Burn (B19), 2007 Burn

(B07), Peat Plateau (P), Plateau Edge (PE), Young Bog (YB), and Mature Bog (MB), at three sites (Lutose, Scotty Creek, and Smith Creek). Each symbol is an individual flux measurement, collected monthly throughout the growing season from April to October 2019 from Lutose (n = 7) and Smith Creek (n = 6), but only once in September 2018 at Scotty Creek. Linear regressions use data from all three sites and show the relationship between soil temperature at 5 cm and N₂O and soil respiration, while the temperature at 40 cm is used for CH₄ fluxes. 31

Figure 2.5: Relationship between nitrous oxide (N₂O) fluxes and near-surface soil water-filled pore space (WFPS). Each symbol represents the growing season average N₂O flux and WFPS for individual collars located in different peatland stages, including burned peat plateaus (2019 Burn, 2007 Burn) along with Peat Plateau, Plateau Edge, Young Bog, and Mature Bog. Note the logarithmic scale for the WFPS. Logarithmic regressions are shown for each of the six peatland stages (colored lines, *p* > 0.05), and for the combined data (black line, *p* < 0.001). 32

Figure 2.6: Nitrous oxide (N₂O) fluxes from five peatland ponds. Flux measurements were done on six occasions between May and October 2019 for all sites except pond L2 which was visited three times between July and October 2019. 33

Figure 2.7: Greenhouse gas balances in CO₂-equivalents among peatland stages (in the order from left to right: 2019 Burn, 2007 Burn, Peat Plateau, Plateau Edge, Young Bog, and Mature Bog), comparing (a) soil respiration, (b) CH₄ fluxes, and (c) N₂O fluxes. Boxplots use all flux data measured throughout the 2019 growing season, with black crosses indicating the averages. Conversion to CO₂-equivalents use sustained global warming and cooling potentials (SGWP, SGCP) based on a 100-year time span for CH₄ (45) and N₂O (270) (Neubauer & Megonigal, 2019). Note the difference in the scale of the y-axes. Outliers are not shown. 34

Figure 3.1: Boreal peat landscapes in the discontinuous and sporadic permafrost zones near the southern limit of permafrost in the Taiga Plains ecoregion of western Canada: (a) Map including both sites, peatland cover (Hugelius et al., 2013) and permafrost zonation (S. Gruber, 2012). (b, c) landcover maps including 80% flux footprints (red polygons) and (d, e) drone images of the landscape around the eddy covariance towers (b, d) at Smith Creek (AmeriFlux-ID: CA-SMC, tower location indicated by green star) and (c, e) at Scotty Creek (AmeriFlux-ID: CA-SCC, tower location indicated by blue star), respectively. 63

Figure 3.2: Seasonal patterns of CO₂ and CH₄ fluxes across all years (2017-2022) ± standard deviation as 14-day moving averages (a, b, c, d) of (a) net ecosystem exchange (NEE), (b) gross primary production (GPP), and (c) ecosystem respiration (ER) and (d) methane (CH₄) flux from the two eddy covariance tower sites, Scotty Creek (SCC, sporadic permafrost) and Smith Creek (SMC, discontinuous permafrost). Wilcoxon rank sum tests were applied on daily averages for each season with results portrayed by * *p* < 0.05, ** *p* < 0.01, and *** *p* < 0.001. Line intensity reflects data availability across all years (July 2017 - September 2022, n=0-6). 73

Figure 3.3: Diurnal patterns of generalized annual CO₂ and CH₄ fluxes ± standard deviation of (a) net ecosystem exchange (NEE), (b) gross primary production (GPP), and (c) ecosystem respiration (ER) and (d) methane (CH₄) flux from the two eddy covariance tower sites, Scotty

Creek (SCC, sporadic permafrost) and Smith Creek (SMC, discontinuous permafrost). Line intensity reflects data availability across all years (July 2017 - September 2022, n = 0-6)..... 75

Figure 3.4: Responses of CO₂ and CH₄ fluxes at the sporadic permafrost Scotty Creek (SCC) and the discontinuous permafrost site (SMC) to changes in selected environmental variables, such as (a) photosynthetic active photon flux density (PPFD) and (b, d) air temperature (TA). All measurements were averaged for calendar weeks whereas (a, b) weekly values of light response parameters k and GPP_{max} were calculated with a moving two-week data frame. 77

Figure 3.5: Cumulative carbon gain and loss (a, b) and net radiative greenhouse gas forcing (c, d) of carbon dioxide (CO₂) and methane (CH₄) of generalized annual data (averages of five data years, 2017-2022, for every half hour) (a, c) and as a generalized annual balance (b, d) at the two eddy covariance sites, Scotty Creek (SCC, sporadic permafrost) and Smith Creek (SMC, discontinuous permafrost). *Export of dissolved organic carbon (DOC) were measured for the years 2017 to 2019 at the watershed outflow by (L. Thompson et al., 2023). Error bars represent interannual variability as standard deviations of complete data years (2018 – 2021) only..... 78

Figure 4.1: (a) Map of the research sites around Lutose including both eddy covariance tower locations (CA-STR in the 2019 Burn and CA-LUT in the 2007 Burn; Canadian National Fire Database, 2023). (b, c) Images of the tower locations within the wildfire-affected peatland areas. 93

Figure 4.2: Generalized annual data based on four/five years of measurements from September 2019 to October 2023 as (a) diurnal and (b) seasonal patterns of annual post-fire net ecosystem exchange (NEE) measured by eddy covariance at 2019 Burn and 2007 Burn for the measurement time from September 2019 to October 2023. Seasonal patterns of (c) photosynthetic active photon flux density (PPFD) and (d) Air temperature (measured at 6.0 m and 2.1 m height at CA-LUT at 2007 Burn and CA-STR at 2019 Burn, respectively). 100

Figure 4.3: Soil respiration as (a) boxplots of measurement means (n=8), above which letters indicate statistically significant ($p < 0.05$) differences between sites, accounting for repeated measurements throughout the three growing seasons 2020, 2021, and 2022 and in (b) dependence of soil temperatures at 10 cm depth measured with static dark chambers at 2019 Burn, 2007 Burn, and Unburn (from left to right). 101

Figure 4.4: (a) Average soil temperatures at 20 cm depth displayed as difference to the Unburn mean soil temperature on each measurement date (n=12, four measurements per stage and date). Error bars represent the standard deviation of measurement occasion averages for each season (b) active layer depth for each growing season (n=240, each stage is represented by an 80-point thaw depth grid). Error bars represent the standard deviations of 80 end-of-season-thaw-depth-measurements excluding taliks which turn unfrozen towards the middle of the growing season (see Gibson et al., 2018). Low standard deviations for 2021 and 2022 at the 2007 Burn originate from the exclusion of 95% of measurements (deeper than 150 cm)..... 102

Figure 4.5: Ecosystem recovery and net CO₂-C balance for permafrost peatlands over 20 years after a wildfire. (a) Permafrost peatland succession and CO₂ balance over 20 years after wildfire, including shifts in annual NEE, relative magnitude of soil respiration, vegetation succession,

depth of the seasonally thawed peat, and the development of taliks. Here information on annual NEE before fire and >20 years after fire is based on Schulze et al., in prep., the evidence of increased proportion of soil respiration derived from old peat is based on Estop-Aragonés et al. (2018), and the recovery of vegetation and taliks ~20 years after fire is based on Gibson et al. (2018). (b) Cumulative impact of wildfire on the net CO₂ balance over 20 years after wildfire when compared to an unburned peatland, accounting for both above- and belowground combustion during fire and the difference in annual NEE between a burned and unburned site.

..... 104

Figure 5.1: Summary of findings: (a) Direction of change (downwards = flux decreases, upwards = flux increases) of carbon dioxide (CO₂), methane (CH₄), nitrous oxide (N₂O), latent heat (LE), and sensible heat (H) following wildfire and thermokarst disturbance in permafrost peatlands of the Taiga Plains in comparison to intact peat plateaus. Records of CO₂ and CH₄ were taken from eddy covariance data, while N₂O originates from static chamber measurements. Diagram adapted from Estop-Aragonés et al. (2018). (b) Estimated annual carbon balances of four permafrost peatland sites investigated in this thesis. * Export of dissolved organic carbon (DOC) was measured by L. Thompson et al. (2023) at watershed outlets in the years 2017 to 2019 (c) Estimated net radiative greenhouse gas forcing of four permafrost peatlands investigated in this thesis. Net radiative greenhouse gas forcing of N₂O at Smith Creek and Scotty Creek was estimated based off fluxes measured by static chamber measurements at peat plateaus and mature bog (Figure 2.4) multiplied by their sustained global warming/cooling potentials (SGCP/SGWP) in relation to the two sites' landcover representation (Table 3.1). ... 114

Figure A2.1: (a, b, c, d) Aerial and (e, f) ground photos of sampling locations at (a, b) wildfire-affected and (c, d, e, f) thermokarst-affected permafrost peatland complexes in the Taiga Plains ecozone, including all three permafrost thaws transect (peatland stages in the order left to right: Peat Plateau, Plateau Edge, Young Bog, and Mature Bog) at (c, d) Lutose, (e) Scotty Creek, and (f) Smith Creek 161

Figure A2.2: Sampling scheme including peat landforms (=stages) and peatland ponds and chamber types used. *The Peatland Pond L2 has situated in the middle of the 2007 Burn fire scar and had beaver activity as well 161

Figure A2.3: Soil temperature curves for one entire year at Lutose and Smith Creek at (a, b) 5 cm, (c, d) 20 cm, and (e, f) 40 cm depth 162

Figure A3.1: Energy balance closures of (a) CA-SCC (Scotty Creek, sporadic permafrost) and (b) CA-SMC (Smith Creek, discontinuous permafrost) over the measurement period from July 8, 2017, to September 21, 2022. 167

Figure A3.2: Time series over the measurement period from July 8, 2017, to September 21, 2022 of available gapfilled data for (a, c, e) CA-SCC (Scotty Creek, sporadic permafrost) and (b, d, f) CA-SMC (Smith Creek, discontinuous permafrost) regarding net ecosystem exchange (NEE), methane (CH₄), and air temperature representative of other environmental variables. . 168

Figure A3.3: Yearly (a, c, e) and diurnal (b, d, f) differences in biometeorological variables between the eddy covariance tower sites, Scotty Creek (SCC, sporadic permafrost) and Smith Creek (SMC, discontinuous permafrost) across the study period (July 2017 - September 2022).

..... 169

Figure A3.4: Seasonal (a, c) and diurnal (b, d) patterns of generalized annual energy fluxes \pm standard deviation of (a, b) latent heat (LE), (b) sensible heat (H) flux from the two eddy covariance tower sites, Scotty Creek (SCC, sporadic permafrost) and Smith Creek (SMC, discontinuous permafrost). Line intensity reflects data availability across all years (July 2017 - September 2022, n=0-6).

..... 170

Figure A4.1: Images of eddy covariance tower setup. Left: scaffolding structure at the 2019 Burn to bring high-frequency instrumentation above the tree canopy. Right: tripod structure at 2007 Burn where most burned tree remainders have fallen to the ground and regrowth of vegetation is still below 1 meter in height.

..... 171

Figure A4.2: Drone images of sampled landscapes around the Lutose peatland complex, left: 2019 Burn with distinct burned (black ashy areas) and unburned area (brown and green areas), middle: 2007 Burn where the vegetation is still recovering more than a decade after the wildfire event, right: Unburn with intact black spruce (*Picea mariana*) canopy.

..... 171

List of Abbreviations and Symbology

ANOVA	Analysis of Variance
BD	Bulk density
C	Carbon
CH₄	Methane
CO₂	Carbon dioxide
Cu	Copper
d₀	Displacement height
DOC	Dissolved organic carbon
DON	Dissolved organic nitrogen
DOY	Day of Year
EC	Electrical conductivity
ER	Ecosystem respiration
Fe	Iron
GHG	Greenhouse gas
GWP	Global warming potential
GPP	Gross primary production
H	Sensible heat
k	Half saturation constant
LAI	Leaf area index
LE	Latent heat
N	Nitrogen
N₂	Dinitrogen
N₂O	Nitrous oxide
NECB	Net ecosystem carbon balance
NEE	Net ecosystem exchange
NH₄⁺-N	Ammonium-as-nitrogen
NO₃⁻-N	Nitrate-as-nitrogen
NPOC	Non-purgeable organic carbon
P	Phosphorus
PO₄³⁻-P	Phosphate-as-phosphorus
PPFD	Photosynthetic active photon flux density
RH	Relative humidity
SGCP	Sustained global cooling potential
SGWP	Sustained global warming potential
SWin	Incoming shortwave radiation
TDN	Total dissolved nitrogen
TS	Soil Temperature
VPD	Vapor pressure deficit
WFPS	Water-filled pore space
z₀	Roughness length

1. Introduction

1.1 Carbon and Nitrogen Cycling in Northern Peatlands under a warming Climate

Humans drive climate change by intensifying the global cycles of two key elements, carbon (C) and nitrogen (N) (Gruber & Galloway, 2008). Since the industrialization, C- and N-based radiatively active trace gases, commonly referred to as greenhouse gases (GHG), such as carbon dioxide (CO₂), methane (CH₄), and nitrous oxide (N₂O) have significantly increased in the atmosphere which results in globally observed air temperature increases (IPCC, 2013). Compared to global averages, warming is advancing with a rate about twice as high in the circumpolar region with consequences for the entire biosphere of the tundra and boreal biomes therein situated (Foster et al., 2022; Smith et al., 2019). In northwestern boreal Canada, the study region of my doctoral thesis, warming is advancing even up to four times faster compared to the global average (Price et al., 2013; Rantanen et al., 2022). This warming enhances wildfires and permafrost thaw, resulting in landscape-scale transformation processes with potential further feedback to the global climate as well as C and N cycles.

Amongst northern ecosystems in the boreal and tundra biome, peatlands have the highest C and N stocks (415 ± 150 Pg C and 10 ± 7 Pg N; Hugelius et al., 2020). These stocks accumulated due to limited decomposition rates under wet and cold conditions since the last glaciation (Gorham, 1991). Northern peatlands store C and N mostly belowground and thus differ from other ecosystems, where the majority of C and N is stored and lost aboveground, often by human-made land use changes (Goldstein et al., 2020). Although human land use includes belowground drainage and exploitation of peatlands along with large amounts of GHG release (Dommain et al., 2018; Goldstein et al., 2020; Günther et al., 2020; Ribeiro et al., 2021), peatland exploitation has so far focused on economically feasible areas closer to dense human population and thus only played a minor role in northern peatlands, particular in North America (United Nations Environment Programme, 2022). Belowground storage of C and N in pristine northern peatlands is rather threatened by human-made climate change via both direct and indirect effects of warming. Warmer climate results in warmer air and ground temperatures and longer growing seasons which affect peatland C storage directly by enhanced soil respiration (Wilson et al., 2016). Indirect effects driven by natural disturbances, such as accelerating wildfire regimes

(Wilkinson et al., 2023), result in both drastic biogeochemical and biophysical changes of northern peatland ecosystems, which also impacts C and N cycling (Abbott et al., 2016; Turetsky et al., 2015).

Storage of C and N in northern peatlands is particularly prone to warmer soil temperatures and increasing wildfires when the ground is permafrost-affected (Natali et al., 2022; Voigt et al., 2020). Permafrost is ground that remains frozen for at least two successive years (S. Harris et al., 1988), and almost half of the northern peatland area is currently affected by permafrost (Hugelius et al., 2020). However, permafrost is warming (Biskaborn et al., 2019) and thus shrinking in its global (Grosse et al., 2016) and circumpolar extent (Olefeldt et al., 2016). Overall, one fifth of the circumpolar region is affected by thermokarst (Olefeldt et al., 2016), i.e. ground surface subsidence caused by thawing permafrost (Osterkamp et al., 2009). However, the outcome of thermokarst formation depends on several factors such as topography, ground ice content, and terrestrial zone and is highly variable across the circumpolar region, appearing as wetland, lake, and hillslope thermokarst (Olefeldt et al., 2016). The consequences of ongoing loss of permafrost by thaw is unclear as studies have suggested both losses and accumulation of C after thaw (Hugelius et al., 2020; Schuur et al., 2022). This is why more research is needed to understand the potential release of CO₂ and CH₄ following permafrost thaw with global implications for the Earth's climate (Lenton et al., 2008). The fate, direction and magnitude of previously frozen C and N has remained unclear for remote and understudied northern peatlands threatened by warming directly and by both permafrost thaw and wildfires indirectly.

In a future warmer climate, degradation of permafrost could release C and N via aerobic or anaerobic decomposition, possibly exceeding predicted increases in C uptake across the boreal biome (Koven et al., 2015; O'Donnell et al., 2012; Voigt et al., 2019). With increasing air and soil temperatures, the seasonally thawed active layer (i.e., the upper part of the ground profile above the permafrost ground ice that thaws and refreezes each year) deepens over time, exposing more and more C and N to microbial activity (Keuper et al., 2012). Once unfrozen, C and N can be 1) mobilized for lateral export as dissolved organic carbon (DOC) and dissolved organic nitrogen (DON) downstream to larger hydrological systems (Frey & Smith, 2005; Olefeldt et al., 2013; Wickland et al., 2018) or 2) released as GHGs to the atmosphere via decomposition and other microbial pathways (Hodgkins et al., 2014). The focus of this doctoral thesis is on the latter

one, as the enhanced GHG release from thawing permafrost and boreal wildfires is of global significance but requires more precise regional estimates for future upscaling efforts (Schädel et al., 2024; Schuur et al., 2022; Wilkinson et al., 2023).

The net ecosystem C balance (NECB) determines whether an ecosystem is a contemporary source or sink of C considering both lateral export as DOC and gaseous release or uptake of the GHGs CO₂ and CH₄ (Arias-Ortiz et al., 2021; Olefeldt et al., 2012). Both lateral export and input of DOC via rain and snow are the water-borne part of the NECB. Other components of C fluxes are atmospheric and include the gaseous net exchange of CO₂ and CH₄ as well as other non-methane volatile organic components (Olefeldt et al., 2012). Previous studies on a permafrost peatland in Sweden have found that the annual NECB is dominated by CO₂ (Holmes et al., 2022; Olefeldt et al., 2012). DOC export was smaller and similar in magnitude as total hydrocarbon, of which 75% was CH₄. CH₄ only offset the CO₂ uptake in small quantities and varied for landforms with permafrost (2% for palsas) and without permafrost (17% for fens) (Holmes et al., 2022). However, warming is projected to increase the CH₄ emissions from thawing permafrost peatlands long-term (Helbig, Quinton, et al., 2017) so that studying the effects of decreasing extents of permafrost on the NECB is a crucial research need.

The overall GHG balance of permafrost peatlands mainly depends on the release and uptake of three GHGs, CO₂, CH₄, and N₂O, which all contribute to the net radiative GHG forcing of ecosystems (Frolking et al., 2011). All three GHGs differ in both their residence times in the atmosphere (<37 years for >50% of the CO₂, 12.4 years for CH₄, and 121 years for N₂O; IPCC, 2014; Neubauer & Megonigal, 2015) and their radiative efficiencies ($1.75 \times 10^{-15} \text{ W m}^{-2} (\text{kg CO}_2)^{-1}$, $1.28 \times 10^{-13} \text{ W m}^{-2} (\text{kg CH}_4)^{-1}$, $3.83 \times 10^{-13} \text{ W m}^{-2} (\text{kg N}_2\text{O})^{-1}$; IPCC, 2014; Neubauer & Megonigal, 2015). Assuming a single-pulse emission, the global warming potential approach expresses the cumulative radiative forcing over different time horizons (most commonly 100 years) to compare the effects of different GHGs with each other. Undisturbed peatlands were previously reported as sinks of CO₂ and N₂O (negative effect on net radiative forcing) and sustained sources of CH₄ (positive effect on radiative forcing) (Frolking et al., 2011; Neubauer & Megonigal, 2015). For sustained long-term emissions from ecosystems, the GWP metric is unsuitable as it only considers one-time pulse emissions of a GHG (Neubauer & Megonigal, 2015).

Moving away from the single-pulse assumption, Neubauer & Megonigal (2015, 2019) reintroduced the Sustained Global Warming/Cooling Potential (SGWP/SGCP) which considers the sustained long-term GHG emissions (positive = net warming) or uptake (negative = net cooling) of ecosystems. Opposing trends of different GHGs lead to overall minor differences of net radiative GHG forcing of peatlands (Baird et al., 2019; Günther et al., 2020; Helbig, Chasmer, Kljun, et al., 2017; Johansson et al., 2006; Nugent et al., 2019). Generally, the SGWP is larger than the GWP, except for when N₂O is considered at time scales smaller than 70 years (Neubauer & Megonigal, 2015). Thus, it can depend on whether the GWP or the SCWP is used for CH₄ emissions to conclude whether the overall net radiative GHG forcing of a peatland is negative (cooling) or positive (warming). An ecosystem consistently sequestering 263 kg of CO₂ while emitting 1 kg of N₂O would be considered GHG neutral using the 100-year GWP while the SGWP suggests a net warming effect for the same timescale (compare Neubauer & Megonigal, 2015). As a consequence, the ecosystem's role as GHG source would be underestimated.

Gaseous releases of C and N as GHGs from unmanaged northern peatlands with or without permafrost have not been accounted for in past GHG accounting reports, be it on a global scale (United Nations Environment Programme, 2022) or a Canada-wide scale (Kurz et al., 2013). The extent of warming controls the resulting acceleration of both wildfire cycles and permafrost thaw. Previous studies estimated that northern peatland GHG emissions could potentially amount to 1% of GHG radiative forcing from anthropogenic sources, while emphasizing the high degree of uncertainty (Hugelius et al., 2020). Thus, more research is needed on how warming and associated disturbances, namely wildfire and permafrost thaw, affect the C and N sink and storage function of the entire circumpolar region (Goldstein et al., 2020; Hugelius et al., 2020; Schuur et al., 2015), including the Taiga Plains ecozone in northwestern Canada (Helbig, Pappas, et al., 2016).

1.2 Boreal Peatlands underlain by Permafrost in the Taiga Plains

Northwestern Canada has widespread boreal peatlands (Loisel et al., 2014; Wright et al., 2022), covering about 40% of the area of the Taiga Plains ecozone (Gibson et al., 2018). Boreal peatlands in the Taiga Plains comprise of plateau-wetland complexes with permafrost only found in peat plateaus elevated above the wetter, surrounding wetlands, mostly without trees (Quinton

et al., 2019). Thus, the peatland areas are distinguished by the presence or absence of permafrost (cf. Figure 1.1, histels and histosols in Hugelius et al., 2013). Permafrost area coverage is used to differentiate between four permafrost zones: continuous (90-100%), discontinuous (50-90%), sporadic (10-50%), and isolated (0-10%) (cf. Figure 1.1) (Brown et al., 2002; Gruber, 2012; Obu et al., 2019). In the discontinuous and sporadic permafrost zones, boreal peatlands are often the only ecosystems with permafrost, as the peat acts as insulating material (Camill, 1999) and the shading tree cover keep the deeper ground temperatures below 0°C throughout an entire year. As a consequence, the high area coverage of peatlands in the boreal landscape allows permafrost to a higher extent in lower latitudes in the Taiga Plains than elsewhere.

In the peatlands of the Taiga Plains, permafrost aggregation and degradation historically occurred in long-term cycles corresponding to global climate and air temperatures (Treat & Jones, 2018). The region's current climate is continental, with low precipitation 200 – 600 mm (Ecosystem Classification Group, 2007, Figure 4) and mean annual air temperatures between -5.5°C and -1.5°C (Carpino et al., 2020; Vincent et al., 2012). Governed by topography, annual precipitation decreases with elevation and increases with latitude (Ecosystem Classification Group, 2007). Following a climate and permafrost extent gradient from south to north across the Taiga Plains, my study sites are three boreal peatland complexes: Lutose (59.50°N, 117.20°W), Scotty Creek (61.30°N, 121.30°W), and Smith Creek (63.15°N, 123.25°W). Mean annual air temperatures and annual precipitation are given as follows (Environment and Climate Change Canada, 2020): -1.8°C and 391 mm at Lutose (measured at Meander River), -3.8°C and 356 mm for Scotty Creek (measured at Fort Simpson), and -4.1°C and 333 mm for Smith Creek (measured at the Wrigley airport). Current warming trends lead to large-scale degradation of permafrost in peatlands (Gibson et al., 2021; Treat & Jones, 2018), which is particularly true for the peatlands in the Taiga Plains (Olefeldt et al., 2016; Wright et al., 2022).

Belowground, the three peatland complexes studied in this thesis vary in organic layer depths, ranging from 1.5 m at Smith Creek to 6 m at the southernmost site Lutose. The peatland development history of Lutose and Scotty Creek are similar. In Lutose, peatland development started off as non-permafrost fens 8,000 - 10,000 years ago that transitioned into poor fens (Heffernan et al., 2020). Permafrost aggregation started after peat initiation (= epigenetic) (Loisel et al., 2014), 4,000 years ago at Scotty Creek and 1,200 years ago at Lutose, respectively. The

formation of ground ice raises the accumulated peat to a plateau (Zoltai & Tarnocai, 1975), which leads to drainage and thus affects the peat accumulation in terms of peat quality and type (Heffernan et al., 2020). Therefore, the deeper parts of the peat profile originate from earlier development stages and are characterized by *Sphagnum* peat (Zoltai, 1993). In contrast, the sylvic peat above developed from residues of ericaceous shrubs, feathermosses, and black spruce (*Picea mariana*) under more oxic conditions (Heffernan et al., 2020). The depth of the transition from *Sphagnum* to sylvic peat in the peat profile therefore determines the age of permafrost formation. Thus, this transition zone lies deeper in the northernmost site Smith Creek followed by Scotty Creek and lastly Lutose.

Aboveground, all three peatland complexes are characterized by a mix of both permafrost-free wetlands, such as bogs and fens, and peat plateaus underlain by permafrost. Compared to the other landcover, intact peat plateaus are raised one or two meters above the surrounding landscape due to the ice expansion during permafrost aggregation and are usually forested with black spruce (*Picea mariana*), tamarack (*Larix laricina*), feathermosses, lichens, and ericaceous shrubs (Robinson & Moore, 2000; Zoltai & Tarnocai, 1975). The landscape coverage of peat plateaus increases with latitude, exceeding 50% when transitioning from sporadic to discontinuous permafrost. There, the dominating black spruce vegetation is less dense and shorter and lichen spp. are more abundant than *Sphagnum* spp. due to the cooler climate and shorter growing season further north (Ecosystem Classification Group, 2007). Further south, Scotty Creek and Lutose in the sporadic permafrost zone in turn have higher percentages of permafrost-free wetlands compared to the Smith Creek site in the discontinuous permafrost zone.

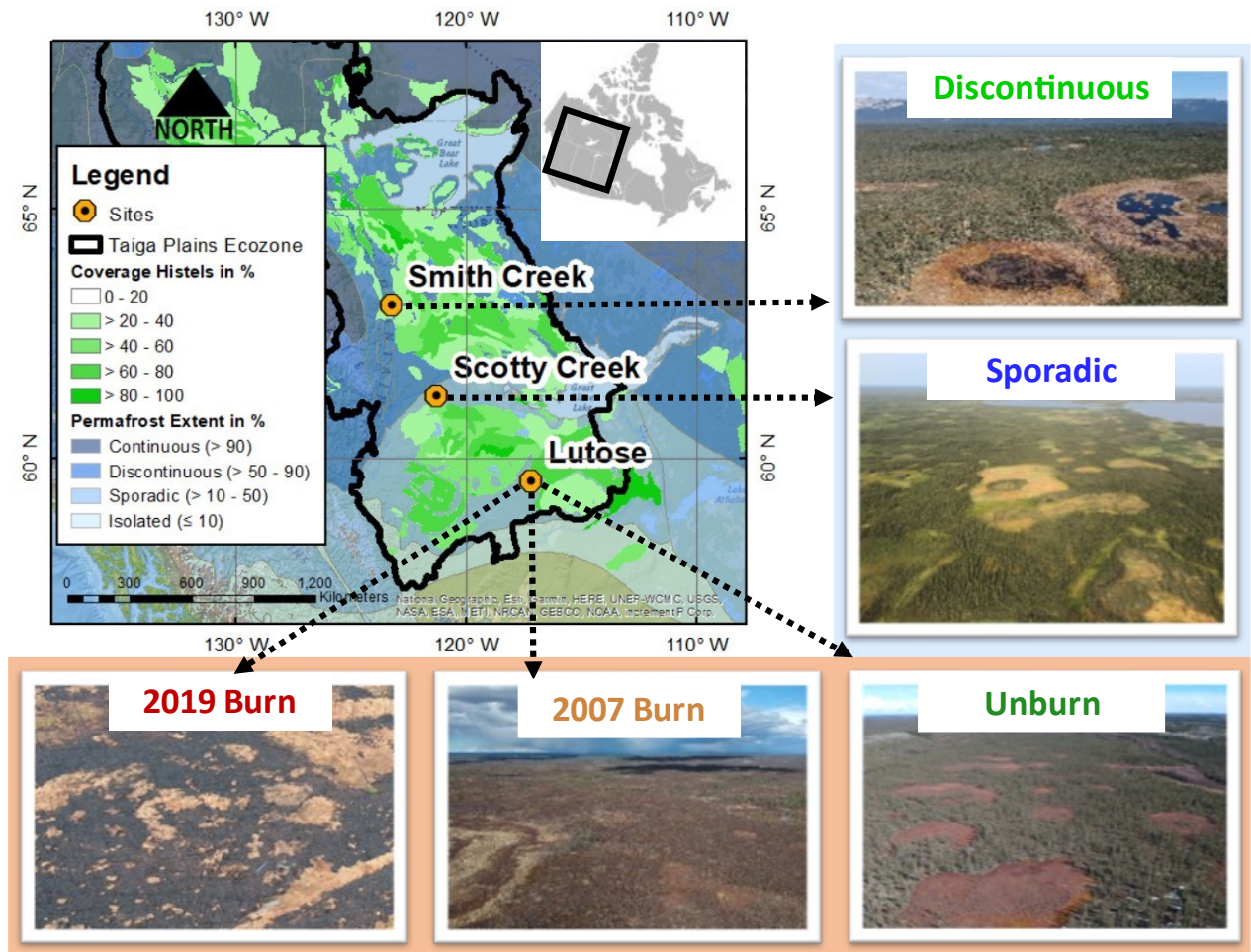


Figure 1.1: Map of study region portraying the Taiga Plains ecozone (Marshall et al., 1999), permafrost zonation based on Obu et al. (2019) and the distribution of histel soils, i.e., peat soils affected by permafrost (Hugelius et al., 2013). The three study sites Lutose (59.50°N, 117.20°W), Scotty Creek (61.30°N, 121.30°W), and Smith Creek (63.15°N, 123.25°W) are peatland complexes underlain by permafrost. Photos are drone images taken by David Olefeldt and show all five measurement locations that are all included in Chapter 2. Blue background of drone images hints at Chapter 3 which investigated Scotty Creek as part of the sporadic permafrost zone and Smith Creek as part of the discontinuous permafrost zone with a higher extent of peat plateaus in the landscape. Red background of images indicates that Lutose was the only peatland complex that had recent wildfire disturbance (2019 and 2007) and is specifically investigated in Chapter 4.

1.3 Out of the Dark, into the Light

1.3.1 Landcover Change in the Taiga Plains – from forested Plateaus to treeless Wetlands

Across the Taiga Plains, warming is accelerating two drivers of landscape change, wildfire and permafrost thaw known as thermokarst (Foster et al., 2022). Wildfires have increased in frequency and severity across all boreal North America (Turetsky et al., 2011). Within the last

decades, the annual total area burned by wildfires has doubled in some boreal regions of northwestern Canada (Flannigan et al., 2009; Stocks et al., 2002). The year 2023 has produced the largest amount of burned area in the Canadian history of wildfire records, twice as much as every other wildfire year recorded before and nine times higher than the average of the last 10 years (Natural Resources Canada, 2023). Within wildfire-affected permafrost peatlands, Gibson et al. (2018) also found significantly higher area proportions of permafrost-free thermokarst bogs and concluded that wildfire also enhances permafrost thaw in the peatlands of the Taiga Plains.

The peatland landcover of the Taiga Plains ecozone gradually shifts from permafrost peat plateaus towards more permafrost-free wetlands and burned peat plateaus with rapidly degrading permafrost (Chasmer & Hopkinson, 2017; J. A. Wang et al., 2020; Wright et al., 2022). Wetland thermokarst dominates major parts of the Taiga Plains ecozones, e.g., more than half of the landscape in the Mackenzie River Valley (Olefeldt et al., 2016). Lake thermokarst often accompanies wetland thermokarst formation in boreal peatlands in the Taiga Plains (Kuhn, Thompson, et al., 2021). Both disturbances wildfire and thermokarst transform the peat landscape from forests with black spruce vegetation (“Out of the Dark”) into open, non-treed and non-permafrost wetlands dominated by mosses or lakes with no vegetation (“Into the Light”). Although there are also biophysical consequences of the changes to landcover and vegetation driven by wildfires and thermokarst, this thesis focuses on the biogeochemical implications of transforming boreal peatland complexes for their landscape-scale GHG fluxes.

The effects of disturbances for landscape-scale GHG fluxes are best monitored using the eddy covariance technique. Eddy covariance includes continuous, non-intrusive, high-frequency measurements of landscape-atmosphere exchange of GHGs, including the C fluxes of CO₂ and CH₄ (Aubinet et al., 1999; Baldocchi, 2003, 2020). In addition to the high-frequency measurements, a variety of biometeorological variables is recorded along with the high-frequency eddy covariance measurements to enable GHG flux calculations and interpretations. So far, there is no study using the eddy covariance technique to measure post-fire CO₂ release of a recently burned permafrost peatland. In general, due to high demand for maintenance and the remoteness of permafrost peatlands in the Taiga Plains, eddy covariance studies comparing more than one permafrost peatland site are scarce. There is thus the need to compare different eddy covariance sites with different extents of permafrost in the landscape to project how the loss of

permafrost might affect both the future net radiative GHG forcing and the NECB of thawing permafrost peatlands.

1.3.2 Changes in Carbon and Nitrogen Cycling - from Frozen-solid in the Ground to Gaseous Release to the Atmosphere

Given the large areal extent and the vast amounts of C and N stored in the peatlands of the study area, the consequences of the warming-driven, landscape-scale transitions are of global significance. Wildfires alter the biogeochemical conditions of permafrost peatlands and promote permafrost thaw and active layer deepening (Gibson et al., 2018; Turetsky et al., 2007, 2015). Compared to intact peat plateaus, burned plateaus present a deeper oxic layer and warmer soil temperatures at depth which cause lower soil respiration rates (Gibson et al., 2019) with a higher contribution of aged C from deeper soil layers (Estop-Aragonés et al., 2018). Losses of old, deeper C after fire are substantial as this C has not been part of the active atmospheric cycle for a long time but is now re-activated (Walker et al., 2018). Additionally, fire leads to increased availability of nutrients such as phosphorus (P) (Burd et al., 2018). Still, slow recovery of peatland productivity and vegetation, mainly Labrador tea (*Rhododendron groenlandicum*) and *Picea mariana* following some years after fire, turns boreal ecosystems into sources of C for one or two decades (Foster et al., 2022). However, past studies often focused on non-permafrost peatlands (e.g., Wieder et al., 2009; Wilkinson et al., 2023).

Thermokarst occurs with the complete loss of permafrost, and the resulting ground subsidence leads to a water table close to the surface along with major changes to C cycling. The water table acts as thermodynamic redox boundary between aerobic and anaerobic conditions (Frolking et al., 2011). Under anaerobic conditions, CO₂ is reduced to CH₄, enhanced by warmer soil temperatures in deeper peat layers than post-thaw (Jones et al., 2017; O'Donnell et al., 2012). Water table depth of thermokarst bogs in the Taiga Plains increases with time since thaw so that recently thawed bogs (~30 years since thaw in Heffernan et al., 2020) often have a water table closer to the surface compared to more mature thaw bogs usually towards the bog center (~200 years since thaw in Heffernan et al., 2020). Main species within the younger bog stage are *Sphagnum riparium* and *Scheuchzeria palustris* which prefer the wet conditions given by a water table close to the surface. The mature bog, however, is dominated by *Sphagnum fuscum* and ericaceous shrubs (Pelletier et al., 2017). Vegetation dynamics and water table depths both

control C and N cycling in peatlands and both vary largely within the short distance of the peat plateau to bog transition zone. In conclusion, biogeochemical changes by thermokarst will impact the GHG exchange of the entire study region if more and more peat plateaus underlain by permafrost develop into permafrost-free bog stages or even completely inundated water bodies.

Past studies at the Lutose peatland site have made use of a space-for-time approach by differentiating between the years after thaw and compared differences in CO₂ and CH₄ fluxes of the intact plateaus underlain by permafrost against the young and mature bog stages free of permafrost using soil static chamber on a plot scale (Heffernan et al., in prep.). The mature bog presented the highest gross primary production (GPP) and ecosystem respiration (ER) whereas net ecosystem exchange (NEE) varied with the annual wetness. In wet years, the mature bog area remained a sink, whereas the younger bog area turned into a source of CO₂. In contrast to wildfire-affected areas, there was almost no contribution of old soil organic C to this potential release detected (Estop-Aragónés et al., 2018). The main variables controlling the fluxes and thus the source and sink function for CO₂ were water table depth and soil temperatures. Due to enhanced soil temperatures, both treeless bog stages were more productive compared to the forested peat plateau. However, past efforts have often overlooked the third important GHG N₂O which can also be measured using the soil static chamber technique at the plot scale.

In addition to impacts on the C cycle, wildfires and thermokarst affect the N cycle of peatlands despite known general limitation of N in many northern ecosystems (Dorrepaal et al., 2005). Active layer deepening post-wildfire can introduce N from deeper layers to plant-available depths and lead to fertilization effects (Keuper et al., 2017). In turn, plant uptake of N is overall limited post-fire (van Beest et al., 2019) when major parts of the previous vegetation have burned down. Ash remainders on otherwise bare surface can affect the pH and restrict key N processing like nitrification and denitrification (Liimatainen et al., 2014). Recent studies have identified N₂O emissions from bare peat surfaces of tundra soils as ‘hot spots’ (McClain et al., 2003) where C to N ratios were low and vegetation was disturbed (Marushchak et al., 2011; Repo et al., 2009; Voigt, Lamprecht, et al., 2017). Given these two controls, potential N₂O hot spots were projected in places where high peatland coverage is accompanied by thermokarst, as given in the Taiga Plains (Voigt, Marushchak, et al., 2017, Figure 5), which requires further investigation. Bare peat surfaces are also commonly found after wildfires (Davidson et al.,

2019), potentially with increased nutrient availability (Burd et al., 2018; van Beest et al., 2019). However, there is only one study on post-fire N₂O emissions including the Taiga Plains, which focused on upland ecosystems instead of wildfire-affected permafrost peatlands (Köster et al., 2017). Thus, there is a need to measure N₂O fluxes from permafrost peatlands post wildfire and thermokarst disturbance.

In conclusion, the storage and sink function of permafrost peatlands for C and N has so far been based off the long-term atmospheric uptake of CO₂, CH₄ and N₂O. Now under a warming climate, intensified disturbances, such as wildfire and thermokarst, are threats to the significant amounts of frozen C and N stored by permafrost peatlands. In the lack of alternative field measurements, current earth system models still rely on C decomposition rates from small-sample size incubation studies in laboratory environments (e.g., Schädel et al., 2016) to project the feedback of thawing permafrost soils in a warming climate and have often not accounted for thermokarst formation nor wildfire (Koven et al., 2015; Lawrence et al., 2012; Schädel et al., 2024). Since thermokarst and wildfires are disturbances with landscape-scale effects, these need to be studied under field conditions and on a wide ecosystem-scale. In a warming world, previously frozen organic compounds of C and N used to be enclosed ‘in the dark’ ground for millennia, but could now be released ‘to the light’ atmosphere as GHGs.

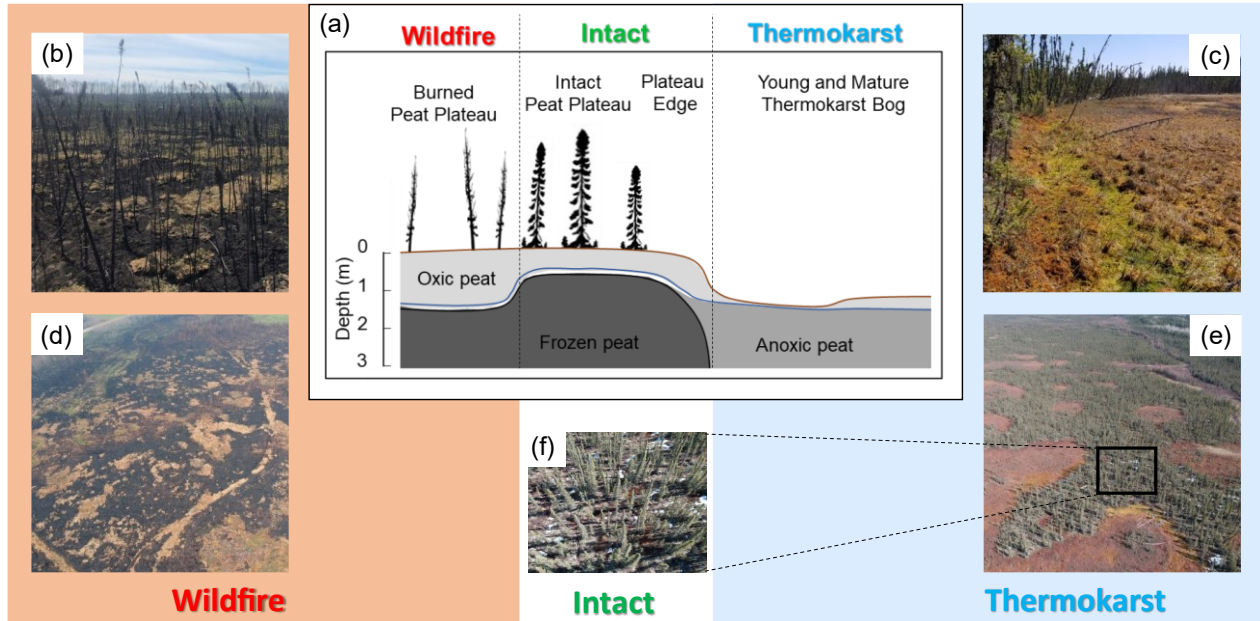


Figure 1.2: (a) Conceptual figure portraying permafrost peatlands characteristic for the Taiga Plains indicating intact permafrost peatlands and both disturbances wildfire and thermokarst (=permafrost thaw) and resulting changes in oxic and anoxic conditions: brown line = peat/ground surface, blue line = water table, black line = frost table. (b, c) Images taken on the ground representing (b) burned and (c) thawed peatlands. (d, e, f) Images taken by drones. Photo Courtesy for (d, e, f): David Olefeldt (University of Alberta)

1.4 Objectives

My research investigates the effects of wildfire and thermokarst on the GHG balance of permafrost peatlands at different spatial scales using two gas flux measurement techniques. To fill existing knowledge gaps, I focused my work on the consequences of wildfire (Chapters 2 & 4) and permafrost thaw (Chapters 2 & 3) on the surface-atmosphere exchange of the three GHGs CO₂, CH₄, and N₂O at different scales (Chapter 2: plot scale, Chapters 3 & 4: ecosystem scale) (Table 1.1). My research objectives are:

O1: Determine the GHG balance of permafrost peatlands and peatland ponds affected by wildfire and permafrost thaw with focus on N₂O.

O2: Assess how different extents of permafrost affect the surface-atmosphere exchange of CO₂ and CH₄ and resulting net radiative forcing and NECB of two peatland complexes within the sporadic and the discontinuous permafrost zone

O3: Quantify the post-fire CO₂ losses of burned permafrost peatlands in comparison to the immediate CO₂ release during wildfire combustion.

Table 1.1: *Overview of peatland complexes, disturbances, flux measurement methods, and GHGs by chapter*

	Peatland complexes			Disturbance		Flux measurement method		GHGs		
	LUT	SCC	SMC	Wildfire	Thermokarst	Static Chambers	Eddy Covariance	CO ₂	CH ₄	N ₂ O
Ch. 2	✓	✓	✓	✓	✓	✓		✓	✓	✓
Ch. 3		✓	✓		✓		✓	✓	✓	
Ch. 4	✓			✓		✓	✓	✓		

Note. LUT = Lutose, SCC = Scotty Creek, SMC = Smith Creek

2. Nitrous Oxide Fluxes in Permafrost Peatlands remain negligible after Wildfire and Thermokarst Disturbance

Abstract

The greenhouse gas (GHG) balance of boreal peatlands in permafrost regions will be affected by climate change through disturbances such as permafrost thaw and wildfire. Although the future GHG balance of boreal peatlands including ponds is dominated by the exchange of both carbon dioxide (CO₂) and methane (CH₄), disturbance impacts on fluxes of the potent GHG nitrous oxide (N₂O) could contribute to shifts in the net radiative balance. Here, we measured monthly (April to October) fluxes of N₂O, CH₄, and CO₂ from three sites located across the sporadic and discontinuous permafrost zones of western Canada. Undisturbed permafrost peat plateaus acted as N₂O sinks (-0.025 mg N₂O m⁻² d⁻¹), but N₂O uptake was lower from burned plateaus (-0.003 mg N₂O m⁻² d⁻¹) and higher following permafrost thaw in the thermokarst bogs (-0.054 mg N₂O m⁻² d⁻¹). The thermokarst bogs had below-ambient N₂O soil gas concentrations, suggesting that denitrification consumed atmospheric N₂O during reduction to dinitrogen. Atmospheric uptake of N₂O in peat plateaus and thermokarst bogs increased with soil temperature and soil moisture, suggesting sensitivity of N₂O consumption to further climate change. Four of five peatland ponds acted as N₂O sinks (-0.018 mg N₂O m⁻² d⁻¹), with no influence of thermokarst expansion. One pond with high nitrate concentrations had high N₂O emissions (0.30 mg N₂O m⁻² d⁻¹). Overall, our study suggests that the future net radiative balance of boreal peatlands will be dominated by impacts of wildfire and permafrost thaw on CH₄ and CO₂ fluxes, while the influence from N₂O is minor.

2.1 Introduction

Northern peatlands cover ~3 million km² (Olefeldt et al., 2021) and impacts of climate change on their future greenhouse gas (GHG) balance may be of global significance (Koven et al., 2015; Lenton et al., 2008; Schuur et al., 2013, 2015). Peatland biogeochemistry is strongly influenced by often waterlogged, cold and nutrient poor soils, which can result in both atmospheric uptake and emissions of all three major GHGs; carbon dioxide (CO₂), methane (CH₄), and nitrous oxide (N₂O) (Frolking et al., 2006, 2011). Of these, N₂O fluxes have been the least studied and impacts of disturbances such as permafrost thaw and wildfires are not well understood across the circumpolar region (Martikainen et al., 1993; Voigt et al., 2020; Voigt, Marushchak, et al., 2017). The discontinuous permafrost zone of the Taiga Plains ecozone in western Canada is the second largest peatland region in Canada with ~250,000 km² peatlands (Olefeldt et al., 2021). Northwestern Canada is currently experiencing some of the fastest climate warming compared to both, the rest of the globe (Rantanen et al., 2022) and across Northern Canada (Bush et al., 2019), accelerating permafrost thaw (Chasmer & Hopkinson, 2017; Gibson et al., 2018), and intensifying fire regimes (Coogan et al., 2019; Turetsky et al., 2011), with uncertain net effects on the GHG balance.

Ecosystem disturbances, such as wildfires and permafrost thaw, can cause long-term shifts in CO₂, CH₄, and N₂O fluxes, potentially shifting from net emission to net uptake or vice versa (Helbig, Chasmer, Desai, et al., 2017; Helbig, Chasmer, Kljun, et al., 2017; Helbig, Pappas, et al., 2016; Voigt et al., 2020). To understand the net effect of an altered GHG balance on atmospheric radiative forcing, it is necessary to account for the differences in sustained global warming (emission) and cooling (uptake) potential (SGWP, SGCP) for each GHG (Neubauer & Megonigal, 2015, 2019). Although N₂O fluxes from pristine, boreal peatlands are generally small (Maljanen et al., 2010; Martikainen et al., 1993; Nadelhoffer et al., 1991), the SGWP and SGCP for N₂O fluxes are 6 and 270 times greater than for CH₄ and CO₂, respectively, when considered on a 100-year horizon (Neubauer & Megonigal, 2019). Thus, even small shifts in N₂O fluxes could affect the net radiative balance of boreal peatlands and the overall impact of disturbances.

Net N₂O emissions from soils are influenced by the balance between N₂O production through both denitrification and nitrification and N₂O consumption which only occurs through denitrification (Butterbach-Bahl et al., 2013; Schlesinger, 2013; Voigt et al., 2020). Nitrification

is an aerobic process where ammonium (NH_4^+) is oxidized to nitrate (NO_3^-), with N_2O as a potential by-product. Denitrification is an anaerobic process which involves both reduction of NO_3^- to N_2O , and reduction of N_2O to nitrogen gas (N_2). Suboxic conditions can favor the initial reduction of NO_3^- to N_2O , and lead to high N_2O emissions (Hendzel et al., 2005; Marushchak et al., 2011; Regina et al., 1998), while fully anoxic conditions under long-term water-saturated conditions favor the complete reduction of NO_3^- to N_2 . Fully anoxic conditions can also lead to N_2O uptake when NO_3^- availability is low and the reduction to N_2 uses atmospheric N_2O that diffuses into the soil (Chapuis-Lardy et al., 2007). Net N_2O emissions from peatlands, including the occurrence of hot spots and hot moments (McClain et al., 2003) of N_2O emissions, are thus driven by complex interactions between soil moisture, availability of inorganic nitrogen (N), competition for inorganic N between microbes and plants, soil temperature, and physical constraints on gas diffusion (Gil et al., 2017, 2021; Marushchak et al., 2021; Repo et al., 2009; Voigt et al., 2020).

Permafrost thaw in peatlands can lead to deepening and warming of the seasonally thawed active layer, but also complete thaw and collapse of the surface which leads to the development of thermokarst bogs and ponds (Quinton et al., 2009). The effect of peatland permafrost thaw on the GHG balance thus varies depending on impacts on environmental conditions and vegetation. Permafrost peatlands, including peat plateaus, are often dominated by lichens, shrubs and stunted trees and have relatively dry soils, yielding a low rate of soil carbon (C) accumulation and low or negligible CH_4 emissions (Helbig, Chasmer, Kljun, et al., 2017; Helbig, Quinton, et al., 2017; Treat et al., 2016; Turetsky et al., 2020). Collapse into thermokarst bogs causes soil saturation and a shift in vegetation to dominance of *Sphagnum* mosses, leading to increased CH_4 emissions and increased rate of peat accumulation – although the net effect on the CO_2 balance is uncertain due to potential mineralization of deep peat layers (Jones et al., 2017). Peatland ponds with thermokarst expansion often emit large amounts of CH_4 and have net emissions of CO_2 (Elder et al., 2021; Walter Anthony et al., 2018), while the effects on pond N_2O fluxes are unknown. Studies of boreal peatland N_2O fluxes in permafrost regions come primarily from northern Europe and have shown generally low N_2O emissions from intact peat plateaus and palsas, but at times very high emissions during initial stages of permafrost thaw and soil warming associated with increased availability of inorganic N and increases in pH (Takatsu et al., 2022; Voigt, Lamprecht, et al., 2017). Thermokarst wetlands with mineral soils have in some regions led to

high N₂O emissions (Abbott & Jones, 2015; Marushchak et al., 2021; Yang et al., 2018), but N₂O emissions did not increase with the development of Tibetan thermokarst bogs (Sun et al., 2021). Lab mesocosm experiments have suggested that development of thermokarst bogs may even lead to N₂O uptake (Voigt et al., 2019), suggesting that impacts of permafrost thaw on N₂O fluxes from peatlands will vary depending on environmental conditions during and after thaw, which may lead to distinct regional differences.

Wildfire in permafrost peatlands causes large immediate emissions of CO₂ through combustion (Mack et al., 2021; Walker et al., 2019, 2020) but can also influence CO₂ fluxes for decades after the fire due to a warmer peat profile and slow vegetation regeneration (Estop-Aragonés et al., 2018; Gibson et al., 2019). The effect of wildfire on N₂O fluxes in permafrost peatlands is unknown, but wildfire has been shown to cause N₂O emissions in burned upland forests (Köster et al., 2017). Absence of vegetation in degrading permafrost peatlands has been linked to high N₂O emissions, due to reduced competition for NO₃⁻ between plants and denitrifying bacteria (Voigt, Lamprecht, et al., 2017; Voigt, Marushchak, et al., 2017). Whether the same processes result in elevated N₂O emissions from permafrost peatlands in the years after wildfire is unknown.

The objective of this study was to assess the impacts of wildfire and permafrost thaw and thus thermokarst development on the GHG balance of peatlands, with a focus on N₂O fluxes. We measured monthly growing season N₂O, CH₄, and CO₂ fluxes from different peat landforms (peatland stages) at three sites across the sporadic and discontinuous permafrost zones of the Taiga Plains ecozone in western Canada, including intact permafrost peat plateaus, peat plateaus affected by wildfire, thermokarst bogs, and peatland ponds. We monitored soil environmental conditions, nutrient availability, and dissolved soil GHG concentrations to assess controls on the GHG fluxes. Using SGWP and SGCPs we compared the net effect on the net radiative balance caused by impacts of wildfire and permafrost thaw on N₂O and CH₄ fluxes. We hypothesized that wildfire would cause increased N₂O emissions due to increased microbial availability and decreased competition for inorganic N, while thermokarst bogs and ponds would have reduced N₂O emissions or even uptake due to stable anoxic conditions favoring complete denitrification to N₂.

2.2 Materials and Methods

2.2.1 Study Sites and Sampling Design

Our study sites are three peatland complexes located within the sporadic and discontinuous permafrost zones of the Taiga Plains ecozone (Obu et al., 2019): Lutose (59.50°N, 117.20°W), Scotty Creek (61.30°N, 121.30°W), and Smith Creek (63.15°N, 123.25°W) (Figure 2.1a and Table A2.1). Mean annual air temperature is -1.0, -2.8, -4.1°C at Lutose, Scotty Creek, and Smith Creek, respectively, while mean annual precipitation is ~380 mm at all sites with ~60% rainfall (Environment and Climate Change Canada, 2020). Peatland initiation occurred at Lutose and Scotty Creek sites ~8,500 cal yr BP (Heffernan et al., 2020; Pelletier et al., 2017), and was followed by transitions through marsh and fen stages until permafrost aggradation occurred ~1,800 and ~5,000 cal yr BP, respectively (Heffernan et al., 2020; Pelletier et al., 2017). The Smith Creek peatland initiation is yet to be studied. Peat depth is ~590, ~330, and ~150 cm at Lutose, Scotty Creek, and Smith Creek. Each peatland complex comprises permafrost-affected peat plateaus, and permafrost-free thermokarst bogs, channel fens, and shallow ponds. Ongoing and accelerating permafrost thaw, leading to the transition of peat plateaus into thermokarst bogs, fens and ponds has been documented at all sites (Chasmer & Hopkinson, 2017; Gibson et al., 2018; Heffernan et al., 2020; Holloway & Lewkowicz, 2020; Kuhn, Thompson, et al., 2021; Pelletier et al., 2017).

At each site, we established sampling transects (20-30 m in length) perpendicular to the peat plateau-thermokarst bog transition. Four distinct peatland stages were included: undisturbed permafrost peat plateau (Peat Plateau), thawing peat plateau edge (Plateau Edge), young thermokarst bogs adjacent to the plateau edge (Young Bog), and mature thermokarst bogs (Mature Bog) (Figures 2.1 and A2.1). The vegetation composition of the peat plateaus at all three sites was comprised of stunted, open canopy of black spruce (*Picea mariana*), low woody shrubs (*Vaccinium vitis-idaea*, *Rhododendron groenlandicum*, *Vaccinium uliginosum*), and a ground cover of lichens (*Cladonia* spp.) and occasional hummocks (*Sphagnum fuscum*, *Sphagnum magellanicum*). The Plateau Edge was found only in a narrow transition (~2-4 m) between the Peat Plateau into Young Bog stage (Figures 2.1b, 2.1d) and had the same vegetation composition as the Peat Plateau, but some black spruce trees were tilted ('drunken trees') or showed evidence of stress from waterlogging. The Young Bog stage was the wettest stage, dominated by

Sphagnum riparium and rannock rush (*Scheuchzeria palustris*), while the drier Mature Bog stage was dominated by *Sphagnum fuscum* and *Sphagnum magellanicum*, bog-rosemary (*Andromeda polifolia*), leatherleaf (*Chamaedaphne calyculata*), and hare's-tail cottongrass (*Eriophorum vaginatum*). Radiocarbon analysis at Lutose and Scotty Creek has dated the time since permafrost thaw to be 30-90 years for Young Bog and ~200-550 years for Mature Bog stages (Heffernan et al., 2020; Pelletier et al., 2017).

Two burned peat plateaus were also included in the study, both located <10 km from the Lutose peatland complex. One of the sites burned in 2007 (2007 Burn) and has previously been studied (Estop-Aragonés et al., 2018; Gibson et al., 2018, 2019), and the other burned in 2019 (2019 Burn), i.e., these sites burned 12 and <1 years prior to the study, respectively. The 2019 Burn had very limited vegetation regrowth and was largely covered by char and singed *Sphagnum fuscum* hummocks. The 2007 Burn had a dense shrub layer of Labrador tea (*Rhododendron groenlandicum*) and regrowth of <1 m tall black spruce. Wildfire changes the soil thermal regime of peat plateaus with ~60% deeper active layers (Gibson et al., 2018) and higher soil temperatures than unburned peat plateaus (Gibson et al., 2019); effects that last for up to 30 years (Gibson et al., 2018).

We also studied five peatland ponds (Figure A2.2), three at Lutose (L1, L2, and L4) and two at Smith Creek (W1 and W2), all of which have been part of previous studies (Kuhn et al., 2021; L. Thompson et al., 2023). All pond depths ranged from 0.5 to 2.5 m and were between 0.5 and 5 ha in area. Ongoing thermokarst expansion affected W1 and L1, as indicated by submerged and tilted black spruce trees. Ponds W2, L2, and L4 had no visible evidence of thermokarst expansion. The surroundings of pond L2 were burned in 2007 and L2 was the only pond with a beaver lodge. All ponds had thick organic sediments, up to 4 m depth above the underlying mineral sediment (Kuhn et al., 2022).

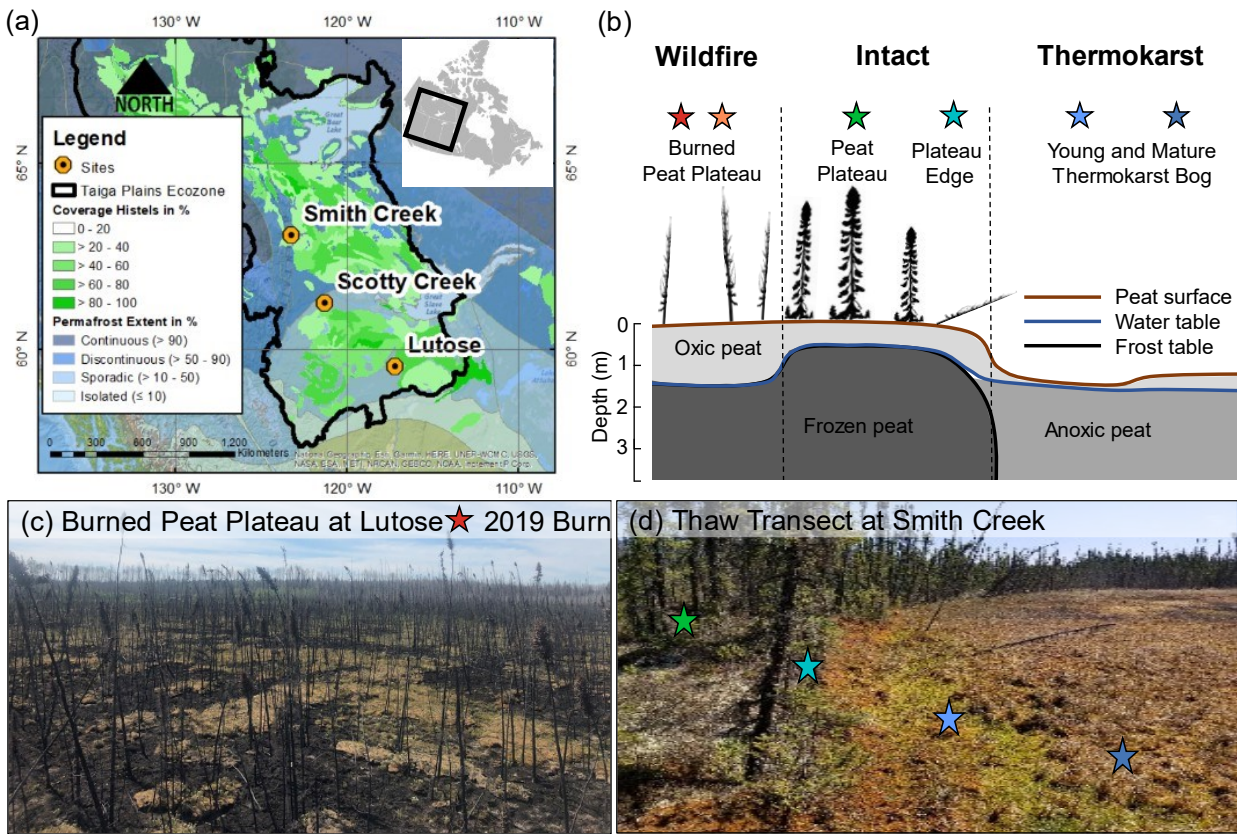


Figure 2.1: (a) Map of study region including permafrost zones (Obu et al., 2019) and distribution of histel soils, i.e., peat soils affected by permafrost (Hugelius et al., 2013) within the Taiga Plains ecozone (Marshall et al., 1999). (b) Peatland disturbances in relation to peatland stages; adapted from Estop-Aragonés et al. (2018). The stars in different colors represent the sampled peatland stages: each peatland stage had a minimum of four replicate collars per site, and the burned stages had eight collars each. Photos of the (c) 2019 Burn at Lutose, and (d) the Smith Creek thermokarst transect with the four corresponding peatland stages indicated.

2.2.2 Greenhouse Gas Flux Measurements

Boardwalks were installed at each site to reduce trampling and minimize ebullitive GHG emissions. Plot-scale fluxes of N_2O , CH_4 , and CO_2 were measured using the static chamber technique (Crill, 1991; Norman et al., 1997; Subke et al., 2021). Flux measurements at Lutose and Smith Creek were made once per month between April and October in 2019 (seven sampling dates at Lutose, six at Smith Creek). At Scotty Creek, measurements were made only once in September 2018 and used different equipment described in Appendix A2.1. The chambers were opaque and the chamber-based flux measurements included ground cover and low-stature vegetation, but excluded the trees present in the peat plateaus; therefore, CO_2 fluxes are thereafter referred to as soil respiration. Circular PVC collars (0.12 m^2) were inserted into the

ground to a depth of 10 cm at least 24 hours prior to the first flux measurement and in few meters distance to the next collar. Each peatland stage was sampled at four collars. To create an adequate seal, each collar had a ring-formed edge filled with water before placing the chamber in the collar. We used chambers with heights of 19 or 38 cm (22.4 L and 44.7 L, respectively). Vegetation height and distance between the collar ring and peat surface were measured for each sampling occasion to account for different chamber volumes. Gas samples (20 mL) were extracted from chambers 5, 10, 15, 30, and 60 min after chamber closure and were subsequently transferred into pre-evacuated 12 mL glass vials (Labco, Lampeter, Wales, United Kingdom). Air temperature in the chambers was monitored during closure using outdoor thermometers with remote sensors (Bios Thermor, Newmarket, ON). A total of 290 chamber flux measurements from peat surfaces were conducted.

GHG concentrations from aquatic surfaces were taken from opaque floating chambers (0.06 m², 13.6 L). The floating chambers were deployed in replicates of four along the edges of the ponds (~1 m from the edge, avoiding the release of artificial bubbles from the sediment) and both chamber outlets were closed after pressure had equilibrated. We concentrated the floating chambers on the shorelines where active thermokarst was visible for the two thermokarst-affected ponds, L1 and W1. Gas sample collection from ponds followed the same protocols as the soil chambers. The calculated pond GHG fluxes were considered to represent total emissions (i.e., the sum of diffusive and ebullitive emissions). We collected a total of 86 chamber flux measurements from pond surfaces.

Gas samples from Smith Creek and Lutose (including pond gas samples) were analyzed at the University of Alberta, Edmonton, for N₂O, CH₄, and CO₂ concentrations on a Varian Model 3800 gas chromatography with a Combi-Pal autosampler (CTC Analytics AG, Zwingen, Switzerland) and an electron capture detector (Varian Inc., Walnut Creek, CA). The instruments' minimum gas concentration detection limits were 0.010 parts per million (ppm) for N₂O, 0.085 ppm for CH₄, and 8.846 ppm for CO₂ (Roman-Perez et al., 2021). Calibration curves were established using at least five standard gases, ranging from 0.25 to 9.77 ppm for N₂O, from 0.83 to 7.99 ppm for CH₄, and from 282 to 10,099 ppm for CO₂ (Roman-Perez et al., 2021). The changes in gas concentrations over time were used to calculate peatland stage and pond GHG fluxes. Each time-series of five gas concentrations were inspected for outliers. For series with

one or two outliers, these specific data points were removed prior to calculating fluxes. Series with more than two outliers were removed completely (18 fluxes). Fluxes were calculated using the method suggested by Hüppi et al. (2018), implemented in the R computing environment (R Core Team, 2020) package ‘gasfluxes’ (Fuß, 2017). Air pressure used in the calculations was retrieved from nearby weather stations (Environment and Climate Change Canada, 2020).

We calculated the SGWP and SGCP of both N₂O and CH₄ fluxes according to Neubauer & Megonigal (2019), i.e., we multiplied both CH₄ fluxes and N₂O fluxes by their corresponding 100-year time span factors 45 and 270, respectively (both emission and uptake). In this way, we obtained comparable GHG fluxes expressed in CO₂-equivalents m⁻² d⁻¹.

2.2.3 Environmental and Soil Data

Frost table, water table, soil moisture, and soil temperature were measured at each collar at each sampling occasion. Frost table position was measured with a 150 cm long probe inserted into the ground until it undoubtedly hit the frozen ground. The water table position was measured in pre-installed 5 mm diameter stilling wells with a blowing tube. Near-surface soil moisture (0-10 cm) was measured with a portable probe (Delta-T HH2, Delta, Cambridge, United Kingdom), averaging five readings around each collar for each occasion. Soil temperature was measured at 5, 10, 20, and 40 cm depths with handheld thermometers (Thermoworks, American Fork, UT). In addition, we inserted soil temperature loggers (Pendant HoboProV2, Onset Corp., Bourne, MA) at 5, 20, and 40 cm depths at one location in each stage. These temperature loggers were installed for a whole year and collected hourly temperature data to describe the soil temperature regimes.

Peat bulk densities (BD) and carbon-to-nitrogen ratios were determined for near-surface (0-20 cm) peat at each stage. We collected triplicate peat samples (est. volume of 200 cm³ pieces taken at 0-5, 5-10, and 10-20 cm depth using a bread knife to cut same-sized chunks) from each peatland stage. The peat samples were weighed both when wet and dried (65°C for over 48 hours) to establish soil water content and BD. According to Carter & Gregorich (2007), water-filled pore space (WFPS) was calculated from volumetric water content and BD, and C and N contents were determined by dry combustion with an elemental analyzer (Thermo Finnigan Flash EA 1112 Series, San Jose, CA).

2.2.4 Porewater Chemistry

Porewater was collected from each peatland stage at Lutose and Smith Creek during the monthly occasions using MacroRhizon samplers with a 0.15 μm pore size (Rhizosphere Research, Wageningen, the Netherlands). The MacroRhizon samplers were inserted to yield porewater at 0-10 cm depth. Porewater samples were collected into two 60 mL acid-washed amber bottles, where one sample was acidified in the field with 0.2 mL 2M HCl. The unacidified sample was analyzed for concentrations of NH_4^+ , NO_3^- , and phosphate (PO_4^{3-}) using a Thermo Scientific Gallery Beermaster Plus Photometric Analyzer (Thermo Fisher Scientific, Waltham, MA), while the acidified samples were analyzed for non-purgeable organic carbon (NPOC) and total dissolved nitrogen (TDN) concentrations using a Shimadzu TOC-L CHP Analyzer (Shimadzu Corporation, Kyoto, Japan). Trace element concentrations including, amongst others, iron (Fe) and copper (Cu) were determined by ICP-OES (iCAP6300 Duo, Thermo Fisher Scientific, Waltham, MA). Pond surface water samples were collected, filtered using a 0.7 μm pore size GF/F filter, and then handled and analyzed in the same way as the porewater samples. The electrical conductivity (EC) and pH of porewater and pond water samples were measured on-site with calibrated PT1 and PT2 Ultrapens (Myron L Company, Carlsbad, CA).

Soil nutrient supply rates were estimated using Plant Root Simulator (PRS) probes (Western AG Innovations, Saskatoon, SK) at Smith Creek and Lutose at each collar. The PRS probes hold ion exchange resins which exchange ions at a rate that depends on the ion activity and diffusion in soils, thus integrating physical, chemical, and biological factors to provide an in-situ relative measure of nutrient supply (Sharifi et al., 2009; M. Wang et al., 2018; Western Ag Innovations, 2000). Paired sets of PRS probes encompassing both cations and anions were inserted at 5 cm depth into the peat adjacent to each flux collar. All PRS probe samplers were kept installed over 40 days, starting mid-July 2019. After rinsing with distilled water, the PRS probes were shipped to and analyzed by Western AG Innovations for supply rates of NH_4^+ -N and NO_3^- -N, and PO_4^{3-} -P as well as other ions.

2.2.5 Soil Gas Concentration Profiles

Soil gas concentration profiles were measured once at all sites. We sampled near the end of the growing season, on 13 September 2018 at Scotty Creek, 19 August 2019 at Lutose, and 26

August 2019 at Smith Creek. We extracted soil gases using vertical metal soil gas probes, with samples from 2, 5, 10, and 20 cm following Marushchak et al. (2021). Each peatland stage had five replicates of depth profiles. In the moist, anoxic peatland stages with the water table near the surface, there was often porewater instead of gas in the attached 35 mL syringe, which was then shaken for one minute to equilibrate the gas concentration of 7 mL porewater with the remaining 28 mL headspace gas. Distributed over the day and different peatland stages, we also took ambient air samples. All gas samples were stored in 12 mL glass vials (Labco, Lampeter, Wales) and analyzed in the same way as the gas samples from Scotty Creek, outlined in A.2.1.

2.2.6 Statistical Analyses

All statistical analyses were done using the R computing environment (R Core Team, 2020). Linear regressions were done to relate peatland fluxes of N₂O, CH₄, and CO₂ to soil temperature at 5 or 40 cm, and to growing season averages of WFPS using ‘stat_cor’ function in R. To assess for differences between sites and peatland stages, we first averaged measurements of GHG fluxes for each collar over the growing season. Data from Scotty Creek was not included in further analysis since we only had one sampling occasion in September 2018. We then checked the data distribution of nutrient concentrations, supply rates, and fluxes of N₂O, CH₄, and CO₂ for normality with the Shapiro-Wilk test using the ‘rstatix’ package (Kassambara, 2021). Next, we ran a two-way ANOVA assessing differences in nutrient concentrations, nutrient supply rates, and GHG fluxes among sites (Lutose and Smith Creek) and among peatland stages (Peat Plateau, Plateau Edge, Young Bog, and Mature Bog), including their interactions. The 2019 Burn and 2007 Burn data was not included in the two-way ANOVA since no burned site was present at the Smith Creek site. In most cases there was no influence of site, and we therefore combined data from peatland stages (Peat Plateau, Plateau Edge, Young Bog, Mature Bog) at Smith Creek and Lutose along with data from the 2019 Burn and 2007 Burn stages into a one-way ANOVA, using the ‘rstatix’ package (Kassambara, 2021). Lastly, to test for differences based on type of disturbance, we ran a one-way ANOVA to test for differences between the intact peat plateau stages (Peat Plateau and Plateau Edge combined), the thermokarst bog stages (Mature Bog and Young Bog combined) and the burned peat plateau stages (2019 Burn and 2007 Burn combined). Combining peatland stages was justified by their similar soil environmental conditions and vegetation composition within the three combined groups.

2.3 Results

2.3.1 Environmental Conditions

There was a consistent order in BD across the three sites with the highest BDs in Peat Plateaus and the lowest in Young Bogs (Table 2.1). Soil temperature, water table position, and WFPS also had consistent order across sites over the growing season, with the warmest and wettest conditions in Young Bogs, followed by Mature Bogs, Plateau Edges, and driest and coolest soils in Peat Plateaus. The 2019 Burn and 2007 Burn had warmer soils than unburned Peat Plateaus (Figure A2.3). The more southern Lutose site generally had warmer soils than the more northern Smith Creek site. The exception was the Mature Bog, which was wetter and warmer at Smith Creek than at Lutose (Table 2.1). The three peatland complexes had acidic soils with pH between 3.95 and 5.46, with no consistent pattern along the thaw transects. The peatland ponds all had pH between 7.4 and 7.9, but concentrations of nutrients varied greatly among ponds (Table 2.1).

Table 2.1: Peatland Stage Properties and Growing Season Environmental Characteristics

Site and peatland stage	pH ^a	Bulk density ^b [g cm ⁻³]	WFPS ^a [%]	Water table depth ^a [cm]	Active layer ^c [cm]	Soil temperature ^a [°C]		
						5 cm	20 cm	40 cm
<i>Lutose</i>								
2019 Burn	4.10 ± 0.30 ^d	0.07	16 ± 4 ^d	29 ± 19 ^d	74	12.2 ^d	5.6 ^d	2.5 ^d
2007 Burn	4.75 ± 0.61	NA	26 ± 16	51 ± 13	107	10.6	5.3	4.0
Peat Plateau	4.63 ± 0.91	0.06	19 ± 5	>40	77	10.3	4.3	1.9
Plateau Edge	3.95 ± 0.06	0.08	25 ± 7	27 ± 10	>150	10.4	5.5	6.0
Young Bog	4.85 ± 0.34	0.02	85 ± 22	7 ± 6	--	11.8	10.0	9.9
Mature Bog	4.91 ± 1.25	0.05	22 ± 8	24 ± 12	--	10.7	6.9	7.4
<i>Scotty Creek</i>								
Peat Plateau	4.39 ^e	0.11 ^f	10 ^g	NA	68 ^g	NA	NA	NA
Plateau Edge	NA	0.11 ^f	29 ^g	NA	65 ^g	NA	NA	NA
Young Bog	NA	0.03 ^f	66 ^g	NA	--	NA	NA	NA
Mature Bog	4.79 ^e	0.05 ^f	60 ^g	NA	--	NA	NA	NA
<i>Smith Creek</i>								
Peat Plateau	5.46 ± 1.92	0.06	19 ± 15	21 ± 14	47	8.2	2.2	0.0

Plateau Edge	4.79 ± 0.30	0.09	40 ± 29	11 ± 5	66	8.0	3.6	1.5
Young Bog	4.34 ± 0.62	0.02	100 ± 0	0 ± 1	--	10.1	7.4	5.2
Mature Bog	4.49 ± 0.80	0.04	79 ± 15	5 ± 4	--	12.8	9.6	8.2

Note. There is no active layer in both permafrost-free bog stages (= --). NA = No data available.

^aGrowing season averages (mean ± standard deviation) of pH, water-filled pore space (WFPS), water table depth, and soil temperatures are based on measurements done during each sampling occasion.

^bBulk densities are averaged for 0-10 cm depth to allow comparison between different sites/approaches.

^cActive layer depth is the average of at least four frost table measurements in September/October.

^dMonthly measurements at 2019 Burn only started in July 2019

^eL. Thompson et al. (2022).

^fPelletier et al. (2017).

^gMeasured only in September 2018.

2.3.2 Porewater Nutrient Concentrations and Supply Rates

Concentrations of NO_3^- , NH_4^+ , and PO_4^{3-} in porewater were highly variable and had only a few consistent trends among peatland sites or peatland stages (Figures 2.2a, 2.2c, 2.2e) (Complete ANOVA results in Tables A2.2, A2.3). Concentrations of NO_3^- were around two times higher at Lutose than at Smith Creek (two-way ANOVA, $F_{1,33} = 7.02$; $p < 0.05$), but there were no differences between peatland stages ($F_{3,33} = 1.53$; $p = 0.23$). Concentrations of NH_4^+ did not vary among sites ($F_{1,33} = 3.37$; $p = 0.08$) or peatland stages ($F_{3,33} = 0.43$; $p = 0.73$). Concentrations of PO_4^{3-} did not vary between sites ($F_{1,33} = 2.01$; $p = 0.17$), but among peatland stages ($F_{3,33} = 5.10$; $p < 0.01$). A one-way ANOVA showed that burned stages had 12 to 25 times higher PO_4^{3-} than intact and thermokarst stages ($F_{2,47} = 10.62$; Tukey HSD $p < 0.001$).

Supply rates of NO_3^- , NH_4^+ , and P did not differ between the Lutose and Smith Creek sites, and only differed for a few peatland stages (Figures 2.2b, 2.2d, 2.2f) (Tables A2.2, A2.3). Nutrient supply rates of NO_3^- varied between peatland stages ($F_{3,24} = 4.48$; $p = 0.012$) with lower rates for Young Bogs than Mature Bogs and Plateau Edges. No differences among peatland stages were found for supply rates of NH_4^+ ($F_{3,24} = 4.48$; $p = 0.012$), but we note the high supply rates for the Young Bog at Lutose and the Mature Bog at Smith Creek which both were fully saturated for much of the growing season. A one-way ANOVA showed that burned stages had higher supply rates of P than either the intact permafrost stages and thermokarst stages ($F_{3,39} = 5.30$; $p = 0.009$).

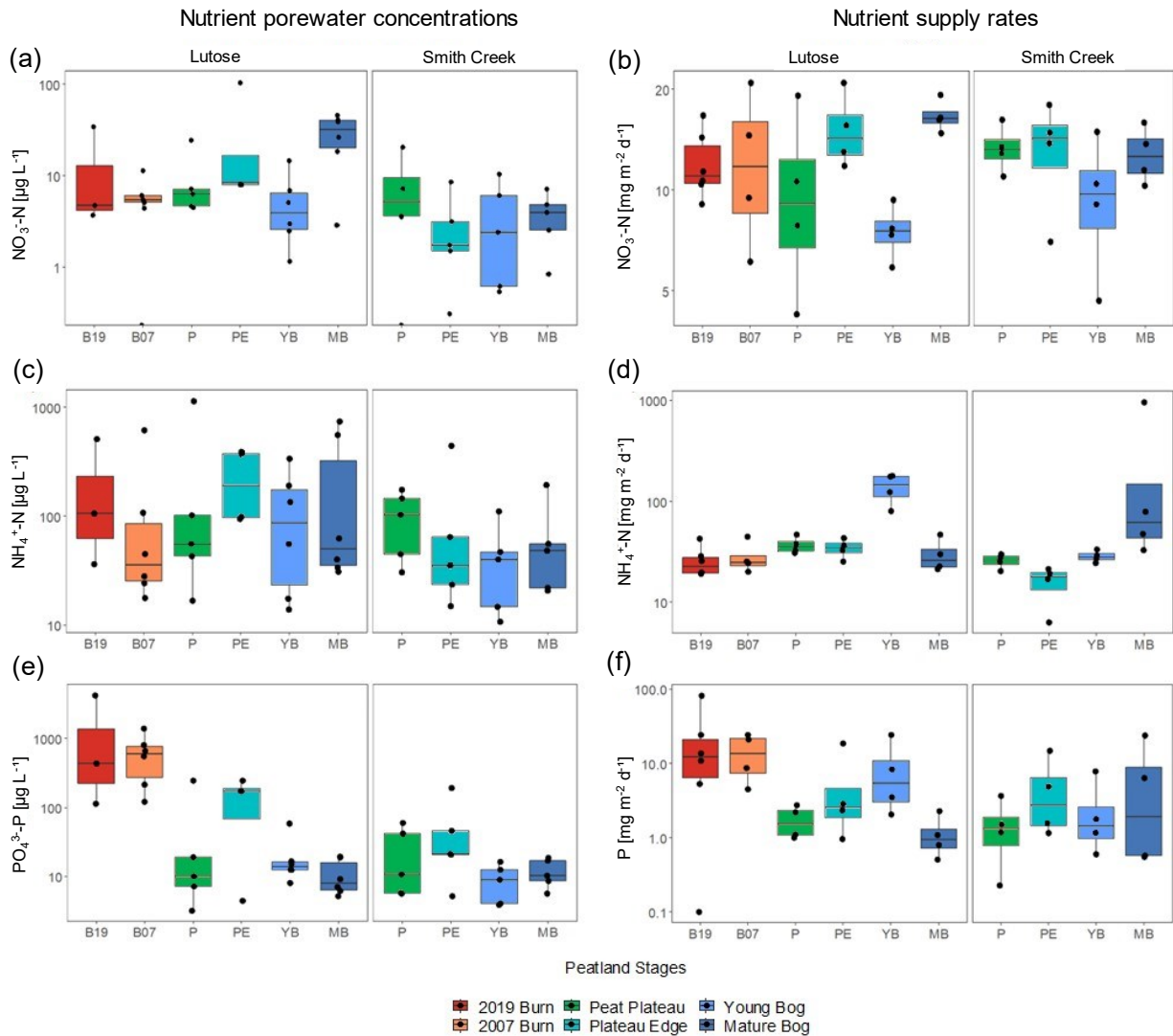


Figure 2.2: Porewater concentrations and supply rates of (a, b) nitrate (NO_3^-), (c, d) ammonium (NH_4^+), and (e) phosphate (PO_4^{3-}) and (f) phosphorus (P) across all peatland stages, i.e., 2019 Burn (B19), 2007 Burn (B07), Peat Plateau (P), Plateau Edge (PE), Young Bog (YB), and Mature Bog (MB) at Lutose and Smith Creek. Measurements were collected over the 2019 growing season. Note the logarithmic scale of all y-axes.

2.3.3 Soil Gas Concentrations

Concentrations of N_2O below the water table were lower than ambient atmospheric N_2O concentrations in all Young Bog and Mature Bog profiles (Figure 2.3a). We observed a decreasing gradient in N_2O concentrations with depth below the water table, while the drier profiles had lesser and more gradual decreases. Out of 60 soil gas concentration profiles, only two Peat Plateau profiles had N_2O concentrations higher than ambient at 20 cm depth (Figure 2.3a). In contrast to N_2O , CH_4 concentrations in the Young Bog and Mature Bog increased with

depth, especially below the water table, and ranged from ambient concentrations at 2 ppm to 30,000 ppm (Figure 2.3b). Under oxic conditions in the peat plateaus, CH₄ concentrations declined with depth to a minimum of 1.5 ppm CH₄. Only a few Peat Plateau and Plateau Edge profiles had elevated CH₄ concentrations, associated with wetter locations. The CO₂ concentrations had similar patterns as CH₄ concentrations in wet sites, with increasing concentrations up to 180,000 ppm below the water table (Figure 2.3c). In contrast to CH₄, CO₂ increased with depth also above the water table, e.g., in dry Peat Plateaus, and CO₂ concentrations were never below ambient.

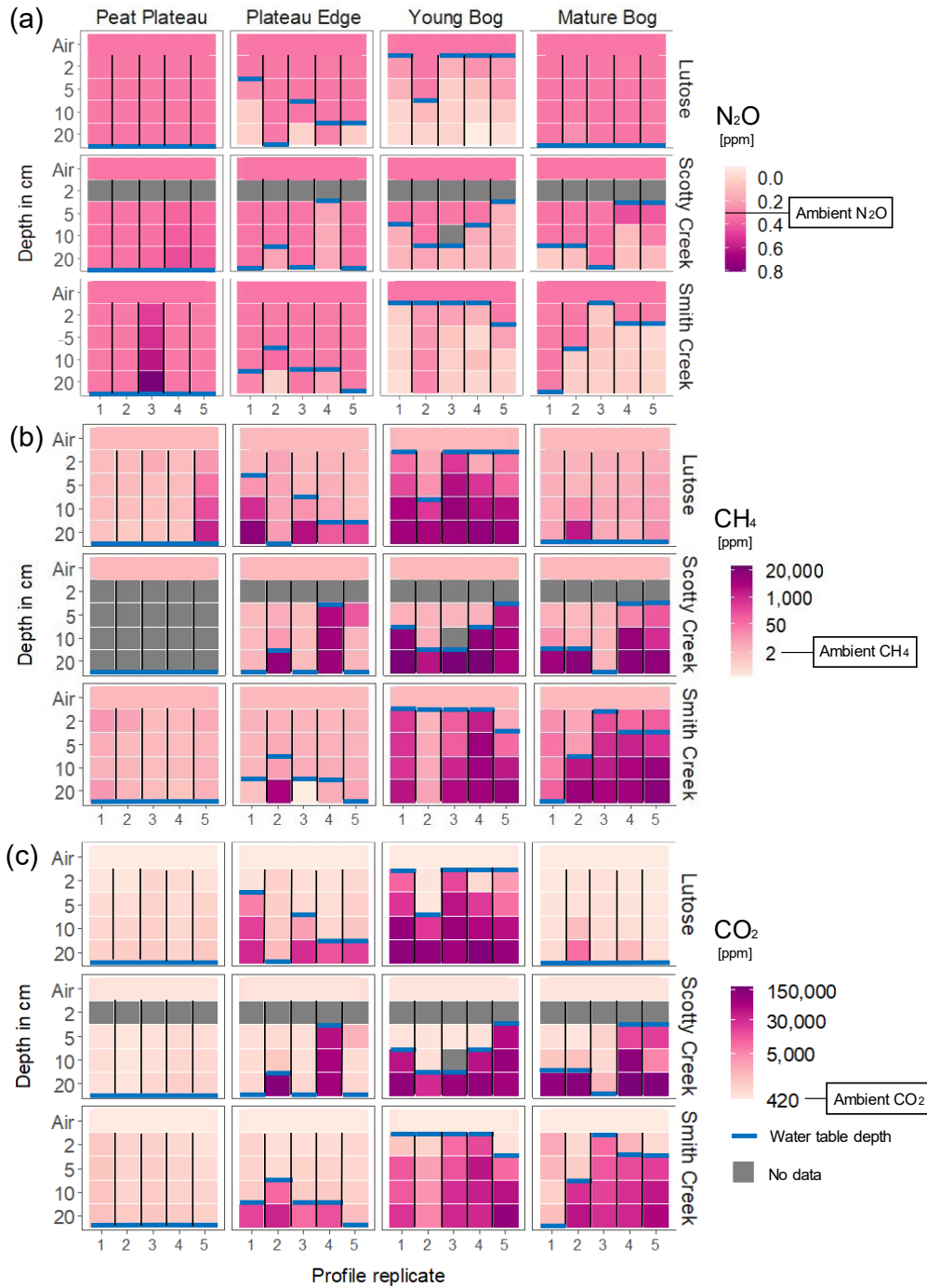


Figure 2.3: Soil gas concentrations of (a) nitrous oxide (N₂O), (b) methane (CH₄), and (c) carbon dioxide (CO₂) for Peat Plateau, Plateau Edge, Young Bog, and Mature Bog depth profiles from three peatland sites (Lutose, Scotty Creek, and Smith Creek). Measurements were done at the end of the growing season, in September 2018 at Scotty Creek and in August 2019 at Lutose and Smith Creek. Water table position is shown for every soil profile, indicated to be above or below the gas sampling depths (2, 5, 10, and 20 cm). Note the logarithmic scale for the CH₄ and CO₂ soil gas concentrations.

2.3.4 Greenhouse Gas Fluxes

There were no differences in N₂O, CH₄ or CO₂ (soil respiration) fluxes between the Lutose and Smith Creek sites when comparing peatland stages present at both sites; Peat Plateau, Plateau Edge, Young Bog, and Mature Bog (Figure 2.4, two-way ANOVA results in Table A2.4). Average growing season N₂O uptake was greatest from the combined thermokarst bog stages (Mature Bog and Young Bog, -0.054 mg N₂O m⁻² d⁻¹), followed by the peat plateau stages (Peat Plateau and Plateau Edge, -0.025 mg N₂O m⁻² d⁻¹), and least for the burned peat plateau stages (2019 Burn and 2007 Burn, -0.003 mg N₂O m⁻² d⁻¹) (one-way ANOVA, $F_{2,45} = 15.1$; $p < 0.001$, Table A2.5). Fluxes from Scotty Creek were not included in statistical analysis since measurements were only done once in September 2018, but we noted some distinct patterns – including N₂O emissions rather than N₂O uptake from the Peat Plateau and Plateau Edge (Figure 2.4a). Uptake of N₂O increased significantly with higher soil temperature at 5 cm depth in the Peat Plateau and Plateau Edge (Figure 2.4b), leading to a seasonal trend of highest uptake in July and August. The influence of soil temperature on N₂O uptake was weaker for Mature Bog and Young Bog and absent at the 2019 Burn and 2007 Burn stages (Figure 2.4b). Seasonal average N₂O uptake was greater from collars with higher near-surface WFPS (Figure 2.5). This trend was present but non-significant within each peatland stage, but significant ($R^2 = 0.24$, $p < 0.001$) when assessed across all collars from all peatland stages.

Emissions of CH₄ were highest from the thermokarst bog stages, where emissions generally increased with higher soil temperatures at 40 cm (Figure 2.4d). Average growing season CH₄ emissions were greatest from the thermokarst bog stages (Mature Bog and Young Bog, 34 and 31 mg CH₄ m⁻² d⁻¹, respectively), while there was no significant difference between the intact peat plateau (Peat Plateau and Plateau Edge, -0.07 and 10.3 mg CH₄ m⁻² d⁻¹, respectively) and burned peat plateau stages (2019 Burn and 2007 Burn, 3.2 and -0.54 mg CH₄ m⁻² d⁻¹, respectively) (one-way ANOVA, $F_{2,45} = 15.1$; $p < 0.001$, Table A2.5). The ranking of average CH₄ emissions among stages closely followed the average water table position (Table 2.1). Emissions of CH₄ from Scotty Creek were not included in the analysis but had a similar pattern.

Soil respiration (dark chamber CO₂ fluxes) had a strong seasonal trend linked to soil temperature at 5 cm at all peatland stages, except at the 2019 Burn stage (Figure 2.4f). The 2019 Burn stage also had the lowest average growing season soil respiration (1,200 mg CO₂ m⁻² d⁻¹), while the

2007 Burn ($3,400 \text{ mg CO}_2 \text{ m}^{-2} \text{ d}^{-1}$) was not different from either the peat plateau stages (Peat Plateau and Plateau Edge, $3,900$ and $4,100 \text{ mg CO}_2 \text{ m}^{-2} \text{ d}^{-1}$, respectively) or the thermokarst bog stages (Mature Bog and Young Bog, $5,200$ and $3,300 \text{ mg CO}_2 \text{ m}^{-2} \text{ d}^{-1}$, respectively) (one-way ANOVA, $F_{5,42} = 3.79$; $p = 0.006$, Table A2.5).

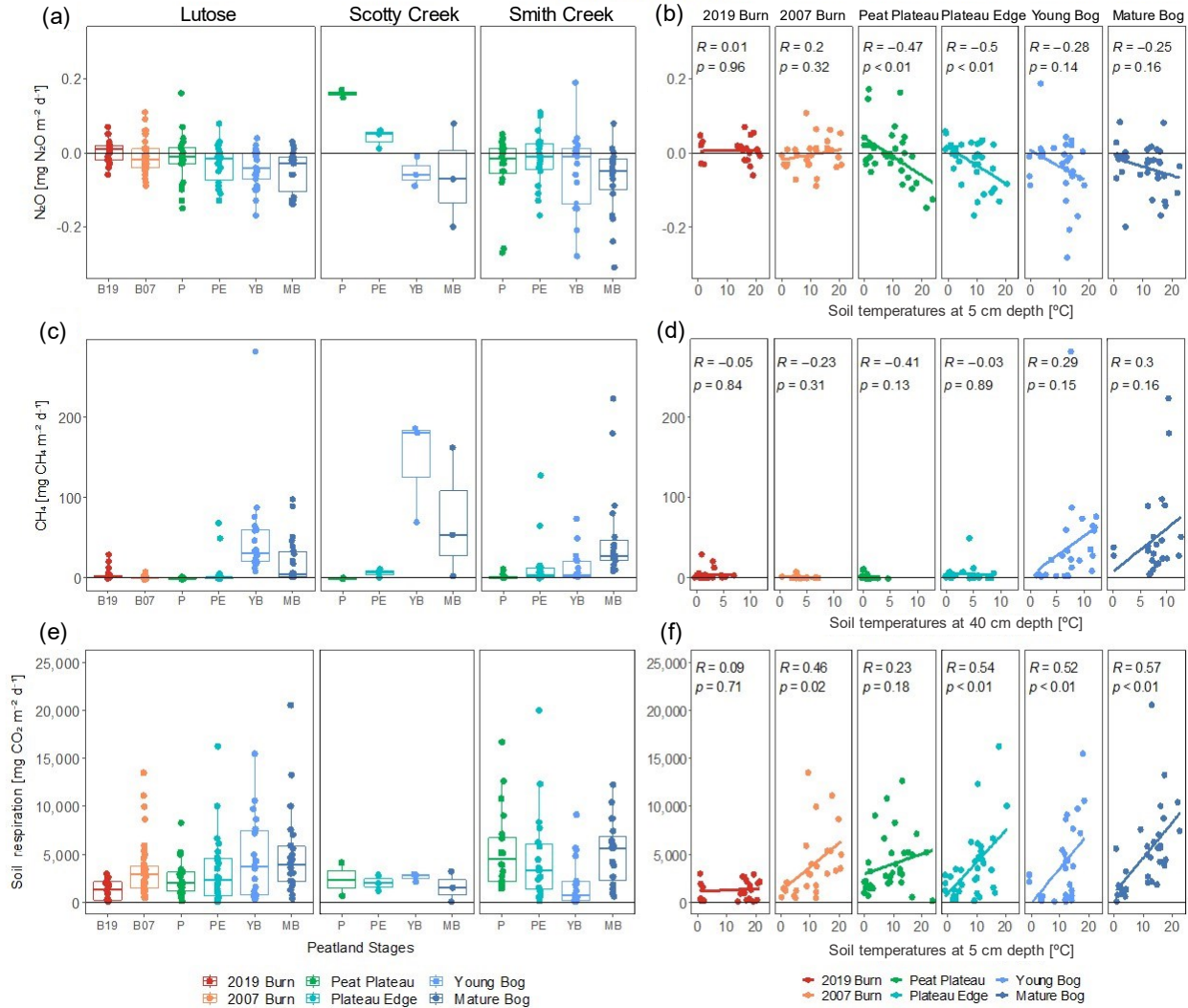


Figure 2.4: Fluxes and temperature dependency of (a, b) nitrous oxide (N₂O), (c, d) methane (CH₄), and (e, f) soil respiration (CO₂) from peatland stages, that is, 2019 Burn (B19), 2007 Burn (B07), Peat Plateau (P), Plateau Edge (PE), Young Bog (YB), and Mature Bog (MB), at three sites (Lutose, Scotty Creek, and Smith Creek). Each symbol is an individual flux measurement, collected monthly throughout the growing season from April to October 2019 from Lutose (n = 7) and Smith Creek (n = 6), but only once in September 2018 at Scotty Creek. Linear regressions use data from all three sites and show the relationship between soil temperature at 5 cm and N₂O and soil respiration, while the temperature at 40 cm is used for CH₄ fluxes.

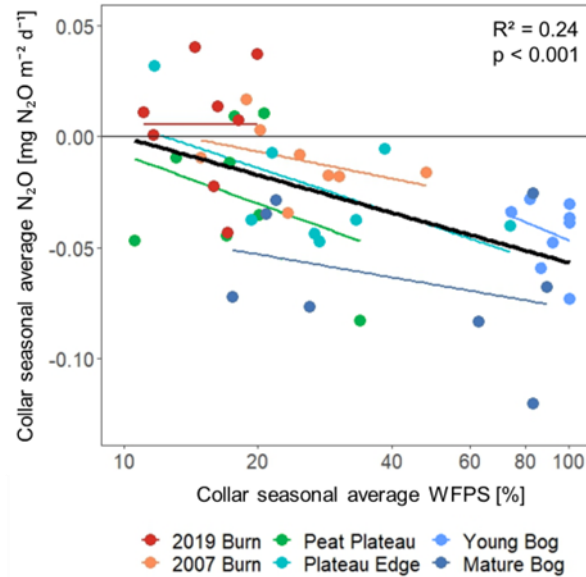


Figure 2.5: Relationship between nitrous oxide (N_2O) fluxes and near-surface soil water-filled pore space (WFPS). Each symbol represents the growing season average N_2O flux and WFPS for individual collars located in different peatland stages, including burned peat plateaus (2019 Burn, 2007 Burn) along with Peat Plateau, Plateau Edge, Young Bog, and Mature Bog. Note the logarithmic scale for the WFPS. Logarithmic regressions are shown for each of the six peatland stages (colored lines, $p > 0.05$), and for the combined data (black line, $p < 0.001$).

2.3.5 N_2O Fluxes from Peatlands Ponds

Four out of five ponds had N_2O uptake, with average rates similar to the peatland stages ($-0.018 mg N_2O m^{-2} d^{-1}$), and no difference between ponds with stable edges and active thermokarst expansion (Figure 2.6). Pond L2 had high average N_2O emissions ($0.30 mg N_2O m^{-2} d^{-1}$), and emissions could reach up to $1.00 mg N_2O m^{-2} d^{-1}$. Ponds near Lutose generally had higher EC, NPOC, TDN, and inorganic nutrients compared to ponds near Smith Creek (Table 2.2). Whether ponds had stable edges or actively thermokarst expansion did not have consistent influences on water chemistry. The L2 pond near Lutose, affected by beaver activity and within a 2007 wildfire, had the highest PO_4^{3-} and the highest ratio between NO_3^- and NH_4^+ (Table 2.2).

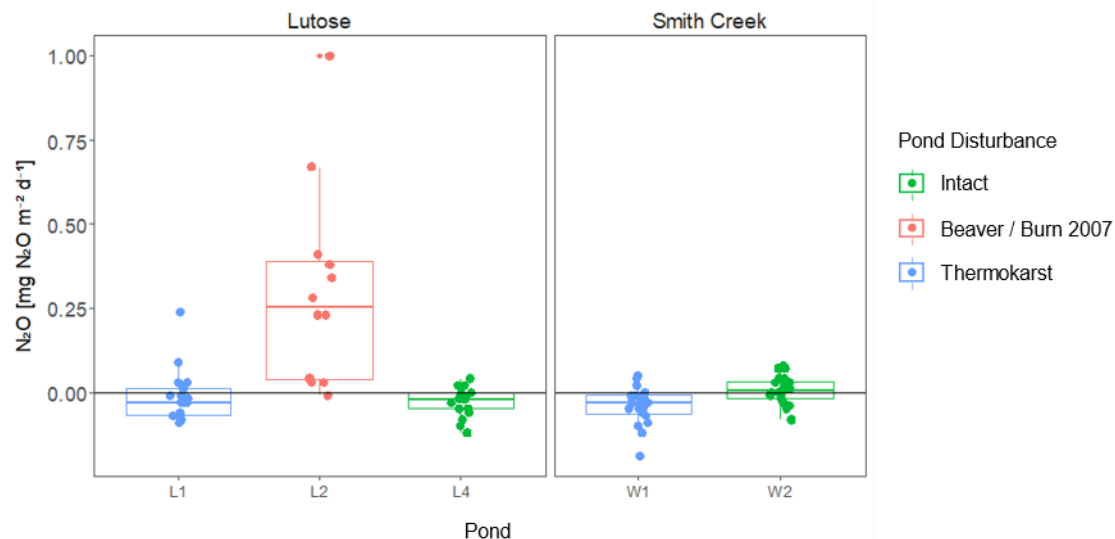


Figure 2.6: Nitrous oxide (N_2O) fluxes from five peatland ponds. Flux measurements were done on six occasions between May and October 2019 for all sites except pond L2 which was visited three times between July and October 2019.

Table 2.2: Peatland pond characteristics

Site and peatland pond	pH	EC [$\mu\text{S cm}^{-1}$]	Fe ^a [mg L^{-1}]	NPOC [mg L^{-1}]	TDN [mg L^{-1}]	Nutrient concentrations [$\mu\text{g L}^{-1}$]		
						NO_3^-	NH_4^+	PO_4^{3-}
<i>Lutose</i>								
L1 ^b	7.89 ± 0.97	366 ± 93	0.1	48.3 ± 15.5	3.04 ± 1.39	25 ± 36	984 ± 1239	126 ± 163
L2 ^c	7.54 ± 0.06^d	144 ± 5^d	1.3^d	44.2 ± 1.4^d	1.41 ± 0.27^d	129 ± 139^d	97.7 ± 29.7^d	195 ± 109^d
L4	7.43 ± 0.94	660 ± 87	0.1	41.3 ± 9.0	2.06 ± 0.56	3.2 ± 2.4	226 ± 323	8.5 ± 7.1
<i>Smith Creek</i>								
W1 ^b	7.27 ± 0.89	111 ± 17	<0.001	18.8 ± 1.7	0.83 ± 0.14	6.3 ± 9.4	50.7 ± 37.7	5.3 ± 1.9
W2	7.20 ± 0.50	90 ± 22	0.1	18.6 ± 1.5	0.88 ± 0.19	7.0 ± 7.7	78.2 ± 85.7	4.5 ± 0.8

Note. Growing season averages (mean \pm standard deviation) of pH, electrical conductivity (EC), Total dissolved nitrogen (TDN), non-purgeable organic carbon (NPOC), nitrate (NO_3^-), ammonium (NH_4^+), and phosphate (PO_4^{3-}) are based on monthly measurements between May and September/October 2019.

^aConcentrations of iron (Fe) were only measured once in 2019.

^bFloating chambers placed at actively expanding thermokarst edges.

^cSituated in 2007 Burn fire scar and beaver activity.

^dMonthly measurements at L2 only started in July 2019.

2.3.6 Impact of Wildfire and Permafrost Thaw on the Net Radiative Balance

We used SGCP and SGWP to assess impacts on the net radiative balance from shifts in CO₂, CH₄, and N₂O fluxes due to wildfire and permafrost thaw (Figure 2.7). The CO₂ fluxes we report only represent soil respiration, and not the full net ecosystem exchange, and can thus not be directly compared to the shifts in CH₄ and N₂O fluxes. Comparing the burned peat plateau stages (2019 Burn and 2007 Burn) with Peat Plateau and Plateau Edge, we found that wildfire led to reduced uptake of N₂O representing +5.9 mg CO₂-eq. m⁻² d⁻¹ (emissions). The reduction of soil respiration between the 2019 Burn and the intact counterpart was -2,700 mg CO₂ m⁻² d⁻¹ but does not represent the full CO₂ balance. Comparing the thermokarst bog stages (Mature Bog and Young Bog) with Peat Plateaus and Plateau Edges, we found that thermokarst led to increased N₂O uptake representing -7.8 mg CO₂-eq. m⁻² d⁻¹ (uptake), while a shift from minor to large CH₄ emissions represented +1,200 mg CO₂-eq. m⁻² d⁻¹ (emissions). Hence, the influence of greater N₂O uptake offset less than 1% of the increased CH₄ emissions following thermokarst bog development, when estimated as CO₂-eq.

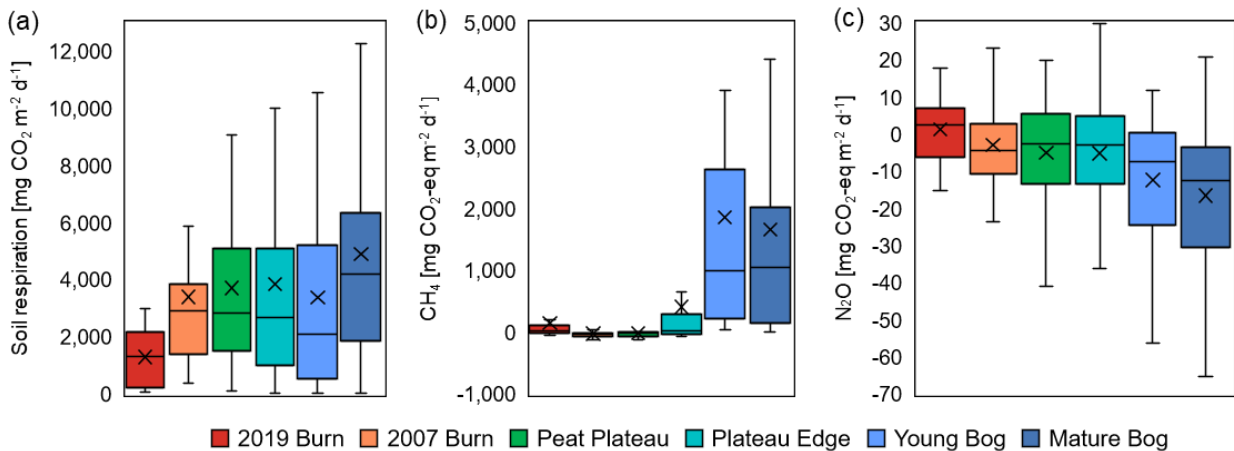


Figure 2.7: Greenhouse gas balances in CO₂-equivalents among peatland stages (in the order from left to right: 2019 Burn, 2007 Burn, Peat Plateau, Plateau Edge, Young Bog, and Mature Bog), comparing (a) soil respiration, (b) CH₄ fluxes, and (c) N₂O fluxes. Boxplots use all flux data measured throughout the 2019 growing season, with black crosses indicating the averages. Conversion to CO₂-equivalents use sustained global warming and cooling potentials (SGWP, SGCP) based on a 100-year time span for CH₄ (45) and N₂O (270) (Neubauer & Megonigal, 2019). Note the difference in the scale of the y-axes. Outliers are not shown.

2.4 Discussion

Here, we explored the impacts of permafrost thaw and wildfire on N₂O, CH₄, and CO₂ fluxes from boreal peatlands in western Canada, with a focus on controls on N₂O fluxes and their contribution to the overall GHG balance. Generally, we observed N₂O uptake rather than emissions from different peatland stages and peatland ponds, and that the rate of N₂O uptake in the studied nutrient-poor peatlands increased with higher soil temperatures and higher soil moisture. As a result, permafrost thaw and development of thermokarst bogs led to increased N₂O uptake, although accompanying increases of CH₄ emissions had a much greater influence on the net radiative balance. In contrast, we found that wildfire led to reduced N₂O uptake, minor changes to CH₄ fluxes, and reduced soil respiration in the first year after fire. We found N₂O uptake from most of the studied peatland ponds, with no clear influence of thermokarst pond expansion, but also that one pond acted as a N₂O emission hot spot. Below we discuss the controls on the GHG balance of each of the studied peatland stages, and the implications of thermokarst and wildfire for the future net radiative balance.

2.4.1 Greenhouse Gas Balance of Peat Plateaus

In the intact Peat Plateaus, the presence of permafrost leads to dry, low nutrient conditions, as displayed by the lowest soil moisture content and soil temperatures in connection with the shallowest active layer when compared to the burned counterparts. The Plateau Edges as the transition zone to the thermokarst bogs had similar vegetation than the plateaus but displayed a deepened active layer and a water table closer to the surface due to ground subsidence. Thus, Peat Plateaus and their Plateau Edges had mostly oxic conditions at shallow depths that facilitate aerobic processes and exhibited near zero N₂O fluxes or small N₂O uptake.

N₂O uptake increased significantly with higher soil temperatures in both, peat plateaus and plateau edges. Soil temperature has been identified as a key control of N₂O fluxes previously (Butterbach-Bahl et al., 2013; Voigt, Lamprecht, et al., 2017). As such, Siljanen et al. (2020) concluded that N₂O production processes in boreal forests are more temperature-sensitive than N₂O consumption processes, as they found N₂O emissions during the warm, dry summer months and N₂O uptake during the wetter, colder shoulder season. However, our results showed the opposite as overall N₂O uptake, and thus N₂O consumption increased with surface soil

temperatures during the peak growing season. Emissions of N₂O are subject to high temporal (hot moments) and spatial (hot spots) variability (Fiencke et al., 2022; Marushchak et al., 2011; McClain et al., 2003). Although we did not observe high N₂O emissions at the soil surface of our study sites, we measured increased N₂O soil gas concentrations at depth in two out of 15 Peat Plateau plots, indicating active N₂O production. In fact, N₂O produced at depth may not necessarily reach the soil surface (Arah et al., 1991). Siljanen et al. (2020) suggested that acid-tolerant denitrifiers, as identified in arctic wetlands (Palmer et al., 2012), consume N₂O via reductase and thus exceed N₂O production.

Besides soil temperatures, porewater nutrient concentrations and soil moisture content usually control the N₂O balance. The effect of active layer deepening caused increased nutrient supply of NO₃⁻ and NH₄⁺ in the Plateau Edges but did not lead to N₂O emissions. In contrast, the Plateau Edges showed slightly increased, non-significant uptake of N₂O consistent over all three sites as the Plateau Edges are slightly wetter than the Peat Plateaus. Thus, we conclude that the effect of soil moisture exceeded the effect of nutrient supply rates under generally low availability of NO₃⁻ and NH₄⁺. The Peat Plateaus in this study had the lowest P supply and PO₄³⁻ porewater concentrations compared to the other stages, which could have limited N₂O emissions (Liimatainen et al., 2018). Besides N₂O uptake, we also observed CH₄ uptake by the peat plateaus due to the oxic soil conditions, similar to other studies on boreal forests (Siljanen et al., 2020) and tundra peat plateaus (Voigt, Lamprecht, et al., 2017). As in Gibson et al. (2019) and Estop-Aragónés et al. (2018), soil respiration was higher in the Peat Plateaus than in burned stages but was lower than in the thermokarst stages.

2.4.2 Greenhouse Gas Balance of Burned Peat Plateaus

We expected wildfire disturbance to lead to increased N₂O emissions linked to enhanced availability of NH₄⁺ and NO₃⁻, possibly caused by 1) reduced plant demand due to a lack of vegetation as observed from bare peat surfaces on palsa and peat plateau surfaces in Eurasia (Fiencke et al., 2022; Marushchak et al., 2011; Repo et al., 2009; Voigt, Lamprecht, et al., 2017), 2) mineralization of organic matter during combustion (Walker et al., 2019, 2020), and 3) increased soil mineralization in the years after wildfire due to warmer soils and a deeper active layer (Gibson et al., 2018), potentially resulting in a flush of higher nutrient supply, specifically

inorganic N, from recently thawed, deeper soil layers (Ackley et al., 2021; Keuper et al., 2012; Ramm et al., 2022; Salmon et al., 2018). In addition to inorganic N, the availability of PO_4^{3-} supply can fuel nitrification and enhance N_2O production (Liimatainen et al., 2018) by stimulating microbial activity (F. Wang et al., 2014). Although our results confirmed an increased supply of P post-fire, we did not observe N_2O emissions, but observed near zero N_2O fluxes from burned peat plateaus.

Three reasons could contribute to the lack of N_2O emissions from the burned peat plateaus. Firstly, although soil respiration almost reached pre-burn rates twelve years after wildfire and increased with soil temperature, N_2O uptake by the wildfire-affected plateaus was not correlated with soil temperature, unlike the intact Peat Plateaus and Plateau Edges. We attribute the absence of temperature sensitivity of N_2O uptake to the fact that microbial communities might have been affected by the fire and require extended time to re-establish. Similarly, high N_2O emissions from thawing yedoma permafrost only occurred in revegetated soils several years after thaw, with re-establishment of the soil microbial communities involved in N-cycling (Marushchak et al., 2021). Köster et al. (2017) found that N_2O emissions only reached pre-fire rates in boreal mineral soils 40 years after fire.

Second, burned wood ash can inhibit N_2O production during nitrification and denitrification in acidic boreal peat soils (Liimatainen et al., 2014). In addition, the loss of labile soil C from combustion could also influence microbial communities to reduce their ability for CH_4 and N_2O uptake, limiting denitrification as well as nitrification and CH_4 oxidation (Gibson et al., 2019; Köster et al., 2017). The lack of labile soil C has been attributed to lower soil respiration following wildfire than unburned surfaces (Gibson et al., 2019).

Lastly, the burned peat plateau stages had the deepest water table and driest conditions (WFPS <30%) in the soil profile. Soil moisture has been identified as an important regulator of N_2O fluxes in permafrost-affected soils (optimum WFPS for N_2O emissions: 40-60%), frequently overruling the effect of temperature (Voigt et al., 2020). Like recent post-wildfire studies on arctic mineral soils in Greenland (Hermesdorf et al., 2022) and subarctic upland forest soils in Northern Canada (Köster et al., 2017), we conclude here that soil moisture also controlled N_2O

fluxes in wildfire-affected peatlands in the western Canadian boreal zone, possibly limiting both, emissions and uptake of N_2O .

2.4.3 Greenhouse Gas Balance of Thermokarst Bogs

The development of thermokarst bogs leads to saturated conditions of the peat profile, particularly during the first few decades. We found that thermokarst formation and subsequent wet conditions promote N_2O uptake in peatlands in the Taiga Plains, which were up to three times greater than uptake from the Peat Plateau and Plateau Edge. Despite the relative differences in soil moisture regimes across the sites, the observed trends of increased N_2O uptake and below ambient N_2O porewater concentrations under anoxic conditions were consistent for all three sites.

Although N_2O uptake can also occur under oxic conditions, observed in polar desert soils (Brummell et al., 2014), the anoxic conditions suggest the prevalence of denitrification, particularly in the mostly anoxic Young Bog stage. Nitrification only produced limited NO_3^- and N_2O under wet conditions, so that concentrations and supply rates of NO_3^- were low. The small amounts of available NO_3^- and N_2O were reduced to N_2 in the denitrification process under the anoxic conditions, which is a typical wetland process also found in thawing yedoma permafrost (Marushchak et al., 2021). In conclusion, the limitations of both NO_3^- and oxygen promote the favorability of N_2O as a terminal electron acceptor, which is eventually reduced to N_2 (Butterbach-Bahl et al., 2013; Voigt et al., 2020). Besides low NO_3^- , the anoxic conditions also lead to high NH_4^+ , aligning with results from an incubation study with peat samples from a collapse-scar bog (Morison et al., 2018) and suggesting well-established and effective denitrification and/or inhibited nitrification under anoxic conditions. Both thermokarst stages had a higher P supply than the Peat Plateaus, associated with increased productivity driven by higher soil temperatures (Figures 2.4f and A2.3); except for the young bog at Smith Creek, where inundation cut off respiration (Figure 2.4e).

Besides WFPS and its effects on redox conditions and nutrient supply, we consider the elevated soil temperatures in the thermokarst bogs as a secondary driver of the increased N_2O uptake, despite non-significant correlations. Although well-established in literature (e.g., Jones et al., 2017), CH_4 emissions also correlated weakly with soil temperatures at 40 cm depth. Therefore,

as expected with climate change, longer, wetter, and warmer summers could further amplify the thermokarst areas' N₂O uptake and CH₄ emissions, respectively.

2.4.4 Greenhouse Gas Balance of Peatland Ponds

Boreal peatland ponds have been identified as potential hot spots for N₂O, CH₄, and CO₂ emissions (Huttunen et al., 2002; Kortelainen et al., 2020; Kuhn, Thompson, et al., 2021) with thermokarst activity enhancing CH₄ and CO₂ emissions (Kuhn et al., 2022). In our study, four of five ponds had minor N₂O uptake similar to the peatland stages. We also found no differences in N₂O exchange between thermokarst and stable edges, despite previous studies on these ponds found higher CH₄ emissions from thermokarst edges (Kuhn et al., 2022), suggesting different controls on CH₄ and N₂O emissions in boreal ponds.

One pond, L2, had N₂O emissions ($\sim 0.30 \text{ mg N}_2\text{O m}^{-2} \text{ d}^{-1}$) similar to those reported for agricultural wetlands ($0.27 \text{ mg N}_2\text{O-N m}^{-2} \text{ d}^{-1}$; Pennock et al., 2010) and was within the global range reported for ponds ($0.12\text{-}0.56 \text{ mg N}_2\text{O-N m}^{-2} \text{ d}^{-1}$; DelSontro et al., 2018). L2 had distinct water chemistry compared to both the four other ponds in this study and to 20 other ponds in the study region (Kuhn, Thompson, et al., 2021), as L2 had five to fifty times higher dissolved NO₃⁻ and Fe concentrations. Differences in NO₃⁻ concentrations and net emission of N₂O were possibly driven by the pond's proximity to a twelve-year-old fire scar or linked to beaver activity. The potential liberation of inorganic N through wildfire has been shown to enhance downstream N₂O emissions from water bodies (Soued et al., 2016). However, this study did not find higher inorganic N concentrations in recently burned peat plateaus for downstream transport into ponds. Further, L2 was the only pond with known beaver activity. The presence of beavers has been shown to alter the biogeochemistry of ecosystems, enhancing N inputs in ponds (Naiman & Melillo, 1984), and potentially driving the observed high N₂O emissions.

Notably, the high magnitude of N₂O released from ponds like L2 can potentially offset all N₂O uptake from thermokarst bog expansion, as L2's relative N₂O-related net radiative balance (not shown) is five to 15 times larger than any other measured net radiative balance in this study (Figure 2.7). However, since we only found N₂O emissions from one out of five ponds, further work is required to identify N₂O hot spots amongst the peatland ponds, which constitute less than 1% of the area in peatland complexes (Olefeldt et al., 2021). In comparison, 5.3% of the

unburned area and 8.3% of the burned areas transitioned into young bogs within the Taiga Plains over 30 years (Gibson et al., 2018).

2.4.5 Implications of Climate Change on the Net Radiative Balance

Although we did not determine the net ecosystem CO₂ exchange of the peat surfaces, it is likely that CO₂ rather than CH₄ dominates shifts in the net radiative balance for wildfire-affected areas, as differences in CH₄ fluxes from the burned plateau and the Peat Plateau were minor. As gross primary production is reduced due to the lack of vegetation, soil respiration will drive net ecosystem exchange post-wildfire disturbance. Previous work showed soil respiration from burned peat plateaus to be lower than the intact Peat Plateau in Lutose (Gibson et al., 2019). Effects of thermokarst bog expansion have shown CH₄ to dominate net radiative forcing rather than CO₂ in the first few decades after permafrost thaw (Helbig, Chasmer, Desai, et al., 2017; Helbig, Chasmer, Kljun, et al., 2017), both governed by the water table position in the peat landscape. The growing season of 2019 was relatively dry, with low water tables compared to site observations at Lutose since 2015 (Heffernan et al., 2021). There, soil respiration signaled high productivity in the thermokarst bog stages (Estop-Aragónés et al., 2018), aligning with the observed N₂O uptake observed in our study. The shallow water table at Smith Creek inhibited soil respiration and moss photosynthesis in the Young Bog (Kou et al., 2022). Except for the inundated Young Bog at Smith Creek, soil respiration in this study showed an inverse correlation to N₂O uptake.

We also found an inverse relationship between N₂O and CH₄ for the peatland stages, in both soil gas concentrations and fluxes. Fundamental biogeochemical redox processes are governed by water table depth and soil moisture contents, controlling the typically inverse CH₄ and N₂O production (Frolking et al., 2011; Maljanen et al., 2010). Completely anoxic conditions in fully saturated soils are conducive to CH₄ production and, in turn, low CH₄ oxidation (Frolking et al., 2011; Maljanen et al., 2010), while the anoxic conditions would also be expected to lead to complete denitrification, producing N₂ rather than N₂O as gaseous end-product. While we found a similar range to a comparable study (Siljanen et al., 2020), N₂O uptake of the peat plateau was only around half of the CH₄ uptake from this yet intact peatland stage when expressed in CO₂-eq. Regarding the thermokarst bogs, the increased N₂O uptake offset less than 1% of their CH₄

emissions. However, the measured N₂O uptake from all peat surfaces of the Taiga Plains (overall average: -0.03 mg N₂O m⁻² d⁻¹) was large compared to previous studies from across the circumpolar region (lower quartile: -0.01 mg N₂O m⁻² d⁻¹; Voigt et al., 2020).

Thus, we conclude that wildfire and thermokarst can shift CO₂, CH₄, and N₂O fluxes, dominated by enhanced CH₄ emissions following thermokarst compared to intact Peat Plateaus displaying uptake of both, N₂O and CH₄. CO₂ fluxes are rather impacted by wildfire, based on our findings and previous studies. Ongoing permafrost thaw is highly likely for at least 6% of the overall study area, i.e., more than 22,000 km² (Gibson et al., 2021). Considering the vast areal extension of peatland thermokarst in the Taiga Plains (Helbig, Pappas, et al., 2016), our findings thus suggest a small counter acting N₂O feedback to the impacts of increasing CH₄ emissions, which has previously been unaccounted for.

2.5 Conclusion

We found a negative feedback from increased N₂O uptake upon thermokarst disturbance and a positive feedback from reduced N₂O uptake following wildfire in the Taiga Plains. Unlike previous studies on permafrost peatlands in northern Eurasia, where abundant hot spots of N₂O emissions have been found, we did not find any such evidence in western Canada. For thermokarst bogs, our results suggest WFPS and soil temperature as major drivers of altered N₂O fluxes in these nutrient-limited environments. Peatland ponds were generally neutral or sinks of N₂O, albeit with a wide range of fluxes and one N₂O hot spot driven by elevated NO₃⁻ supply. From a SGCP/SGWP perspective, the effects of wildfire and permafrost thaw on GHG emissions from boreal peatlands in our study region are likely to be dominated by the responses of CH₄ and CO₂, while N₂O uptake constituted less than 1% of CH₄ emissions from peatland thermokarst.

References

- Abbott, B. W., & Jones, J. B. (2015). Permafrost collapse alters soil carbon stocks, respiration, CH₄, and N₂O in upland tundra. *Global Change Biology*, 21(12), 4570–4587. <https://doi.org/10.1111/gcb.13069>
- Ackley, C., Tank, S. E., Haynes, K. M., Rezanezhad, F., McCarter, C., & Quinton, W. L. (2021). Coupled hydrological and geochemical impacts of wildfire in peatland-dominated regions of discontinuous permafrost. *Science of The Total Environment*, 782, 146841. <https://doi.org/10.1016/j.scitotenv.2021.146841>
- Arah, J. R. M., Smith, K. A., Crichton, I. J., & Li, H. S. (1991). Nitrous oxide production and denitrification in Scottish arable soils. *Journal of Soil Science*, 42, 351–367.
- Brummell, M. E., Farrell, R. E., Hardy, S. P., & Siciliano, S. D. (2014). Greenhouse gas production and consumption in High Arctic deserts. *Soil Biology and Biochemistry*, 68, 158–165. <https://doi.org/10.1016/j.soilbio.2013.09.034>
- Bush, E. & Lemmen, D.S. (Eds.) (2019). *Canada's Changing Climate Report*. Government of Canada, Ottawa, Ontario, Canada. 444. <https://publications.gc.ca/pub?id=9.870430&sl=0>

Butterbach-Bahl, K., Baggs, E. M., Dannenmann, M., Kiese, R., & Zechmeister-Boltenstern, S. (2013). Nitrous oxide emissions from soils: how well do we understand the processes and their controls? *Philosophical Transactions of the Royal Society B: Biological Sciences*, 368(1621), 20130122–20130122. <https://doi.org/10.1098/rstb.2013.0122>

Carter M.R., & Gregorich E.G. (2007). *Soil Sampling and Methods of Analysis* (2nd ed.). Canadian Society of Soil Science, Taylor & Francis Group, CRC Press. <https://doi.org/10.1201/9781420005271>

Chapuis-Lardy, L., Wrage, N., Metay, A., Chotte, J.-L., & Bernoux, M. (2007). Soils, a sink for N₂O? A review. *Global Change Biology*, 13(1), 1–17. <https://doi.org/10.1111/j.1365-2486.2006.01280.x>

Chasmer, L., & Hopkinson, C. (2017). Threshold loss of discontinuous permafrost and landscape evolution. *Global Change Biology*, 23(7), 2672–2686. <https://doi.org/10.1111/gcb.13537>

Coogan, S. C. P., Robinne, F.-N., Jain, P., & Flannigan, M. D. (2019). Scientists' warning on wildfire — a Canadian perspective. *Canadian Journal of Forest Research*, 49(9), 1015–1023. <https://doi.org/10.1139/cjfr-2019-0094>

Crill, P. M. (1991). Seasonal patterns of methane uptake and carbon dioxide release by a temperate woodland soil. *Global Biogeochemical Cycles*, 5(4), 319–334. <https://doi.org/10.1029/91GB02466>

DelSontro, T., Beaulieu, J. J., & Downing, J. A. (2018). Greenhouse gas emissions from lakes and impoundments: Upscaling in the face of global change. *Limnology and Oceanography Letters*, 3(3), 64–75. <https://doi.org/10.1002/lol2.10073>

Elder, C. D., Thompson, D. R., Thorpe, A. K., Chandanpurkar, H. A., Hanke, P. J., Hasson, N., James, S. R., Minsley, B. J., Pastick, N. J., Olefeldt, D., Walter Anthony, K. M., & Miller, C. E. (2021). Characterizing Methane Emission Hotspots From Thawing Permafrost. *Global Biogeochemical Cycles*, 35(12), e2020GB006922. <https://doi.org/10.1029/2020GB006922>

Environment and Climate Change Canada. (2020). Historical Data. https://climate.weather.gc.ca/historical_data/search_historic_data_e.html [accessed in October 2022]

Estop-Aragonés, C., Czimczik, C. I., Heffernan, L., Gibson, C., Walker, J. C., Xu, X., & Olefeldt, D. (2018). Respiration of aged soil carbon during fall in permafrost peatlands enhanced by active layer deepening following wildfire but limited following thermokarst. *Environmental Research Letters*, 13(8), 85002. <https://doi.org/10.1088/1748-9326/aad5f0>

Fiencke, C., Marushchak, M. E., Sanders, T., Wegner, R., & Beer, C. (2022). Microbiogeochemical Traits to Identify Nitrogen Hotspots in Permafrost Regions. *Nitrogen*, 3(3), 458–501. <https://doi.org/10.3390/nitrogen3030031>

Frolking, S., Roulet, N., & Fuglestvedt, J. (2006). How northern peatlands influence the Earth's radiative budget: Sustained methane emission versus sustained carbon sequestration. *Journal of Geophysical Research: Biogeosciences*, 111(G1). <https://doi.org/10.1029/2005JG000091>

Frolking, S., Talbot, J., Jones, M. C., Treat, C. C., Kauffman, J. B., Tuittila, E., & Roulet, N. (2011). Peatlands in the Earth's 21st century climate system. *Environmental Reviews*, 19, 371–396. <https://doi.org/10.1139/a11-014>

Fuß, R. (2017). *gasfluxes: Greenhouse Gas Flux Calculation from Chamber Measurements*. <https://cran.r-project.org/web/packages/gasfluxes/index.html>.

Gibson, C., Cottenie, K., Gingras-Hill, T., Kokelj, S. v, Baltzer, J., Chasmer, L., & Turetsky, M. (2021). Mapping and understanding the vulnerability of northern peatlands to permafrost thaw at scales relevant to community adaptation planning. *Environmental Research Letters*. <http://iopscience.iop.org/article/10.1088/1748-9326/abe74b>

Gibson, C. M., Chasmer, L. E., Thompson, D. K., Quinton, W. L., Flannigan, M. D., & Olefeldt, D. (2018). Wildfire as a major driver of recent permafrost thaw in boreal peatlands. *Nature Communications*, 9(1), 3041. <https://doi.org/10.1038/s41467-018-05457-1>

Gibson, C. M., Estop-Aragonés, C., Flannigan, M., Thompson, D. K., & Olefeldt, D. (2019). Increased deep soil respiration detected despite reduced overall respiration in permafrost peat

plateaus following wildfire. *Environmental Research Letters*, 14(12), 125001. <https://doi.org/10.1088/1748-9326/ab4f8d>

Gil, J. A., Marushchak, M. E., Rütting, T., Baggs, E. M., Pérez, T., Novakovskiy, A., Trubnikova, T., Kaverin, D., Martikainen, P. J., & Biasi, C. (2021). Sources of nitrous oxide and fate of mineral nitrogen in sub-Arctic permafrost peat soils. *Biogeosciences Discussions*, 2021, 1–25. <https://doi.org/10.5194/bg-2021-228>

Gil, J., Pérez, T., Boering, K., Martikainen, P. J., & Biasi, C. (2017). Mechanisms responsible for high N₂O emissions from subarctic permafrost peatlands studied via stable isotope techniques. *Global Biogeochemical Cycles*, 31(1), 172–189. <https://doi.org/10.1002/2015GB005370>

Heffernan, L., Estop-Aragonés, C., Knorr, K.-H., Talbot, J., & Olefeldt, D. (2020). Long-term Impacts of Permafrost Thaw on Carbon Storage in Peatlands: Deep Losses Offset by Surficial Accumulation. *Journal of Geophysical Research: Biogeosciences*, 125(3), e2019JG005501. <https://doi.org/10.1029/2019JG005501>

Heffernan, L., Jassey, V. E. J., Frederickson, M., MacKenzie, M. D., & Olefeldt, D. (2021). Constraints on potential enzyme activities in thermokarst bogs: Implications for the carbon balance of peatlands following thaw. *Global Change Biology*, 27(19), 4711–4726. <https://doi.org/10.1111/gcb.15758>

Helbig, M., Chasmer, L. E., Desai, A. R., Kljun, N., Quinton, W. L., & Sonnentag, O. (2017). Direct and indirect climate change effects on carbon dioxide fluxes in a thawing boreal forest–wetland landscape. *Global Change Biology*, 23(8), 3231–3248. <https://doi.org/10.1111/gcb.13638>

Helbig, M., Chasmer, L. E., Kljun, N., Quinton, W. L., Treat, C. C., & Sonnentag, O. (2017). The positive net radiative greenhouse gas forcing of increasing methane emissions from a thawing boreal forest-wetland landscape. *Global Change Biology*, 23(6), 2413–2427. <https://doi.org/10.1111/gcb.13520>

- Helbig, M., Pappas, C., & Sonnentag, O. (2016). Permafrost thaw and wildfire: Equally important drivers of boreal tree cover changes in the Taiga Plains, Canada. *Geophysical Research Letters*, 43(4), 1598–1606. <https://doi.org/10.1002/2015GL067193>
- Helbig, M., Quinton, W. L., & Sonnentag, O. (2017). Warmer spring conditions increase annual methane emissions from a boreal peat landscape with sporadic permafrost. *Environmental Research Letters*, 12(11), 115009. <https://doi.org/10.1088/1748-9326/aa8c85>
- Hendzel, L. L., Matthews, C. J. D., Venkiteswaran, J. J., St. Louis, V. L., Burton, D., Joyce, E. M., & Bodaly, R. A. (2005). Nitrous Oxide Fluxes in Three Experimental Boreal Forest Reservoirs. *Environmental Science & Technology*, 39(12), 4353–4360. <https://doi.org/10.1021/es049443j>
- Hermesdorf, L., Elberling, B., D’Imperio, L., Xu, W., Lambæk, A., & Ambus, P. L. (2022). Effects of fire on CO₂, CH₄, and N₂O exchange in a well-drained Arctic heath ecosystem. *Global Change Biology*, 28(16), 4882–4899. <https://doi.org/10.1111/gcb.16222>
- Holloway, J. E., & Lewkowicz, A. G. (2020). Half a century of discontinuous permafrost persistence and degradation in western Canada. *Permafrost and Periglacial Processes*, 31(1), 85–96. <https://doi.org/10.1002/ppp.2017>
- Hugelius, G., Tarnocai, C., Broll, G., Canadell, J. G., Kuhry, P., & Swanson, D. K. (2013). The Northern Circumpolar Soil Carbon Database: spatially distributed datasets of soil coverage and soil carbon storage in the northern permafrost regions. *Earth System Science Data*, 5(1), 3–13. <https://doi.org/10.5194/essd-5-3-2013>
- Hüppi, R., Felber, R., Krauss, M., Six, J., Leifeld, J., & Fuß, R. (2018). Restricting the nonlinearity parameter in soil greenhouse gas flux calculation for more reliable flux estimates. *PLOS ONE*, 13(7), e0200876. <https://doi.org/10.1371/journal.pone.0200876>
- Huttunen, J. T., Väisänen, T. S., Heikkinen, M., Hellsten, S., Nykänen, H., Nenonen, O., & Martikainen, P. J. (2002). Exchange of CO₂, CH₄ and N₂O between the atmosphere and two northern boreal ponds with catchments dominated by peatlands or forests. *Plant and Soil*, 242(1), 137–146. <https://doi.org/10.1023/A:1019606410655>

Jones, M. C., Harden, J., O'Donnell, J., Manies, K., Jorgenson, T., Treat, C., & Ewing, S. (2017). Rapid carbon loss and slow recovery following permafrost thaw in boreal peatlands. *Global Change Biology*, 23(3), 1109–1127. <https://doi.org/10.1111/gcb.13403>

Kassambara, A. (2021). *rstatix: Pipe-Friendly Framework for Basic Statistical Tests*. *R package version 0.7.0*, <https://rpkgs.datanovia.com/rstatix/>. Retrieved from <https://github.com/kassambara/rstatix/releases/tag/v0.7.0>

Keuper, F., van Bodegom, P. M., Dorrepaal, E., Weedon, J. T., van Hal, J., van Logtestijn, R. S. P., & Aerts, R. (2012). A frozen feast: thawing permafrost increases plant-available nitrogen in subarctic peatlands. *Global Change Biology*, 18(6), 1998–2007. <https://doi.org/10.1111/j.1365-2486.2012.02663.x>

Kortelainen, P., Larmola, T., Rantakari, M., Juutinen, S., Alm, J., & Martikainen, P. J. (2020). Lakes as nitrous oxide sources in the boreal landscape. *Global Change Biology*, 26(3), 1432–1445. <https://doi.org/10.1111/gcb.14928>

Köster, E., Köster, K., Berninger, F., Aaltonen, H., Zhou, X., & Pumpanen, J. (2017). Carbon dioxide, methane and nitrous oxide fluxes from a fire chronosequence in subarctic boreal forests of Canada. *Science of The Total Environment*, 601–602, 895–905. <https://doi.org/https://doi.org/10.1016/j.scitotenv.2017.05.246>

Kou, D., Virtanen, T., Treat, C. C., Tuovinen, J.-P., Räsänen, A., Juutinen, S., Mikola, J., Aurela, M., Heiskanen, L., Heikkilä, M., Weckström, J., Juselius, T., Piilo, S. R., Deng, J., Zhang, Y., Chaudhary, N., Huang, C., Välikanta, M., Biasi, C., ... Shurpali, N. J. (2022). Peatland Heterogeneity Impacts on Regional Carbon Flux and Its Radiative Effect Within a Boreal Landscape. *Journal of Geophysical Research: Biogeosciences*, 127(9), e2021JG006774. <https://doi.org/10.1029/2021JG006774>

Koven, C. D., Schuur, E. A. G., Schädel, C., Bohn, T. J., Burke, E. J., Chen, G., Chen, X., Ciais, P., Grosse, G., Harden, J. W., Hayes, D. J., Hugelius, G., Jafarov, E. E., Krinner, G., Kuhry, P., Lawrence, D. M., MacDougall, A. H., Marchenko, S. S., McGuire, A. D., ... Turetsky, M. (2015). A simplified, data-constrained approach to estimate the permafrost carbon–climate

feedback. *Philosophical Transactions of the Royal Society A: Mathematical, Physical and Engineering Sciences*, 373(2054), 20140423. <https://doi.org/10.1098/rsta.2014.0423>

Kuhn, M. A., Thompson, L. M., Winder, J. C., Braga, L. P. P., Tanentzap, A. J., Bastviken, D., & Olefeldt, D. (2021). Opposing Effects of Climate and Permafrost Thaw on CH₄ and CO₂ Emissions From Northern Lakes. *AGU Advances*, 2(4), e2021AV000515. <https://doi.org/10.1029/2021AV000515>

Kuhn, M., Schmidt, M., Heffernan, L., Stührenberg, J., Knorr, K. H., Estop-Aragonés, C., Broder, T., Gonzalez Moguel, R., Douglas, P., & Olefeldt, D. (2022). High ebullitive, millennial-aged greenhouse gas emissions from thermokarst expansion of peatland lakes in boreal western Canada. *Limnology & Oceanography*. <https://doi.org/10.1002/lno.12288>

Lenton, T. M., Held, H., Kriegler, E., Hall, J. W., Lucht, W., Rahmstorf, S., & Schellnhuber, H. J. (2008). Tipping elements in the Earth's climate system. *Proceedings of the National Academy of Sciences of the United States of America*, 105(6), 1786–1793. <https://doi.org/10.1073/pnas.0705414105>

Liimatainen, M., Martikainen, P. J., & Maljanen, M. (2014). Why granulated wood ash decreases N₂O production in boreal acidic peat soil? *Soil Biology and Biochemistry*, 79, 140–148. <https://doi.org/10.1016/j.soilbio.2014.09.016>

Liimatainen, M., Voigt, C., Martikainen, P. J., Hytönen, J., Regina, K., Óskarsson, H., & Maljanen, M. (2018). Factors controlling nitrous oxide emissions from managed northern peat soils with low carbon to nitrogen ratio. *Soil Biology and Biochemistry*, 122(November 2017), 186–195. <https://doi.org/10.1016/j.soilbio.2018.04.006>

Mack, M. C., Walker, X. J., Johnstone, J. F., Alexander, H. D., Melvin, A. M., Jean, M., & Miller, S. N. (2021). Carbon loss from boreal forest wildfires offset by increased dominance of deciduous trees. *Science*, 372(6539), 280 LP – 283. <https://doi.org/10.1126/science.abf3903>

Maljanen, M., Sigurdsson, B. D., Guðmundsson, J., Óskarsson, H., Huttunen, J. T., & Martikainen, P. J. (2010). Greenhouse gas balances of managed peatlands in the Nordic countries

– present knowledge and gaps. *Biogeosciences*, 7(9), 2711–2738. <https://doi.org/10.5194/bg-7-2711-2010>

Marshall, I. B., Schut, P. H., & Ballard, M. (1999). A National Ecological Framework for Canada. Agriculture and Agri-Food Canada, Research Branch, Centre for Land and Biological Resources Research, and Environment Canada, State of the Environment Directorate, Ecozone Analysis Branch. Ottawa/Hull. <https://sis.agr.gc.ca/cansis/nsdb/ecostrat/index.html>

Martikainen, P. J., Nykänen, H., Crill, P., & Silvola, J. (1993). Effect of a lowered water table on nitrous oxide fluxes from northern peatlands. *Nature*, 366(6450), 51–53. <https://doi.org/10.1038/366051a0>

Marushchak, M. E., Kerttula, J., Diáková, K., Faguet, A., Gil, J., Grosse, G., Knoblauch, C., Lashchinskiy, N., Martikainen, P. J., Morgenstern, A., Nykamb, M., Ronkainen, J. G., Siljanen, H. M. P., van Delden, L., Voigt, C., Zimov, N., Zimov, S., & Biasi, C. (2021). Thawing Yedoma permafrost is a neglected nitrous oxide source. *Nature Communications*, 12(1), 7107. <https://doi.org/10.1038/s41467-021-27386-2>

Marushchak, M. E., Pitkämäki, A., Koponen, H., Biasi, C., Seppälä, M., & Martikainen, P. J. (2011). Hot spots for nitrous oxide emissions found in different types of permafrost peatlands. *Global Change Biology*, 17(8), 2601–2614. <https://doi.org/10.1111/j.1365-2486.2011.02442.x>

McClain, M. E., Boyer, E. W., Dent, C. L., Gergel, S. E., Grimm, N. B., Groffman, P. M., Hart, S. C., Harvey, J. W., Johnston, C. A., Mayorga, E., McDowell, W. H., & Pinay, G. (2003). Biogeochemical Hot Spots and Hot Moments at the Interface of Terrestrial and Aquatic Ecosystems. *Ecosystems*, 6(4), 301–312. <https://doi.org/10.1007/s10021-003-0161-9>

Morison, M. Q., Macrae, M. L., Petrone, R. M., & Fishback, L. (2018). Climate-induced changes in nutrient transformations across landscape units in a thermokarst subarctic peatland. *Arctic, Antarctic, and Alpine Research*, 50(1), e1519366. <https://doi.org/10.1080/15230430.2018.1519366>

Nadelhoffer, K. J., Giblin, A. E., Shaver, G. R., & Laundre, J. A. (1991). Effects of Temperature and Substrate Quality on Element Mineralization in Six Arctic Soils. *Ecology*, 72(1), 242–253. <https://doi.org/10.2307/1938918>

Naiman, R. J., & Melillo, J. M. (1984). Nitrogen budget of a subarctic stream altered by beaver (*Castor canadensis*). *Oecologia*, 62(2), 150–155. <https://doi.org/10.1007/BF00379007>

Neubauer, S. C., & Megonigal, J. P. (2015). Moving Beyond Global Warming Potentials to Quantify the Climatic Role of Ecosystems. *Ecosystems*, 18(6), 1000–1013. <http://www.jstor.org/stable/43677758>

Neubauer, S. C., & Megonigal, J. P. (2019). Correction to: Moving Beyond Global Warming Potentials to Quantify the Climatic Role of Ecosystems. *Ecosystems*, 22(8), 1931–1932. <https://doi.org/10.1007/s10021-019-00422-5>

Norman, J. M., Kucharik, C. J., Gower, S. T., Baldocchi, D. D., Crill, P. M., Rayment, M., Savage, K., & Striegl, R. G. (1997). A comparison of six methods for measuring soil-surface carbon dioxide fluxes. *Journal of Geophysical Research: Atmospheres*, 102(D24), 28771–28777. <https://doi.org/10.1029/97JD01440>

Obu, J., Westermann, S., Bartsch, A., Berdnikov, N., Christiansen, H. H., Dashtseren, A., Delaloye, R., Elberling, B., Etzelmüller, B., Kholodov, A., Khomutov, A., Kääh, A., Leibman, M. O., Lewkowicz, A. G., Panda, S. K., Romanovsky, V., Way, R. G., Westergaard-Nielsen, A., Wu, T., ... Zou, D. (2019). Northern Hemisphere permafrost map based on TTOP modelling for 2000–2016 at 1 km² scale. *Earth-Science Reviews*, 193, 299–316. <https://doi.org/10.1016/j.earscirev.2019.04.023>

Olefeldt, D., Hovemyr, M., Kuhn, M. A., Bastviken, D., Bohn, T. J., Connolly, J., Crill, P., Euskirchen, E. S., Finkelstein, S. A., Genet, H., Grosse, G., Harris, L. I., Heffernan, L., Helbig, M., Hugelius, G., Hutchins, R., Juutinen, S., Lara, M. J., Malhotra, A., ... Watts, J. D. (2021). The Boreal-Arctic Wetland and Lake Dataset (BAWLD). *Earth System Science Data*, 13(11), 5127–5149. <https://doi.org/10.5194/essd-13-5127-2021>

Palmer, K., Biasi, C., & Horn, M. A. (2012). Contrasting denitrifier communities relate to contrasting N₂O emission patterns from acidic peat soils in arctic tundra. *The ISME Journal*, 6(5), 1058–1077. <https://doi.org/10.1038/ismej.2011.172>

Pelletier, N., Talbot, J., Olefeldt, D., Turetsky, M., Blodau, C., Sonnentag, O., & Quinton, W. L. (2017). Influence of Holocene permafrost aggradation and thaw on the paleoecology and carbon storage of a peatland complex in northwestern Canada. *The Holocene*, 27(9), 1391–1405. <https://doi.org/10.1177/0959683617693899>

Pennock, D., Yates, T., Bedard-Haughn, A., Phipps, K., Farrell, R., & Mcdougal, R. (2010). Landscape controls on N₂O and CH₄ emissions from freshwater mineral soil wetlands of the Canadian Prairie Pothole region. *Geoderma*, 155(3–4), 308–319. <https://doi.org/10.1016/j.geoderma.2009.12.015>

Quinton, W. L., Bemrose, R. K., Zhang, Y., & Carey, S. K. (2009). The influence of spatial variability in snowmelt and active layer thaw on hillslope drainage for an alpine tundra hillslope. *Hydrological Processes*, 23(18), 2628–2639. <https://doi.org/10.1002/hyp.7327>

R Core Team. (2020). R: A language and environment for statistical computing (3.6.3). R Foundation for Statistical Computing. <https://www.r-project.org/>.

Ramm, E., Liu, C., Ambus, P., Butterbach-Bahl, K., Hu, B., Martikainen, P. J., Marushchak, M. E., Mueller, C. W., Rennenberg, H., Schloter, M., Siljanen, H. M. P., Voigt, C., Werner, C., Biasi, C., & Dannenmann, M. (2022). A review of the importance of mineral nitrogen cycling in the plant-soil-microbe system of permafrost-affected soils changing the paradigm. *Environmental Research Letters*, 17(1), 13004. <https://doi.org/10.1088/1748-9326/ac417e>

Rantanen, M., Karpechko, A. Yu., Lipponen, A., Nordling, K., Hyvärinen, O., Ruosteenoja, K., Vihma, T., & Laaksonen, A. (2022). The Arctic has warmed nearly four times faster than the globe since 1979. *Communications Earth & Environment*, 3(1), 168. <https://doi.org/10.1038/s43247-022-00498-3>

Regina, K., Nykänen, H., Maljanen, M., Silvola, J., & Martikainen, P. J. (1998). Emissions of N₂O and NO and net nitrogen mineralization in a boreal forested peatland treated with different

nitrogen compounds. *Canadian Journal of Forest Research*, 28(1), 132–140.
<https://doi.org/10.1139/x97-198>

Repo, M. E., Susiluoto, S., Lind, S. E., Jokinen, S., Elsakov, V., Biasi, C., Virtanen, T., & Martikainen, P. J. (2009). Large N₂O emissions from cryoturbated peat soil in tundra. *Nature Geoscience*, 2(3), 189–192. <https://doi.org/10.1038/ngeo434>

Roman-Perez, C. C., Hernandez-Ramirez, G., Kryzanowski, L., Puurveen, D., & Lohstraeter, G. (2021). Greenhouse gas emissions, nitrogen dynamics and barley productivity as impacted by biosolids applications. *Agriculture, Ecosystems and Environment*, 320. <https://doi.org/10.1016/j.agee.2021.107577>

Salmon, V. G., Schädel, C., Bracho, R., Pegoraro, E., Celis, G., Mauritz, M., Mack, M. C., & Schuur, E. A. G. (2018). Adding Depth to Our Understanding of Nitrogen Dynamics in Permafrost Soils. *Journal of Geophysical Research: Biogeosciences*, 123(8), 2497–2512. <https://doi.org/10.1029/2018JG004518>

Schlesinger, W. H. (2013). An estimate of the global sink for nitrous oxide in soils. *Global Change Biology*, 19(10), 2929–2931. <https://doi.org/10.1111/gcb.12239>

Schuur, E. A. G., Abbott, B. W., Bowden, W. B., Brovkin, V., Camill, P., Canadell, J. G., Chanton, J. P., Chapin, F. S., Christensen, T. R., Ciais, P., Crosby, B. T., Czimczik, C. I., Grosse, G., Harden, J., Hayes, D. J., Hugelius, G., Jastrow, J. D., Jones, J. B., Kleinen, T., ... Zimov, S. A. (2013). Expert assessment of vulnerability of permafrost carbon to climate change. *Climatic Change*, 119(2), 359–374. <https://doi.org/10.1007/s10584-013-0730-7>

Schuur, E. A. G., McGuire, A. D., Schädel, C., Grosse, G., Harden, J. W., Hayes, D. J., Hugelius, G., Koven, C. D., Kuhry, P., Lawrence, D. M., Natali, S. M., Olefeldt, D., Romanovsky, V. E., Schaefer, K., Turetsky, M. R., Treat, C. C., & Vonk, J. E. (2015). Climate change and the permafrost carbon feedback. *Nature*, 520(7546), 171–179. <https://doi.org/10.1038/nature14338>

Sharifi, M., Lynch, D. H., Zebarth, B. J., Zheng, Z., & Martin, R. C. (2009). Evaluation of Nitrogen Supply Rate Measured by in situ Placement of Plant Root Simulator™ Probes as a

Predictor of Nitrogen Supply from Soil and Organic Amendments in Potato Crop. *American Journal of Potato Research*, 86(5), 356–366. <https://doi.org/10.1007/s12230-009-9090-2>

Siljanen, H. M. P., Welti, N., Voigt, C., Heiskanen, J., Biasi, C., & Martikainen, P. J. (2020). Atmospheric impact of nitrous oxide uptake by boreal forest soils can be comparable to that of methane uptake. *Plant and Soil*, 454(1), 121–138. <https://doi.org/10.1007/s11104-020-04638-6>

Soued, C., del Giorgio, P. A., & Maranger, R. (2016). Nitrous oxide sinks and emissions in boreal aquatic networks in Québec. *Nature Geoscience*, 9(2), 116–120. <https://doi.org/10.1038/ngeo2611>

Subke, J.-A., Kutzbach, L., & Risk, D. (2021). Soil Chamber Measurements. In T. Foken (Ed.), *Springer Handbook of Atmospheric Measurements* (pp. 1603–1624). Springer International Publishing. https://doi.org/10.1007/978-3-030-52171-4_60

Sun, X., Wang, H., Song, C., Jin, X., Richardson, C. J., & Cai, T. (2021). Response of Methane and Nitrous Oxide Emissions from Peatlands to Permafrost Thawing in Xiaoxing'an Mountains, Northeast China. *Atmosphere*, 12(2). <https://doi.org/10.3390/atmos12020222>

Takatsu, Y., Miyamoto, T., Tahvanainen, T., & Hashidoko, Y. (2022). Nitrous Oxide Emission in Response to pH from Degrading Palsa Mire Peat Due to Permafrost Thawing. *Current Microbiology*, 79(2), 56. <https://doi.org/10.1007/s00284-021-02690-8>

Thompson, L. M., Olefeldt, D., Mangal, V., & Knorr, K. H. (2022). Soil and porewater chemistry from peatlands of the Interior Plains, Northwestern Canada (dataset). University of Alberta Education & Research Archive. <https://doi.org/10.7939/r3-vp5e-aj53>

Thompson L.M., Kuhn M.A., Winder J.C., Braga L.P.P., Hutchins R.H.S., Tanentzap A.J., St. Louis V.L., & Olefeldt D. (2023). Controls on methylmercury concentrations in lakes and streams of peatland-rich catchments along a 1700 km permafrost gradient. *Limnology & Oceanography*. <https://doi.org/10.1002/lno.12296>

Treat, C. C., Jones, M. C., Camill, P., Gallego-Sala, A., Garneau, M., Harden, J. W., Hugelius, G., Klein, E. S., Kokfelt, U., Kuhry, P., Loisel, J., Mathijssen, P. J. H., O'Donnell, J. A., Oksanen, P. O., Ronkainen, T. M., Sannel, A. B. K., Talbot, J., Tarnocai, C., & Väiliranta, M.

(2016). Effects of permafrost aggradation on peat properties as determined from a pan-Arctic synthesis of plant macrofossils. *Journal of Geophysical Research: Biogeosciences*, 121(1), 78–94. <https://doi.org/10.1002/2015JG003061>

Turetsky, M. R., Abbott, B. W., Jones, M. C., Anthony, K. W., Olefeldt, D., Schuur, E. A. G., Grosse, G., Kuhry, P., Hugelius, G., Koven, C., Lawrence, D. M., Gibson, C., Sannel, A. B. K., & McGuire, A. D. (2020). Carbon release through abrupt permafrost thaw. *Nature Geoscience*, 13(2), 138–143. <https://doi.org/10.1038/s41561-019-0526-0>

Turetsky, M. R., Kane, E. S., Harden, J. W., Ottmar, R. D., Manies, K. L., Hoy, E., & Kasischke, E. S. (2011). Recent acceleration of biomass burning and carbon losses in Alaskan forests and peatlands. *Nature Geoscience*, 4(1), 27–31. <https://doi.org/10.1038/ngeo1027>

Voigt, C., Lamprecht, R. E., Marushchak, M. E., Lind, S. E., Novakovskiy, A., Aurela, M., Martikainen, P. J., & Biasi, C. (2017). Warming of subarctic tundra increases emissions of all three important greenhouse gases – carbon dioxide, methane, and nitrous oxide. *Global Change Biology*, 23(8), 2929–3432. <https://doi.org/10.1111/gcb.13563>

Voigt, C., Marushchak, M. E., Abbott, B. W., Biasi, C., Elberling, B., Siciliano, S. D., Sonntag, O., Stewart, K. J., Yang, Y., & Martikainen, P. J. (2020). Nitrous oxide emissions from permafrost-affected soils. *Nature Reviews Earth and Environment*, 1(8), 420–434. <https://doi.org/10.1038/s43017-020-0063-9>

Voigt, C., Marushchak, M. E., Lamprecht, R. E., Jackowicz-Korczyński, M., Lindgren, A., Mastepanov, M., Granlund, L., Christensen, T. R., Tahvanainen, T., Martikainen, P. J., & Biasi, C. (2017). Increased nitrous oxide emissions from Arctic peatlands after permafrost thaw. *Proceedings of the National Academy of Sciences of the United States of America*, 114(24), 6238–6243. <https://doi.org/10.1073/pnas.1702902114>

Voigt, C., Marushchak, M. E., Mastepanov, M., Lamprecht, R. E., Christensen, T. R., Dorodnikov, M., Jackowicz-Korczyński, M., Lindgren, A., Lohila, A., Nykänen, H., Oinonen, M., Oksanen, T., Palonen, V., Treat, C. C., Martikainen, P. J., & Biasi, C. (2019). Ecosystem carbon response of an Arctic peatland to simulated permafrost thaw. *Global Change Biology*, 25(5), 1746–1764. <https://doi.org/10.1111/gcb.14574>

Walker, X. J., Baltzer, J. L., Cumming, S. G., Day, N. J., Ebert, C., Goetz, S., Johnstone, J. F., Potter, S., Rogers, B. M., Schuur, E. A. G., Turetsky, M. R., & Mack, M. C. (2019). Increasing wildfires threaten historic carbon sink of boreal forest soils. *Nature*, *572*(7770), 520–523. <https://doi.org/10.1038/s41586-019-1474-y>

Walker, X. J., Rogers, B. M., Veraverbeke, S., Johnstone, J. F., Baltzer, J. L., Barrett, K., Bourgeau-Chavez, L., Day, N. J., de Groot, W. J., Dieleman, C. M., Goetz, S., Hoy, E., Jenkins, L. K., Kane, E. S., Parisien, M.-A., Potter, S., Schuur, E. A. G., Turetsky, M., Whitman, E., & Mack, M. C. (2020). Fuel availability not fire weather controls boreal wildfire severity and carbon emissions. *Nature Climate Change*, *10*(12), 1130–1136. <https://doi.org/10.1038/s41558-020-00920-8>

Walter Anthony, K., Schneider von Deimling, T., Nitze, I., Frohking, S., Emond, A., Daanen, R., Anthony, P., Lindgren, P., Jones, B., & Grosse, G. (2018). 21st-century modeled permafrost carbon emissions accelerated by abrupt thaw beneath lakes. *Nature Communications*. <https://doi.org/10.1038/s41467-018-05738-9>

Wang, F., Li, J., Wang, X., Zhang, W., Zou, B., Neher, D. A., & Li, Z. (2014). Nitrogen and phosphorus addition impact soil N₂O emission in a secondary tropical forest of South China. *Scientific Reports*, *4*(1), 5615. <https://doi.org/10.1038/srep05615>

Wang, M., Talbot, J., & Moore, T. R. (2018). Drainage and fertilization effects on nutrient availability in an ombrotrophic peatland. *Science of The Total Environment*, *621*, 1255–1263. <https://doi.org/10.1016/j.scitotenv.2017.10.103>

Western Ag Innovations. (2000). Plant Root Simulator™ (PRS) probes are an effective tool for measuring nutrient supplies to plant roots. <https://www.westernag.ca/innovations/publications/techupdates?view=tu&id=3>. [accessed in October 2022]

Yang, G., Peng, Y., Marushchak, M. E., Chen, Y., Wang, G., Li, F., Zhang, D., Wang, J., Yu, J., Liu, L., Qin, S., Kou, D., & Yang, Y. (2018). Magnitude and Pathways of Increased Nitrous Oxide Emissions from Uplands Following Permafrost Thaw. *Environmental Science & Technology*, *52*(16), 9162–9169. <https://doi.org/10.1021/acs.est.8b02271>

3. Permafrost extent controls landscape-scale fluxes of greenhouse gases in boreal peatlands in northwestern Canada

Abstract

Extensive peatlands in the discontinuous permafrost zone store vast amounts of carbon (C), potentially released as greenhouse gases (GHG) upon permafrost thaw with ongoing climate change. In the Taiga Plains Ecoregion in boreal western Canada, current warming rates accelerate loss of forested permafrost peat plateaus along with the expansion of treeless thermokarst wetlands, altering landscape-scale fluxes of carbon dioxide (CO₂) and methane (CH₄). However, we still lack an understanding of whether and how the extent of permafrost controls ecosystem C fluxes on a landscape-scale. In this study, we compare five years of concurrent eddy covariance measurements (2017-2022) at Scotty Creek (sporadic permafrost) and Smith Creek (discontinuous permafrost) to assess differences in net exchanges of CH₄ as well as CO₂ and its two component fluxes, gross primary productivity (GPP) and ecosystem respiration (ER). A lower extent of permafrost at the sporadic permafrost site (50% permafrost peat plateau vs. 50% permafrost-free wetland) caused significantly higher CH₄ emissions (daily means for March to November: 21.5 ± 13.7 vs. 4.38 ± 8.93 mg C m⁻² d⁻¹) throughout the year compared to the discontinuous permafrost site (80% permafrost peat plateau vs. 20% permafrost-free wetland). There, the higher proportion of permafrost peat plateaus resulted in higher GPP (1.78 ± 0.75 vs. 2.33 ± 1.06 g C m⁻² d⁻¹), and ER (1.61 ± 0.65 vs. 2.24 ± 0.89 g C m⁻² d⁻¹). The difference of $1.1 \mu\text{mol m}^{-2} \text{ s}^{-1}$ in nighttime ER led to a difference of $44.7 \text{ g C m}^{-2} \text{ yr}^{-1}$ in net CO₂ exchange between the two sites. From a net radiative GHG forcing perspective, potential CO₂ uptake following wetland expansion is offset by the enhanced CH₄ emissions. Our study suggests that climate warming and permafrost thaw will increase the CO₂ uptake while also increasing CH₄ emissions, leading to modest gains in C and increases in net radiative warming.

3.1 Introduction

Boreal forests are crucial for regulating our global climate (Bonan, 2008), contributing ~30 % of the area (Brandt et al., 2013) and ~20% to the carbon (C) sink function (Pan et al., 2011) of all forest ecosystems of the Earth (Gauthier et al., 2015). Amongst all boreal ecosystems, boreal peatland complexes have throughout the Holocene accumulated the most significant stores of soil carbon (C). This implies that boreal peatlands have been acting as C sinks for millennia, but the rate of C accumulation decreased once permafrost conditions set in (Treat et al., 2015; Yu et al., 2010). Permafrost is perennially frozen ground (S. Harris et al., 1988), which stores around $1,035 \pm 150$ Pg C near the surface across the northern circumpolar region (Hugelius et al., 2013; Schuur et al., 2022). Across the region, climate change now leads to widespread permafrost thaw, exposing soil organic matter to microbial processes (Lenton et al., 2008; Schuur et al., 2022). Microbial decomposition transforms the previously frozen C into greenhouse gases (GHG), such as carbon dioxide (CO₂) and methane (CH₄). Alternatively, warming could increase the CO₂ uptake of boreal peatlands (Mekonnen & Riley, 2023), so far often limited by cold temperatures and short growing seasons, leading to C accumulation in new peat as permafrost starts degrading (Germain Chartrand et al., 2023; Heffernan et al., 2020). Thus, the net effects of permafrost thaw and their magnitude are still unknown regarding the C balance and net radiative GHG forcing of boreal peatlands.

Both the areal extent and C sink strength of boreal peatlands underlain by permafrost are threatened by different anthropogenic and natural disturbances intensified by global warming (Foster et al., 2022; Lindgren et al., 2018; McGuire et al., 2018), such as permafrost thaw (Turetsky et al., 2020). The extent of permafrost in the landscape is categorized and has been mapped into four zones, namely continuous (>90%), discontinuous (>50-90%), sporadic (>10-50%), and isolated (<10%) (S. Gruber, 2012). Globally, permafrost ground temperature has increased by $0.29 \pm 0.12^\circ\text{C}$ measured in boreholes near the depth of zero annual amplitude, whereas discontinuous permafrost temperature has risen around $0.20 \pm 0.10^\circ\text{C}$ (Biskaborn et al., 2019). Across the boreal biome of North America, the permafrost zonation is therefore shifting rapidly (Brown et al., 2002; Tarnocai & Bockheim, 2011), albeit over different timescales depending on both the soil landscape (Jorgenson et al., 2013) and the rate of warming (Bush et al., 2019).

Northwestern Canada is currently undergoing high rates of warming with consequences for the boreal peatland complexes, their permafrost extent and resulting landcover composition (Bush et al., 2019; Foster et al., 2022; Helbig, Pappas, et al., 2016). In northwestern Canada, the Taiga Plains ecoregion is the third largest peatland area of the circumpolar region after the West Siberian Lowlands and the Hudson Bay lowlands and is situated near the southern limit of permafrost, ranging in permafrost extent from sporadic to discontinuous (Zoltai & Tarnocai, 1975). In the boreal peatland complexes in the Taiga Plains, permafrost aggregation elevated peat plateaus above the surrounding permafrost-free wetland landscape (Robinson & Moore, 2000). Near the southern limit of permafrost, amplified climate change is now largely shrinking the permafrost extent of the peatland complexes, often resulting in thaw-induced thermokarst wetland expansion (Helbig, Pappas, et al., 2016; Wright et al., 2022). Consequently, peat plateaus underlain by permafrost are replaced by thermokarst lakes and permafrost-free wetlands (Quinton et al., 2009), at recent loss rates of 0.58% per year at the sporadic permafrost site Scotty Creek (Chasmer & Hopkinson, 2017). We currently lack understanding of the consequences of these landscape-wide transitions as recently thawed peatlands could differ in their net GHG exchange and C balances from their non-permafrost equivalents south of the permafrost boundary.

The loss of permafrost could alter the landscape C balance and net radiative GHG forcing, mostly determined by fluxes of potent GHGs such as CO₂ and CH₄ (Frolking et al., 2011). Land cover types of boreal peatland complexes with permafrost largely differ from such without permafrost, particularly in their vegetation and moisture conditions (Carpino et al., 2018). While peat plateaus are forested and usually dry, the surrounding, lower parts of the landscape are treeless and have saturated soil profiles (Baltzer et al., 2014). Wetlands are known sources of CH₄ due to saturated soils (Olefeldt et al., 2017; Perryman et al., 2020) and can turn into emission hot spots after land subsidence following permafrost thaw (Abbott & Jones, 2015; Elder et al., 2021). Climate change thus enhances CH₄ emissions by expansion of thermokarst wetlands (Helbig, Chasmer, Kljun, et al., 2017; Treat et al., 2021). In summary, the peatland landcover can be broadly divided into two ecosystem types, i.e., peat plateaus with permafrost and wetlands without permafrost both with distinct net CO₂ and CH₄ exchange. The ongoing shift towards more wetlands is an indirect effect of climate change on land surface-atmosphere

interactions including fluxes of CO₂ and CH₄ on a landscape-scale (Helbig, Chasmer, Desai, et al., 2017).

Climate change also alters ecosystem fluxes of CO₂ and CH₄ directly, as some environmental variables are altered (Beer et al., 2010; Desai et al., 2008), e.g. increasing air and soil temperature result in immediate ecosystem reactions to the changing environment (Helbig, Chasmer, Desai, et al., 2017; Richardson et al., 2013; Schuur et al., 2007). Consequently, longer growing seasons driven by higher air temperatures might lead to extended CO₂ uptake due to decreased temperature-limitation of CO₂ uptake during the shoulder seasons (Helbig, Chasmer, Desai, et al., 2017). However, overall net CO₂ losses of northern ecosystems were observed in response to autumn warming and higher decomposition rates (Piao et al., 2008). Furthermore, warmer air and soil temperatures during shoulder seasons could also increase annual CH₄ emissions by up to 30% in saturated wetland soils (Helbig, Quinton, et al., 2017). In conclusion, the overall landscape C and net radiative GHG forcing are affected by both direct and indirect effects of climate change, the first driven by altered environmental variables and the latter being determined by the area ratio of permafrost vs. non-permafrost landcover. There is a strong need for research approaches accounting for both direct and indirect effects of climate change at ecosystem-scale.

Continuous long-term and year-round measurements are needed to capture ecosystem responses to environmental changes under a warming climate (Baldocchi, 2020). At ecosystem-scale, the eddy covariance method is used to measure gaseous fluxes of C (CO₂ and CH₄) and water (H₂O) continuously and with high-frequency, supported by measurements of biometeorological variables (Aubinet et al., 1999; Baldocchi, 2003). Biometeorological variables are crucial to derive biogeophysical characteristics, such as albedo and net radiation (e.g., Rohatyn et al., 2023), that determine the net radiative balance together with the water fluxes, namely sensible heat (H) and latent heat (LE), and C fluxes. In addition, the C fluxes also affect the net ecosystem C balance (NECB) (Chapin et al., 2006), that also requires water monitoring efforts to estimate the downstream export of dissolved organic carbon (Olefeldt & Roulet, 2012). There are only a few studies (e.g., Arias-Ortiz et al., 2021; Dinsmore et al., 2010) that consider net exchanges of CH₄ and CO₂ with implications for both the net radiative GHG forcing and NECB.

Net CO₂ exchange is controlled by its component fluxes, gross primary production (GPP) and ecosystem respiration (ER), which also depend on various environmental variables; many of them directly impacted by climate change. Effects of environmental variables on the ecosystem-scale component fluxes are often investigated by multi-site-comparison approaches and differentiate between abiotic variables, such as photosynthetic active photon flux density (PPFD), water table depths, air temperature, growing season length, and vapor pressure deficit (VPD) (Evans et al., 2021; Lindroth et al., 2007; Lund et al., 2010) as well as biotic variables, such as aboveground biomass and leaf area index (LAI) (Humphreys et al., 2006). In a multi-site comparison study, ER and GPP followed the latitude due to limited PPFD in northern latitudes so that with the southernmost site had the highest rates for GPP and ER (Lindroth et al., 2007). As permafrost extent also follows a north-south gradient, this would suggest for our study region that GPP and ER are higher at sites further south with less permafrost in the landscape. However, many of the multi-site comparison studies only included peatland sites without permafrost or did not account for different extents of permafrost in the boreal peatland complexes. Hence, we still require a better understanding of how different extents of permafrost affect the component fluxes of net CO₂ exchange.

In addition to multi-site-approaches, there are studies at local scales that have compared ecosystems with permafrost against non-permafrost ecosystems at one boreal peatland complex (e.g., Euskirchen et al., 2024; Helbig, Chasmer, Desai, et al., 2017; Johansson et al., 2006). Only a few studies however have been able to address both permafrost thaw and temperature in the same study. Upon thaw, bogs had similar NEE rates and higher CH₄ emissions than the overall wetland-forest landscape, shown by nested eddy covariance data from the sporadic permafrost site, Scotty Creek (Helbig, Chasmer, Desai, et al., 2017; Helbig, Chasmer, Kljun, et al., 2017). But larger GPP and ER on the landscape than on the thermokarst wetland scale suggest that warming itself affected peat landscape's NEE more than the indirect effects of wetland expansion (Helbig, Chasmer, Desai, et al., 2017). Warmer climate could increase the CO₂ sink function of fen and bog ecosystems, if not affected by droughts (Helbig et al., 2022). From a net radiative perspective, their increased CH₄ emissions could potentially outweigh the cooling effects of CO₂ uptake by higher rates of net ecosystem production rates (Fofana et al., 2022; Helbig, Chasmer, Desai, et al., 2017; Schuur et al., 2022). Thus, the future net radiative GHG forcing and NECB of peatland complexes depend on both the individual net exchange of CO₂

and CH₄ of those specific permafrost and non-permafrost landforms and their abundance in the landscape. Studies comparing two sites with different permafrost extents are still sparse as often situated in inaccessible, remote locations.

Using concurrent eddy covariance and supporting measurements made over two thawing boreal peatland complexes ca. 300 km apart from each other, we examined their net C ecosystem exchanges between 2017 and 2022. The two peatland complexes, Scotty Creek and Smith Creek, were characterized by high and low proportions of thermokarst wetlands, respectively. Situated in the sporadic (Scotty Creek) and discontinuous (Smith Creek) permafrost zones of the southern Taiga Plains ecoregion, the resulting differences in landscape heterogeneity expressed as wetland-to-forest ratio were assumed to broadly reflect latitudinal differences in permafrost conditions (e.g., areal extent, temperature, active layer thickness). The goal was to shed light on how landscape heterogeneity due to latitudinal permafrost zonation affected surface-atmosphere interactions near the southern limit of permafrost distribution in western Canada. To meet this goal, our objectives were to a) compare diurnal and seasonal patterns in half-hourly and daily CO₂ and CH₄ fluxes, and to b) compare the NECB and the net radiative GHG forcing of two boreal peatland complexes with different extents of permafrost.

3.2 Materials and methods

3.2.1 Study Sites

This study compares two peatland sites within the Taiga Plains ecoregion (Ecoregion 3.3 according to United States Environmental Protection Agencies' Level II Ecoregions of North America) in the Northwest Territories, Canada; Scotty Creek (61.30°N, 121.30°W, AmeriFlux-ID: CA-SCC) and Smith Creek (63.15°N, 123.25°W, AmeriFlux-ID: CA-SMC) (Figure 3.1). The climate is subarctic and currently experiencing a period of rapid warming since the mid-1990s (Quinton et al., 2019). Peatlands are the dominating landform in the Taiga Plains ecoregion wherever flat, fine-grained lacustrine deposits prevent effective drainage in contrast to the till areas of the region which more often support upland forests. In the Taiga Plains, peatlands often include permafrost whose thaw drives the expansion of thermokarst wetlands along with the loss of peat plateaus (Wright et al., 2022).

Scotty Creek is part of the sporadic permafrost zone with a slightly warmer mean annual air temperature of -2.4°C and 379 mm of annual precipitation than Smith Creek with -3.7°C and 341 mm (climate normal 1991-2020; T. Wang et al., 2016) which is part of the discontinuous permafrost zone with (S. Gruber, 2012). Thus, more than half of the Smith Creek landscape (~80%) still contains permafrost, found in elevated peat plateaus forested by black spruce (*Picea mariana*) and few tamaracks (*Larix laricina*). The remaining landcover is without permafrost and consists of non-treed wetlands such as thermokarst bogs and channel fens. These wetter landforms are dominated by hydrophilic vegetation, such as *Sphagnum* mosses in the bogs and sedges and shrubs in the fens (Quinton et al., 2009). Both sites have shallow (<3 m deep) peatland ponds with organic-rich sediments found within 300 m from the towers.

The major difference between the two peatland complexes is given by the different extents of permafrost, governing landscape and vegetation composition; there are however further site-specific characteristics in the fetch area of both towers. While both sites have coarse-grained lacustrine deposits derived from limestone/dolomite bedrock, they were only part of the footprint of one eddy covariance tower, that is CA-SMC at Smith Creek (Figure 3.1). These few locations are sandy outwash moraines originating from the glacial retreat, on which the peat is thin or absent and the trees are taller and include white spruce (*Picea glauca*) and aspen (*Populus*

tremuloides) ('Upland Moraine' in Figure 3.1). Overall, Smith Creek has a shallower peat depth with ~ 150 cm compared to ~330 cm at Scotty Creek. We also observed differences in ground cover, with more extensive lichens at Smith Creek compared to more widespread *Sphagnum* hummocks and dense woody shrubs at the Scotty Creek plateaus.

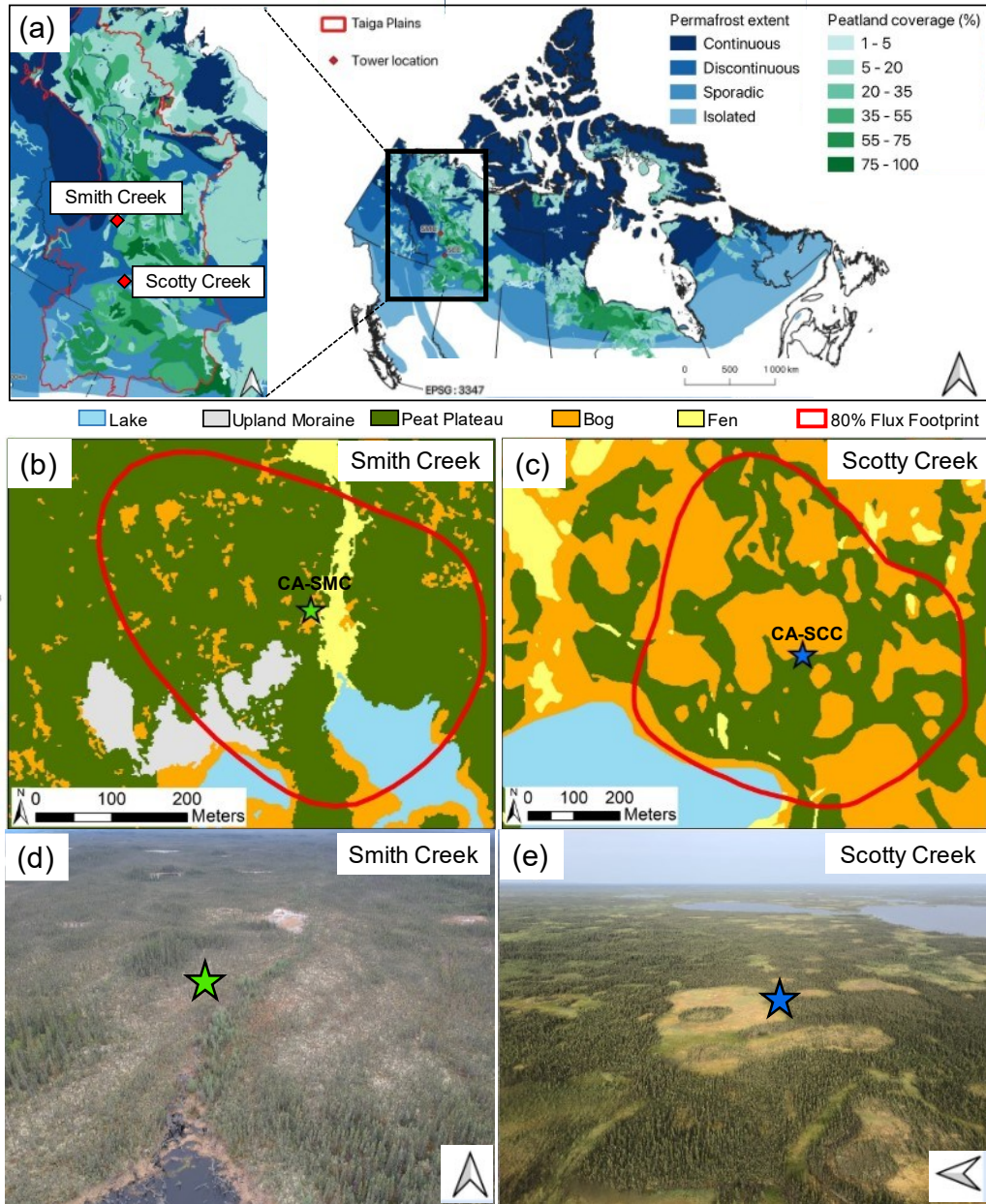


Figure 3.1: Boreal peat landscapes in the discontinuous and sporadic permafrost zones near the southern limit of permafrost in the Taiga Plains ecoregion of western Canada: (a) Map including both sites, peatland cover (Hugelius et al., 2013) and permafrost zonation (S. Gruber, 2012). (b, c) landcover maps including 80% flux footprints (red polygons) and (d, e) drone images of the landscape around the eddy covariance towers (b, d) at Smith Creek (AmeriFlux-ID: CA-SMC, tower location indicated by green star) and (c, e) at Scotty Creek (AmeriFlux-ID: CA-SCC, tower location indicated by blue star), respectively.

3.2.2 Eddy Covariance Measurements

We used the eddy covariance technique to measure vertical turbulence fluxes above the tree canopy. Two eddy covariance landscape towers have been set up at Scotty Creek (running since April 2013) and Smith Creek (running since July 2017). Our datasets included concurrent measurements at both sites from 8 July 2017 to 21 September 2022. The measurement height is 15.2 m at Scotty Creek and 14.9 m at Smith Creek, respectively. High-frequency fluctuations in wind velocities were measured by three-dimensional sonic anemometers (CSAT3A, Campbell Scientific, Logan, UT). High-frequency variations in gas concentrations of CO₂ and H₂O were measured by infrared gas analyzers, a LI-7200 with an enclosed path at Smith Creek (LI-COR Biosciences, Lincoln, NE) and an open-path EC150 at CA-SCC (EC150; Campbell Scientific). A previous study compared the open-path sensor (EC150) to one with an enclosed path (LI-7200) at Scotty Creek combined with the same CSAT3A and only found minor differences in net CO₂ fluxes (<5% and 8% for cumulative) (Helbig, Wischnewski, Gosselin, et al., 2016). CH₄ concentrations were measured at both sites using a fast-response open-path methane analyzer (LI-7700, LI-COR Biosciences) with mirror heating and washing. At both sites, high frequency (all instruments at 10 Hz) data were recorded and stored using a Campbell CR 3000 datalogger (Campbell Scientific).

3.2.3 Supporting Measurements

The additional instrumentation measuring biometeorological variables at the CA-SCC tower has already been described elsewhere (Helbig, Wischnewski, Kljun, et al., 2016). At both sites, air temperature and pressure as well as relative humidity (RH) were measured at 2 m and 15 m above the ground, respectively (HMP45C, Vaisala, Helsinki, Finland). An additional wind sensor (R.M. Young 05103 Wind Monitor, Traverse City, MI) recorded wind direction and windspeed. Ground heat flux was measured with four heat flux plates (HFP01, Hukseflux Thermal Sensors, Delft, the Netherlands) at each site; two replicates placed in peat plateau hollows and two in plateau hummocks. Also installed in both hollows and hummocks, soil water content reflectometers (CS616, Campbell Scientific) recorded soil water content in 10, 20, and 30 cm depth and soil thermocouple probes (TCAV, Campbell Scientific) measured soil temperatures at depths of 5, 10, 20, 30, 40, 50, 60, and 70 cm. Four-component net radiometers (CNRX, Kipp & Zonen, Delft, the Netherlands) were installed at south-facing poles to measure incoming and

outcoming radiation at the height of 13.44 m at CA-SCC and at 13.25 m at CA-SMC, respectively. Precipitation was recorded by tipping buckets (TE525WS-L, Campbell Scientific) and a rain gauge (OTT Pluvio, OTT HydroMet GmbH, Germany). Snow depth was measured by an ultrasonic distance sensor (SR50, Campbell Scientific). All of the above-described environmental data were stored as 30-min averages in two CR3000 dataloggers per site (Campbell Scientific).

Leaf Area Index (LAI) measurements were carried out along four 100-m transects in four cardinal directions centered on the eddy covariance towers on 8 and 9 September 2019 at Smith Creek and Scotty Creek, respectively. We used a LAI-2200 plant canopy analyzer (LI-COR Biosciences) to measure effective LAI of trees and shrubs separately and calculated LAI accordingly (Ryu et al., 2010; Sonnentag et al., 2007, 2008).

3.2.4 Data Processing

3.2.4.1 Eddy Covariance Data

Flux calculation and data post-processing are performed described in Helbig et al. (Helbig, Chasmer, Desai, et al., 2017; Helbig, Chasmer, Kljun, et al., 2017; Helbig, Wischnewski, Kljun, et al., 2016). Half-hourly turbulent fluxes of CO₂, LE, H, and CH₄ were calculated with the EddyPro software (version 7.0.6, LI-COR Biosciences, Lincoln, NE). The software applied double-rotation rotating the coordinate system of the sonic anemometer (Wilczak et al., 2001) and the spike removal within the high-frequency flux data (Vickers & Mahrt, 1997). Furthermore, the software corrected both CO₂ and LE fluxes for spectral attenuation (Moncrieff et al., 1997; 2004), effects of humidity (Van Dijk et al., 2004), and air density fluctuations (Webb et al., 1980).

Further data operations were done in the Matlab computing environment (version R2020b, The MathWorks, Natick, MA) by the Laboratory in Atmospheric Biogeosciences in high latitudes (ATMOSBIOS, Université de Montréal, Montréal, QC). The three-class quality flag system was used to filter poor quality data (data flagged >1) (Mauder & Foken, 2011). Further post-processing including filtering of the datasets followed Papale et al. (2006) and Reichstein et al. (2005), where friction velocity thresholds were set to 0.1 m s⁻¹ for both sites to not underestimate CO₂ emissions during low-turbulence periods at night (Falge et al., 2001; Gu et al., 2005; Papale

et al., 2006). Over the entire study period, 53% (daytime: 43%; nighttime: 64%) and 36% (daytime: 27%; nighttime: 49%) of measured NEE were discarded due to low quality at Scotty Creek and Smith Creek, respectively. NEE gapfilling used the marginal distribution sampling method by Reichstein et al. (2005) and included the variables SWin, air temperature, and VPD. Data coverage for NEE after gapfilling was 73% for the Scotty Creek data and 51% for the Smith Creek data. Regarding CH₄, 70% and 48% of measured CH₄ fluxes at Scotty Creek and Smith Creek did not pass the quality control and were replaced by CH₄ gapfilling using a marginal distribution sampling algorithm (Reichstein et al., 2005). After gapfilling, half hourly CH₄ data was available for 67% and 50% of the overall study period at Scotty Creek and Smith Creek, respectively.

Positive NEE and CH₄ fluxes represent net losses of CO₂ and CH₄ from the ecosystem and negative fluxes indicate uptake of CO₂ and CH₄, respectively. All turbulent fluxes were corrected with their corresponding storage fluxes to arrive at the final half-hour flux values. We further ensured comparability of flux measurements of the two sites by investigating the energy balance closure for the months June and July. After removal of fluxes of H and LE fluxes with low quality flags (flagged >0), energy balance closure was 0.70 for Scotty Creek and 0.73 for Smith Creek, respectively (Figure A3.1). Helbig, Wischnewski, Kljun, et al. (2016) previously reported 0.79 at Scotty Creek and other wetlands sites were within a similar range, i.e., 0.76 ± 0.13 (Stoy et al., 2013).

3.2.4.2 Partitioning Net Ecosystem Exchange into Component Fluxes

Partitioning of NEE into GPP and ER made use of ER modelling following nighttime temperature regression models (Reichstein et al., 2005; Runkle et al., 2013). Nighttime was determined by incoming shortwave radiation (SWin) <20 W m⁻². In addition, we derived the model parameters of a Michaelis-Menten curve applying the r-package ‘nlme’ (Pinheiro et al., 2023) and the following formula (Baird et al., 2019):

$$NEE = \frac{GPP_{max} \times PPF D}{k + PPF D} + R_T$$

The theoretical maximum GPP (GPP_{max}) can be thought of as the asymptotic limit whereas k is referred to as the half saturation constant which determines the rate approaching GPP_{max} . R_T was assumed to be constant and associated with ER (Baird et al., 2019). The model considered ‘Year’

as a random factor so that all data of different years were compiled in two-week moving data frames for each calendar week (i.e., week 35.5 included data from week 35 and 36 of the years 2017-2022) which yielded more robust trends than one-week-data frames. Only NEE measurements meeting the highest quality (data flagged =0) were included in the data frames described above.

3.2.4.3 Annual Balances and Sustained Global Warming/Cooling Potential

Data gaps from both sites precluded the estimation of cumulative annual fluxes for individual years (Figure A3.2). Hence, to compare the GHG fluxes for the two sites, we calculated generalized annual flux datasets. These datasets were created by averaging all flux variables for each half hour period of the year separately ($n = 0-6$), creating generalized annual datasets. In this way, we reduced the daily and half-hourly variability due to different environmental conditions in different years and overcame long data gaps. Similarly, generalized annual datasets for environmental variables were calculated in the same way, including for air temperature, rainfall, PPFD, VPD, RH, SWin.

Due to the lack of power supply in winter, CA-SMC had no available data from 16 November to 9 February in any of the measurement years. To fill this gap and arrive at an annual balance, we averaged adjacent days of the generalized mean dataset from 1) November for early winter (to the end of the calendar year) and 2) from February for late winter (starting from the beginning of the calendar year) and compared it against modeled literature values. Our values for early ($0.31 \text{ g C m}^{-2} \text{ yr}^{-1}$) and late ($0.14 \text{ g C m}^{-2} \text{ yr}^{-1}$) winter NEE were in a similar range than modelled CO_2 losses (boreal: $0.07 \pm 0.5 \text{ g C m}^{-2} \text{ yr}^{-1}$; Watts et al., 2021) and differences between the sites were minor during winter. The cumulated differences for this time period between the two sites were 2.0 g C m^{-2} for CO_2 and 0.9 g C m^{-2} for CH_4 , respectively, and thus negligible compared to the overall difference in the annual carbon balance (44.7 g C m^{-2}). To contrast the net radiative GHG forcing effects of CO_2 and CH_4 in CO_2 -equivalents, we applied the sustained global warming potentials (SGWP) and sustained global cooling potentials (SGCP) for a 100-year time span based on Neubauer & Megonigal (2015, 2019).

3.2.5 Landcover Classification and Footprint Modeling

The Lidar data were collected at Scotty Creek and at Smith Creek in 2017 (Teledyne Optech Inc. Titan multi-spectral airborne lidar). Data were classified into ground and non-ground returns, followed by the derivation of structural and topographic data products, including a digital elevation model and a canopy height model at 2 m spatial resolution. Laser return intensity in three wavelengths (average for all returns) was interpolated across three laser wavelengths: green (532 nm), near infrared (1064 nm), and shortwave infrared (1550 nm) for differentiation of moss species and moisture characteristics found within bogs vs. fens in lieu of Worldview-2 data (which were not available in 2017). Additional data derivatives were also developed from the lidar data products, including slope, aspect, curvature, and topographic position index (100 m radius), which together are used to identify topographically elevated areas from depressions and the location at which flat peatlands increase in elevation to form plateaus. Vegetation structural metrics, including canopy height, are used to identify forests on plateaus, shrubs, and open areas characteristic of plateaus, transition zones, and areas of drying/shrub encroachment at both sites.

The data derivatives were then ingested into a hierarchical decision tree classification described in Chasmer et al. (2014). This provides an opportunity to mimic the methods associated with a landcover classification over the Scotty Creek watershed in 2010, applied to data collected in 2017 at Scotty Creek and Smith Creek to ensure similarity in procedures and for the purpose of area-based change detection. The landcover classification derived using this method consists of five different landcover types, including ‘lake’, ‘upland moraine’, ‘peat plateau’, ‘fen’, and ‘bog’. Based on these data products, we derived our landcover classifications for both of our two sites. From the lidar-based land cover classification at Scotty Creek and Smith Creek in 2017, landcover classes were then reclassified into new classes appropriate for this study using ArcGIS (version 10.8.2, ESRI, Redlands, CA). These were based on our knowledge from site visits. The landcover classifications were used as inputs to a footprint model to determine the origin of the fluxes within the peatland landscape.

The footprint models for both sites were based on Kljun et al. (2015) and applied to both sites, which yielded two-dimensional half-hourly flux footprints, i.e. probabilities, for the time period from 1 September 2017 to 31 July 2019. The half-hourly probabilities for each of the five landcover types (Figure 3.1) were assigned to their corresponding half-hourly flux

measurements. Input parameters such as roughness length (z_0), displacement height (d_0), wind direction, and SW_{in} for the footprint models were derived from the eddy covariance data and additional environmental variables.

3.2.6 Statistical Analyses

All statistical tests and figures were done in the R computing environment (R Core Team, 2020). There, linear regressions were done to relate peatland fluxes of CO_2 and CH_4 to air temperature at 15 m height applying the 'stat_cor' function in the 'ggpubr' package (Kassambara, 2023). The same R-package was used to apply paired Wilcoxon rank sum tests to check for significant differences between the two sites' daily averages of the generalized annual dataset which was grouped into the different meteorological seasons of the year according to the following classification: late winter (Day of Year (DOY) 1-59, Spring (DOY 60-151), early summer (DOY 152-197), late summer (DOY 198-243), fall (DOY 244-334), and early winter (DOY >335).

3.3 Results

3.3.1 Landscape Composition and Flux Footprints

The annual air temperature during the study period at Scotty Creek was -1.4°C compared to -3.5°C for Smith Creek, both warmer than their long-term climate normal. Air temperature, PPFD, and VPD were higher throughout the year at the more southern site Scotty Creek (Figure A3.3). Scotty Creek received a slightly higher PPFD (+2%) and SWin (+11%) than Smith Creek. Rainfall, however, was similar across all four seasons with an annual sum of 294 mm at Scotty Creek and 311 mm at Smith Creek, respectively, with over 60-80% of rainfall at both sites during the summer months. RH was around 4% lower throughout all four seasons at Scotty Creek than at Smith Creek, with the highest values (77% vs. 81%) during fall and winter. Soil surface temperatures measured at the peat plateaus (averaged for 10–20 cm) varied more at Scotty Creek, ranging from -6.0°C in winter to 15.2°C in summer, whereas topsoil temperatures at Smith Creek oscillated from -3.0°C in winter to 10.7°C . However, these differences in soil surface temperature were more related to measurement locations and their microtopography or depths than actual differences between sites. Deeper soil temperatures were higher at Scotty Creek except for summer but the differences were overall minor, not exceeding 1.0°C .

The 90% footprint climatology followed the extent of permafrost in the landscape so that fluxes around Smith Creek originated mostly from forested landcover forms, of which peat plateaus contributed the large major majority compared to negligible flux contributions from upland moraines. In contrast, treeless wetland form as bogs and fens contributed around two thirds of the overall landscape flux at Scotty Creek (Table 1). The peat plateaus at both sites were similar tree LAIs at the two sites (LAI_{mean} : 0.69 ± 0.20 vs. $0.63 \pm 0.17 \text{ m}^2 \text{ m}^{-2}$ at Scotty Creek and Smith Creek, respectively) with minimums and maximums in the same range. Shrub LAIs were twice as high at Scotty Creek than at Smith Creek and more variable.

Table 3.1: Comparison of characteristics for Scotty Creek and Smith Creek study sites, including land cover, leaf area index, and climate.

	Scotty Creek	Smith Creek
<i>Flux origins [probability in %]</i>		
Peat plateau	33.6	81.4
Bog	64.0	8.4
Fen	1.3	8.0
Upland moraine	0.1	1.1
Lake	1.0	1.1
<i>LAI (peat plateau) [$m^2 m^{-2}$]</i>		
Tree LAI	0.69 ± 0.20	0.63 ± 0.17
Shrub LAI	0.69 ± 0.31	0.38 ± 0.18
<i>Air temperature [$^{\circ}C$]</i>		
Annual (long term, 1991-2020) ^a	-2.4 ^a	-3.7 ^a
Annual (years of study; >95% data)	-1.4 ± 0.6 (2018-2021)	-3.5 ± 0.9 (2019-2021)
<i>Soil temperature [$^{\circ}C$] (peat plateau)</i>		
Annual average 10-20 cm	1.7 ± 0.3 (2018-2020)	1.7 ± 0.2 (2018-2020)
Annual average 60 cm	0.1 ± 0.1 (2018-2020)	-0.1 ± 0.3 (2018-2020)
<i>Precipitation [mm]</i>		
Annual (long term, 1991-2020) ^a	379 ^a	341 ^a
<i>Rainfall [mm]</i>		
Annual (years of study; >95% data)	294 ± 125 (2018-2021)	311 ± 10 (2019-2021)
<i>SWin [$W m^{-2}$]</i>		
	123 ± 10	111 ± 12
<i>PPFD [$\mu mol m^{-2} s^{-1}$]</i>		
	237 ± 17	232 ± 26

Note. Averages (mean ± standard deviation) of air temperature, soil temperature, precipitation, rainfall, incoming shortwave radiation (SWin), and photosynthetic active photon flux density (PPFD) are based on complete (coverage >95%) data years only (2019-2021)

^aT. Wang et al. (2016)

3.3.2 Seasonal Patterns of Fluxes of CH₄ and CO₂

Both CH₄ and CO₂ fluxes (including NEE, GPP, and ER) had distinct seasonal patterns, and clear differences between the two sites. Daily average NEE of the generalized annual data (NEE_{mean Mar-Oct} ± corresponding daily averaged standard deviation of generalized annual data) was more negative at Scotty Creek from March to October (NEE_{mean Mar-Oct}: -0.30 ± 0.80 g C m⁻² d⁻¹) than at Smith Creek (NEE_{mean Mar-Oct}: -0.03 ± 1.10 g C m⁻² d⁻¹). NEE during late and early winter was in a similar range at both sites, 0.21 ± 0.18 g C m⁻² d⁻¹ at Scotty Creek and 0.19 ± 0.08 g C m⁻² d⁻¹ at Smith Creek. NEE at Scotty Creek increased until DOY 182 reaching -2.01 ± 1.48 μmol C m⁻² d⁻¹, whereas NEE at Smith Creek already peaked on DOY 157 with a maximum

average daily uptake of $-1.47 \pm 0.91 \text{ g C m}^{-2} \text{ d}^{-1}$ (Figure 3.2a). Differences between the two sites' NEE occurred in late winter, early summer, late summer, and fall ($p < 0.001$) as well as in early winter ($p < 0.05$).

From spring to fall, daily averages of GPP were lower at Scotty Creek ($\text{GPP}_{\text{mean Mar-Oct}}: 1.78 \pm 0.75 \text{ g C m}^{-2} \text{ d}^{-1}$) than at Smith Creek ($\text{GPP}_{\text{mean Mar-Oct}}: 2.33 \pm 1.06 \text{ g C m}^{-2} \text{ d}^{-1}$), culminating with a maximum daily average of $5.58 \pm 1.00 \text{ g C m}^{-2} \text{ d}^{-1}$ during late summer on DOY 212 at Scotty Creek vs. $7.05 \pm 1.15 \text{ g C m}^{-2} \text{ d}^{-1}$ during early summer at Smith Creek on DOY 180 (Figure 3.2b). Early summer was the period with the most significant difference ($p < 0.001$) in GPP, whereas late summer and fall were less significant ($p < 0.05$). Daily averages of ER during spring, summer, and fall were also lower at Scotty Creek ($\text{ER}_{\text{mean Mar-Oct}}: 1.61 \pm 0.65 \text{ g C m}^{-2} \text{ d}^{-1}$) than at Smith Creek ($\text{ER}_{\text{mean Mar-Oct}}: 2.24 \pm 0.89 \text{ g C m}^{-2} \text{ d}^{-1}$). ER reached its maximum at both sites during late summer, $5.70 \pm 0.94 \text{ g C m}^{-2} \text{ d}^{-1}$ at Smith Creek and $4.80 \pm 1.70 \text{ g C m}^{-2} \text{ d}^{-1}$ at Scotty Creek, respectively (Figure 3.2c).

Late summer was also the time when differences in CH_4 emissions were highest, but differences were significant throughout the entire year except for early winter (Figure 3.2d, $p < 0.001$). Thus, Scotty Creek, with greater wetland cover, had a higher daily average CH_4 from March to October than Smith Creek, $21.5 \pm 13.7 \text{ mg C m}^{-2} \text{ d}^{-1}$ and $4.38 \pm 8.93 \text{ mg C m}^{-2} \text{ d}^{-1}$, respectively. The highest daily average emissions of CH_4 occurred during July with $70.2 \pm 24.3 \text{ mg C m}^{-2} \text{ d}^{-1}$ at Scotty Creek and $17.6 \pm 12.0 \text{ mg C m}^{-2} \text{ d}^{-1}$ at Smith Creek.

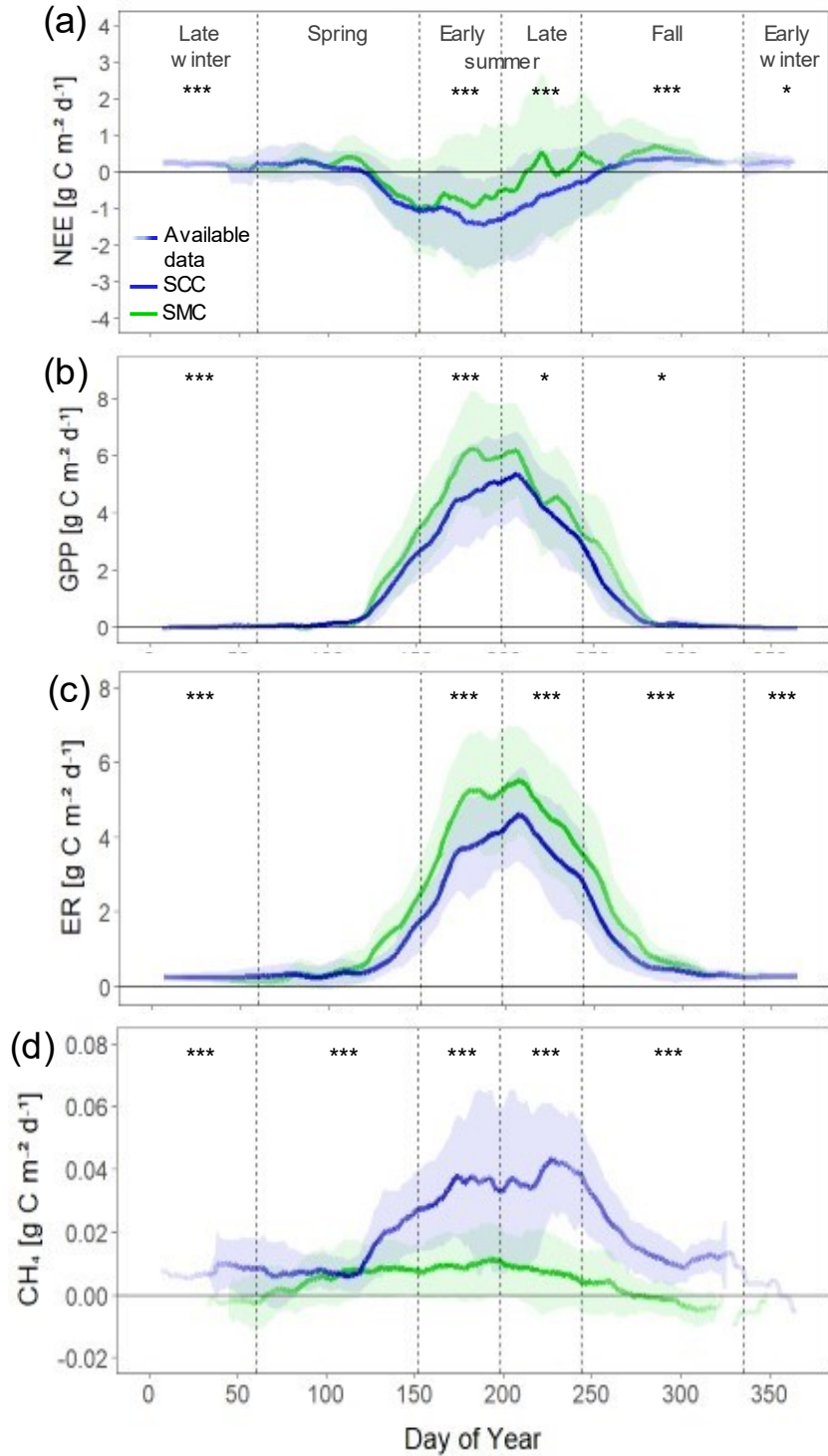


Figure 3.2: Seasonal patterns of CO₂ and CH₄ fluxes across all years (2017-2022) ± standard deviation as 14-day moving averages (a, b, c, d) of (a) net ecosystem exchange (NEE), (b) gross primary production (GPP), and (c) ecosystem respiration (ER) and (d) methane (CH₄) flux from the two eddy covariance tower sites, Scotty Creek (SCC, sporadic permafrost) and Smith Creek (SMC, discontinuous permafrost). Wilcoxon rank sum tests were applied on daily averages for each season with results portrayed by * $p < 0.05$, ** $p < 0.01$, and *** $p < 0.001$. Line intensity reflects data availability across all years (July 2017 - September 2022, n=0-6).

3.3.3 Diurnal Patterns of Fluxes of CH₄ and CO₂

Diurnal patterns of NEE were similar during winter and spring whereas most noticeable differences in NEE occurred during nighttime in late summer. The diurnal pattern showed that CO₂ release during nighttime in late summer was lower at Scotty Creek with $2.7 \pm 1.0 \mu\text{mol C m}^{-2} \text{ s}^{-1}$ compared to Smith Creek with $3.8 \pm 1.5 \mu\text{mol C m}^{-2} \text{ s}^{-1}$. The CO₂ uptake during daytime was similar with $-4.3 \mu\text{mol C m}^{-2} \text{ s}^{-1}$ (± 1.6 at Scotty Creek, ± 2.2 at Smith Creek) $\mu\text{mol C m}^{-2} \text{ s}^{-1}$ at both sites during late summer (Figure 3.3a). GPP peaked at $8.4 \pm 2.1 \mu\text{mol C m}^{-2} \text{ s}^{-1}$ at Scotty Creek compared to $9.9 \pm 2.5 \mu\text{mol C m}^{-2} \text{ s}^{-1}$ during late summer at Smith Creek, suggesting that Smith Creek had a 18% larger maximum photosynthetic capacity (Figure 3.3b). Unlike GPP and NEE, ER peaked in the afternoon (late summer: $4.8 \pm 1.5 \mu\text{mol C m}^{-2} \text{ s}^{-1}$ at Scotty Creek and at $6.3 \pm 1.5 \mu\text{mol C m}^{-2} \text{ s}^{-1}$ at Smith Creek). The site difference in daytime ER was highest during early summer whereas the difference in nighttime ER was highest during late summer (Figure 3.3c). While CH₄ emissions at Scotty Creek reached maximum on DOY 209 at $0.068 \pm 0.023 \mu\text{mol C m}^{-2} \text{ s}^{-1}$, Smith Creek reached a maximum daily average of $0.017 \pm 0.012 \mu\text{mol C m}^{-2} \text{ s}^{-1}$ on DOY 187. Scotty Creek's diurnal pattern of CH₄ flux was much less pronounced than at Smith Creek where the diurnal CH₄ flux reached a maximum of $0.027 \pm 0.016 \mu\text{mol C m}^{-2} \text{ s}^{-1}$ during afternoon in early summer (Figure 3.3d).

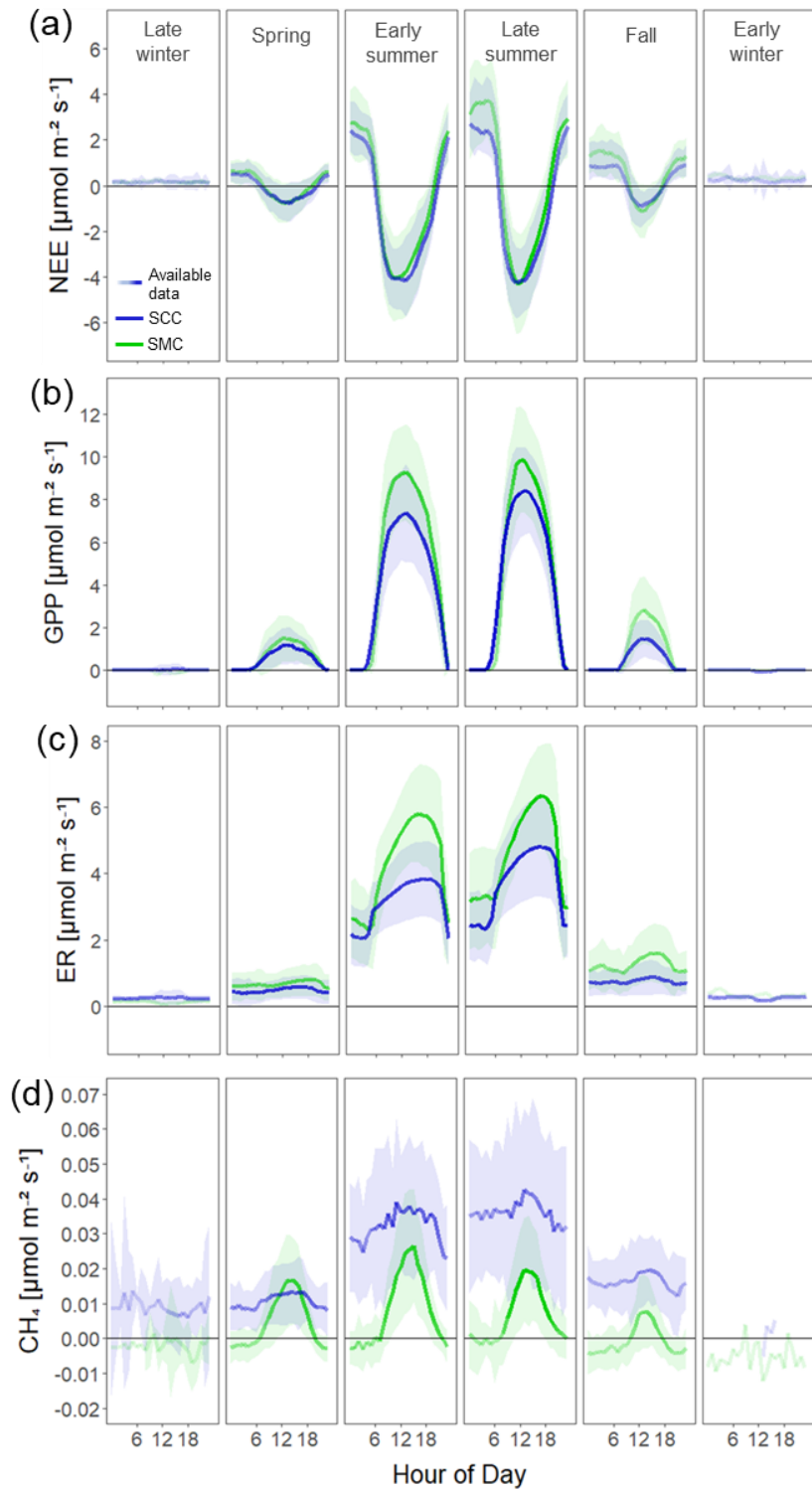


Figure 3.3: Diurnal patterns of generalized annual CO₂ and CH₄ fluxes \pm standard deviation of (a) net ecosystem exchange (NEE), (b) gross primary production (GPP), and (c) ecosystem respiration (ER) and (d) methane (CH₄) flux from the two eddy covariance tower sites, Scotty Creek (SCC, sporadic permafrost) and Smith Creek (SMC, discontinuous permafrost). Line intensity reflects data availability across all years (July 2017 - September 2022, n = 0-6).

3.3.4 Relationships between Environmental Variables and Fluxes of CH₄ and CO₂

Environmental conditions were in a similar range at the two sites regarding both air temperature and PPFD and small differences mostly followed the difference in latitude. Towards the start of the growing season, the GPP_{max} (= photosynthetic capacity when light is unlimited) only responded when average daily air temperatures were $>0^{\circ}C$ which happened concurrently at both sites (Figure 3.4a). GPP_{max} was lower at Scotty Creek with the largest between-site differences in GPP_{max} during late summer (calendar week 32). The second light response parameter k was higher at Scotty Creek almost throughout the entire growing season, i.e. vegetation at Scotty Creek needed more light to reach its photosynthetic capacity GPP_{max} (Figure 3.4b). Therefore, the two sites' ratios between observed midday GPP and GPP_{max} only diverged later in the season when Scotty Creek dropped around calendar week 35 until the end of the growing season around calendar week 42. Emissions of CH₄ increased with air temperatures at both sites, with a slightly higher temperature sensitivity at Scotty Creek (Figure 3.4c). ER increased with warmer air temperatures, with a higher respiration towards the end of the growing season compared to the start of the growing season at similar temperatures (Figure 3.4d).

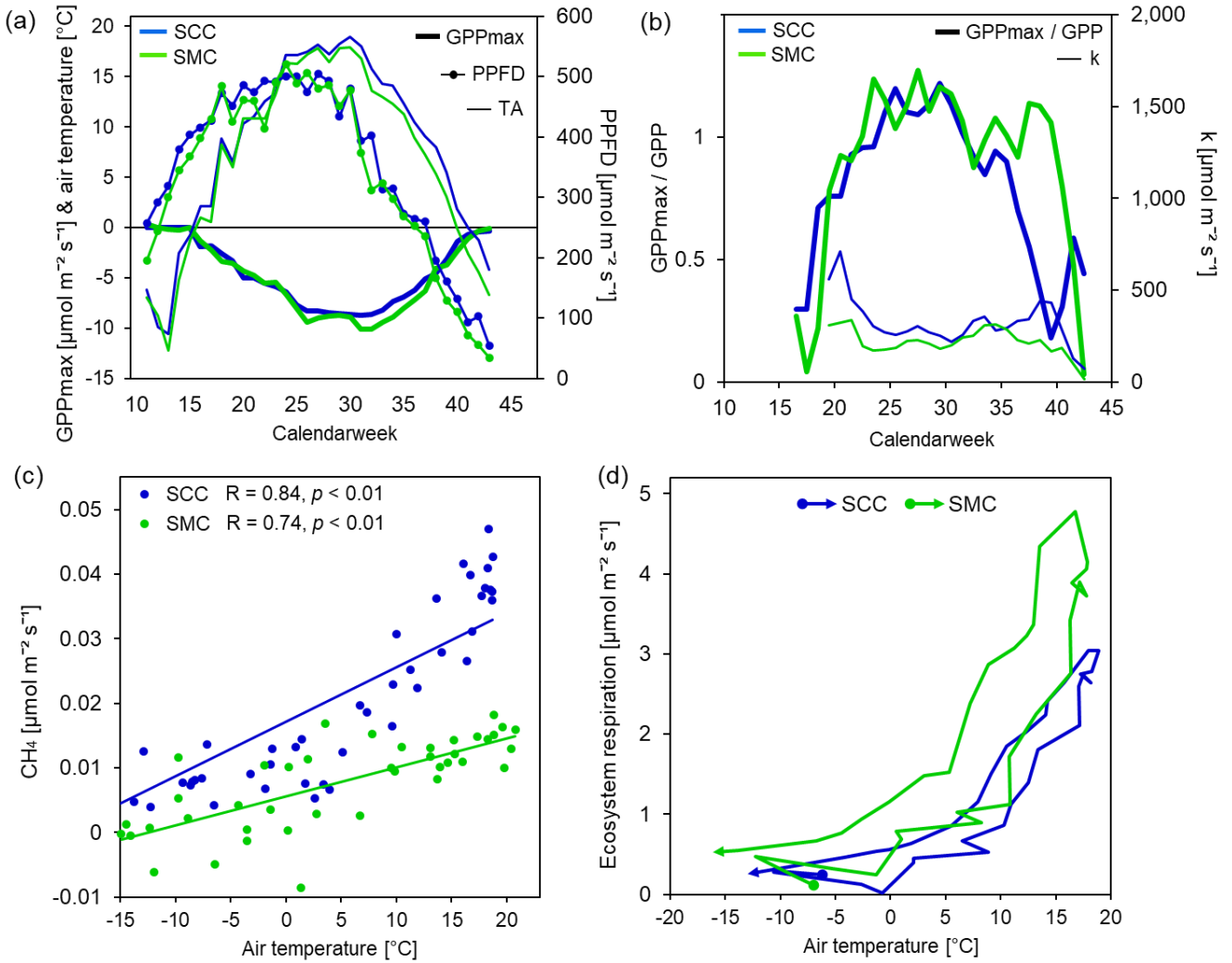


Figure 3.4: Responses of CO₂ and CH₄ fluxes at the sporadic permafrost Scotty Creek (SCC) and the discontinuous permafrost site (SMC) to changes in selected environmental variables, such as (a) photosynthetic active photon flux density (PPFD) and (b, d) air temperature (TA). All measurements were averaged for calendar weeks whereas (a, b) weekly values of light response parameters k and GPP_{max} were calculated with a moving two-week data frame.

3.3.5 Carbon Balance and Net Radiative Greenhouse Gas Forcing

The peatlands at Scotty Creek and Smith Creek had NECBs of $-16.2 \pm 12.2 \text{ g C m}^{-2} \text{ yr}^{-1}$ and $28.5 \pm 3.3 \text{ g C m}^{-2} \text{ yr}^{-1}$, respectively (Figures 3.5a and 3.5b); a difference of $44.7 \text{ g C m}^{-2} \text{ yr}^{-1}$. The largest flux for both sites' overall NECB was CO₂ ($-23.5 \pm 10.7 \text{ g C m}^{-2} \text{ yr}^{-1}$ at Scotty Creek vs. $25.8 \pm 3.1 \text{ g C m}^{-2} \text{ yr}^{-1}$ at Smith Creek), compared to C losses via CH₄ emissions ($5.9 \pm 1.3 \text{ g C m}^{-2} \text{ yr}^{-1}$ at Scotty Creek vs. $1.0 \pm 0.2 \text{ g C m}^{-2} \text{ yr}^{-1}$ at Smith Creek) and DOC export measured at the watershed outlet (1.4 ± 0.2 vs. $1.6 \pm 0.2 \text{ g C m}^{-2} \text{ yr}^{-1}$ at Scotty Creek and Smith Creek, respectively) by L. Thompson et al. (2023). The net radiative GHG forcing of both peatland

landscapes was strongly influenced by CH₄ emissions. At Scotty Creek, the net radiative warming from CH₄ flux was ~ 4 times greater (354 ± 78 g CO₂-eq. m⁻² yr⁻¹) than the cooling by CO₂ (-86 ± 39 g CO₂-eq. m⁻² yr⁻¹) (Figures 3.5c and 3.5d). At Smith Creek, CO₂ (95 ± 11 g CO₂-eq. m⁻² yr⁻¹) and CH₄ (62 ± 13 g CO₂-eq. m⁻² yr⁻¹) were in a similar range regarding their net radiative GHG forcing. Overall, both sites' net radiative GHG balances were similar (268 ± 117 vs. 157 ± 24 g CO₂-eq. m⁻² yr⁻¹ at Scotty Creek and Smith Creek, respectively).

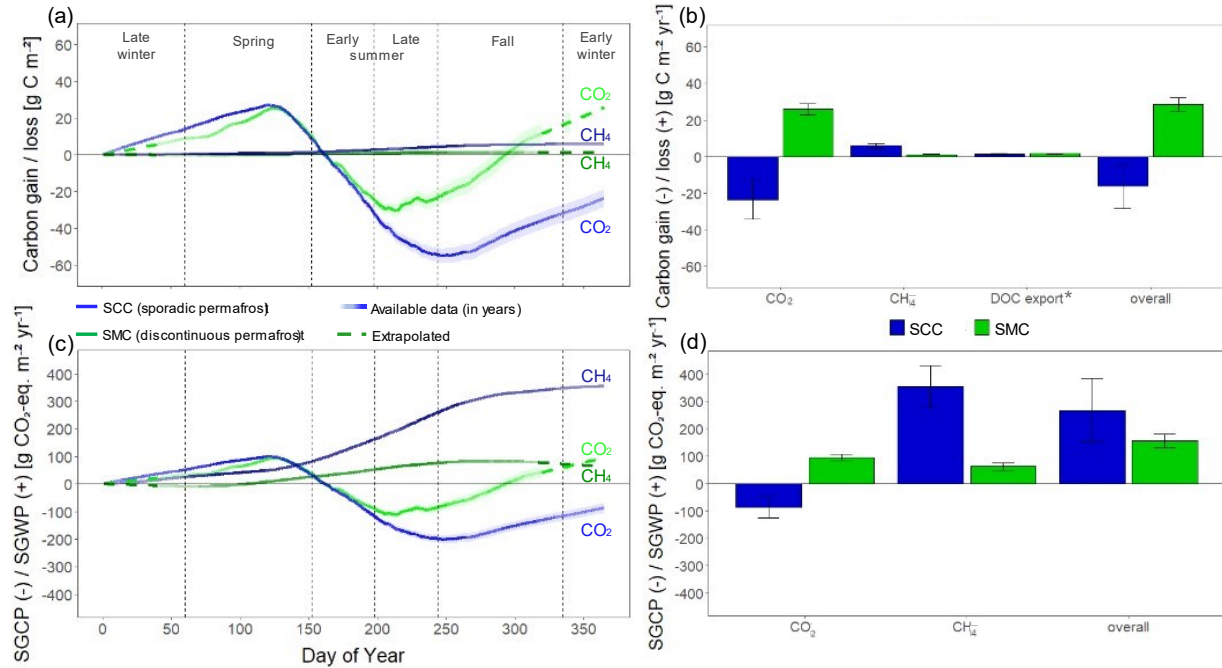


Figure 3.5: Cumulative carbon gain and loss (a, b) and net radiative greenhouse gas forcing (c, d) of carbon dioxide (CO₂) and methane (CH₄) of generalized annual data (averages of five data years, 2017-2022, for every half hour) (a, c) and as a generalized annual balance (b, d) at the two eddy covariance sites, Scotty Creek (SCC, sporadic permafrost) and Smith Creek (SMC, discontinuous permafrost). *Export of dissolved organic carbon (DOC) were measured for the years 2017 to 2019 at the watershed outflow by (L. Thompson et al., 2023). Error bars represent interannual variability as standard deviations of complete data years (2018 – 2021) only.

3.4 Discussion

We followed a space-for-time approach in this study by comparing two sites with different extents of permafrost, sporadic vs. discontinuous, in the same ecoregion with similar boreal climate and peatland vegetation. Our results suggested that the difference in permafrost extent is the main driver of site differences. In a few decades from current time, the discontinuous permafrost site will have slowly transformed into a sporadic permafrost site due to ongoing thaw as an indirect consequence of climate change (Chasmer & Hopkinson, 2017; Gibson et al., 2021). While direct effects of climate change will alter selected environmental variables, such as increasing air and soil temperatures, other variables such as PPFD will remain constant. All these environmental variables as well as different Holocene developmental histories leading to different quantity and quality of soil C will have played into our findings to a certain degree. Thus, projecting future ecosystem fluxes needs to consider the indirect effects of warming, i.e. landscape transitions following landscape-wide permafrost thaw along with wetland extension. CH₄ emissions were higher at the sporadic permafrost site, while GPP and ER were greater at the discontinuous permafrost site, despite lower air and soil temperatures as well as lesser PPFD given by the latitudinal position further north. Overall, Scotty Creek was a C sink while Smith Creek was a C source and the difference in NEE between the sites was mostly driven by higher ER at nighttime. Below we discuss the differences of landscape-scale ecosystem fluxes and how they were mostly driven by the contrasting extent of permafrost.

3.4.1 CH₄

CH₄ fluxes followed the permafrost extent so that CH₄ emissions were greater at the sporadic permafrost site due to the larger abundance of wetlands (Helbig, Chasmer, Kljun, et al., 2017). The higher wetland-to-forest ratio also led to a higher LE flux and a lower H flux at the sporadic permafrost site Scotty Creek, respectively (Figure A3.4). The wetland areas, often thermokarst bogs or fens, had near-surface water table, and are thus often anaerobic in contrast to the aerobic peat plateaus underlain by permafrost (Estop-Aragonés et al., 2022; Helbig, Quinton, et al., 2017; Jones et al., 2017; Osterkamp et al., 2009). Although CH₄ emissions are known to be quite variable in space and time (Elder et al., 2021; McClain et al., 2003; Reuss-Schmidt et al., 2019), the magnitude of CH₄ flux followed the area percentage of wetlands within the two footprints. At a sporadic permafrost site in Finland, wetland area only covered a quarter of the area but

accounted for 90% of the CH₄ emissions while only contributing 22% to the landscape's CO₂ uptake (Kou et al., 2022). The amount of wetland area is a proxy for the non-permafrost landcover of permafrost peatland complexes and as such key to predict landscape CH₄ emissions.

We found a strong diurnal pattern for CH₄ emissions, especially at the northern discontinuous permafrost site Smith Creek. Previous studies using chambers in a boreal black spruce forest floor in Alaska (Ueyama et al., 2023) and eddy covariance in a Canadian peatland (Long et al., 2010) reported diurnal patterns of CH₄ emissions and suggested CH₄ diffusion via aerenchyma and CH₄ preferentially released during daytime when the stomata are open (Ding et al., 2005). In this way, the more diffuse diurnal patterns of CH₄ flux at the sporadic site could then be explained by poor stomatal control of hydrophilic wetland plant types, such as sedges, that are more dominant in the landscape. Additionally, wetland trees can emit CH₄ through the stem, reaching a magnitude of up to 20% of peat soils underneath (Gauci et al., 2010). Thus, this pattern could alternatively result from CH₄ storage under the canopy during calm wind conditions. Generally higher wind speeds at Scotty Creek result from lower roughness length facilitated by less abundant forest structures, elevating the wind profile above the canopy. Either way, this pattern is also a consequence of the higher extent of permafrost at Smith Creek and underlines the importance of considering biosphere-atmosphere interactions and their effects on exchange of CH₄ and CO₂.

Warming will consequently increase CH₄ emissions, directly by warmer air temperatures and indirectly by wetland expansion. Projected into the future, the discontinuous permafrost landscape will evolve into a sporadic permafrost landscape with higher landcover of thermokarst bog areas. There, recent thaw features emit CH₄ at a rate three times higher than older thaw (Heffernan et al., 2022). Besides wetland expansion, warming will increase CH₄ emissions simply by warmer air and soil temperatures (Rößger et al., 2022), along with substantial temporal and spatial variation and seasonal hysteresis with higher emissions during fall than at spring at the same temperature (Chang et al., 2021). However, the majority of CH₄ emissions occurs during peak growing season in June and July, driven by both warming and ecosystem productivity gains (Yuan et al., 2024). Our results suggest a proportional increase of CH₄ emissions with shrinking permafrost extent so that we project at least four times higher CH₄ emissions for Smith Creek than at the current extent of permafrost. More warming could further

amplify future CH₄ emissions by warmer air and soil temperatures expanding the frost-free growing seasons and productivity.

3.4.2 GPP and ER

Both GPP and ER were higher at the northern site with discontinuous permafrost despite both cooler air and soil temperatures. Air temperature is known to limit GPP in high latitudes by setting the length of the growing season (Helbig, Chasmer, Desai, et al., 2017). Increased GPP results in both more fresh organic material to be decomposed by heterotrophic bacteria, and higher autotrophic respiration, a main component of ER. Peatland ecosystems typically have low-productive aboveground biomass so that heterotrophic respiration of belowground biomass is proportionally more important, making shallow soil temperature an important predictor variable for ER (Baird et al., 2019). Although the presence of trees can lead to slightly increased soil temperatures in tundra and boreal ecosystems (Kropp et al., 2021), the large differences in shallow soil temperatures are governed by the presence or absence of permafrost at both of our sites. Following permafrost thaw, a wet soil regime has a higher thermal conductivity. However, warmer soil temperatures in the more abundant thermokarst bogs did not lead to higher overall ER of Scotty Creek nor did warmer air temperatures. If abiotic variables as soil and air temperatures did not align with the difference in ER (as in Helbig, Chasmer, Desai, et al., 2017), biotic factors like landcover composition or vegetation dynamics must explain the difference between the sites.

Smith Creek had minor areas of sandy upland moraine with mature and high trees including deciduous species near the tower, but these areas were unlikely to be the reason for higher GPP and ER at Smith Creek. In temperate climate, old growth forests with LAIs around four are known to have higher respiration than comparably younger forests with higher LAIs ($\sim 5 \text{ m}^2 \text{ m}^{-2}$) (Desai et al., 2005). In boreal peatlands, the upland areas did have larger trees and greater LAI, but they only represented $\sim 1\%$ of the footprint compared to 0.1% within the 90%-footprint range of Scotty Creek. Regarding the structure of the dominating peat plateau forests, tree LAIs at both sites were in the very same range. Furthermore, these relatively thin black spruce trees have been found to contribute little to the overall ecosystem evapotranspiration rates (Perron et al., 2023), which are closely tied to GPP (Keenan et al., 2013).

It is unlikely that site differences in soil moisture, peat depth or below-canopy vegetation caused the higher GPP and ER at Smith Creek. Shrub LAI was lower at Smith Creek and thus unlikely to drive the higher GPP (Ueyama et al., 2023). The organic soil layer however is generally shallower at Smith Creek (~150 cm) compared to Scotty Creek (~ 330 cm), which could then imply an overall tendency towards upland ecosystem characteristics, usually more productive than lowland ecosystems in the Taiga Plains (Startsev et al., 2016). However, both sites reach organic layer depth of over 150 cm so that the contribution of deep peat layers to overall ER is minor, even upon permafrost thaw (Estop-Aragonés et al., 2018). In terms of soil moisture status, waterlogging or dry stress, both as potential consequences of permafrost thaw, are further factors to consider as controls on GPP and ER (Baltzer et al., 2014). Sniderhan et al. (2020) predicted advantages for black spruce at northern sites whereas growth might become more limited by dry stress on thawing peat plateaus further south. However, dry stress and waterlogging would have also affected net CO₂ uptake, which was actually greater at Scotty Creek.

Higher GPP and ER at the Smith Creek site was most likely due to the greater proportion of peat plateau compared to Scotty Creek. Helbig, Chasmer, Desai, et al. (2017) found in their intra-site comparison at Scotty Creek that the overall landscape GPP and ER including the peat plateaus were higher than the equivalent fluxes from wetland area only. Our study compared two peatlands with a different latitudinal position which can be a major factor, as light limitation caused low-arctic ecosystems to have four times higher gross ecosystem productivity rates compared to high-arctic ones (Lafleur et al., 2012). However, our results suggest that GPP became light-limited only at the site with higher PPFD. Smith Creek had a higher maximum photosynthetic rate (i.e., GPP_{max}) at light saturation while also achieving higher GPP at lower PPFD rates towards the end of the growing season. GPP_{max} in peatlands is rather driven by biotic factors compared to abiotic factors (Peichl et al., 2018), underlining the importance of site differences in vegetation composition and rather than PPFD and air temperatures. In addition, *Sphagnum* mosses can be photo-inhibited under high light conditions in open canopy settings (Murray et al., 1993), indicated by a lower photosynthetic capacity than under the shading canopy of shrubs and trees (Hájek et al., 2009). The tall structure of trees allows them to compete for light more effectively than mosses in the ground layer, but the daytime advantage comes at the cost of high maintenance indicated by higher ER. Consequently, forested peat plateaus have both higher GPP and ER than treeless thermokarst bogs which are less abundant at Smith Creek.

And the difference in nighttime ER is the most crucial factor for between-sites differences in NEE.

3.4.3 NEE

Peatland ecosystems at comparable latitudes were previously reported as small net atmospheric CO₂ sinks (Humphreys et al., 2006; Lund et al., 2010). Our results (-23.5 to +25.8 g C m⁻² yr⁻¹) align with those of other high-latitude ecosystems in the discontinuous (black spruce forest in Alaska: -20 to -60 g C m⁻² yr⁻¹, Ueyama et al., 2006; permafrost palsamire: -50 g C m⁻², Olefeldt et al., 2012) and continuous permafrost zone (arctic meadow: -80 g C m⁻² yr⁻¹, Emmerton et al., 2016). When looking at previous peatland studies, there were no clear patterns of NEE along climate and permafrost gradients. A multi-site comparison cannot inform whether permafrost thaw will lead to increased/decreased CO₂ uptake due to the variety of different factors, such as peatland types, vegetation, site histories, and different study periods. All these likely obscure inferences on how permafrost extent influence site NEE. In our study however, we compared two sites with very similar characteristics, in the same ecoregion, and the measurements were done in the same years so that differences between the sites are more likely to be attributed to differences in permafrost extents than elsewhere.

The annual NEE of our sites indicated that Scotty Creek was a sink of -23.5 g C m⁻² while Smith Creek was a source of +25.8 g C m⁻² yr⁻¹. This difference between the sites is large enough that we consider the sites to have actual differences in long term NEE, despite uncertainties introduced from gap-filling methods including recently found biases at northern latitude sites (Vekuri et al., 2023), large interannual variability found at other permafrost peatland sites (± 100 g C m⁻² yr⁻¹ in annual NEE; Euskirchen et al., 2024), and the eddy covariance method in general (± 60 g C m⁻² yr⁻¹ in annual NEE; Baldocchi, 2020). However, we cannot determine our sites to be long-term CO₂ sinks or sources. Our data suggests that the site in the sporadic permafrost zone had a lower NEE (i.e., more of a sink or less of a source) compared to the site in the discontinuous permafrost zone and we thus focus on differences in NEE rather than absolute values.

From a seasonal perspective, we found the largest differences in NEE starting in July after solstice. While NEE at Scotty Creek only peaked in the beginning of July after solstice, Smith

Creek already had the greatest NEE uptake in the beginning of June. We again suspect the difference in permafrost extent behind the difference in seasonal NEE. The water table in wetlands has been found to be a major control of net CO₂ exchange (Helbig et al., 2022; Lindroth et al., 2007; Sulman et al., 2010). Wetland inundation in bogs and fens can suppress net CO₂ exchange early in the season, sustained into later in the season in wet years (Sulman et al., 2010). In dry years, a too low water table during late summer can however turn peatlands into interannual CO₂ sinks (Helbig et al., 2022), suggesting ER dominating over GPP under dry conditions. Late in the year in fall and winter, ER determines whether ecosystems act as CO₂ sources or sinks despite frozen soils (Ueyama et al., 2014; Watts et al., 2021).

Looking at the diurnal patterns, daytime differences in NEE between the two sites were minor compared to the differences during nighttime, which suggests ER as the main driver behind the difference in NEE. Increased wetland extent is likely to reduce respiration, especially during nighttime, which is why Scotty Creek acted as a sink while Smith Creek was a source. Previous work at Scotty Creek using nested eddy covariance has shown that there was no difference in NEE rates between the wetland and the sporadic permafrost landscape's overall NEE (Helbig, Chasmer, Desai, et al., 2017). If the nighttime ER at Smith Creek is lowered to the current rate of Scotty Creek, increasing wetland ratios Smith Creek in future might come along with more negative NEE like at the sporadic permafrost site Scotty Creek.

As of now, NEE seems rather limited by cold temperatures rather than by low rates of PPFD during the shoulder seasons whereas light-limitation was only observed at Scotty Creek. Thus, warming could extend the growing season at Smith Creek. However, the more northern peatland complex at Smith Creek could become even more light-limited in future as Scotty Creek is now when wetlands expand on the costs of light-efficient forest ecosystems. In a tundra ecosystem in Alaska, enhanced ER did outweigh gains in GPP due to increased temperatures and persistent permafrost thaw (Schuur et al., 2021). Expansion of thermokarst wetlands in a warming climate at Smith Creek could result in GPP getting light limited in fall - similar to the status quo at Scotty Creek.

3.4.4 Net Ecosystem Carbon Balance and Net Radiative Greenhouse Gas Forcing

The overall difference of $44.7 \text{ g C m}^{-2} \text{ yr}^{-1}$ in the carbon balance was mostly driven by NEE rather than the similar DOC export (L. Thompson et al., 2023) and the higher CH_4 emissions at the sporadic permafrost site Scotty Creek (Miner et al., 2022; Watts et al., 2023). Like Scotty Creek, other peatland sites have been found to be minor C sinks ($\sim -20 \text{ g C m}^{-2} \text{ yr}^{-1}$) and NEE measured by eddy covariance was often the main driver in terms of overall magnitude and variability in different NECB studies (Dinsmore et al., 2010; Nilsson et al., 2008; Roulet et al., 2007). Previous work from a sporadic permafrost peatland complex in Sweden found CH_4 emissions of bogs and fens to only offset 7% and 17% of the CO_2 uptake, respectively (Holmes et al., 2022). Hydrologic export of C is more relevant to tidal wetland ecosystems (e.g., Arias-Ortiz et al., 2021), where large proportion of their net atmospheric C uptake was lost via hydrologic export. Thus, effects of shrinking permafrost extent on NEE is crucial to predict the direction of change in permafrost peatland C storage.

Determining the NECB of peatlands after thaw has been approached by different methods with different spatial and temporal boundaries which has led to varying results. Recent work including Scotty Creek and Smith Creek found accelerated *Sphagnum* growth suggesting increased C uptake and highlighting the need for a complete C budgeting with palaeoecological analysis of peat surface cores (Germain Chartrand et al., 2023). At Scotty Creek, full peat core analysis showed that surface peat accumulated at a rate of $22 \text{ g C m}^{-2} \text{ yr}^{-1}$ (L. Harris et al., 2023). Following permafrost thaw however, analyses of plateau-bog chronosequences indicated a net C loss, where 13% of the peat C was lost over 600 years, with even higher losses C from deeper peat (L. Harris et al., 2023; Jones et al., 2017). In contrast, flux measurements of respired ^{14}C - CO_2 by static chambers suggest that permafrost thaw leads to preservation of old, deeper C (Estop-Aragonés et al., 2018). Peat core analyses can only conclude on consequences of permafrost thaw under historically colder climatic conditions. Furthermore, biometric methods such as peat core analyses and chamber-based flux measurements tend to underestimate net primary production when compared to estimates based on eddy covariance, especially in boreal forests where C fluxes are relatively small (Campioli et al., 2016). Meanwhile, eddy covariance measurements, like presented here, undergo a high degree of standardization in the data

processing and now also include CH₄ fluxes (Arias-Ortiz et al., 2021), in contrast to previous studies using chamber-based measurements (e.g., Dinsmore et al., 2010; Nilsson et al., 2008).

The enhanced CH₄ emissions following permafrost thaw are more important from a net radiative GHG forcing perspective (Frolking & Roulet, 2007; Helbig, Chasmer, Desai, et al., 2017; Knoblauch et al., 2018). Johansson et al. (2006) found that increases in CO₂ uptake of 16% were outweighed by a 22% increase of CH₄ emissions over a 30-year-period at a sporadic permafrost site, resulting in a 47% higher net radiative GHG forcing on a 100-year time scale. Our results suggest an almost linear increase of CH₄ emissions with increasing wetland expansion (cf. Elder et al., 2021; Kuhn, Varner, et al., 2021; Miner et al., 2022; Treat et al., 2021), potentially even further amplified by future warming and longer growing seasons (Helbig, Quinton, et al., 2017; Rößger et al., 2022). Wetland expansion will likely increase the uptake of the third important GHG, nitrous oxide, but with minor consequences for the overall net radiative GHG balance (Dinsmore et al., 2010; Schulze et al., 2023). Overall, we will likely see an increase of net radiative GHG forcing along with permafrost loss across the discontinuous peat landscape, with high uncertainties and increasing interannual variability in CO₂ (Helbig et al., 2022) and CH₄ (Yuan et al., 2024). Our study suggests that climate warming and permafrost thaw will enhance the CO₂ uptake while also increasing CH₄ emissions, leading to modest increases in both C storage and net radiative warming.

3.5 Conclusion

Continued warming and permafrost thaw will lead to increased peatland C uptake due to increased CO₂ uptake but also increased net radiative GHG forcing due to increased CH₄ emissions. The wetland-to-forest ratio governed by the extent of permafrost was a key control for all ecosystem GHG fluxes including ER and GPP which were higher at the more northern site despite lower air temperatures and light supply. Differences in NEE were driven by the higher respiration during nighttime, most likely given by the higher tree cover and more abundant peat plateaus in the discontinuous permafrost landscape. Given the limited light supplies in fall, the GPP is unlikely to increase with ongoing wetland expansion. Even if the landcover transition accompanied by a loss of permafrost led to lower respiration rates as currently portrayed by the sporadic permafrost site, ongoing warming would rather increase overall ER. The CH₄ balance is certainly crucial from a net radiative GHG forcing point of view. Warmer air temperatures and more wetland expansion only allow for one direction of change: further warming by increasing CH₄ emissions. Our study suggests an increase of CH₄ emissions with increasing abundance of fens and bogs in the landscape along with a decline of permafrost extent, likely leading to an increase of net radiative GHG forcing.

4. Large Losses of Carbon Dioxide and Carbon from Burned Permafrost Peatlands in the First Years after Wildfire

Abstract

Across northwestern Canada, boreal peatlands underlain by permafrost have accumulated vast amounts of carbon (C) over millennia despite regularly burning in natural wildfire cycles. Ongoing climate change shortens fire return intervals and intensifies fire severity, possibly transforming the ecosystems of this vast region into long-term future C sources. Losses of C occur during wildfire as well as in the years post-fire due to reduced vegetative uptake of CO₂, a potent greenhouse gas (GHG). Here, I report the first eddy covariance measurements (2020-2023) of net carbon dioxide (CO₂) exchange from a recently burned permafrost peatland complex ('2019 Burn') in the first four years after the fire and compare them to concurrent measurements at a nearby burned peat plateau recovering from a wildfire in 2007 ('2007 Burn'). The 2019 Burn released over 100 g C m⁻² yr⁻¹ as CO₂ for each of the first years after the wildfire, while the 2007 Burn has returned to an annual net CO₂ sink by 2023, i.e., 16 years post-fire. Thaw depths and soil temperature were higher, but soil respiration was lower at both burned sites compared to unburned peat plateaus. My results thus suggest large net CO₂ losses in the first years after fire but a quick recovery of net CO₂ gains of burned peatland complexes 16 years after fire. However, accentuated active layer deepening post-fire and warmer soil temperatures at depth are likely to promote the release of deep, old C. Future work must account for both, the significant magnitude and origin of post-fire CO₂ emissions, as previously frozen, old C is being reintroduced to the atmospheric C cycle, fueling further global warming.

4.1 Introduction

Wildfires have increased in frequency, extent, and severity across boreal Canada due to climate change (Flannigan et al., 2009; French et al., 2020; Stocks et al., 2002), with globally non-negligible emissions of potent greenhouse gases (GHG) resulting in a positive, i.e., warming, feedback to the climate system (Gibson et al., 2018; Schuur et al., 2022). Despite the boreal biome's large areal extent (Gauthier et al., 2015) and carbon (C) sink function (Goodale et al., 2002), there is a lack of predictive understanding on ecosystem-scale effects of wildfires on net CO₂ fluxes in the years post-fire (Oliveira et al., 2021). The foregoing particularly applies to boreal peatland complexes which are treed and relatively dry, and thus carry fire (Nelson et al., 2021). As such, permafrost peatlands are most significant in storing C and several studies have shown that the direct combustion losses from treed permafrost peatlands are substantial (Walker et al., 2018, 2019). However, it remains unknown for permafrost peatlands how much post-fire CO₂ is released in the years after fire before they start to return to a C sink via vegetation regrowth.

Globally, boreal peatlands store around 400,000 Tg of C covering 3.7 million km² (Hugelius et al., 2020). In boreal western Canada, the Taiga Plains ecozone spans around ~550,000 km² and is characterized by flat to undulating topography on sedimentary bedrock, sporadic to continuous permafrost, and widespread boreal peatlands (~50 % of the area) (Castilla et al., 2022). As part of the boreal biome, the Taiga Plains is susceptible to wildfires as more than one third of the Taiga Plains (approximately 140,000 km²) has burned in the years from 1959 to 1997, resulting in an annual burned area of 3,600 km² (0.7%) per year (Stocks et al., 2002). In the 2010s, almost 70,000 km² in total burned, suggesting that the annual burned area per year doubled (Castilla et al., 2022). When the long-term sequestration rate of C by Canadian peatlands was estimated at 23 Tg per year (Carlson et al., 2010), CO₂ emissions from combustion and post-fire were not considered (Kurz et al., 2013).

Many studies on wildfires have focused on combustion losses and ignored post-fire losses by assuming an instant ecosystem recovery of CO₂ capacity (Mack et al., 2021; Turetsky et al., 2015; Walker et al., 2020). The few available studies on post-fire CO₂ losses investigated boreal forest ecosystems (Amiro et al., 2010) or peatlands without permafrost (Wieder et al., 2009), and suggested that many forest ecosystems will only start to regain net C after 10 to 20 years of

forest regrowth (Liu et al., 2011). Combustion losses from boreal forests generally depend on the burn severity driven by soil moisture regime (Turetsky et al., 2015; Walker et al., 2018), depth of burn (Walker et al., 2019), and fuel availability (Walker et al., 2020). Compared to tropical peatlands characterized by large amounts of aboveground forest biomass, combustion losses from forested northern peatland complexes are relatively small (Loisel et al., 2020), e.g., 5 Tg C per year from Alaskan wetlands (Lyu et al., 2018). Across boreal northwestern North America, wildfires caused losses of about 789 Tg C compared to gains of 649 Tg C following post-fire recovery over a 30-year time span (Wang et al., 2021). Although wildfires lead to short-term fertilization effects (Neff et al., 2005; Schulze et al., 2023; van Beest et al., 2019), boreal peatlands are particularly slow in their vegetation regrowth due to their nutrient-poor status (Wang et al., 2018) and low soil temperatures, especially when associated with permafrost (Gibson et al., 2018; Robinson & Moore, 2000). For permafrost peatlands, there is in fact no previous study contrasting both combustion losses of CO₂ and post-fire CO₂ losses.

Post-fire atmospheric CO₂ losses from non-permafrost peatlands are dominated by heterotrophic respiration, whereas photosynthetic uptake and autotrophic respiration are small due to missing or slowly recovering vegetation (O'Donnell et al., 2009; Wieder et al., 2009). In permafrost peatlands, post-wildfire heterotrophic respiration by microbes in deeper soil layers is fueled by both higher oxygen availability and higher soil temperatures at around 40 cm depth (Gibson et al., 2019). Increased soil temperatures at depth after a wildfire accelerate thaw (Gibson et al., 2018) and cause permafrost degradation (Nossov et al., 2013) and thus increase deep soil respiration rates (Estop-Aragonés et al., 2018; Gibson et al., 2019). Wildfire can lead to large-scale reductions in tree cover along with wetland expansion (Helbig, Pappas, et al., 2016), which then affects both evapotranspiration (Kettridge et al., 2015) and net radiative forcing by long-term net changes in GHG exchange (Köster et al., 2017), albedo, and black C deposition (Potter et al., 2020; Randerson et al., 2006). Increased lateral C export is an additional consequence of wildfire in peatlands with permafrost (Burd et al., 2018) and without permafrost (Orlova et al., 2020) and can lead to further CO₂ emissions downstream (Dinsmore et al., 2010; Olefeldt et al., 2013).

Previous estimates of post-fire C losses have only included burned peatlands without permafrost (Wieder et al., 2009; Wilkinson et al., 2023) or used the static chamber method instead of the

eddy covariance technique (Myers-Smith et al., 2007). The eddy covariance approach is characterized by continuous and non-intrusive GHG flux measurements on an ecosystem-scale (Baldocchi, 2020). To date there have been no published studies using the eddy covariance technique to quantify net CO₂ fluxes between burned permafrost peatland complexes and the atmosphere. Thus, the goal of this study is to understand how losses of CO₂ from burned permafrost peat plateaus in the years post-fire compare to those during combustion before returning to net CO₂ sinks. To meet this goal, our objectives were to quantify a) the C combustion losses and net ecosystem CO₂ exchanges (NEE) of two burned permafrost peat plateaus in the first four (2019) and sixteen years after the wildfire (2007) using the eddy covariance technique (2019-2023). The two burned peat plateaus were located in northernmost Alberta, in the sporadic permafrost zone of the Taiga Plains. To shed light on the respiratory contributions from the burned peat plateau surfaces to ecosystem-scale fluxes, the eddy covariance measurements were supported by chamber-based soil respiration measurements, frost table, and soil temperature measurements in comparison to a nearby unburned peat plateau.

4.2 Materials and methods

4.2.1 Study Sites

This study was carried out at three peatland complexes located <18 km apart in northernmost Alberta, Canada (Figure 4.1a). Two of the peatlands were affected by wildfires in 2019 and 2007, while the third has not burned for at least 60 years based on tree ring observations. Due to the short distance between the sites, the three peatlands experience similar climatical conditions, and likely had similar vegetation composition prior to the wildfires. We installed identical eddy covariance systems at the recently burned peatland (2019) (59.59°N 117.29°W; AmeriFlux-ID ‘CA-STR’ at the ‘2019 Burn’) and at the peatland which burned in 2007 (59.44°N 117.24°W; AmeriFlux-ID ‘CA-LUT’ at the ‘2007 Burn’). The unburned third site was the Lutose unburned peatland site (59.48°N 117.18°W; ‘Unburn’, see Heffernan et al. 2020). I collected soil chamber flux measurements and established thaw depth measurement grids at all three sites (Figure 4.1a).

All three sites are peatland complexes with sporadic permafrost (<50%), characterized by a mosaic of peat plateaus where permafrost is present and thermokarst bogs and channel fens where permafrost is absent. Peat plateaus are elevated 1-2 m above their surroundings due to excess ground ice, which leads to relatively dry conditions by drainage. Peat plateaus have an open canopy of stunted <6 m tall black spruce (*Picea mariana*), a ground cover of Labrador tea shrubs (*Rhododendron groenlandicum*), lichens (*Cladonia* spp.), and sparse hummocks with *Sphagnum fuscum* moss. Thermokarst bogs are wetter and are dominated by mosses (*Sphagnum fuscum*, *Sphagnum angustifolium*, and *Sphagnum riparium*), Leather leaf (*Chamaedaphne calyculata*) and Bog Rosemary (*Andromeda polifolia*) shrubs, and sparse Rannoch-rush sedges (*Scheuchzeria palustris*). Channel fens are wetter and have a varied vegetation composition, but no channel fens were located within 120 m of the eddy covariance instrumentation, and no soil chamber flux measurements were done in fens or bogs. Peat depths of the three sites were 150 cm at the 2019 Burn, 220 cm at the 2007 Burn, and 550 cm at the Unburn. The climate is continental, with a mean annual average temperature of -1.1°C for the period 2011 to 2020 and a mean annual precipitation of 355 mm (T. Wang et al., 2016). Wildfire has already affected at least one quarter of permafrost peatlands in the sporadic and discontinuous permafrost zone of the Taiga Plains (Gibson et al., 2018). During wildfire recovery, peatlands in the study region are

very similar in their succession stages, independent from burn severity, depth of burn, and peat depth (Gibson et al., 2018).

The 2019 Burn burned in late May of 2019 (Alberta Fire Number: HWF066-2019, 65,000 ha). The Fire Weather Index, a numeric rating of general fire danger based on weather and fuel moisture, was at the start of the fire >30 , i.e., extreme (<https://cwfis.cfs.nrcan.gc.ca/maps>). The fire was of high severity as defined by Kasischke et al. (2008), with all low shrubs consumed by fire, all trees deceased and with all needles, tertiary, secondary branches consumed and $<30\%$ of primary branches remaining. *Sphagnum* mosses in thermokarst bogs and on hummocks of the peat plateaus were singed but not combusted. Most tree boles were standing after the fire, but all were severely charred, and the ground previously covered by lichens was also charred (Figure 4.1b).

The 2007 Burn burned in late June 2007 (Alberta Fire Number: HWF119-2007, 2,200 ha). The Fire Weather Index at the initiation of the fire was between 10 and 20, i.e. moderate. Assessing fire severity at the 2007 Burn at the start of this study was not possible due to the time since the fire. However, no black spruce trees had survived the fire and lichens were completely absent, which suggests that the site had at least moderate fire severity. By 2019, most charred tree boles had fallen over, and vegetation recovery was dominated by dense Labrador tea shrubs (~ 40 cm tall) and sparse regenerating black spruce (<1 m tall) (Figure 4.1c).

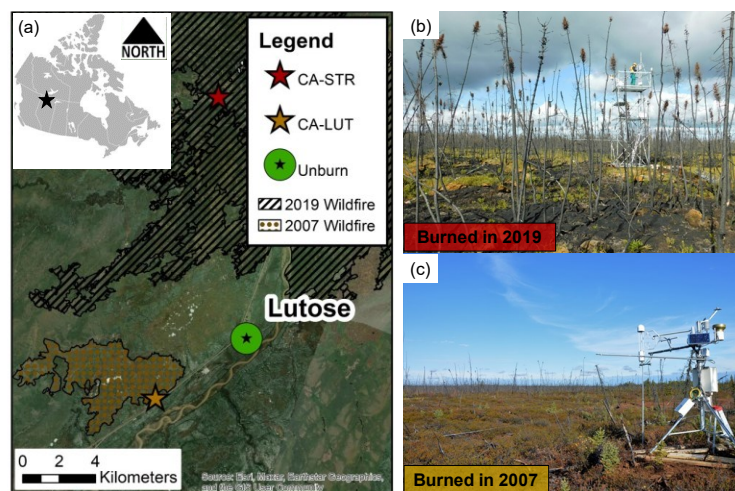


Figure 4.1: (a) Map of the research sites around Lutose including both eddy covariance tower locations (CA-STR in the 2019 Burn and CA-LUT in the 2007 Burn; Canadian National Fire Database, 2023). (b, c) Images of the tower locations within the wildfire-affected peatland areas.

4.2.2 Eddy Covariance Measurements

In September 2019, I established the first eddy covariance system at the 2007 Burn followed by the 2019 Burn in June 2020, respectively. At both sites, flux footprints originated from elevated burned peat plateaus and wetter, unburned bog areas in depressions; both equal in their coverage ratios throughout the two wildfire scars. The eddy covariance instruments were identical at both sites but installed on different structures: at the 2019 Burn, a measurement height of 6.0 m was required to surpass the height of standing dead trees (~4 m in height), which was achieved by using a scaffolding structure with a west-facing boom (length >1m) directed outwards of the tower structure (Figure 4.1b). At the 2007 Burn, the dead trees from the fire had fallen over so that the instrumentation was installed on a west-facing boom (length >1m) at 2.1 m height at a tripod (Figure 4.1c). Fluctuations of vertical wind speed and sonic temperature were recorded by sonic anemometers (CSAT3, Campbell Scientific, Logan, UT) at high frequency (10 Hz). Operating at the same frequency and measurement heights in colocation to the sonic anemometers, enclosed-path infrared gas analyzers (LI-7200, LI-COR Biosciences, Lincoln, NE) measured densities of water vapor and CO₂. To the turbulent net flux of CO₂, the storage term was added to derive NEE between ecosystem and atmosphere. Positive NEE fluxes indicate net losses of CO₂ from the ecosystem to the atmosphere and negative fluxes indicate uptake of CO₂, respectively.

Site visits and checks including cleaning of optical pathways on the high frequency instrumentations occurred monthly during the growing seasons 2020, 2021, and quarterly starting from the growing season 2022. The calibration of the gas analyzers was done on a yearly basis. The high-frequency data were stored by CR3000-XT dataloggers (Campbell Scientific, Logan, UT), which also recorded additional environmental measurements as half-hour averages, including net radiation, rainfall, air and soil temperature at 10 cm depth, photosynthetic active photon flux density (PPFD), soil moisture content, and ground heat flux (see Table A4.1 for information on sensors).

Half-hourly fluxes were computed using the software EddyPro (v. 7.0.9, LI-COR Biosciences, Lincoln, NE). The software allowed to double-rotate the anemometers' coordination systems according to Wilczak et al. (2001), to apply spike removal followed Vickers & Mahrt (1997) and to correct for spectral attenuation according to Moncrieff et al. (1997, 2004), air density

fluctuations (Webb et al., 1980), and humidity effects (Van Dijk et al., 2004). The three-class quality flag system by Mauder & Foken (2011) was applied to filter poor quality data (data flagged >1). Further filtering of the eddy covariance datasets followed Papale et al. (2006) and Reichstein et al. (2005) and included the dismissal of low-turbulence periods during nighttime (Falge et al., 2001; Gu et al., 2005; Papale et al., 2006). To be able to differentiate between daytime and nighttime as described in Helbig, Wischniewski, et al. (2016) despite the lack of measurements of incoming short-wave radiation (SWin), I calculated SWin based on PPFd using an approximation factor (0.495) as suggested by Hassika & Berbigier (1998). Nighttime NEE was bootstrapped (100 times) to derive the 95% confidence interval and friction velocity thresholds according to Papale et al. (2006).

4.2.3 Net Annual CO₂ Fluxes

I estimated the net annual net CO₂ balance for the 2019 Burn and 2007 Burn by summing the average measured flux for each half-hour throughout the year, i.e. with up to four - five values for each half-hour (measurement period at 2007 Burn lasted from September 2019 to October 2023, i.e., half hours in September and October could have years to enter the standard deviation calculation). This approach enabled data coverage of 90% and 81% of all 17,520 half hour fluxes of a generalized annual dataset and ignored Day of Year (DOY) 366 of the intercalary year 2020. Standard deviations were also calculated for each half hour of the year accordingly. I chose to estimate an average net annual CO₂ flux rather than individual net CO₂ fluxes for each of the four years mostly due to several summer data gaps longer than three weeks and winter data gaps. Data gaps were more pronounced during winter due to low solar power potential which could not always supply sufficient power to the battery systems connected to all the instruments. From DOY 305 to DOY 59, data coverage was 71% and 43% for CA-STR and CA-LUT, respectively. To arrive at a complete annual estimate of net CO₂ exchange, we therefore assumed low diurnal and seasonal variability (standard deviation ~ 0.002 g C m⁻² per half hour flux for both sites) of winter fluxes at both sites between November and February and averaged all available NEE values of the generalized annual data from a) 1 November to 31 December and d) from 1 January to 28 February to gapfill all missing NEE values for the corresponding periods. Moreover, different meteorological seasons were grouped into the following classification: late winter

(DOY 1-59), Spring (DOY 60-151), early summer (DOY 152-197), late summer (DOY 198-243), fall (DOY 244-334), and early winter (DOY >335).

4.2.4 Static Chamber Soil Respiration

I measured soil respiration at the 2019 Burn, 2007 Burn, and Unburn using the static chamber approach (Crill, 1991; Norman et al., 1997; Subke et al., 2021). At each site, I installed four to six circular collars (0.12 m²), where the collars were placed to represent the heterogeneous peat plateau vegetation, and included dominance of char, Labrador tea, and singed *Sphagnum* moss at the 2019 Burn and 2007 Burn, and of lichens, Labrador tea, and live *Sphagnum* moss at the Unburn site. No trees or saplings were in the collars. I used opaque chambers (19 cm height, 22.4 L volume) covered with reflective foil insulation to reduce warming inside the chamber. The chambers fit in a 5 mm ring-formed edge on top of the collars where water was added to seal the chambers during measurements. The concentration of CO₂ in the chamber was measured with a portable infrared gas analyzer (EGM-4, PP Systems, Amesbury, MA), connected to the chamber with ~1 m silicone tubes. Chambers were deployed for eight minutes, and readings of CO₂ concentration were taken every 30 seconds. Soil respiration fluxes were calculated based on the change in CO₂ concentration between three to eight minutes of the chamber deployment, using the ideal gas law. Air temperature and air pressure required for the flux calculation used measurements from the nearby (<1 km) eddy covariance instrumentations (see above). For each flux measurement I also measured depth to frost table, water table position, soil moisture, and soil temperatures at 5, 10, 20, and 40 cm. There were three occasions of flux measurements in 2020 and 2021, and two in 2022, for a total of 108 soil respiration measurements. For all eight measurement occasions, I averaged all soil respiration rates for each site and applied repeated measures ANOVA using the ‘rstatix’ package (Kassambara, 2021) in the R computing environment (R Core Team, 2020).

4.2.5 Depth to Frost Table Position

I measured the depth to the frost table two to four times each year between 2019 and 2022, including one occasion each year between mid-September and mid-October when the deepest seasonal frost table position can be expected to occur (i.e., the active layer). An 80-point sampling grid (10 rows x 8 columns) was established with 5 m spacing between points within

peat plateaus covering 2,000 m² at each of the three sites. Depth to the frost table at each point was measured using a 150 cm soil probe, and I noted when the depth to the frost table was >150 cm. At each point, I recorded the microtopography (hummock or hollow) and ground cover (lichen, char, or *Sphagnum*). The presence of taliks (i.e., areas with continuously non-frozen peat above the frost table, indicating permafrost degradation) was indicated when the depth to frost table was >150 cm at the end of the season (Gibson et al., 2018). For example, at the 2007 Burn, taliks were found at 76 out of 80 grid points at the end of the measurements in October 2022. A representative measure of depth to the frost table for points without taliks was estimated by applying a kernel density estimation (Gibson et al., 2018; Wessa, 2015). This central estimate of depth to frost table measured in mid-September to mid-October represents the active layer for non-talik points and thus indicate differences in cumulative annual ground heat flux if peat properties (bulk density, soil moisture) are not different between sites.

4.2.6 Estimation of Combustion C Losses

I estimated combustion C losses only at 2019 Burn, given the long time since fire at 2007 Burn. Combustion C losses were estimated for both above- and belowground, following the method described by Walker et al. (2018). Two 2×20 m transects running north-south were randomly placed within the burned peat plateaus of the 2019 Burn and Unburn. Stand age at the 2019 Burn and the Unburn were assessed from tree rings of three basal tree discs from each site using the CooRecorder software (Cybis Elektronik & Data AB, described in Maxwell & Larsson, 2021). In each transect, I counted all trees and measured the diameters at breast height for trees >1.3 m and at the base for smaller trees. Aboveground biomass and C losses were assessed using allometric equations for black spruce stands according to Lambert et al. (2005), and I assumed total combustion of foliage, branches, and bark and an average C content of 50% (Walker et al., 2018). For all trees >1.3 m tall in each transect, I measured the distance between the top of the highest adventitious roots to the peat surface. Belowground C loss at the 2019 Burn site also required soil C content in the top 4.8 cm at the Unburn site. I collected 15 surface peat samples at the Unburn, 4.8 cm thick and 5 cm diameter, which were dried (60°C for 84 hours) and then combusted (550°C for 4 hours). The C content of the peat organic matter was assumed to be 45% (Heffernan et al., 2020). Aerial imagery from the 2019 Burn allowed us to estimate that 50% of the peat surface within 200 m from the tower with eddy covariance instrumentation had had soil

combustion, while the other 50% of the site had singed *Sphagnum* moss which I assumed had no soil C combustion.

Uncertainty (95% confidence intervals) of above-, belowground-, and total combustion C losses at the 2019 Burn were estimated using a Monte Carlo simulation (10,000 iterations) which accounted for the uncertainty of each factor. For the aboveground combustion losses, uncertainty of biomass losses used 1.96 standard error based on the two transects (n=2), and an assumed 95% CI of biomass C content ($50 \pm 5\%$) based on literature (Walker et al., 2018). For belowground combustion losses, uncertainty of depth of burn used 1.96 standard error based on the two transects (n=2), uncertainty of peat bulk density used 1.96 standard error based on the fifteen samples (n=15), and uncertainty of the peat C content used the reported 95% CI by Heffernan et al. (2020) which was done at the same (Unburn) site.

4.2.7 Net CO₂ Balance over 20 Years after Fire

To estimate the impact of wildfire on the net CO₂-C balance of permafrost peatlands over 20 years, I accounted for both combustion CO₂ emissions during wildfire (above- and belowground) and the difference in the annual NEE between a burned and unburned permafrost peatland. My study measured NEE during years 1 to 4 (2019 Burn) and years 13 to 16 (2007 Burn) after wildfire, and we used the 5-years-average NEE of -24 g CO₂-C observed at the Scotty Creek peatland complex (61.30°N, 121.30°W, AmeriFlux-ID: CA-SCC, see Helbig, Chasmer, Desai, et al., 2017), located 300 km northwest of the 2019 Burn, to represent an unburned peat plateau with similar vegetation and peat depth (Schulze et al., in prep.). I used linear interpolation for missing NEE between the observed periods and assumed that NEE of a burned site returned to pre-fire unburn NEE 20 years after the fire. Studies in the region have shown that the peat plateau soil thermal regime returns to pre-fire conditions ~25 years after fire, and that vegetation recovery at 20 years after fire includes the return of lichens and regrowth of young black spruce trees (Gibson et al., 2018).

4.3 Results

4.3.1 Eddy Covariance CO₂ Fluxes

I split the year into seasons for comparison of diurnal and daily patterns of NEE between the two sites (Figure 4.2). During winter, I found no diurnal pattern and no difference between the sites with NEE ranges of 0.24-0.33 $\mu\text{mol C m}^{-2} \text{s}^{-1}$ for 2019 Burn and 0.25-0.27 $\mu\text{mol C m}^{-2} \text{s}^{-1}$ for 2007 Burn (Figure 4.2a). Differences between the sites started around DOY 130, when 2007 Burn switched to a net daily CO₂ sink while 2019 Burn remained a net source throughout the entire year (Figure 4.2b). During the summer, I found only a small difference in NEE between the sites during nighttime with averages at midnight of 2.4 ± 0.9 vs. 2.0 ± 0.9 $\mu\text{mol C m}^{-2} \text{s}^{-1}$ at 2019 Burn and 2007 Burn, respectively. Differences during midday were much larger, NEE was on average -1.9 ± 0.9 and -3.7 ± 1.4 $\mu\text{mol C m}^{-2} \text{s}^{-1}$ for 2019 Burn and 2007 Burn, respectively. The greatest daily CO₂ emissions occurred in fall when daytime CO₂ uptake was light-limited, but soils remained relatively warm (Figure 4.2b). I estimated that the average cumulative annual NEE for years 1 to 4 after fire was $+104 \text{ g C m}^{-2} \text{yr}^{-1}$, while NEE for years 13 to 16 after fire was $-35 \text{ g C m}^{-2} \text{yr}^{-1}$. Due to the proximity of both sites, PPFD and air temperature were very similar over the measurement period (Figures 4.2c and 4.2d).

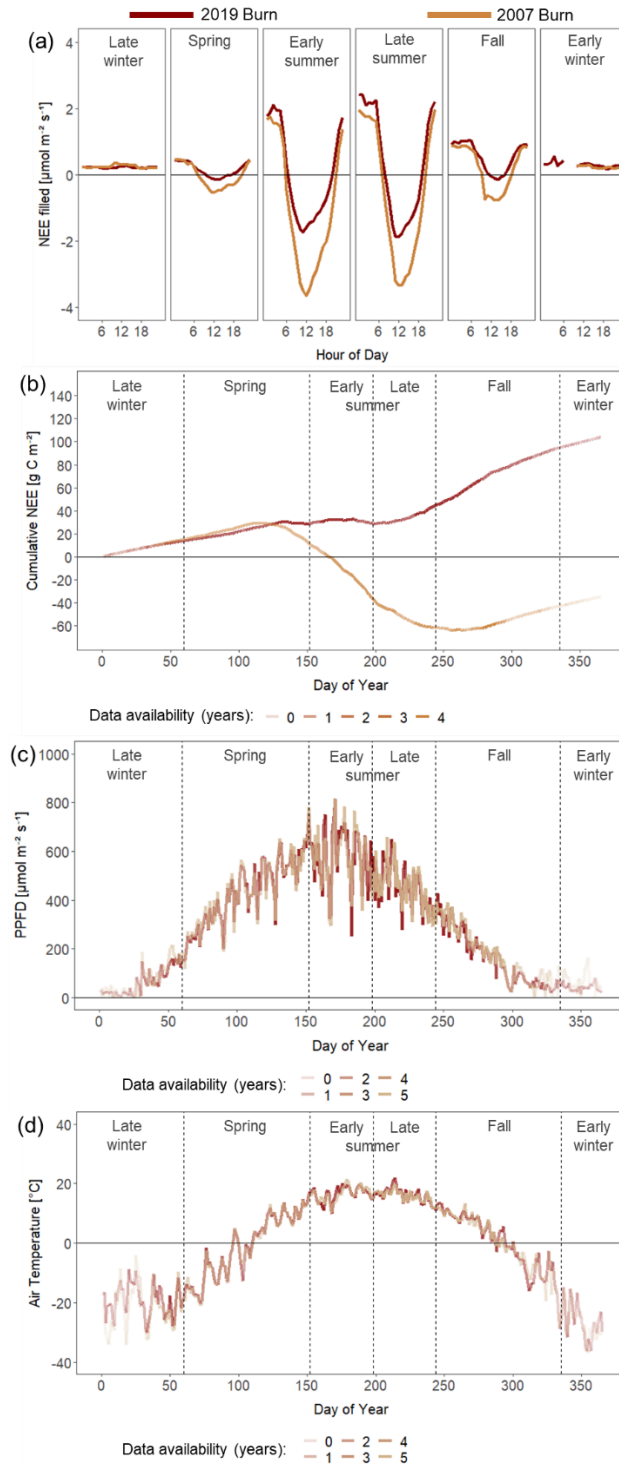


Figure 4.2: Generalized annual data based on four/five years of measurements from September 2019 to October 2023 as (a) diurnal and (b) seasonal patterns of annual post-fire net ecosystem exchange (NEE) measured by eddy covariance at 2019 Burn and 2007 Burn for the measurement time from September 2019 to October 2023. Seasonal patterns of (c) photosynthetic active photon flux density (PPFD) and (d) Air temperature (measured at 6.0 m and 2.1 m height at CA-LUT at 2007 Burn and CA-STR at 2019 Burn, respectively).

4.3.1 Soil Respiration

Soil respiration was lowest at the 2019 Burn site (average $1.15 \mu\text{mol C m}^{-2} \text{s}^{-1}$) followed by the 2007 Burn ($1.58 \mu\text{mol C m}^{-2} \text{s}^{-1}$) and Unburn ($1.79 \mu\text{mol C m}^{-2} \text{s}^{-1}$) (repeated measures ANOVA, $p = 0.045$, $F(2, 14) = 3.9$) (Figure 4.3a). The 2019 Burn also had the weakest relationship between soil respiration and soil temperature at 10 cm depth, while the Unburn had the strongest relationship (Figure 4.3b). Eight measurement occasions over the three-year period were not sufficient to assess differences between years, as the timing of measurements were not comparable.

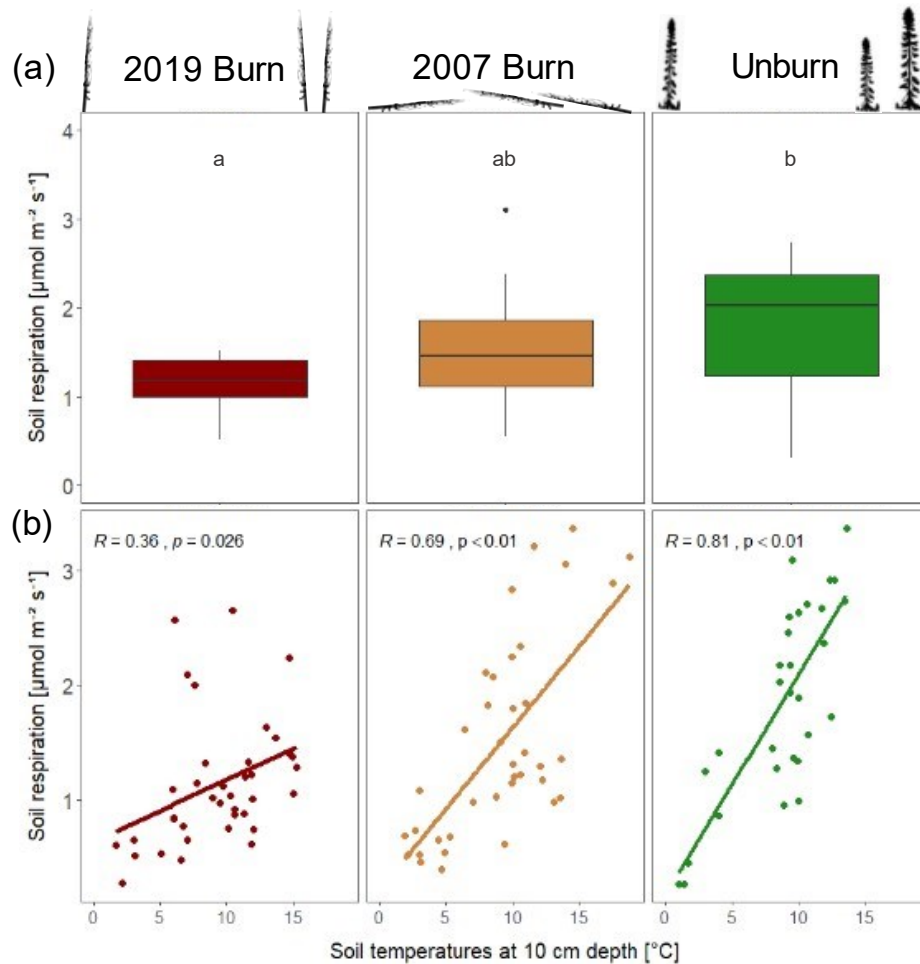


Figure 4.3: Soil respiration as (a) boxplots of measurement means ($n=8$), above which letters indicate statistically significant ($p < 0.05$) differences between sites, accounting for repeated measurements throughout the three growing seasons 2020, 2021, and 2022 and in (b) dependence of soil temperatures at 10 cm depth measured with static dark chambers at 2019 Burn, 2007 Burn, and Unburn (from left to right).

4.3.2 Soil Thermal Regime

Compared to the Unburn, the 2019 Burn and 2007 Burn both had warmer soil temperatures at 20 cm depth, spatially more extensive taliks, and deeper active layer (Figure 4.4a). The 2019 Burn and 2007 Burn had average soil temperatures at 20 cm that were 1.1 and 1.6°C warmer than the Unburn throughout the study. The 2019 Burn and 2007 Burn had on average 43% and 95% of the grid-points indicated as taliks (end of season thaw >150 cm), compared to 28% at the Unburn site. The active layer depth of non-talik grid-points was shallowest for the Unburn (average 52 cm over 4 years) and was deepest for the 2007 Burn (~120 cm), while the 2019 Burn had a strong trend during the study, from 52 cm in year 1 (2019) to 89 cm in year 4 (2022) (Figure 4.4b).

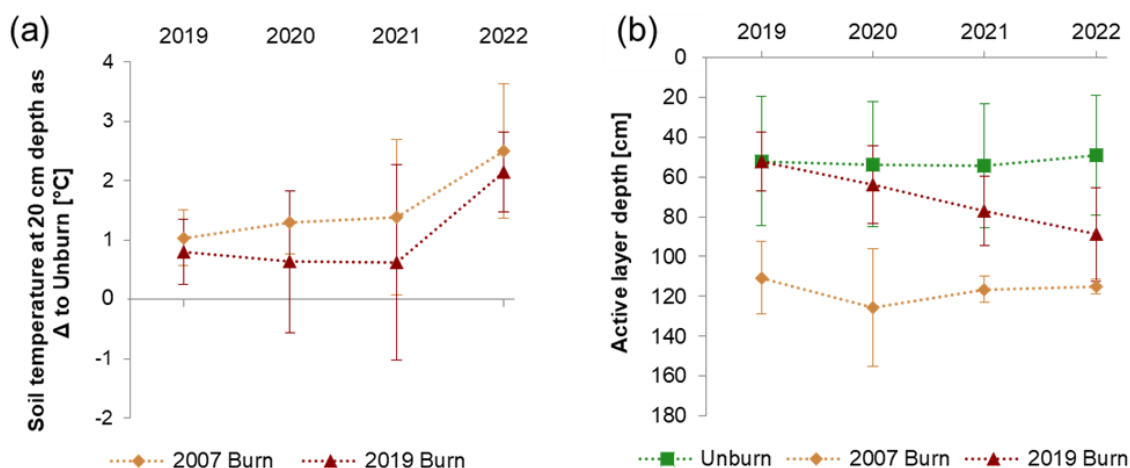


Figure 4.4: (a) Average soil temperatures at 20 cm depth displayed as difference to the Unburn mean soil temperature on each measurement date ($n=12$, four measurements per stage and date). Error bars represent the standard deviation of measurement occasion averages for each season (b) active layer depth for each growing season ($n=240$, each stage is represented by an 80-point thaw depth grid). Error bars represent the standard deviations of 80 end-of-season-thaw-depth-measurements excluding taliks which turn unfrozen towards the middle of the growing season (see Gibson et al., 2018). Low standard deviations for 2021 and 2022 at the 2007 Burn originate from the exclusion of 95% of measurements (deeper than 150 cm).

4.3.3 Wildfire Carbon Losses

I estimated that the total combustion C loss at the 2019 Burn was $1,700 \pm 570$ (95% CI) g C m^{-2} of which 24% was due to aboveground combustion and 76% due to belowground soil combustion (Table 4.1). The distance to peat at the 2019 Burn sites was 4.8 cm greater than the Unburn, providing an estimate of the depth of soil combustion. This depth of burn represented

the largest sources of uncertainty for belowground C losses, along with the assessment of burned dry mass for aboveground C losses.

Table 4.1: *Combustion carbon losses during the wildfire at 2019 Burn.*

Aboveground	Mean \pm 1.96SE (95% CI)
Burned dry mass (foliage, bark, branches)	790 \pm 340 g m ⁻²
Biomass C content ¹	50 \pm 5.0%
<i>Aboveground combustion C loss</i>	<i>400 \pm 170 g C m⁻²</i>
Belowground	
Proportion ground area burned ²	50 \pm 5.0%
Depth of burn	0.049 \pm 0.017 m
Surface 0-5 cm peat bulk density	0.12 \pm 0.013 g cm ⁻³
Peat C content ³	45 \pm 3.6%
<i>Belowground combustion C loss</i>	<i>1,300 \pm 540 g C m⁻²</i>
Total Combustion Losses	1,700 \pm 570 g C m⁻²

¹Assumption from Walker et al. (2018);

²Estimate and uncertainty based on drone imagery.

³Data from Heffernan et al. (2020).

4.3.4 Net CO₂ Balance over 20 Years after Fire

Based on the measured NEE for years 1 to 4 (CA-STR) and 12 to 16 (CA-LUT) after fire, I estimated that a burned peat plateau will have a cumulative NEE over 20 years of +380 g C m⁻². I assumed return to pre-fire conditions after 20 years (Figure 4.5a), and linear recovery of annual NEE between the measured periods. The nearby unburned peatland at Scotty Creek had an annual NEE of -24 g C m⁻², suggesting a cumulative NEE of -480 g C m⁻² over 20 years (Schulze et al., in prep.). Hence the difference in NEE between a burned and an unburned peat plateau was estimated to be 860 g C m⁻² over 20 years (Figure 4.5b). Thus, differences in NEE are about one third (33%) of the combustion losses for the total impact of wildfire (67%) on the long-term CO₂-C balance of permafrost peatlands.

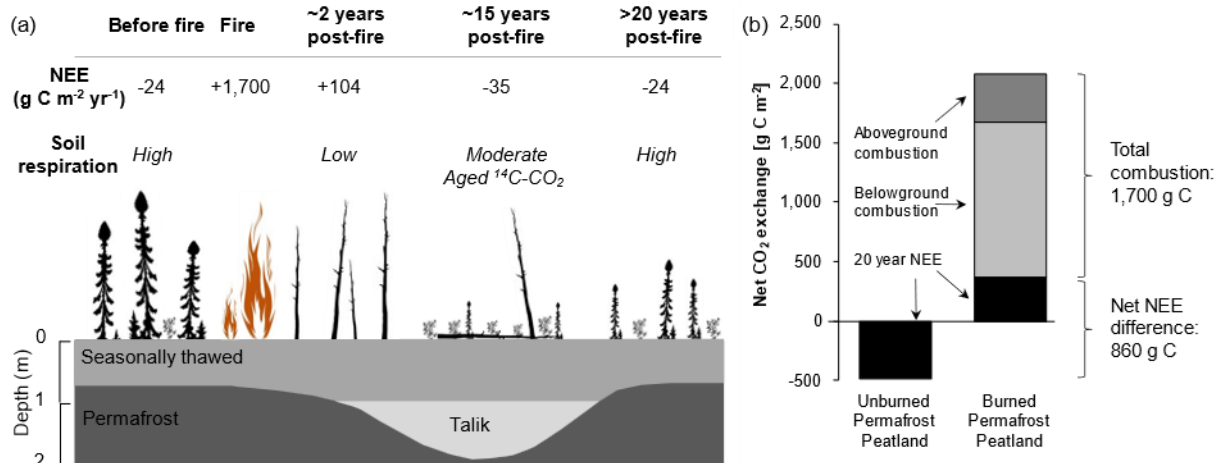


Figure 4.5: Ecosystem recovery and net CO₂-C balance for permafrost peatlands over 20 years after a wildfire. (a) Permafrost peatland succession and CO₂ balance over 20 years after wildfire, including shifts in annual NEE, relative magnitude of soil respiration, vegetation succession, depth of the seasonally thawed peat, and the development of taliks. Here information on annual NEE before fire and >20 years after fire is based on Schulze et al., in prep., the evidence of increased proportion of soil respiration derived from old peat is based on Estop-Aragonés et al. (2018), and the recovery of vegetation and taliks ~20 years after fire is based on Gibson et al. (2018). (b) Cumulative impact of wildfire on the net CO₂ balance over 20 years after wildfire when compared to an unburned peatland, accounting for both above- and belowground combustion during fire and the difference in annual NEE between a burned and unburned site.

4.4 Discussion

Here I investigated the effects of wildfire on the net CO₂-C balance of two burned permafrost peatland complexes in Northern Alberta using eddy covariance and compared both burned sites' soil respiration and ground thermal regimes with a third, intact peat plateau area as an unburned equivalent. During the wildfire, CO₂-C combustion losses were large and in a similar range to previous reports (e.g., Walker et al., 2018). In the immediate years after fire, ecosystem-scale flux measurements of post-fire peatland NEE are rare and a high research need (Wilkinson et al., 2023). Therefore, post-fire NEE has not often been considered when projecting the CO₂ balance of permafrost peatlands. Our findings revealed large CO₂ losses in the years post-fire with a positive NEE >100 g C m⁻² yr⁻¹, mostly driven by limited CO₂ uptake by sparse revegetation rather than increased soil respiration. However, we also observed the return of CO₂ uptake similar to unburned permafrost peatlands already a decade after the wildfire. Lowered soil respiration of burned peat plateaus was measured in the years post-fire compared to the Unburn, suggesting a shift in prevalence from autotrophic and heterotrophic respiration of young surface C to mostly heterotrophic respiration of deeper, older C post-fire.

My estimate of C combustion losses was similar to previous studies at comparable sites in the Taiga Plains and distinguished between above- and belowground C combustion losses. My combustion release estimate of 1.7 kg C m⁻² is below the median of 2.5 kg C m⁻² across different Alaskan landcovers reported by Veraverbeke et al. (2015) and in the lower middle of the boreal wildfire range from 0.5 to 4.0 kg C m⁻² (Moubarak et al., 2023; Rogers et al., 2014; Walker et al., 2018, 2020). Unlike other ecosystems, peatland C combustion is often dominated by belowground losses due to the high C density of peat and thus depends on the depth of burn, soil moisture status, and organic layer depth (Turetsky et al., 2015; Walker et al., 2018). Further north in the discontinuous permafrost zone of the Taiga Plains, combustion C losses of black-spruce-dominated boreal forests widely varied from 0.1 to 9.3 kg C m⁻² with an average release of 3.90 kg C m⁻² of which 90 % originated from belowground combustion (Walker et al., 2018). Following Walker et al. (2018), my approach likely overestimates belowground combustion C losses, as it measured the depth of burn using the highest adventitious root of wooden species which can carry the fire deeper into the ground compared to unvegetated or mossy areas nearby. Including different shallow-rooting vegetation as additional markers could have reduced this

potential bias (Moubarak et al., 2023). Regarding aboveground CO₂ combustion losses, forest structure and vegetation species composition are relevant to conclude on aboveground combustion losses (Rogers et al., 2015; Walker et al., 2018). Although peatland C combustion losses generally need to be determined on a regional scale due to small-scale variations in both vegetation aboveground and soil composition belowground (Mack et al., 2011; Moubarak et al., 2023; Walker et al., 2020), the study sites and my results can be assumed to be generally representative for permafrost peatlands of the sporadic permafrost zone of the Taiga Plains (Gibson et al., 2018, 2019).

Wildfires can affect the soil thermal regime and vegetation for multiple decades (Köster et al., 2017; Nossov et al., 2013). As there is no more shading of intact tree foliage, sunlight reaches the peat surface still covered in black ash and the decreasing albedo results in enhanced ground heat flux post-fire (Ackley et al., 2021; Randerson et al., 2006). As a result, soil temperatures increase and the active layer deepens (Ackley et al., 2021; Li et al., 2023); both reflected in my results (see Figure 4.4). Additionally, winter snowpack may be important for inhibiting the freezing up of the soil in a burned peat plateau. Compared to unburned peat plateaus, Gibson et al. (2018) previously reported around 4°C warmer soils at 40 cm depth and 90 cm deeper active layers, accompanied by large drops in thaw depth due to talik formation (continuously thawed soil layer; e.g., Ackley et al., 2021; Connon et al., 2018; Gibson et al., 2018; Nossov et al., 2013). 20-30 years after fire, the soil thermal regime as well as accompanying vegetation either fully recovers or both are irreversibly altered if accelerated permafrost thaw leads to ground subsistence known as thermokarst, promoting a shift in vegetation from tree to moss dominance (Jorgenson et al., 2013; Robinson & Moore, 2000).

Boreal peatlands and their often moss-dominated ground cover vegetation are characterized by both slow nutrient cycling (Moore et al., 2005) and vegetation growth (Turetsky et al., 2010) due to cold and wet conditions, particularly for peatlands underlain by permafrost (Schuur et al., 2022). In permafrost-free bogs, colonizing moss species peaked in abundance in the first decade after fire, whereas it took over three decades in permafrost peatlands, depending on fire severity (Turetsky et al., 2010). Independent of fire severity, lichens take three decades to regrow on peat plateaus within the study region (Bernier et al., 2011; Gibson et al., 2018). However, more severe fires can cause higher nutrient losses in deeper ground (Jiang et al., 2017). Ash residues

and acid pH further affect nutrient cycling post-fire (Liimatainen et al., 2014). However, modelling results have suggested that the regrowth of vegetation is rather restricted by limited photosynthetic capacity of sparse intact vegetation than a lack of nutrients in the years after fire (Jiang et al., 2015). Higher inorganic loads of N and even more so P did not indicate a lack of nutrients at burned sites compared to unburned ones (Neff et al., 2005; Schulze et al., 2023; van Beest et al., 2019). In summary, fire severity has been found to affect post-fire succession in upland forest sites (Johnstone et al., 2011; Shenoy et al., 2011) and peatlands without permafrost (Morison et al., 2021), observations from permafrost peatlands suggest that fire severity is not a strong determinant of post-fire succession (Kuosmanen et al., 2023; Mallon et al., 2016).

My results showed that the recently burned site had lower soil respiration when compared to unburned peat plateaus. This aligns with previous studies (O'Donnell et al., 2009), of which some included the 2007 Burn (Estop-Aragónés et al., 2018; Gibson et al., 2018). Lower soil respiration at the burned sites was despite the much deeper organic layer depth of around 5.5 meters of the intact peat plateau (Heffernan et al., 2020), which would suggest lower respiration rates compared to the sites with more shallow peat depths (Gibson et al., 2019). However, the soil respiration from the recently burned peat plateau was not only lower than at the unburned peat plateau equivalent; there was also only a weak correlation to soil surface temperatures (O'Donnell et al., 2009; Schulze et al., 2023). Soil respiration rates at the burned peat plateaus (also in Gibson et al., 2019) could be impacted by several factors, including the amount of fresh surface labile C burned during the fire correlating with the depth of burn (Turetsky et al., 2011), the degree of impact and recovery rate of plants (autotrophic respiration), lichen, and microbial communities (heterotrophic respiration) (Xiang et al., 2014). Therefore, in the first few years post fire, soil respiration was low, primarily because the top layer of peat and live vegetation was combusted, and near-surface peat is much more labile than deeper peat (Estop-Aragónés et al., 2018; Gibson et al., 2019). However, soil respiration gradually recovered when comparing the year of the fire event (cf. Schulze et al., 2023) to the first three years post fire. Since the correlation to topsoil temperatures is still weak in the first years after fire, the increase in overall soil respiration at 2019 Burn is likely driven by a gradual deepening of the active layer and warmer soil temperatures at depth, along with slowly increasing availability of fresh organic matter originating from vegetation regrowth.

Regarding the decade after wildfire, Gibson et al. (2019) found similar respiration rates of the 2007 Burn and a close-by peatland that burned in 2000, both lower than at the Unburn. In my study however, there was no significant difference between 2007 Burn and the Unburn, suggesting an almost complete recovery of ecosystem respiration 16 years post-fire. While partly this could be due to vegetation recovery, autotrophic respiration and respiration based on root exudates, previous studies at the 2007 Burn have shown that deep, old peat layers have a greater contribution to the overall respiration (Estop-Aragónés et al., 2018; Gibson et al., 2019). This is supported by the overall weaker correlation of soil respiration to topsoil temperatures at 10 cm depth compared to the Unburn. In conclusion, the presence of taliks and warmer soils, in combination with the low water table position in peat plateaus appear to enhance mineralization of deep peat.

At the ecosystem scale, our eddy covariance data from both burned sites indicated that site differences in NEE largely originated from GPP rather than ER, shown by the large difference in day-time NEE between the two sites and no significant differences in soil respiration of burned patches. A reduced ecosystem photosynthetic capacity upon wildfire appears obvious due to major parts (at our sites ~50%) of the landscapes' vegetation having burned off in the fire. Therefore, in the immediate years post-fire, net CO₂ losses originate from a fire-induced and sustained prevalence of ecosystem respiration over photosynthetic uptake by both limited regeneration of Labrador tea on dry burned peat plateaus and unburned wetter areas with live *Sphagnum* vegetation. The latter is important for many plant species throughout the entire boreal landscape, enhancing the formation of fire refugia (Kuntzemann et al., 2023) and allowing plant species to resettle on burned patches quickly after fire, as *Sphagnum* mosses even increase in abundance long-term (Kuosmanen et al., 2023). If soil respiration of burned patches is not significantly different and the contributions to NEE of unburned areas are assumed similar, the recovered GPP by vegetation regrowth must be conclusively the main driver of the difference in NEE between the two permafrost peatlands burned in 2007 and 2019, respectively.

Permafrost peatlands are large sources of CO₂ in the immediate years after fire and shift from source to sink 16 years post fire. Generally, boreal uplands and lowlands largely vary in terms of vegetation regrowth, permafrost degradation, and species decomposition post-fire (Jorgenson et al., 2013; Mallon et al., 2016), all of which determine C accumulation (Quillet et al., 2013) and

soil decomposition rates belowground (Turetsky, 2004). Permafrost-free bogs in Alberta returned to C sinks 13 years after fire and remain overall C sinks under current fire return cycles due to the regrowth of shrubs and mosses (Wieder et al., 2009). Kuosmanen et al. (2023) found that mosses also recover quickly after fire in peatlands with sporadic permafrost and concluded that fires may not have a long-term impact on the C function of peatlands. However, burned permafrost peatlands had large NEE losses in the first few years, which is not the case for non-permafrost peatlands.

My study is the first eddy covariance study of permafrost peatlands directly after the wildfire and estimated the post-fire net CO₂ balance at losses of 380 g C m⁻² over 20 years, likely with a significant contribution of older C release from deeper layer along with talik formation and the active layer deepening. Adding the combustion losses of 1,700 g C m⁻², I arrive at a difference of 2,560 g C m⁻² compared to the 20-years-NEE of an unburned peatland (-24 g C m⁻² yr⁻¹). Robinson & Moore (2000) used peat core analyses down to White River Ash (35-40 cm depth), suggesting that each time a peat plateau is affected by wildfire, its C accumulation rate is reduced by ~2,000 g C m⁻² accounting for both combustion and post-fire soil mineralization. Thus, my findings were about 1,000 g C m⁻² higher, mostly because losses from deeper peat layers were accounted for in my approach in contrast to Robinson & Moore (2000). Post-fire contribution of deeper soil respiration can reach up to a quarter (0.12 g C m⁻² d⁻¹) of the overall soil respiration (Estop-Aragonés et al., 2018), driven by warmer soil temperatures at depth and resulting active layer deepening under the burned soil surface (Gibson et al., 2018). Gibson et al. (2019) projected losses of 500 g C m⁻² only from deeper soil layers over a timeframe of 25 years, which is reintroduced to the atmospheric C cycle after being frozen for millennia (Walker et al., 2019). When old, formerly inactive soil C from deeper layers is reintroduced to the atmospheric C cycle via combustion during the fire (Turetsky et al., 2015) or decomposition post-fire (Estop-Aragonés et al., 2018; Gibson et al., 2019), ‘legacy carbon’ from historic fire cycles can be included (Walker et al., 2019) and be seen as ‘irrecoverable’ with implications for the global climate (Goldstein et al., 2020). Increased contributions of deeper soil layers are also indicated by our results, a) by the poor relationship between overall soil respiration and surface soil temperatures and b) by the gradual deepening of the active layer across the recently burned peatland in the immediate years after the fire.

The impact of wildfire on the CO₂ balance likely dominates the impact on net radiative forcing – with effects on albedo (Bernier et al., 2011; Chambers et al., 2005; D. Thompson et al., 2015) and other trace gases (Moubarak et al., 2023) being minor in comparison. However, if future wildfires cause complete permafrost thaw and transition into thermokarst bogs with high CH₄ emissions, the net impact of wildfire will be substantially different. Combustion losses in wildfire studies are commonly reported as overall C losses but are however dominated by CO₂ (Moubarak et al., 2023). Regarding post-fire alterations of fluxes of GHGs, my study showed major changes in the net CO₂ balance whereas CH₄ and N₂O were found negligible for permafrost peatlands in the study region (Schulze et al., 2023). Thus, the net CO₂ balance of burned permafrost peatlands and their post-fire recovery strongly impact the future net radiative balance of the entire Taiga Plains ecozone. As over one quarter of the ecozone has burned already since 1965, wildfire is an equally important driver of tree cover loss in boreal forests as permafrost thaw (Helbig, Pappas, et al., 2016). Gibson et al. (2018) have shown that wildfire can even accelerate permafrost thaw, thus burned peat plateaus transition more often into thermokarst bogs and fens instead of recovering to peat plateaus with permafrost. These thermokarst landforms then have their own distinct GHG balances and albedo, possibly leading to long-term productivity gains or losses and net cooling or warming effects (Randerson et al., 2006; Rogers et al., 2014; Yue et al., 2013).

Previous research has often ignored immediate and short-term post-fire CO₂ losses due to a lack of studies and data (Wilkinson et al., 2023), particularly across the permafrost region. Here, I quantified the net CO₂ losses of burned permafrost peatlands both during combustion and 20 years post-fire. Following research must consider both past fire history and future scenarios including predicted decreases in snowpack, fire return intervals (Lyons et al., 2008; Potter et al., 2020; Wieder et al., 2009), and rising number of lightning strikes (Bieniek et al., 2020; Chen et al., 2021), starting even more wildfires with positive climate change feedback (Moubarak et al., 2023).

4.5 Conclusion

CO₂ post-fire losses of permafrost peatlands accumulate to half in magnitude as the combustion CO₂ losses during fire and leads to reduced C storage compared to unburned peatlands. The long-term loss of CO₂ from burned permafrost peatlands is similar to the effect of wildfire on other boreal ecosystems which recover within the next decade after the fire. Nevertheless, my findings suggest major changes in burned permafrost peat plateaus regarding the ground thermal regime including warmer soil temperatures and a gradual deepening year by year. This is accompanied by reduced soil respiration, indicating a shift in respiration from autotrophic and heterotrophic young C to older, deeper C. Given the abundance of peat plateaus in western Canada along with the intensifying fire regime, the post-fire NEE is crucial to account for, if we are to understand the overall C balance of the region. This will be of particular importance given the region's extreme fire year 2023, which will lead to large CO₂ losses over the coming decades.

5. Summary, conclusions, and directions for future research

5.1 Summary of Findings

In my research, I examined the effects of wildfire and permafrost thaw on GHG exchange between atmosphere and the peatland landscape of the Taiga Plains ecozone in northwestern Canada. Wildfire and permafrost thaw transform the landcover of the peatland landscape and alter environmental variables, that control the ecosystem release and uptake of the three important GHGs, CO₂, CH₄, and N₂O. What has remained enclosed in the dark underground for millennia, could now be released as GHG into the atmosphere ('Out of the Dark, into the Light').

For burned peatlands, there are immediate GHG losses in the fire as well as in the years after the fire. The recovery of vegetation and microbial communities is slow during succession, so that the GHG balance is characterized by both the lack of C uptake by vegetation and reduced N₂O uptake by microbes. Overall reduced respiration is driven by losses of slowly increasing amounts of labile C near the surface and increasing contributions of deeper soil C, as burned peat plateaus experience a gradual active layer deepening towards the end of the growing season in the years post-fire. For peatlands affected by thermokarst, there are also shifts in vegetation, caused by the complete thaw of ground ice. The surface collapse results in a water table close to the surface and warmer soils due to heat conductance, which enhances CH₄ emissions and N₂O uptake.

Chapter 2 focused on the plot-scale exchange of N₂O following both wildfire and permafrost thaw across three permafrost peatlands sites in northwestern Canada. In Eurasia, non-vegetated palsas were major N₂O hotspots, whereas I did not find bare burned peat plateaus to be N₂O hotspots in my study region. Still, burned peat plateaus had less N₂O uptake than intact peat plateaus, whereas thaw bog stages had enhanced N₂O uptake along with below-ambient N₂O soil gas concentrations. N₂O uptake increased with higher soil temperature and moisture, which may be even more enhanced under wetter and warmer climate in future. Like the rest of the landscape, peatland ponds were mostly minor N₂O sinks, regardless of active thermokarst at the pond edge. One peatland pond with beaver activity within a twelve-year-old fire scar had elevated NO₃⁻ concentrations and was thus identified a N₂O hot spot. From a net radiative GHG forcing perspective, the enhanced N₂O uptake rates were negligible compared to the warming caused by CH₄ emissions, particularly from the wet thermokarst areas.

In Chapter 3, differences in landscape-scale ecosystem fluxes of CO₂ and CH₄ were associated with different ratios of remaining intact peat plateaus in the landscape in a space-for-time comparison between a sporadic and a discontinuous permafrost peatland. Landcover underlain by intact permafrost are forested, in contrast to permafrost-free and treeless wetlands. Thus, the landscape of the sporadic permafrost site characterized by a higher wetland-to-forest ratio had higher CH₄ as well as more negative NEE (CO₂ uptake). Higher GPP and ER were also related to the higher contribution of peat plateaus to the landscape flux at the discontinuous permafrost site. With ongoing climate change along with permafrost thaw, the discontinuous permafrost site will evolve into a sporadic permafrost site with increased CH₄ emissions and enhanced CO₂ uptake, leading to increases in both C storage and net radiative warming.

In Chapter 4, I quantified the CO₂ balance of burned permafrost peatlands post-fire. A recently burned permafrost peatland was a major source of CO₂, with losses over 100 g C m⁻² yr⁻¹ in the first years following the wildfire, whereas a fire recovery site (12 to 16 years post-fire) had similar NEE (-35 g C m⁻² yr⁻¹) compared to intact peatland sites. Both burned peatlands had warmer soil temperatures and deeper active layers, which did not lead to higher soil respiration rates. Soil respiration was thus apparently limited by the availability of fresh labile organic material – much of which was lost to combustion during wildfire. Similarly, daytime NEE rates were restricted to the CO₂ uptake by the sparse vegetation, particularly at the recently burned site, which only recovered slowly in the first few years after the fire event. My study suggests that post-fire CO₂ losses (i.e., the cumulative NEE over 20 years following wildfire) were half of the C combustion losses during the fire, both aboveground and belowground. This needs to be accounted for when we assess the impact of wildfire on GHGs in the boreal region.

From a C balance perspective, wildfire was the more relevant disturbance, with large CO₂ losses resulting from both combustion and post-fire NEE during succession. Permafrost thaw had a lesser influence on the NECB, where CO₂ uptake was counteracted by increased CH₄ losses. In contrast to the NECB, both wildfire and permafrost thaw caused increased net radiative warming, driven by the increased CH₄ emissions following thaw (Chapter 2 and 3) and CO₂ losses post-fire (Chapter 4). The effects of N₂O fluxes were negligible following both wildfire and thermokarst disturbance (Chapter 2), when comparing their net radiative GHG forcing in CO₂-equivalents per area unit (Figure 2.7). Helbig, Pappas, et al. (2016) previously quantified

the areal extents of both disturbances as equally important for changes in tree cover across the Taiga Plains. My work suggests that wildfire and permafrost thaw are also equally important for shifts in net radiative GHG forcing (Figure 5.1).

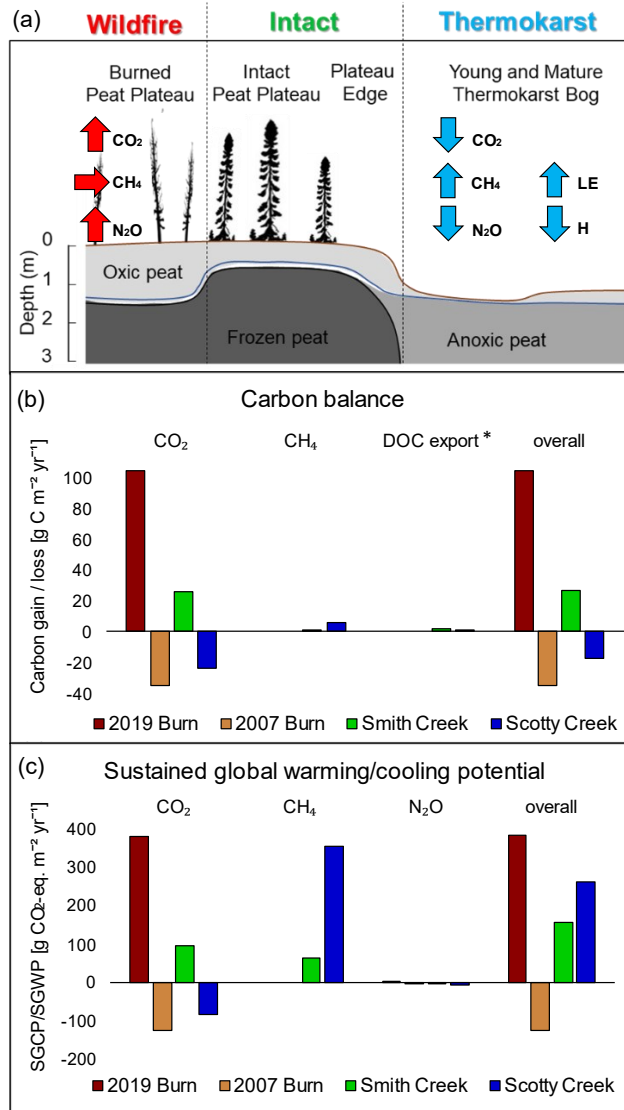


Figure 5.1: Summary of findings: (a) Direction of change (downwards = flux decreases, upwards = flux increases) of carbon dioxide (CO₂), methane (CH₄), nitrous oxide (N₂O), latent heat (LE), and sensible heat (H) following wildfire and thermokarst disturbance in permafrost peatlands of the Taiga Plains in comparison to intact peat plateaus. Records of CO₂ and CH₄ were taken from eddy covariance data, while N₂O originates from static chamber measurements. Diagram adapted from Estop-Aragonés et al. (2018). (b) Estimated annual carbon balances of four permafrost peatland sites investigated in this thesis. * Export of dissolved organic carbon (DOC) was measured by L. Thompson et al. (2023) at watershed outlets in the years 2017 to 2019 (c) Estimated net radiative greenhouse gas forcing of four permafrost peatlands investigated in this thesis. Net radiative greenhouse gas forcing of N₂O at Smith Creek and Scotty Creek was estimated based off fluxes measured by static chamber measurements at peat plateaus and mature bog (Figure 2.4) multiplied by their sustained global warming/cooling potentials (SGCP/SGWP) in relation to the two sites' landcover representation (Table 3.1).

5.2 Directions for future Research

Future research can be undertaken in a variety of directions to build upon the findings of this doctoral thesis. As this thesis mostly considered landscape transformation processes as indirect effects of climate change, it is important to also consider the direct effects, such as alternating precipitation patterns or warming. Due to further warming towards the end of the century, Helbig, Chasmer, Desai, et al. (2017) suggested that higher air temperatures will increase ER and reduce net CO₂ uptake of boreal peat landscapes. Thus, direct effects of climate change could outweigh indirect effects of landscape transformation processes discussed in this thesis.

This work has not considered all potential landcover shifts equally. With ongoing permafrost thaw throughout the peat landscape, more and more bog areas could hydrologically connect with fens, receiving higher nutrient input. Amongst all landcover types of boreal peat landscapes (introduced in Chapter 3), the fens are systematically understudied. However, fen CH₄ emissions are generally higher than bogs across the circumpolar region (Kuhn, Varner, et al., 2021). In comparison to bogs, fens have higher nutrient loads, so that their uptake potential for N₂O may be limited. As a consequence of wide thaw across the peat landscape, more fen area may thus impact the net radiative GHG balance the most.

Net radiative GHG balances must be based on the entire year including all four meteorological seasons, but a lot of research including this thesis relied on growing season data. Albeit winter fluxes outside the growing season period are generally smaller, the length of this period - almost half of the year - is too long to be ignored. It is often the winter and fall season that determines whether a site represents a C sink or source. According to results in Chapter 4, the time from October to March accounts for about 57 % of the overall CO₂ losses. Using CO₂ soil flux sensors during the non-growing season could be a way to cross-validate the magnitude of eddy covariance fluxes during winter, where data records became patchy due to low solar power supply (Chapter 4). Furthermore, our wildfire research was limited to the Lutose and Steen River sites in northern Alberta. Before finalizing this thesis, the Scotty Creek site has burned by a wildfire in fall 2022, which represents a unique opportunity given the ten years of pre-fire eddy covariance measurements.

The amount of data years is equally important as the completeness of individual years. I have observed high interannual variability of environmental variables, first and foremost the variation in water table depth at Lutose, during my five years of fieldwork and during my data analyses in Chapter 3. Climatic trends can only be identified with long-term environmental monitoring and site maintenance. To yield long-term and continuous eddy covariance or chamber flux datasets, highly qualified personnel are needed to run and maintain remote research sites in boreal Canada. For this, future research should include local Indigenous skillsets, knowledge, priorities, needs, and workforce. Ultimately, our research shall serve and benefit local northern communities that are most affected by climate change and its accompanying disturbances, wildfire and permafrost thaw.

In conclusion, I suggest tackling the above-mentioned weaknesses and shortcomings of my work to build upon my colleagues' and my own findings to conclude on the overall future net radiative balance of permafrost peatlands across the Taiga Plains. This shall include different warming and wildfire scenarios as well as all three important GHGs. Only in this way, we will be able to arrive at a conclusive and complete projection of the future net radiative GHG forcing of the permafrost peatlands of the Taiga Plains ecozone, which continues to transform from 'out of the dark, into the light'.

References

Abbott, B. W., & Jones, J. B. (2015). Permafrost collapse alters soil carbon stocks, respiration, CH₄, and N₂O in upland tundra. *Global Change Biology*, 21(12), 4570–4587. <https://doi.org/10.1111/gcb.13069>

Abbott, B. W., Jones, J. B., Schuur, E. A. G., Stuart Chapin III, F., Bowden, W. B., Bret-Harte, M. S., Epstein, H. E., Flannigan, M. D., Harms, T. K., Hollingsworth, T. N., Mack, M. C., McGuire, A. D., Natali, S. M., Rocha, A. V., Tank, S. E., Turetsky, M. R., Vonk, J. E., Wickland, K. P., Aiken, G. R., ... Zimov, S. (2016). Biomass offsets little or none of permafrost carbon release from soils, streams, and wildfire: an expert assessment. *Environmental Research Letters*, 11(3), 034014. <https://doi.org/10.1088/1748-9326/11/3/034014>

Ackley, C., Tank, S. E., Haynes, K. M., Rezaeehad, F., McCarter, C., & Quinton, W. L. (2021). Coupled hydrological and geochemical impacts of wildfire in peatland-dominated regions of discontinuous permafrost. *Science of The Total Environment*, 782, 146841. <https://doi.org/10.1016/j.scitotenv.2021.146841>

Amiro, B. D., Barr, A. G., Barr, J. G., Black, T. A., Bracho, R., Brown, M., Chen, J., Clark, K. L., Davis, K. J., Desai, A. R., Dore, S., Engel, V., Fuentes, J. D., Goldstein, A. H., Goulden, M. L., Kolb, T. E., Lavigne, M. B., Law, B. E., Margolis, H. A., ... Xiao, J. (2010). Ecosystem carbon dioxide fluxes after disturbance in forests of North America. *Journal of Geophysical Research: Biogeosciences*, 115(G4). <https://doi.org/10.1029/2010JG001390>

Arah, J. R. M., Smith, K. A., Crichton, I. J., & Li, H. S. (1991). Nitrous oxide production and denitrification in Scottish arable soils. *Journal of Soil Science*, 42(3), 351–367. <https://doi.org/10.1111/j.1365-2389.1991.tb00414.x>

Arias-Ortiz, A., Oikawa, P. Y., Carlin, J., Masqué, P., Shahan, J., Kanneg, S., Paytan, A., & Baldocchi, D. D. (2021). Tidal and Nontidal Marsh Restoration: A Trade-Off Between Carbon Sequestration, Methane Emissions, and Soil Accretion. *Journal of Geophysical Research: Biogeosciences*, 126(12), e2021JG006573. <https://doi.org/10.1029/2021JG006573>

Aubinet, M., Grelle, A., Ibrom, A., Rannik, Ü., Moncrieff, J., Foken, T., Kowalski, A. S., Martin, P. H., Berbigier, P., Bernhofer, Ch., Clement, R., Elbers, J., Granier, A., Grünwald, T., Morgenstern, K., Pilegaard, K., Rebmann, C., Snijders, W., Valentini, R., & Vesala, T. (1999). Estimates of the Annual Net Carbon and Water Exchange of Forests: The EUROFLUX Methodology (A. H. Fitter & D. G. Raffaelli, Eds.; Vol. 30, pp. 113–175). Academic Press. [https://doi.org/10.1016/S0065-2504\(08\)60018-5](https://doi.org/10.1016/S0065-2504(08)60018-5)

Baird, A. J., Green, S. M., Brown, E., & Dooling, G. P. (2019). Modelling time-integrated fluxes of CO₂ and CH₄ in peatlands: A review. *Mires and Peat*, 24, 1-15. Article 16. <https://doi.org/10.19189/MaP.2019.DW.395>

Baldocchi, D. (2003). Assessing the eddy covariance technique for evaluating carbon dioxide exchange rates of ecosystems: past, present and future. *Global Change Biology*, 9(4), 479–492. <https://doi.org/10.1046/j.1365-2486.2003.00629.x>

Baldocchi, D. D. (2020). How eddy covariance flux measurements have contributed to our understanding of Global Change Biology. *Global Change Biology*, 26(1), 242–260. <https://doi.org/10.1111/gcb.14807>

Baltzer, J. L., Veness, T., Chasmer, L. E., Sniderhan, A. E., & Quinton, W. L. (2014). Forests on thawing permafrost: fragmentation, edge effects, and net forest loss. *Global Change Biology*, 20(3), 824–834. <https://doi.org/10.1111/gcb.12349>

Beer, C., Reichstein, M., Tomelleri, E., Ciais, P., Jung, M., Carvalhais, N., Rödenbeck, C., Arain, M. A., Baldocchi, D., Bonan, G. B., Bondeau, A., Cescatti, A., Lasslop, G., Lindroth, A., Lomas, M., Luyssaert, S., Margolis, H., Oleson, K. W., Rouspard, O., ... Papale, D. (2010). Terrestrial Gross Carbon Dioxide Uptake: Global Distribution and Covariation with Climate. *Science*, 329(5993), 834 LP – 838. <https://doi.org/10.1126/science.1184984>

Bernier, P. Y., Desjardins, R. L., Karimi-Zindashty, Y., Worth, D., Beaudoin, A., Luo, Y., & Wang, S. (2011). Boreal lichen woodlands: A possible negative feedback to climate change in eastern North America. *Agricultural and Forest Meteorology*, 151(4), 521–528. <https://doi.org/10.1016/j.agrformet.2010.12.013>

Bieniek, P. A., Bhatt, U. S., York, A., Walsh, J. E., Lader, R., Strader, H., Ziel, R., Jandt, R. R., & Thoman, R. L. (2020). Lightning Variability in Dynamically Downscaled Simulations of Alaska's Present and Future Summer Climate. *Journal of Applied Meteorology and Climatology*, 59(6), 1139–1152. <https://doi.org/10.1175/JAMC-D-19-0209.1>

Biskaborn, B. K., Smith, S. L., Noetzli, J., Matthes, H., Vieira, G., Streletskiy, D. A., Schoeneich, P., Romanovsky, V. E., Lewkowicz, A. G., Abramov, A., Allard, M., Boike, J., Cable, W. L., Christiansen, H. H., Delaloye, R., Diekmann, B., Drozdov, D., Etzelmüller, B., Grosse, G., ... Lantuit, H. (2019). Permafrost is warming at a global scale. *Nature Communications*, 10(1), 264. <https://doi.org/10.1038/s41467-018-08240-4>

Bonan, G. B. (2008). Forests and Climate Change: Forcings, Feedbacks, and the Climate Benefits of Forests. *Science*, 320(5882), 1444–1449. <https://doi.org/10.1126/science.1155121>

Brandt, J. P., Flannigan, M. D., Maynard, D. G., Thompson, I. D., & Volney, W. J. A. (2013). An introduction to Canada's boreal zone: ecosystem processes, health, sustainability, and environmental issues. *Environmental Reviews*, 21(4), 207–226. <https://doi.org/10.1139/er-2013-0040>

Brown, J., Ferrians, O., Heginbottom, J. A., & Melnikov, E. (2002). Circum-Arctic Map of Permafrost and Ground-Ice Conditions, Version 2. Boulder, Colorado USA. NSIDC: National Snow and Ice Data Center. <https://nsidc.org/data/ggd318>

Brummell, M. E., Farrell, R. E., Hardy, S. P., & Siciliano, S. D. (2014). Greenhouse gas production and consumption in High Arctic deserts. *Soil Biology and Biochemistry*, 68, 158–165. <https://doi.org/10.1016/j.soilbio.2013.09.034>

Burd, K., Tank, S. E., Dion, N., Quinton, W. L., Spence, C., Tanentzap, A. J., & Olefeldt, D. (2018). Seasonal shifts in export of DOC and nutrients from burned and unburned peatland-rich catchments, Northwest Territories, Canada. *Hydrology and Earth System Sciences*, 22(8), 4455–4472. <https://doi.org/10.5194/hess-22-4455-2018>

Bush, E. & Lemmen, D.S. (Eds.) (2019). Canada's Changing Climate Report. Government of Canada, Ottawa, Ontario, Canada. 444. <https://publications.gc.ca/pub?id=9.870430&sl=0>

Butterbach-Bahl, K., Baggs, E. M., Dannenmann, M., Kiese, R., & Zechmeister-Boltenstern, S. (2013). Nitrous oxide emissions from soils: how well do we understand the processes and their controls? *Philosophical Transactions of the Royal Society B: Biological Sciences*, 368(1621), 20130122–20130122. <https://doi.org/10.1098/rstb.2013.0122>

Camill, P. (1999). Peat accumulation and succession following permafrost thaw in the boreal peatlands of Manitoba, Canada. *Écoscience*, 6(4), 592–602. <https://doi.org/10.1080/11956860.1999.11682561>

Campioli, M., Malhi, Y., Vicca, S., Luysaert, S., Papale, D., Peñuelas, J., Reichstein, M., Migliavacca, M., Arain, M. A., & Janssens, I. A. (2016). Evaluating the convergence between eddy-covariance and biometric methods for assessing carbon budgets of forests. *Nature Communications*, 7(1), 13717. <https://doi.org/10.1038/ncomms13717>

Carlson, M., Chen, J., Elgie, S., Henschel, C., Montenegro, Á., Roulet, N., Scott, N., Tarnocai, C., & Wells, J. (2010). Maintaining the role of Canada's forests and peatlands in climate regulation. *The Forestry Chronicle*, 86(4), 434–443. <https://doi.org/10.5558/tfc86434-4>

Carpino, O. A., Berg, A. A., Quinton, W. L., & Adams, J. R. (2018). Climate change and permafrost thaw-induced boreal forest loss in northwestern Canada. *Environmental Research Letters*, 13(8), 084018. <https://doi.org/10.1088/1748-9326/aad74e>

Carpino, O., Haynes, K., Connon, R., Craig, J., Devoie, É., & Quinton, W. (2020). The trajectory of landcover change in peatland complexes with discontinuous permafrost, northwestern Canada. *Hydrology and Earth System Sciences Discussions*, 2020, 1–40. <https://doi.org/10.5194/hess-2020-411>

Carter M.R., & Gregorich E.G. (2007). *Soil Sampling and Methods of Analysis* (2nd ed.). Canadian Society of Soil Science, Taylor & Francis Group, CRC Press. <https://doi.org/10.1201/9781420005271>

Castilla, G., Hall, R. J., Skakun, R., Filiatrault, M., Beaudoin, A., Gartrell, M., Smith, L., Groenewegen, K., Hopkinson, C., & van der Sluijs, J. (2022). The Multisource Vegetation

Inventory (MVI): A Satellite-Based Forest Inventory for the Northwest Territories Taiga Plains. *Remote Sensing*, 14(5). <https://doi.org/10.3390/rs14051108>

Chambers, S. D., Beringer, J., Randerson, J. T., & Chapin III, F. S. (2005). Fire effects on net radiation and energy partitioning: Contrasting responses of tundra and boreal forest ecosystems. *Journal of Geophysical Research: Atmospheres*, 110(D9). <https://doi.org/10.1029/2004JD005299>

Chang, K.-Y., Riley, W. J., Knox, S. H., Jackson, R. B., McNicol, G., Poulter, B., Aurela, M., Baldocchi, D., Bansal, S., Bohrer, G., Campbell, D. I., Cescatti, A., Chu, H., Delwiche, K. B., Desai, A. R., Euskirchen, E., Friborg, T., Goeckede, M., Helbig, M., ... Zona, D. (2021). Substantial hysteresis in emergent temperature sensitivity of global wetland CH₄ emissions. *Nature Communications*, 12(1), 2266. <https://doi.org/10.1038/s41467-021-22452-1>

Chapin, F. S., Woodwell, G. M., Randerson, J. T., Rastetter, E. B., Lovett, G. M., Baldocchi, D. D., Clark, D. A., Harmon, M. E., Schimel, D. S., Valentini, R., Wirth, C., Aber, J. D., Cole, J. J., Goulden, M. L., Harden, J. W., Heimann, M., Howarth, R. W., Matson, P. A., McGuire, A. D., ... Schulze, E.-D. (2006). Reconciling Carbon-cycle Concepts, Terminology, and Methods. *Ecosystems*, 9(7), 1041–1050. <https://doi.org/10.1007/s10021-005-0105-7>

Chapuis-Lardy, L., Wrage, N., Metay, A., Chotte, J.-L., & Bernoux, M. (2007). Soils, a sink for N₂O? A review. *Global Change Biology*, 13(1), 1–17. <https://doi.org/10.1111/j.1365-2486.2006.01280.x>

Chasmer, L., & Hopkinson, C. (2017). Threshold loss of discontinuous permafrost and landscape evolution. *Global Change Biology*, 23(7), 2672–2686. <https://doi.org/10.1111/gcb.13537>

Chasmer, L., Hopkinson, C., Veness, T., Quinton, W., & Baltzer, J. (2014). A decision-tree classification for low-lying complex land cover types within the zone of discontinuous permafrost. *Remote Sensing of Environment*, 143, 73–84. <https://doi.org/10.1016/J.RSE.2013.12.016>

Chen, Y., Romps, D. M., Seeley, J. T., Veraverbeke, S., Riley, W. J., Mekonnen, Z. A., & Randerson, J. T. (2021). Future increases in Arctic lightning and fire risk for permafrost carbon. *Nature Climate Change*, 11(5), 404–410. <https://doi.org/10.1038/s41558-021-01011-y>

Connon, R., Devoie, É., Hayashi, M., Veness, T., & Quinton, W. (2018). The Influence of Shallow Taliks on Permafrost Thaw and Active Layer Dynamics in Subarctic Canada. *Journal of Geophysical Research: Earth Surface*, 123(2), 281–297. <https://doi.org/10.1002/2017JF004469>

Coogan, S. C. P., Robinne, F.-N., Jain, P., & Flannigan, M. D. (2019). Scientists' warning on wildfire — a Canadian perspective. *Canadian Journal of Forest Research*, 49(9), 1015–1023. <https://doi.org/10.1139/cjfr-2019-0094>

Crill, P. M. (1991). Seasonal patterns of methane uptake and carbon dioxide release by a temperate woodland soil. *Global Biogeochemical Cycles*, 5(4), 319–334. <https://doi.org/10.1029/91GB02466>

Davidson, S. J., Van Beest, C., Petrone, R., & Strack, M. (2019). Wildfire overrides hydrological controls on boreal peatland methane emissions. *Biogeosciences*, 16(13), 2651–2660. <https://doi.org/10.5194/bg-16-2651-2019>

DelSontro, T., Beaulieu, J. J., & Downing, J. A. (2018). Greenhouse gas emissions from lakes and impoundments: Upscaling in the face of global change. *Limnology and Oceanography Letters*, 3(3), 64–75. <https://doi.org/10.1002/lol2.10073>

Desai, A. R., Bolstad, P. V., Cook, B. D., Davis, K. J., & Carey, E. V. (2005). Comparing net ecosystem exchange of carbon dioxide between an old-growth and mature forest in the upper Midwest, USA. *Agricultural and Forest Meteorology*, 128(1), 33–55. <https://doi.org/10.1016/j.agrformet.2004.09.005>

Desai, A. R., Richardson, A. D., Moffat, A. M., Kattge, J., Hollinger, D. Y., Barr, A., Falge, E., Noormets, A., Papale, D., Reichstein, M., & Stauch, V. J. (2008). Cross-site evaluation of eddy covariance GPP and RE decomposition techniques. *Agricultural and Forest Meteorology*, 148(6), 821–838. <https://doi.org/10.1016/j.agrformet.2007.11.012>

Ding, W., Cai, Z., & Tsuruta, H. (2005). Plant species effects on methane emissions from freshwater marshes. *Atmospheric Environment*, 39(18), 3199–3207. <https://doi.org/10.1016/j.atmosenv.2005.02.022>

- Dinsmore, K. J., Billett, M. F., Skiba, U. T. E. M., Rees, R. M., Drewer, J., & Helfter, C. (2010). Role of the aquatic pathway in the carbon and greenhouse gas budgets of a peatland catchment. *Global Change Biology*, 16(10), 2750–2762. <https://doi.org/10.1111/j.1365-2486.2009.02119.x>
- Dommain, R., Frohling, S., Jeltsch-Thömmes, A., Joos, F., Couwenberg, J., & Glaser, P. H. (2018). A radiative forcing analysis of tropical peatlands before and after their conversion to agricultural plantations. *Global Change Biology*, 24(11), 5518–5533. <https://doi.org/10.1111/gcb.14400>
- Dorrepaal, E., Cornelissen, J. H. C., Aerts, R., Wallén, B., & Van Logtestijn, R. S. P. (2005). Are growth forms consistent predictors of leaf litter quality and decomposability across peatlands along a latitudinal gradient? *Journal of Ecology*, 93(4), 817–828. <https://doi.org/10.1111/j.1365-2745.2005.01024.x>
- Ecosystem Classification Group. (2007). Ecological Regions of the Northwest Territories – Taiga Plains. <http://www.enr.gov.nt.ca/index.html>. Government of the Northwest Territories, 1-184 p.
- Elder, C. D., Thompson, D. R., Thorpe, A. K., Chandanpurkar, H. A., Hanke, P. J., Hasson, N., James, S. R., Minsley, B. J., Pastick, N. J., Olefeldt, D., Walter Anthony, K. M., & Miller, C. E. (2021). Characterizing Methane Emission Hotspots From Thawing Permafrost. *Global Biogeochemical Cycles*, 35(12), e2020GB006922. <https://doi.org/10.1029/2020GB006922>
- Emmerton, C. A., St. Louis, V. L., Humphreys, E. R., Gamon, J. A., Barker, J. D., & Pastorello, G. Z. (2016). Net ecosystem exchange of CO₂ with rapidly changing high Arctic landscapes. *Global Change Biology*, 22(3), 1185–1200. <https://doi.org/10.1111/gcb.13064>
- Environment and Climate Change Canada. (2020). Historical Data. https://climate.weather.gc.ca/historical_data/search_historic_data_e.html
- Estop-Aragonés, C., Czimczik, C. I., Heffernan, L., Gibson, C., Walker, J. C., Xu, X., & Olefeldt, D. (2018). Respiration of aged soil carbon during fall in permafrost peatlands enhanced by active layer deepening following wildfire but limited following thermokarst. *Environmental Research Letters*, 13(8), 85002. <https://doi.org/10.1088/1748-9326/aad5f0>

Estop-Aragonés, C., Heffernan, L., Knorr, K.-H., & Olefeldt, D. (2022). Limited Potential for Mineralization of Permafrost Peatland Soil Carbon Following Thermokarst: Evidence From Anoxic Incubation and Priming Experiments. *Journal of Geophysical Research: Biogeosciences*, 127(12), e2022JG006910. <https://doi.org/10.1029/2022JG006910>

Euskirchen, E. S., Edgar, C. W., Kane, E. S., Waldrop, M. P., Neumann, R. B., Manies, K. L., Douglas, T. A., Dieleman, C., Jones, M. C., & Turetsky, M. R. (2024). Persistent net release of carbon dioxide and methane from an Alaskan lowland boreal peatland complex. *Global Change Biology*, 30(1), e17139. <https://doi.org/10.1111/gcb.17139>

Evans, C. D., Peacock, M., Baird, A. J., Artz, R. R. E., Burden, A., Callaghan, N., Chapman, P. J., Cooper, H. M., Coyle, M., Craig, E., Cumming, A., Dixon, S., Gauci, V., Grayson, R. P., Helfter, C., Heppell, C. M., Holden, J., Jones, D. L., Kaduk, J., ... Morrison, R. (2021). Overriding water table control on managed peatland greenhouse gas emissions. *Nature*, 593(7860), 548–552. <https://doi.org/10.1038/s41586-021-03523-1>

Falge, E., Baldocchi, D., Olson, R., Anthoni, P., Aubinet, M., Bernhofer, C., Burba, G., Ceulemans, R., Clement, R., Dolman, H., Granier, A., Gross, P., Grünwald, T., Hollinger, D., Jensen, N.-O., Katul, G., Keronen, P., Kowalski, A., Lai, C. T., ... Wofsy, S. (2001). Gap filling strategies for defensible annual sums of net ecosystem exchange. *Agricultural and Forest Meteorology*, 107(1), 43–69. [https://doi.org/https://doi.org/10.1016/S0168-1923\(00\)00225-2](https://doi.org/https://doi.org/10.1016/S0168-1923(00)00225-2)

Fiencke, C., Marushchak, M. E., Sanders, T., Wegner, R., & Beer, C. (2022). Microbiogeochemical Traits to Identify Nitrogen Hotspots in Permafrost Regions. *Nitrogen*, 3(3), 458–501. <https://doi.org/10.3390/nitrogen3030031>

Flannigan, M., Stocks, B., Turetsky, M., & Wotton, M. (2009). Impacts of climate change on fire activity and fire management in the circumboreal forest. *Global Change Biology*, 15(3), 549–560. <https://doi.org/10.1111/j.1365-2486.2008.01660.x>

Fofana, A., Anderson, D., McCalley, C. K., Hodgkins, S., Wilson, R. M., Cronin, D., Raab, N., Torabi, M., Varner, R. K., Crill, P., Saleska, S. R., Chanton, J. P., Tfaily, M. M., & Rich, V. I. (2022). Mapping substrate use across a permafrost thaw gradient. *Soil Biology and Biochemistry*, 175, 108809. <https://doi.org/10.1016/j.soilbio.2022.108809>

Foster, A. C., Wang, J. A., Frost, G. V., Davidson, S. J., Hoy, E., Turner, K. W., Sonnentag, O., Epstein, H., Berner, L. T., Armstrong, A. H., Kang, M., Rogers, B. M., Campbell, E., Miner, K. R., Orndahl, K. M., Bourgeau-Chavez, L. L., Lutz, D. A., French, N., Chen, D., ... Goetz, S. (2022). Disturbances in North American boreal forest and Arctic tundra: impacts, interactions, and responses. *Environmental Research Letters*, 17(11), 113001. <https://doi.org/10.1088/1748-9326/ac98d7>

French, N. H. F., Graham, J., Whitman, E., & Bourgeau-Chavez, L. L. (2020). Quantifying surface severity of the 2014 and 2015 fires in the Great Slave Lake area of Canada. *International Journal of Wildland Fire*, 29(10), 892–906. <https://doi.org/10.1071/WF20008>

Frey, K. E., & Smith, L. C. (2005). Amplified carbon release from vast West Siberian peatlands by 2100. *Geophysical Research Letters*, 32(9), L09401. <https://doi.org/10.1029/2004GL022025>

Frolking, S., Roulet, N., & Fuglestedt, J. (2006). How northern peatlands influence the Earth's radiative budget: Sustained methane emission versus sustained carbon sequestration. *Journal of Geophysical Research: Biogeosciences*, 111(G1). <https://doi.org/10.1029/2005JG000091>

Frolking, S., & Roulet, N. T. (2007). Holocene radiative forcing impact of northern peatland carbon accumulation and methane emissions. *Global Change Biology*, 13(5), 1079–1088. <https://doi.org/10.1111/j.1365-2486.2007.01339.x>

Frolking, S., Talbot, J., Jones, M. C., Treat, C. C., Kauffman, J. B., Tuittila, E., & Roulet, N. (2011). Peatlands in the Earth's 21st century climate system. *Environmental Reviews*, 19, 371–396. <https://doi.org/10.1139/a11-014>

Fuß, R. (2017). gasfluxes: Greenhouse Gas Flux Calculation from Chamber Measurements. <https://cran.r-project.org/web/packages/gasfluxes/index.html>.

Gauci, V., Gowing, D. J. G., Hornibrook, E. R. C., Davis, J. M., & Dise, N. B. (2010). Woody stem methane emission in mature wetland alder trees. *Atmospheric Environment*, 44(17), 2157–2160. <https://doi.org/10.1016/j.atmosenv.2010.02.034>

Gauthier, S., Bernier, P., Kuuluvainen, T., Shvidenko, A. Z., & Schepaschenko, D. G. (2015). Boreal forest health and global change. *Science*, 349(6250), 819–822. <https://doi.org/10.1126/science.aaa9092>

Germain Chartrand, P., Sonnentag, O., Sanderson, N. K., & Garneau, M. (2023). Recent peat and carbon accumulation on changing permafrost landforms along the Mackenzie River valley, Northwest Territories, Canada. *Environmental Research Letters*, 18(9), 095002. <https://doi.org/10.1088/1748-9326/ace9ed>

Gibson, C., Cottenie, K., Gingras-Hill, T., Kokelj, S. V., Baltzer, J., Chasmer, L., & Turetsky, M. (2021). Mapping and understanding the vulnerability of northern peatlands to permafrost thaw at scales relevant to community adaptation planning. *Environmental Research Letters*. <http://iopscience.iop.org/article/10.1088/1748-9326/abe74b>

Gibson, C. M., Chasmer, L. E., Thompson, D. K., Quinton, W. L., Flannigan, M. D., & Olefeldt, D. (2018). Wildfire as a major driver of recent permafrost thaw in boreal peatlands. *Nature Communications*, 9(1), 3041. <https://doi.org/10.1038/s41467-018-05457-1>

Gibson, C. M., Estop-Aragónés, C., Flannigan, M., Thompson, D. K., & Olefeldt, D. (2019). Increased deep soil respiration detected despite reduced overall respiration in permafrost peat plateaus following wildfire. *Environmental Research Letters*, 14(12), 125001. <https://doi.org/10.1088/1748-9326/ab4f8d>

Gil, J. A., Marushchak, M. E., Rütting, T., Baggs, E. M., Pérez, T., Novakovskiy, A., Trubnikova, T., Kaverin, D., Martikainen, P. J., & Biasi, C. (2021). Sources of nitrous oxide and fate of mineral nitrogen in sub-Arctic permafrost peat soils. *Biogeosciences Discussions*, 2021, 1–25. <https://doi.org/10.5194/bg-2021-228>

Gil, J., Pérez, T., Boering, K., Martikainen, P. J., & Biasi, C. (2017). Mechanisms responsible for high N₂O emissions from subarctic permafrost peatlands studied via stable isotope techniques. *Global Biogeochemical Cycles*, 31(1), 172–189. <https://doi.org/10.1002/2015GB005370>

Goldstein, A., Turner, W. R., Spawn, S. A., Anderson-Teixeira, K. J., Cook-Patton, S., Fargione, J., Gibbs, H. K., Griscom, B., Hewson, J. H., Howard, J. F., Ledezma, J. C., Page, S., Koh, L. P.,

- Rockström, J., Sanderman, J., & Hole, D. G. (2020). Protecting irrecoverable carbon in Earth's ecosystems. *Nature Climate Change*, 10(4), 287–295. <https://doi.org/10.1038/s41558-020-0738-8>
- Goodale, C. L., Apps, M. J., Birdsey, R. A., Field, C. B., Heath, L. S., Houghton, R. A., Jenkins, J. C., Kohlmaier, G. H., Kurz, W., Liu, S., Nabuurs, G.-J., Nilsson, S., & Shvidenko, A. Z. (2002). Forest carbon sinks in the northern hemisphere. *Ecological Applications*, 12(3), 891–899. [https://doi.org/10.1890/1051-0761\(2002\)012\[0891:FCSITN\]2.0.CO;2](https://doi.org/10.1890/1051-0761(2002)012[0891:FCSITN]2.0.CO;2)
- Gorham, E. (1991). Northern Peatlands: Role in the Carbon Cycle and Probable Responses to Climatic Warming. *Ecological Applications*, 1(2), 182–195. <https://doi.org/10.2307/1941811>
- Grosse, G., Goetz, S., McGuire, A. D., Romanovsky, V. E., & Schuur, E. A. G. (2016). Changing permafrost in a warming world and feedbacks to the Earth system. *Environmental Research Letters*, 11(4), 040201. <https://doi.org/10.1088/1748-9326/11/4/040201>
- Gruber, N., & Galloway, J. N. (2008). An Earth-system perspective of the global nitrogen cycle. *Nature* 451(7176), 293–296. <https://doi.org/10.1038/nature06592>
- Gruber, S. (2012). Derivation and analysis of a high-resolution estimate of global permafrost zonation. *The Cryosphere*, 6(1), 221–233. <https://doi.org/10.5194/tc-6-221-2012>
- Gu, L., Falge, E. M., Boden, T., Baldocchi, D. D., Black, T. A., Saleska, S. R., Suni, T., Verma, S. B., Vesala, T., Wofsy, S. C., & Xu, L. (2005). Objective threshold determination for nighttime eddy flux filtering. *Agricultural and Forest Meteorology*, 128(3), 179–197. <https://doi.org/10.1016/j.agrformet.2004.11.006>
- Günther, A., Barthelmes, A., Huth, V., Joosten, H., Jurasinski, G., Koebisch, F., & Couwenberg, J. (2020). Prompt rewetting of drained peatlands reduces climate warming despite methane emissions. *Nature Communications*, 11(1), 1644. <https://doi.org/10.1038/s41467-020-15499-z>
- Hájek, T., Tuittila, E.-S., Ilomets, M., & Laiho, R. (2009). Light responses of mire mosses – a key to survival after water-level drawdown? *Oikos*, 118(2), 240–250. <https://doi.org/10.1111/j.1600-0706.2008.16528.x>

Harris, L. I., Olefeldt, D., Pelletier, N., Blodau, C., Knorr, K.-H., Talbot, J., Heffernan, L., & Turetsky, M. (2023). Permafrost thaw causes large carbon loss in boreal peatlands while changes to peat quality are limited. *Global Change Biology*, 29(19), 5720–5735. <https://doi.org/10.1111/gcb.16894>

Harris, S. A., French, H. M., Heginbottom, J. A., Johnston, G. H., Ladanyi, B., Segó, D. C., & van Everdingen, R. O. (1988). Glossary of permafrost and related ground-ice terms. In Technical Memorandum (National Research Council of Canada. Associate Committee on Geotechnical Research); no. ACGR-TM-142. National Research Council of Canada. Associate Committee on Geotechnical Research. Permafrost Subcommittee. <https://doi.org/10.4224/20386561>

Hassika, P., & Berbigier, P. (1998). Annual cycle of photosynthetically active radiation in maritime pine forest. *Agricultural and Forest Meteorology*, 90(3), 157–171. [https://doi.org/10.1016/S0168-1923\(98\)00054-9](https://doi.org/10.1016/S0168-1923(98)00054-9)

Heffernan, L., Cavaco, M. A., Bhatia, M. P., Estop-Aragonés, C., Knorr, K.-H., & Olefeldt, D. (2022). High peatland methane emissions following permafrost thaw: enhanced acetoclastic methanogenesis during early successional stages. *Biogeosciences*, 19(12), 3051–3071. <https://doi.org/10.5194/bg-19-3051-2022>

Heffernan, L., Estop-Aragonés, C., Knorr, K.-H., Olefeldt, D. (in prep.). Asynchronous interannual variability of the greenhouse gas exchange of young and mature thermokarst bogs due to differences in dominant environmental controls.

Heffernan, L., Estop-Aragonés, C., Knorr, K.-H., Talbot, J., & Olefeldt, D. (2020). Long-term Impacts of Permafrost Thaw on Carbon Storage in Peatlands: Deep Losses Offset by Surficial Accumulation. *Journal of Geophysical Research: Biogeosciences*, 125(3), e2019JG005501. <https://doi.org/10.1029/2019JG005501>

Heffernan, L., Jassey, V. E. J., Frederickson, M., MacKenzie, M. D., & Olefeldt, D. (2021). Constraints on potential enzyme activities in thermokarst bogs: Implications for the carbon balance of peatlands following thaw. *Global Change Biology*, 27(19), 4711–4726. <https://doi.org/10.1111/gcb.15758>

- Helbig, M., Chasmer, L. E., Desai, A. R., Kljun, N., Quinton, W. L., & Sonnentag, O. (2017). Direct and indirect climate change effects on carbon dioxide fluxes in a thawing boreal forest–wetland landscape. *Global Change Biology*, 23(8), 3231–3248. <https://doi.org/10.1111/gcb.13638>
- Helbig, M., Chasmer, L. E., Kljun, N., Quinton, W. L., Treat, C. C., & Sonnentag, O. (2017). The positive net radiative greenhouse gas forcing of increasing methane emissions from a thawing boreal forest-wetland landscape. *Global Change Biology*, 23(6), 2413–2427. <https://doi.org/10.1111/gcb.13520>
- Helbig, M., Pappas, C., & Sonnentag, O. (2016). Permafrost thaw and wildfire: Equally important drivers of boreal tree cover changes in the Taiga Plains, Canada. *Geophysical Research Letters*, 43(4), 1598–1606. <https://doi.org/10.1002/2015GL067193>
- Helbig, M., Quinton, W. L., & Sonnentag, O. (2017). Warmer spring conditions increase annual methane emissions from a boreal peat landscape with sporadic permafrost. *Environmental Research Letters*, 12(11), 115009. <https://doi.org/10.1088/1748-9326/aa8c85>
- Helbig, M., Wischniewski, K., Gosselin, G. H., Biraud, S. C., Bogoev, I., Chan, W. S., Euskirchen, E. S., Glenn, A. J., Marsh, P. M., Quinton, W. L., & Sonnentag, O. (2016). Addressing a systematic bias in carbon dioxide flux measurements with the EC150 and the IRGASON open-path gas analyzers. *Agricultural and Forest Meteorology*, 228–229, 349–359. <https://doi.org/10.1016/j.agrformet.2016.07.018>
- Helbig, M., Wischniewski, K., Kljun, N., Chasmer, L. E., Quinton, W. L., Detto, M., & Sonnentag, O. (2016). Regional atmospheric cooling and wetting effect of permafrost thaw-induced boreal forest loss. *Global Change Biology*, 22(12), 4048–4066. <https://doi.org/10.1111/gcb.13348>
- Helbig, M., Živković, T., Alekseychik, P., Aurela, M., El-Madany, T. S., Euskirchen, E. S., Flanagan, L. B., Griffis, T. J., Hanson, P. J., Hattakka, J., Helfter, C., Hirano, T., Humphreys, E. R., Kiely, G., Kolka, R. K., Laurila, T., Leahy, P. G., Lohila, A., Mammarella, I., ... Zaehle, S. (2022). Warming response of peatland CO₂ sink is sensitive to seasonality in warming trends. *Nature Climate Change*, 12(8), 743–749. <https://doi.org/10.1038/s41558-022-01428-z>

Hendzel, L. L., Matthews, C. J. D., Venkiteswaran, J. J., St. Louis, V. L., Burton, D., Joyce, E. M., & Bodaly, R. A. (2005). Nitrous Oxide Fluxes in Three Experimental Boreal Forest Reservoirs. *Environmental Science & Technology*, 39(12), 4353–4360. <https://doi.org/10.1021/es049443j>

Hermesdorf, L., Elberling, B., D’Imperio, L., Xu, W., Lambæk, A., & Ambus, P. L. (2022). Effects of fire on CO₂, CH₄, and N₂O exchange in a well-drained Arctic heath ecosystem. *Global Change Biology*, 28(16), 4882–4899. <https://doi.org/10.1111/gcb.16222>

Hodgkins, S. B., Tfaily, M. M., McCalley, C. K., Logan, T. A., Crill, P. M., Saleska, S. R., Rich, V. I., & Chanton, J. P. (2014). Changes in peat chemistry associated with permafrost thaw increase greenhouse gas production. *Proceedings of the National Academy of Sciences*, 111(16), 5819–5824. <https://doi.org/10.1073/pnas.1314641111>

Holloway, J. E., & Lewkowicz, A. G. (2020). Half a century of discontinuous permafrost persistence and degradation in western Canada. *Permafrost and Periglacial Processes*, 31(1), 85–96. <https://doi.org/10.1002/ppp.2017>

Holmes, M. E., Crill, P. M., Burnett, W. C., McCalley, C. K., Wilson, R. M., Frohling, S., Chang, K.-Y., Riley, W. J., Varner, R. K., Hodgkins, S. B., Coordinators, I. P., Team, I. F., McNichol, A. P., Saleska, S. R., Rich, V. I., & Chanton, J. P. (2022). Carbon Accumulation, Flux, and Fate in Stordalen Mire, a Permafrost Peatland in Transition. *Global Biogeochemical Cycles*, 36(1), e2021GB007113. <https://doi.org/10.1029/2021GB007113>

Hugelius, G., Loisel, J., Chadburn, S., Jackson, R. B., Jones, M., MacDonald, G., Marushchak, M., Olefeldt, D., Packalen, M., Siewert, M. B., Treat, C., Turetsky, M., Voigt, C., & Yu, Z. (2020). Large stocks of peatland carbon and nitrogen are vulnerable to permafrost thaw. *Proceedings of the National Academy of Sciences*, 117(34), 20438–20446. <https://doi.org/10.1073/pnas.1916387117>

Hugelius, G., Tarnocai, C., Broll, G., Canadell, J. G., Kuhry, P., & Swanson, D. K. (2013). The Northern Circumpolar Soil Carbon Database: spatially distributed datasets of soil coverage and soil carbon storage in the northern permafrost regions. *Earth System Science Data*, 5(1), 3–13. <https://doi.org/10.5194/essd-5-3-2013>

Humphreys, E. R., Lafleur, P. M., Flanagan, L. B., Hedstrom, N., Syed, K. H., Glenn, A. J., & Granger, R. (2006). Summer carbon dioxide and water vapor fluxes across a range of northern peatlands. *Journal of Geophysical Research: Biogeosciences*, 111(G4). <https://doi.org/10.1029/2005JG000111>

Hüppi, R., Felber, R., Krauss, M., Six, J., Leifeld, J., & Fuß, R. (2018). Restricting the nonlinearity parameter in soil greenhouse gas flux calculation for more reliable flux estimates. *PLOS ONE*, 13(7), e0200876. <https://doi.org/10.1371/journal.pone.0200876>

Huttunen, J. T., Väisänen, T. S., Heikkinen, M., Hellsten, S., Nykänen, H., Nenonen, O., & Martikainen, P. J. (2002). Exchange of CO₂, CH₄ and N₂O between the atmosphere and two northern boreal ponds with catchments dominated by peatlands or forests. *Plant and Soil*, 242(1), 137–146. <https://doi.org/10.1023/A:1019606410655>

Intergovernmental Panel on Climate Change (IPCC) (2014). Anthropogenic and Natural Radiative Forcing. In *Climate Change 2013: The Physical Science Basis. Contribution of Working Group I Contribution to the Fifth Assessment Report of the Intergovernmental Panel on Climate Change* [Stocker, T.F., D. Qin, G.-K. Plattner, M. Tignor, S.K. Allen, J. Boschung, A. Nauels, Y. Xia, V. Bex and P.M. Midgley (eds.)]. Cambridge University Press, Cambridge, United Kingdom and New York, NY, USA. 659-740. <https://doi.org/10.1017/CBO9781107415324.018>

Intergovernmental Panel on Climate Change (IPCC) (2013). Summary for Policymakers. In *Climate Change 2013: The Physical Science Basis. Contribution of Working Group I to the Fifth Assessment Report of the Intergovernmental Panel on Climate Change* [Stocker, T.F., D. Qin, G.-K. Plattner, M. Tignor, S.K. Allen, J. Boschung, A. Nauels, Y. Xia, V. Bex and P.M. Midgley (eds.)]. Cambridge University Press, Cambridge, United Kingdom and New York, NY, USA. 1-30. <https://doi.org/10.1017/CBO9781107415324.004>

Jiang, Y., Rastetter, E. B., Rocha, A. V, Pearce, A. R., Kwiatkowski, B. L., & Shaver, G. R. (2015). Modeling carbon–nutrient interactions during the early recovery of tundra after fire. *Ecological Applications*, 25(6), 1640–1652. <https://doi.org/10.1890/14-1921.1>

- Jiang, Y., Rastetter, E. B., Shaver, G. R., Rocha, A. V., Zhuang, Q., & Kwiatkowski, B. L. (2017). Modeling long-term changes in tundra carbon balance following wildfire, climate change, and potential nutrient addition. *Ecological Applications*, 27(1), 105–117. <https://doi.org/10.1002/eap.1413>
- Johansson, T., Malmer, N., Crill, P. M., Friborg, T., Åkerman, J. H., Mastepanov, M., & Christensen, T. R. (2006). Decadal vegetation changes in a northern peatland, greenhouse gas fluxes and net radiative forcing. *Global Change Biology*, 12(12), 2352–2369. <https://doi.org/10.1111/j.1365-2486.2006.01267.x>
- Johnstone, J. F., Rupp, T. S., Olson, M., & Verbyla, D. (2011). Modeling impacts of fire severity on successional trajectories and future fire behavior in Alaskan boreal forests. *Landscape Ecology*, 26(4), 487–500. <https://doi.org/10.1007/s10980-011-9574-6>
- Jones, M. C., Harden, J., O'Donnell, J., Manies, K., Jorgenson, T., Treat, C., & Ewing, S. (2017). Rapid carbon loss and slow recovery following permafrost thaw in boreal peatlands. *Global Change Biology*, 23(3), 1109–1127. <https://doi.org/10.1111/gcb.13403>
- Kasischke, E. S., Turetsky, M. R., Ottmar, R. D., French, N. H. F., Hoy, E. E., & Kane, E. S. (2008). Evaluation of the composite burn index for assessing fire severity in Alaskan black spruce forests. *International Journal of Wildland Fire*, 17(4), 515–526. <https://doi.org/10.1071/WF08002>
- Kassambara, A. (2021). rstatix: Pipe-Friendly Framework for Basic Statistical Tests. R package version 0.7.0, <https://rpkgs.datanovia.com/rstatix/>. Retrieved from <https://github.com/kassambara/rstatix/releases/tag/v0.7.0>
- Kassambara, A. (2023). ggpubr: 'ggplot2' Based Publication Ready Plots. R package version 0.6.0, <https://rpkgs.datanovia.com/ggpubr/>
- Keenan, T. F., Hollinger, D. Y., Bohrer, G., Dragoni, D., Munger, J. W., Schmid, H. P., & Richardson, A. D. (2013). Increase in forest water-use efficiency as atmospheric carbon dioxide concentrations rise. *Nature*, 499(7458), 324–327. <https://doi.org/10.1038/nature12291>

Kettridge, N., Turetsky, M. R., Sherwood, J. H., Thompson, D. K., Miller, C. A., Benscoter, B. W., Flannigan, M. D., Wotton, B. M., & Waddington, J. M. (2015). Moderate drop in water table increases peatland vulnerability to post-fire regime shift. *Scientific Reports*, 5(1), 8063. <https://doi.org/10.1038/srep08063>

Keuper, F., Dorrepaal, E., van Bodegom, P. M., van Logtestijn, R., Venhuizen, G., van Hal, J., & Aerts, R. (2017). Experimentally increased nutrient availability at the permafrost thaw front selectively enhances biomass production of deep-rooting subarctic peatland species. *Global Change Biology*, 23(10), 4257–4266. <https://doi.org/10.1111/gcb.13804>

Keuper, F., van Bodegom, P. M., Dorrepaal, E., Weedon, J. T., van Hal, J., van Logtestijn, R. S. P., & Aerts, R. (2012). A frozen feast: thawing permafrost increases plant-available nitrogen in subarctic peatlands. *Global Change Biology*, 18(6), 1998–2007. <https://doi.org/10.1111/j.1365-2486.2012.02663.x>

Kljun, N., Calanca, P., Rotach, M. W., & Schmid, H. P. (2015). A simple two-dimensional parameterisation for Flux Footprint Prediction (FFP). *Geoscientific Model Development*, 8(11), 3695–3713. <https://doi.org/10.5194/gmd-8-3695-2015>

Knoblauch, C., Beer, C., Liebner, S., & Grigoriev, M. N. (2018). Methane production as key to the greenhouse gas budget of thawing permafrost. *Nature Climate Change*, 8, 309–312. <https://doi.org/10.1038/s41558-018-0095-z>

Kortelainen, P., Larmola, T., Rantakari, M., Juutinen, S., Alm, J., & Martikainen, P. J. (2020). Lakes as nitrous oxide sources in the boreal landscape. *Global Change Biology*, 26(3), 1432–1445. <https://doi.org/10.1111/gcb.14928>

Köster, E., Köster, K., Berninger, F., Aaltonen, H., Zhou, X., & Pumpanen, J. (2017). Carbon dioxide, methane and nitrous oxide fluxes from a fire chronosequence in subarctic boreal forests of Canada. *Science of The Total Environment*, 601–602, 895–905. <https://doi.org/10.1016/j.scitotenv.2017.05.246>

Kou, D., Virtanen, T., Treat, C. C., Tuovinen, J.-P., Räsänen, A., Juutinen, S., Mikola, J., Aurela, M., Heiskanen, L., Heikkilä, M., Weckström, J., Juselius, T., Piilo, S. R., Deng, J., Zhang, Y.,

Chaudhary, N., Huang, C., Väiliranta, M., Biasi, C., ... Shurpali, N. J. (2022). Peatland Heterogeneity Impacts on Regional Carbon Flux and Its Radiative Effect Within a Boreal Landscape. *Journal of Geophysical Research: Biogeosciences*, 127(9), e2021JG006774. <https://doi.org/10.1029/2021JG006774>

Koven, C. D., Lawrence, D. M., & Riley, W. J. (2015). Permafrost carbon–climate feedback is sensitive to deep soil carbon decomposability but not deep soil nitrogen dynamics. *Proceedings of the National Academy of Sciences*, 112(12), 3752 LP – 3757. <https://doi.org/10.1073/pnas.1415123112>

Kropp, H., Loranty, M. M., Natali, S. M., Kholodov, A. L., Rocha, A. V, Myers-Smith, I., Abbot, B. W., Abermann, J., Blanc-Betes, E., Blok, D., Blume-Werry, G., Boike, J., Breen, A. L., Cahoon, S. M. P., Christiansen, C. T., Douglas, T. A., Epstein, H. E., Frost, G. V, Goeckede, M., ... Lund, M. (2021). Shallow soils are warmer under trees and tall shrubs across Arctic and Boreal ecosystems. *Environmental Research Letters*, 16(1), 015001. <https://doi.org/10.1088/1748-9326/abc994>

Kuhn, M. A., Schmidt, M., Heffernan, L., Stührenberg, J., Knorr, K.-H., Estop-Aragonés, C., Broder, T., Gonzalez Moguel, R., Douglas, P. M. J., & Olefeldt, D. (2022). High ebullitive, millennial-aged greenhouse gas emissions from thermokarst expansion of peatland lakes in boreal western Canada. *Limnology and Oceanography*, 68(2), 498-513. <https://doi.org/10.1002/lno.12288>

Kuhn, M. A., Thompson, L. M., Winder, J. C., Braga, L. P. P., Tanentzap, A. J., Bastviken, D., & Olefeldt, D. (2021). Opposing Effects of Climate and Permafrost Thaw on CH₄ and CO₂ Emissions From Northern Lakes. *AGU Advances*, 2(4), e2021AV000515. <https://doi.org/10.1029/2021AV000515>

Kuhn, M. A., Varner, R. K., Bastviken, D., Crill, P., MacIntyre, S., Turetsky, M., Walter Anthony, K., McGuire, A. D., & Olefeldt, D. (2021). BAWLD-CH₄: a comprehensive dataset of methane fluxes from boreal and arctic ecosystems. *Earth System Science Data*, 13(11), 5151–5189. <https://doi.org/10.5194/essd-13-5151-2021>

- Kuntzemann, C. E., Whitman, E., Stralberg, D., Parisien, M.-A., Thompson, D. K., & Nielsen, S. E. (2023). Peatlands promote fire refugia in boreal forests of northern Alberta, Canada. *Ecosphere*, 14(5), e4510. <https://doi.org/10.1002/ecs2.4510>
- Kuosmanen, N., Väiliranta, M., Piilo, S., Tuittila, E.-S., Oksanen, P., & Wallenius, T. (2023). Repeated fires in forested peatlands in sporadic permafrost zone in Western Canada. *Environmental Research Letters*, 18(9), 094051. <https://doi.org/10.1088/1748-9326/acf05b>
- Kurz, W. A., Shaw, C. H., Boisvenue, C., Stinson, G., Metsaranta, J., Leckie, D., Dyk, A., Smyth, C., & Neilson, E. T. (2013). Carbon in Canada's boreal forest — A synthesis. *Environmental Reviews*, 21(4), 260–292. <https://doi.org/10.1139/er-2013-0041>
- Lafleur, P. M., Humphreys, E. R., St. Louis, V. L., Myklebust, M. C., Papakyriakou, T., Poissant, L., Barker, J. D., Pilote, M., & Swystun, K. A. (2012). Variation in Peak Growing Season Net Ecosystem Production Across the Canadian Arctic. *Environmental Science & Technology*, 46(15), 7971–7977. <https://doi.org/10.1021/es300500m>
- Lambert, M.-C., Ung, C.-H., & Raulier, F. (2005). Canadian national tree aboveground biomass equations. *Canadian Journal of Forest Research*, 35(8), 1996–2018. <https://doi.org/10.1139/x05-112>
- Lawrence, D. M., Slater, A. G., & Swenson, S. C. (2012). Simulation of Present-Day and Future Permafrost and Seasonally Frozen Ground Conditions in CCSM4. *Journal of Climate*, 25(7), 2207–2225. <http://www.jstor.org/stable/26191314>
- Lenton, T. M., Held, H., Kriegler, E., Hall, J. W., Lucht, W., Rahmstorf, S., & Schellnhuber, H. J. (2008). Tipping elements in the Earth's climate system. *Proceedings of the National Academy of Sciences of the United States of America*, 105(6), 1786–1793. <https://doi.org/10.1073/pnas.0705414105>
- Li, X., Jin, H., He, R., Wang, H., Sun, L., Luo, D., Li, Y., Huang, Y., Yang, X., Jin, X., Chang, X., Wang, L., Wei, C., & Zhang, Z. (2023). Influence of wildfire on the rapidly changing features of patchy permafrost, Northeast China. *Land Degradation & Development*, 34(9), 2652–2667. <https://doi.org/10.1002/ldr.4637>

Liimatainen, M., Martikainen, P. J., & Maljanen, M. (2014). Why granulated wood ash decreases N₂O production in boreal acidic peat soil? *Soil Biology and Biochemistry*, 79, 140–148. <https://doi.org/10.1016/j.soilbio.2014.09.016>

Liimatainen, M., Voigt, C., Martikainen, P. J., Hytönen, J., Regina, K., Óskarsson, H., & Maljanen, M. (2018). Factors controlling nitrous oxide emissions from managed northern peat soils with low carbon to nitrogen ratio. *Soil Biology and Biochemistry*, 122, 186–195. <https://doi.org/10.1016/j.soilbio.2018.04.006>

Lindgren, A., Hugelius, G., & Kuhry, P. (2018). Extensive loss of past permafrost carbon but a net accumulation into present-day soils. *Nature*, 560(7717), 219–222. <https://doi.org/10.1038/s41586-018-0371-0>

Lindroth, A., Lund, M., Nilsson, M., Aurela, M., Christensen, T. R., Laurila, T., Rinne, J., Riutta, T., Sagerfors, J., Ström, L., Tuovinen, J.-P., & Vesala, T. (2007). Environmental controls on the CO₂ exchange in north European mires. *Tellus B*, 59(5), 812–825. <https://doi.org/10.1111/j.1600-0889.2007.00310.x>

Liu, S., Bond-Lamberty, B., Hicke, J. A., Vargas, R., Zhao, S., Chen, J., Edburg, S. L., Hu, Y., Liu, J., McGuire, A. D., Xiao, J., Keane, R., Yuan, W., Tang, J., Luo, Y., Potter, C., & Oeding, J. (2011). Simulating the impacts of disturbances on forest carbon cycling in North America: Processes, data, models, and challenges. *Journal of Geophysical Research: Biogeosciences*, 116(G4). <https://doi.org/10.1029/2010JG001585>

Loisel, J., Gallego-Sala, A. V, Amesbury, M. J., Magnan, G., Anshari, G., Beilman, D. W., Benavides, J. C., Blewett, J., Camill, P., Charman, D. J., Chawchai, S., Hedgpeth, A., Kleinen, T., Korhola, A., Large, D., Mansilla, C. A., Müller, J., van Bellen, S., West, J. B., ... Wu, J. (2020). Expert assessment of future vulnerability of the global peatland carbon sink. *Nature Climate Change*, 11, 70–77. <https://doi.org/10.1038/s41558-020-00944-0>

Loisel, J., Yu, Z., Beilman, D. W., Camill, P., Alm, J., Amesbury, M. J., Anderson, D., Andersson, S., Bochicchio, C., Barber, K., Belyea, L. R., Bunbury, J., Chambers, F. M., Charman, D. J., De Vleeschouwer, F., Fiałkiewicz-Kozieł, B., Finkelstein, S. A., Gałka, M., Garneau, M., ... Zhou, W. (2014). A database and synthesis of northern peatland soil properties

and Holocene carbon and nitrogen accumulation. *The Holocene*, 24(9), 1028–1042. <https://doi.org/10.1177/0959683614538073>

Long, K. D., Flanagan, L. B., & Cai, T. (2010). Diurnal and seasonal variation in methane emissions in a northern Canadian peatland measured by eddy covariance. *Global Change Biology*, 16(9), 2420–2435. <https://doi.org/10.1111/j.1365-2486.2009.02083.x>

Lund, M., Lafleur, P. M., Roulet, N. T., Lindroth, A., Christensen, T. R., Aurela, M., Chojnicki, B. H., Flanagan, L. B., Humphreys, E. R., Laurila, T., Oechel, W. C., Olejnik, J., Rinne, J., Schubert, P., & Nilsson, M. B. (2010). Variability in exchange of CO₂ across 12 northern peatland and tundra sites. *Global Change Biology*, 16(9), 2436–2448. <https://doi.org/10.1111/j.1365-2486.2009.02104.x>

Lyons, E. A., Jin, Y., & Randerson, J. T. (2008). Changes in surface albedo after fire in boreal forest ecosystems of interior Alaska assessed using MODIS satellite observations. *Journal of Geophysical Research: Biogeosciences*, 113(G2). <https://doi.org/10.1029/2007JG000606>

Lyu, Z., Genet, H., He, Y., Zhuang, Q., McGuire, A. D., Bennett, A., Breen, A., Clein, J., Euskirchen, E. S., Johnson, K., Kurkowski, T., Pastick, N. J., Rupp, T. S., Wylie, B. K., & Zhu, Z. (2018). The role of environmental driving factors in historical and projected carbon dynamics of wetland ecosystems in Alaska. *Ecological Applications*, 28(6), 1377–1395. <https://doi.org/10.1002/eap.1755>

Mack, M. C., Bret-Harte, M. S., Hollingsworth, T. N., Jandt, R. R., Schuur, E. A. G., Shaver, G. R., & Verbyla, D. L. (2011). Carbon loss from an unprecedented Arctic tundra wildfire. *Nature*, 475(7357), 489–492. <https://doi.org/10.1038/nature10283>

Mack, M. C., Walker, X. J., Johnstone, J. F., Alexander, H. D., Melvin, A. M., Jean, M., & Miller, S. N. (2021). Carbon loss from boreal forest wildfires offset by increased dominance of deciduous trees. *Science*, 372(6539), 280 – 283. <https://doi.org/10.1126/science.abf3903>

Maljanen, M., Sigurdsson, B. D., Guðmundsson, J., Óskarsson, H., Huttunen, J. T., & Martikainen, P. J. (2010). Greenhouse gas balances of managed peatlands in the Nordic countries

– present knowledge and gaps. *Biogeosciences*, 7(9), 2711–2738. <https://doi.org/10.5194/bg-7-2711-2010>

Mallon, E. E., Turetsky, M. R., Thompson, I. D., Fryxell, J. M., & Wiebe, P. A. (2016). Effects of disturbance on understory succession in upland and lowland boreal forests and implications for woodland caribou (*Rangifer tarandus caribou*). *Forest Ecology and Management*, 364, 17–26. <https://doi.org/10.1016/j.foreco.2015.12.001>

Marshall, I. B., Schut, P. H., & Ballard, M. (1999). A National Ecological Framework for Canada. Agriculture and Agri-Food Canada, Research Branch, Centre for Land and Biological Resources Research, and Environment Canada, State of the Environment Directorate, Ecozone Analysis Branch. <https://sis.agr.gc.ca/cansis/nsdb/ecostrat/index.html>

Martikainen, P. J., Nykänen, H., Crill, P., & Silvola, J. (1993). Effect of a lowered water table on nitrous oxide fluxes from northern peatlands. *Nature*, 366(6450), 51–53. <https://doi.org/10.1038/366051a0>

Marushchak, M. E., Kerttula, J., Diáková, K., Faguet, A., Gil, J., Grosse, G., Knoblauch, C., Lashchinskiy, N., Martikainen, P. J., Morgenstern, A., Nykamb, M., Ronkainen, J. G., Siljanen, H. M. P., van Delden, L., Voigt, C., Zimov, N., Zimov, S., & Biasi, C. (2021). Thawing Yedoma permafrost is a neglected nitrous oxide source. *Nature Communications*, 12(1), 7107. <https://doi.org/10.1038/s41467-021-27386-2>

Marushchak, M. E., Pitkämäki, A., Koponen, H., Biasi, C., Seppälä, M., & Martikainen, P. J. (2011). Hot spots for nitrous oxide emissions found in different types of permafrost peatlands. *Global Change Biology*, 17(8), 2601–2614. <https://doi.org/10.1111/j.1365-2486.2011.02442.x>

Mauder, M., & Foken, T. (2011). Documentation and Instruction Manual of the Eddy Covariance Software Package TK3, 1-60, Univ. Bayreuth, Abt. Mikrometeorologie, Bayreuth, Germany. (ISSN 1614-8916). Retrieved from <https://core.ac.uk/download/pdf/33805297.pdf>

Maxwell, R. S., & Larsson, L.-A. (2021). Measuring tree-ring widths using the CooRecorder software application (Technical Note), *Dendrochronologia*, 67(June 2021), 125841. <https://doi.org/10.1016/j.dendro.2021.125841>

McClain, M. E., Boyer, E. W., Dent, C. L., Gergel, S. E., Grimm, N. B., Groffman, P. M., Hart, S. C., Harvey, J. W., Johnston, C. A., Mayorga, E., McDowell, W. H., & Pinay, G. (2003). Biogeochemical Hot Spots and Hot Moments at the Interface of Terrestrial and Aquatic Ecosystems. *Ecosystems*, 6(4), 301–312. <https://doi.org/10.1007/s10021-003-0161-9>

McGuire, A. D., Lawrence, D. M., Koven, C., Klein, J. S., Burke, E., Chen, G., Jafarov, E., MacDougall, A. H., Marchenko, S., Nicolsky, D., Peng, S., Rinke, A., Ciais, P., Gouttevin, I., Hayes, D. J., Ji, D., Krinner, G., Moore, J. C., Romanovsky, V., ... Zhuang, Q. (2018). Dependence of the evolution of carbon dynamics in the northern permafrost region on the trajectory of climate change. *Proceedings of the National Academy of Sciences*, 115(15), 3882–3887. <https://doi.org/10.1073/pnas.1719903115>

Mekonnen, Z. A., & Riley, W. J. (2023). Climate Change Will Increase Biomass Proportion of Global Forest Carbon Stocks Under an SSP5–8.5 Climate Trajectory. *Geophysical Research Letters*, 50(23), e2023GL104612. <https://doi.org/10.1029/2023GL104612>

Miner, K. R., Turetsky, M. R., Malina, E., Bartsch, A., Tamminen, J., McGuire, A. D., Fix, A., Sweeney, C., Elder, C. D., & Miller, C. E. (2022). Permafrost carbon emissions in a changing Arctic. *Nature Reviews Earth & Environment*, 3(1), 55–67. <https://doi.org/10.1038/s43017-021-00230-3>

Moncrieff, J. B., Massheder, J. M., de Bruin, H., Elbers, J., Friborg, T., Heusinkveld, B., Kabat, P., Scott, S., Soegaard, H., & Verhoef, A. (1997). A system to measure surface fluxes of momentum, sensible heat, water vapour and carbon dioxide. *Journal of Hydrology*, 188–189, 589–611. [https://doi.org/10.1016/S0022-1694\(96\)03194-0](https://doi.org/10.1016/S0022-1694(96)03194-0)

Moncrieff, J., Clement, R., Finnigan, J., & Meyers, T. (2004). Averaging, Detrending, and Filtering of Eddy Covariance Time Series. In W. and L. B. Lee Xuhui and Massman (Ed.), Lee, X., Massman, W., Law, B. (eds) *Handbook of Micrometeorology: A Guide for Surface Flux Measurement and Analysis*, 7–31. Springer, The Netherlands. https://doi.org/10.1007/1-4020-2265-4_2

- Moore, T., Blodau, C., Turunen, J., Roulet, N., & Richard, P. J. H. (2005). Patterns of nitrogen and sulfur accumulation and retention in ombrotrophic bogs, eastern Canada. *Global Change Biology*, 11(2), 356–367. <https://doi.org/10.1111/j.1365-2486.2004.00882.x>
- Morison, M. Q., Macrae, M. L., Petrone, R. M., & Fishback, L. (2018). Climate-induced changes in nutrient transformations across landscape units in a thermokarst subarctic peatland. *Arctic, Antarctic, and Alpine Research*, 50(1), e1519366. <https://doi.org/10.1080/15230430.2018.1519366>
- Morison, M., van Beest, C., Macrae, M., Nwaishi, F., & Petrone, R. (2021). Deeper burning in a boreal fen peatland 1-year post-wildfire accelerates recovery trajectory of carbon dioxide uptake. *Ecohydrology*, 14(3), e2277. <https://doi.org/10.1002/eco.2277>
- Moubarak, M., Sistla, S., Potter, S., Natali, S. M., & Rogers, B. M. (2023). Carbon emissions and radiative forcings from tundra wildfires in the Yukon–Kuskokwim River Delta, Alaska. *Biogeosciences*, 20(8), 1537–1557. <https://doi.org/10.5194/bg-20-1537-2023>
- Murray, K. J., Tenhunen, J. D., & Nowak, R. S. (1993). Photoinhibition as a control on photosynthesis and production of Sphagnum mosses. *Oecologia*, 96(2), 200–207. <https://doi.org/10.1007/BF00317733>
- Myers-Smith, I. H., McGuire, A. D., Harden, J. W., & Chapin III, F. S. (2007). Influence of disturbance on carbon exchange in a permafrost collapse and adjacent burned forest. *Journal of Geophysical Research: Biogeosciences*, 112(G4). <https://doi.org/10.1029/2007JG000423>
- Nadelhoffer, K. J., Giblin, A. E., Shaver, G. R., & Laundre, J. A. (1991). Effects of Temperature and Substrate Quality on Element Mineralization in Six Arctic Soils. *Ecology*, 72(1), 242–253. <https://doi.org/10.2307/1938918>
- Naiman, R. J., & Melillo, J. M. (1984). Nitrogen budget of a subarctic stream altered by beaver (*Castor canadensis*). *Oecologia*, 62(2), 150–155. <https://doi.org/10.1007/BF00379007>
- Natali, S. M., Bronen, R., Cochran, P., Holdren, J. P., Rogers, B. M., & Treharne, R. (2022). Incorporating permafrost into climate mitigation and adaptation policy. *Environmental Research Letters*, 17(9), 091001. <https://doi.org/10.1088/1748-9326/ac8c5a>

- Natural Resources Canada (2023). Canada's record-breaking wildfires in 2023: A fiery wake-up call. Retrieved from <https://natural-resources.canada.ca/simply-science/canadas-record-breaking-wildfires-2023-fiery-wake-call/25303>
- Neff, J. C., Harden, J. W., & Gleixner, G. (2005). Fire effects on soil organic matter content, composition, and nutrients in boreal interior Alaska. *Canadian Journal of Forest Research*, 35(9), 2178–2187. <https://doi.org/10.1139/x05-154>
- Nelson, K., Thompson, D., Hopkinson, C., Petrone, R., & Chasmer, L. (2021). Peatland-fire interactions: A review of wildland fire feedbacks and interactions in Canadian boreal peatlands. *Science of The Total Environment*, 769, 145212. <https://doi.org/10.1016/j.scitotenv.2021.145212>
- Neubauer, S. C., & Megonigal, J. P. (2015). Moving Beyond Global Warming Potentials to Quantify the Climatic Role of Ecosystems. *Ecosystems*, 18(6), 1000–1013. <http://www.jstor.org/stable/43677758>
- Neubauer, S. C., & Megonigal, J. P. (2019). Correction to: Moving Beyond Global Warming Potentials to Quantify the Climatic Role of Ecosystems. *Ecosystems*, 22(8), 1931–1932. <https://doi.org/10.1007/s10021-019-00422-5>
- Nilsson, M., Sagerfors, J., Buffam, I., Laudon, H., Eriksson, T., Grelle, A., Klemedtsson, L., Weslien, P. E. R., & Lindroth, A. (2008). Contemporary carbon accumulation in a boreal oligotrophic minerogenic mire – a significant sink after accounting for all C-fluxes. *Global Change Biology*, 14(10), 2317–2332. <https://doi.org/10.1111/j.1365-2486.2008.01654.x>
- Norman, J. M., Kucharik, C. J., Gower, S. T., Baldocchi, D. D., Crill, P. M., Rayment, M., Savage, K., & Striegl, R. G. (1997). A comparison of six methods for measuring soil-surface carbon dioxide fluxes. *Journal of Geophysical Research: Atmospheres*, 102(D24), 28771–28777. <https://doi.org/10.1029/97JD01440>
- Nossov, D. R., Torre Jorgenson, M., Kielland, K., & Kanevskiy, M. Z. (2013). Edaphic and microclimatic controls over permafrost response to fire in interior Alaska. *Environmental Research Letters*, 8(3), 035013. <https://doi.org/10.1088/1748-9326/8/3/035013>

Nugent, K. A., Strachan, I. B., Roulet, N. T., Strack, M., Frohking, S., & Helbig, M. (2019). Prompt active restoration of peatlands substantially reduces climate impact. *Environmental Research Letters*, 14(12), 124030. <https://doi.org/10.1088/1748-9326/ab56e6>

Obu, J., Westermann, S., Bartsch, A., Berdnikov, N., Christiansen, H. H., Dashtseren, A., Delaloye, R., Elberling, B., Etzelmüller, B., Kholodov, A., Khomutov, A., Kääh, A., Leibman, M. O., Lewkowicz, A. G., Panda, S. K., Romanovsky, V., Way, R. G., Westergaard-Nielsen, A., Wu, T., ... Zou, D. (2019). Northern Hemisphere permafrost map based on TTOP modelling for 2000–2016 at 1 km² scale. *Earth-Science Reviews*, 193, 299–316. <https://doi.org/10.1016/j.earscirev.2019.04.023>

O'Donnell, J. A., Jorgenson, M. T., Harden, J. W., McGuire, A. D., Kanevskiy, M. Z., & Wickland, K. P. (2012). The Effects of Permafrost Thaw on Soil Hydrologic, Thermal, and Carbon Dynamics in an Alaskan Peatland. *Ecosystems*, 15(2), 213–229. <https://doi.org/10.1007/s10021-011-9504-0>

O'Donnell, J. A., Turetsky, M. R., Harden, J. W., Manies, K. L., Pruett, L. E., Shetler, G., & Neff, J. C. (2009). Interactive Effects of Fire, Soil Climate, and Moss on CO₂ Fluxes in Black Spruce Ecosystems of Interior Alaska. *Ecosystems*, 12(1), 57–72. <https://doi.org/10.1007/s10021-008-9206-4>

Olefeldt, D., Devito, K. J., & Turetsky, M. R. (2013). Sources and fate of terrestrial dissolved organic carbon in lakes of a Boreal Plains region recently affected by wildfire. *Biogeosciences*, 10(10), 6247–6265. <https://doi.org/10.5194/bg-10-6247-2013>

Olefeldt, D., Euskirchen, E. S., Harden, J., Kane, E., McGuire, A. D., Waldrop, M. P., & Turetsky, M. R. (2017). A decade of boreal rich fen greenhouse gas fluxes in response to natural and experimental water table variability. *Global Change Biology*, 23(6), 2428–2440. <https://doi.org/10.1111/gcb.13612>

Olefeldt, D., Goswami, S., Grosse, G., Hayes, D., Hugelius, G., Kuhry, P., McGuire, A. D., Romanovsky, V. E., Sannel, A. B. K., Schuur, E. A. G., & Turetsky, M. R. (2016). Circumpolar distribution and carbon storage of thermokarst landscapes. *Nature Communications*, 7, 13043. <https://doi.org/10.1038/ncomms13043>

Olefeldt, D., Hovemyr, M., Kuhn, M. A., Bastviken, D., Bohn, T. J., Connolly, J., Crill, P., Euskirchen, E. S., Finkelstein, S. A., Genet, H., Grosse, G., Harris, L. I., Heffernan, L., Helbig, M., Hugelius, G., Hutchins, R., Juutinen, S., Lara, M. J., Malhotra, A., ... Watts, J. D. (2021). The Boreal-Arctic Wetland and Lake Dataset (BAWLD). *Earth System Science Data*, 13(11), 5127–5149. <https://doi.org/10.5194/essd-13-5127-2021>

Olefeldt, D., & Roulet, N. T. (2012). Effects of permafrost and hydrology on the composition and transport of dissolved organic carbon in a subarctic peatland complex. *Journal of Geophysical Research: Biogeosciences*, 117(G1). <https://doi.org/10.1029/2011JG001819>

Olefeldt, D., Roulet, N. T., Bergeron, O., Crill, P., Bäckstrand, K., & Christensen, T. R. (2012). Net carbon accumulation of a high-latitude permafrost palsa mire similar to permafrost-free peatlands. *Geophysical Research Letters*, 39(3). <https://doi.org/10.1029/2011GL050355>

Oliveira, B. R. F., Schaller, C., Keizer, J. J., & Foken, T. (2021). Estimating immediate post-fire carbon fluxes using the eddy-covariance technique. *Biogeosciences*, 18(1), 285–302. <https://doi.org/10.5194/bg-18-285-2021>

Orlova, J., Olefeldt, D., Yasinski, J. H., & Anderson, A. E. (2020). Effects of Prescribed Burn on Nutrient and Dissolved Organic Matter Characteristics in Peatland Shallow Groundwater. *Fire*, 3(3). <https://doi.org/10.3390/fire3030053>

Osterkamp, T. E., Jorgenson, M. T., Schuur, E. A. G., Shur, Y. L., Kanevskiy, M. Z., Vogel, J. G., & Tumskey, V. E. (2009). Physical and ecological changes associated with warming permafrost and thermokarst in Interior Alaska. *Permafrost and Periglacial Processes*, 20(3), 235–256. <https://doi.org/10.1002/ppp.656>

Palmer, K., Biasi, C., & Horn, M. A. (2012). Contrasting denitrifier communities relate to contrasting N₂O emission patterns from acidic peat soils in arctic tundra. *The ISME Journal*, 6(5), 1058–1077. <https://doi.org/10.1038/ismej.2011.172>

Pan, Y., Birdsey, R. A., Fang, J., Houghton, R., Kauppi, P. E., Kurz, W. A., Phillips, O. L., Shvidenko, A., Lewis, S. L., Canadell, J. G., Ciais, P., Jackson, R. B., Pacala, S. W., McGuire, A. D., Piao, S., Rautiainen, A., Sitch, S., & Hayes, D. (2011). A Large and Persistent Carbon

Sink in the World's Forests. *Science*, 333(6045), 988–993.
<https://doi.org/10.1126/science.1201609>

Papale, D., Reichstein, M., Aubinet, M., Canfora, E., Bernhofer, C., Kutsch, W., Longdoz, B., Rambal, S., Valentini, R., Vesala, T., & Yakir, D. (2006). Towards a standardized processing of Net Ecosystem Exchange measured with eddy covariance technique: algorithms and uncertainty estimation. *Biogeosciences*, 3(4), 571–583. <https://doi.org/10.5194/bg-3-571-2006>

Peichl, M., Gažovič, M., Vermeij, I., de Goede, E., Sonnentag, O., Limpens, J., & Nilsson, M. B. (2018). Peatland vegetation composition and phenology drive the seasonal trajectory of maximum gross primary production. *Scientific Reports*, 8(1), 8012. <https://doi.org/10.1038/s41598-018-26147-4>

Pelletier, N., Talbot, J., Olefeldt, D., Turetsky, M., Blodau, C., Sonnentag, O., & Quinton, W. L. (2017). Influence of Holocene permafrost aggradation and thaw on the paleoecology and carbon storage of a peatland complex in northwestern Canada. *The Holocene*, 27(9), 1391–1405. <https://doi.org/10.1177/0959683617693899>

Pennock, D., Yates, T., Bedard-Haughn, A., Phipps, K., Farrell, R., & Mcdougal, R. (2010). Landscape controls on N₂O and CH₄ emissions from freshwater mineral soil wetlands of the Canadian Prairie Pothole region. *Geoderma*, 155(3–4), 308–319. <https://doi.org/10.1016/j.geoderma.2009.12.015>

Perron, N., Baltzer, J. L., & Sonnentag, O. (2023). Spatial and temporal variation in forest transpiration across a forested boreal peatland complex. *Hydrological Processes*, 37(2), e14815. <https://doi.org/10.1002/hyp.14815>

Perryman, C. R., McCalley, C. K., Malhotra, A., Fahnestock, M. F., Kashi, N. N., Bryce, J. G., Giesler, R., & Varner, R. K. (2020). Thaw Transitions and Redox Conditions Drive Methane Oxidation in a Permafrost Peatland. *Journal of Geophysical Research: Biogeosciences*, 125(3), e2019JG005526. <https://doi.org/10.1029/2019JG005526>

Piao, S., Ciais, P., Friedlingstein, P., Peylin, P., Reichstein, M., Luysaert, S., Margolis, H., Fang, J., Barr, A., Chen, A., Grelle, A., Hollinger, D. Y., Laurila, T., Lindroth, A., Richardson,

A. D., & Vesala, T. (2008). Net carbon dioxide losses of northern ecosystems in response to autumn warming. *Nature*, 451(7174), 49–52. <https://doi.org/10.1038/nature06444>

Pinheiro, J., Bates, D., DebRoy, S., Sarkar, D., EISPACK authors, Heisterkamp, S., van Willigen, B., Ranke, J., & R Core Team. (2023). nlme: Linear and nonlinear mixed effects models. R package version 3.1-164, <https://CRAN.R-project.org/package=nlme>. Retrieved from <https://svn.r-project.org/R-packages/trunk/nlme/>

Potter, S., Solvik, K., Erb, A., Goetz, S. J., Johnstone, J. F., Mack, M. C., Randerson, J. T., Román, M. O., Schaaf, C. L., Turetsky, M. R., Veraverbeke, S., Walker, X. J., Wang, Z., Massey, R., & Rogers, B. M. (2020). Climate change decreases the cooling effect from postfire albedo in boreal North America. *Global Change Biology*, 26(3), 1592–1607. <https://doi.org/10.1111/gcb.14888>

Price, D. T., Alfaro, R. I., Brown, K. J., Flannigan, M. D., Fleming, R. A., Hogg, E. H., Girardin, M. P., Lakusta, T., Johnston, M., McKenney, D. W., Pedlar, J. H., Stratton, T., Sturrock, R. N., Thompson, I. D., Trofymow, J. A., & Venier, L. A. (2013). Anticipating the consequences of climate change for Canada’s boreal forest ecosystems. *Environmental Reviews*, 21(4), 322–365. <https://doi.org/10.1139/er-2013-0042>

Quillet, A., Garneau, M., & Frohling, S. (2013). Sobol’ sensitivity analysis of the Holocene Peat Model: What drives carbon accumulation in peatlands? *Journal of Geophysical Research: Biogeosciences*, 118(1), 203–214. <https://doi.org/10.1029/2012JG002092>

Quinton, W., Berg, A., Braverman, M., Carpino, O., Chasmer, L., Connon, R., Craig, J., Devoie, É., Hayashi, M., Haynes, K., Olefeldt, D., Pietroniro, A., Rezanezhad, F., Schincariol, R., & Sonnentag, O. (2019). A synthesis of three decades of hydrological research at Scotty Creek, NWT, Canada. *Hydrology & Earth System Sciences*, 23(4), 2015–2039. <http://10.0.20.74/hess-23-2015-2019>

Quinton, W. L., Hayashi, M., & Chasmer, L. E. (2009). Peatland Hydrology of Discontinuous Permafrost in the Northwest Territories: Overview and Synthesis. *Canadian Water Resources Journal / Revue Canadienne Des Ressources Hydriques*, 34(4), 311–328. <https://doi.org/10.4296/cwrj3404311>

R Core Team. (2020). R: A language and environment for statistical computing (3.6.3). R Foundation for Statistical Computing. <https://www.r-project.org/>.

Ramm, E., Liu, C., Ambus, P., Butterbach-Bahl, K., Hu, B., Martikainen, P. J., Marushchak, M. E., Mueller, C. W., Rennenberg, H., Schloter, M., Siljanen, H. M. P., Voigt, C., Werner, C., Biasi, C., & Dannenmann, M. (2022). A review of the importance of mineral nitrogen cycling in the plant-soil-microbe system of permafrost-affected soils — changing the paradigm. *Environmental Research Letters*, 17(1), 13004. <https://doi.org/10.1088/1748-9326/ac417e>

Randerson, J. T., Liu, H., Flanner, M. G., Chambers, S. D., Jin, Y., Hess, P. G., Pfister, G., Mack, M. C., Treseder, K. K., Welp, L. R., Chapin, F. S., Harden, J. W., Goulden, M. L., Lyons, E., Neff, J. C., Schuur, E. A. G., & Zender, C. S. (2006). The Impact of Boreal Forest Fire on Climate Warming. *Science*, 314(5802), 1130–1132. <https://doi.org/10.1126/science.1132075>

Rantanen, M., Karpechko, A. Yu., Lipponen, A., Nordling, K., Hyvärinen, O., Ruosteenoja, K., Vihma, T., & Laaksonen, A. (2022). The Arctic has warmed nearly four times faster than the globe since 1979. *Communications Earth & Environment*, 3(1), 168. <https://doi.org/10.1038/s43247-022-00498-3>

Regina, K., Nykänen, H., Maljanen, M., Silvola, J., & Martikainen, P. J. (1998). Emissions of N₂O and NO and net nitrogen mineralization in a boreal forested peatland treated with different nitrogen compounds. *Canadian Journal of Forest Research*, 28(1), 132–140. <https://doi.org/10.1139/x97-198>

Reichstein, M., Falge, E., Baldocchi, D., Papale, D., Aubinet, M., Berbigier, P., Bernhofer, C., Buchmann, N., Gilmanov, T., Granier, A., Grünwald, T., Havránková, K., Ilvesniemi, H., Janous, D., Knohl, A., Laurila, T., Lohila, A., Loustau, D., Matteucci, G., ... Valentini, R. (2005). On the separation of net ecosystem exchange into assimilation and ecosystem respiration: review and improved algorithm. *Global Change Biology*, 11(9), 1424–1439. <https://doi.org/10.1111/j.1365-2486.2005.001002.x>

Repo, M. E., Susiluoto, S., Lind, S. E., Jokinen, S., Elsakov, V., Biasi, C., Virtanen, T., & Martikainen, P. J. (2009). Large N₂O emissions from cryoturbated peat soil in tundra. *Nature Geoscience*, 2(3), 189–192. <https://doi.org/10.1038/ngeo434>

- Reuss-Schmidt, K., Levy, P., Oechel, W., Tweedie, C., Wilson, C., & Zona, D. (2019). Understanding spatial variability of methane fluxes in Arctic wetlands through footprint modelling. *Environmental Research Letters*, 14(12), 125010. <https://doi.org/10.1088/1748-9326/ab4d32>
- Ribeiro, K., Pacheco, F. S., Ferreira, J. W., de Sousa-Neto, E. R., Hastie, A., Krieger Filho, G. C., Alvalá, P. C., Forti, M. C., & Ometto, J. P. (2021). Tropical peatlands and their contribution to the global carbon cycle and climate change. *Global Change Biology*, 27(3), 489–505. <https://doi.org/10.1111/gcb.15408>
- Richardson, A. D., Keenan, T. F., Migliavacca, M., Ryu, Y., Sonnentag, O., & Toomey, M. (2013). Climate change, phenology, and phenological control of vegetation feedbacks to the climate system. *Agricultural and Forest Meteorology*, 169, 156–173. <https://doi.org/10.1016/J.AGRFORMET.2012.09.012>
- Robinson, S. D., & Moore, T. R. (2000). The Influence of Permafrost and Fire upon Carbon Accumulation in High Boreal Peatlands, Northwest Territories, Canada. *Arctic, Antarctic, and Alpine Research*, 32(2), 155–166. <https://doi.org/10.1080/15230430.2000.12003351>
- Rogers, B. M., Soja, A. J., Goulden, M. L., & Randerson, J. T. (2015). Influence of tree species on continental differences in boreal fires and climate feedbacks. *Nature Geoscience*, 8(3), 228–234. <https://doi.org/10.1038/ngeo2352>
- Rogers, B. M., Veraverbeke, S., Azzari, G., Czimczik, C. I., Holden, S. R., Mouteva, G. O., Sedano, F., Treseder, K. K., & Randerson, J. T. (2014). Quantifying fire-wide carbon emissions in interior Alaska using field measurements and Landsat imagery. *Journal of Geophysical Research: Biogeosciences*, 119(8), 1608–1629. <https://doi.org/10.1002/2014JG002657>
- Rohatyn, S., Rotenberg, E., Tatarinov, F., Carmel, Y., & Yakir, D. (2023). Large variations in afforestation-related climate cooling and warming effects across short distances. *Communications Earth & Environment*, 4(1), 18. <https://doi.org/10.1038/s43247-023-00678-9>
- Roman-Perez, C. C., Hernandez-Ramirez, G., Kryzanowski, L., Puurveen, D., & Lohstraeter, G. (2021). Greenhouse gas emissions, nitrogen dynamics and barley productivity as impacted by

biosolids applications. *Agriculture, Ecosystems and Environment*, 320, 107577. <https://doi.org/10.1016/j.agee.2021.107577>

Rößger, N., Sachs, T., Wille, C., Boike, J., & Kutzbach, L. (2022). Seasonal increase of methane emissions linked to warming in Siberian tundra. *Nature Climate Change*, 12(11), 1031–1036. <https://doi.org/10.1038/s41558-022-01512-4>

Roulet, N. T., Lafleur, P. M., Richard, P. J. H., Moore, T. I. M. R., Humphreys, E. R., & Bubier, J. (2007). Contemporary carbon balance and late Holocene carbon accumulation in a northern peatland. *Global Change Biology*, 13(2), 397–411. <https://doi.org/10.1111/j.1365-2486.2006.01292.x>

Runkle, B. R. K., Sachs, T., Wille, C., Pfeiffer, E.-M., & Kutzbach, L. (2013). Bulk partitioning the growing season net ecosystem exchange of CO₂ in Siberian tundra reveals the seasonality of its carbon sequestration strength. *Biogeosciences*, 10(3), 1337–1349. <https://doi.org/10.5194/bg-10-1337-2013>

Ryu, Y., Sonnentag, O., Nilson, T., Vargas, R., Kobayashi, H., Wenk, R., & Baldocchi, D. D. (2010). How to quantify tree leaf area index in an open savanna ecosystem: A multi-instrument and multi-model approach. *Agricultural and Forest Meteorology*, 150(1), 63–76. <https://doi.org/10.1016/j.agrformet.2009.08.007>

Salmon, V. G., Schädel, C., Bracho, R., Pegoraro, E., Celis, G., Mauritz, M., Mack, M. C., & Schuur, E. A. G. (2018). Adding Depth to Our Understanding of Nitrogen Dynamics in Permafrost Soils. *Journal of Geophysical Research: Biogeosciences*, 123(8), 2497–2512. <https://doi.org/10.1029/2018JG004518>

Schädel, C., Bader, M. K. F., Schuur, E. A. G., Biasi, C., Bracho, R., Capek, P., De Baets, S., Diáková, K., Ernakovich, J., Estop-Aragones, C., Graham, D. E., Hartley, I. P., Iversen, C. M., Kane, E., Knoblauch, C., Lupascu, M., Martikainen, P. J., Natali, S. M., Norby, R. J., ... Wickland, K. P. (2016). Potential carbon emissions dominated by carbon dioxide from thawed permafrost soils. *Nature Climate Change*, 6(10), 950–953. <https://doi.org/10.1038/nclimate3054>

Schädel, C., Rogers, B. M., Lawrence, D. M., Koven, C. D., Brovkin, V., Burke, E. J., Genet, H., Huntzinger, D. N., Jafarov, E., McGuire, A. D., Riley, W. J., & Natali, S. M. (2024). Earth system models must include permafrost carbon processes. *Nature Climate Change*. <https://doi.org/10.1038/s41558-023-01909-9>

Schlesinger, W. H. (2013). An estimate of the global sink for nitrous oxide in soils. *Global Change Biology*, 19(10), 2929–2931. <https://doi.org/10.1111/gcb.12239>

Schulze, C., Olefeldt, D., Kljun, N., Chasmer, L., Detto, M., Gosselin, G. H., Helbig, M., Hopkinson, C., & Sonnentag, O. (in prep.). Permafrost extent controls landscape-scale fluxes of greenhouse gases in boreal peatlands in northwestern Canada.

Schulze, C., Sonnentag, O., Voigt, C., Thompson, L., van Delden, L., Heffernan, L., Hernandez-Ramirez, G., Kuhn, M., Lin, S., & Olefeldt, D. (2023). Nitrous Oxide Fluxes in Permafrost Peatlands Remain Negligible After Wildfire and Thermokarst Disturbance. *Journal of Geophysical Research: Biogeosciences*, 128(4), e2022JG007322. <https://doi.org/10.1029/2022JG007322>

Schuur, E. A. G., Abbott, B. W., Bowden, W. B., Brovkin, V., Camill, P., Canadell, J. G., Chanton, J. P., Chapin, F. S., Christensen, T. R., Ciais, P., Crosby, B. T., Czimeczik, C. I., Grosse, G., Harden, J., Hayes, D. J., Hugelius, G., Jastrow, J. D., Jones, J. B., Kleinen, T., ... Zimov, S. A. (2013). Expert assessment of vulnerability of permafrost carbon to climate change. *Climatic Change*, 119(2), 359–374. <https://doi.org/10.1007/s10584-013-0730-7>

Schuur, E. A. G., Abbott, B. W., Commane, R., Ernakovich, J., Euskirchen, E., Hugelius, G., Grosse, G., Jones, M., Koven, C., Leshyk, V., Lawrence, D., Lorant, M. M., Mauritz, M., Olefeldt, D., Natali, S., Rodenhizer, H., Salmon, V., Schädel, C., Strauss, J., ... Turetsky, M. (2022). Permafrost and Climate Change: Carbon Cycle Feedbacks From the Warming Arctic. *Annual Review of Environment and Resources*, 47(1), 343–371. <https://doi.org/10.1146/annurev-environ-012220-011847>

Schuur, E. A. G., Bracho, R., Celis, G., Belshe, E. F., Ebert, C., Ledman, J., Mauritz, M., Pegoraro, E. F., Plaza, C., Rodenhizer, H., Romanovsky, V., Schädel, C., Schirokauer, D., Taylor, M., Vogel, J. G., & Webb, E. E. (2021). Tundra Underlain By Thawing Permafrost

Persistently Emits Carbon to the Atmosphere Over 15 Years of Measurements. *Journal of Geophysical Research: Biogeosciences*, 126(6), e2020JG006044. <https://doi.org/10.1029/2020JG006044>

Schuur, E. A. G., Crummer, K. G., Vogel, J. G., & Mack, M. C. (2007). Plant Species Composition and Productivity following Permafrost Thaw and Thermokarst in Alaskan Tundra. *Ecosystems*, 10(2), 280–292. <https://doi.org/10.1007/s10021-007-9024-0>

Schuur, E. A. G., McGuire, A. D., Schädel, C., Grosse, G., Harden, J. W., Hayes, D. J., Hugelius, G., Koven, C. D., Kuhry, P., Lawrence, D. M., Natali, S. M., Olefeldt, D., Romanovsky, V. E., Schaefer, K., Turetsky, M. R., Treat, C. C., & Vonk, J. E. (2015). Climate change and the permafrost carbon feedback. *Nature*, 520(7546), 171–179. <https://doi.org/10.1038/nature14338>

Sharifi, M., Lynch, D. H., Zebarth, B. J., Zheng, Z., & Martin, R. C. (2009). Evaluation of Nitrogen Supply Rate Measured by in situ Placement of Plant Root Simulator™ Probes as a Predictor of Nitrogen Supply from Soil and Organic Amendments in Potato Crop. *American Journal of Potato Research*, 86(5), 356–366. <https://doi.org/10.1007/s12230-009-9090-2>

Shenoy, A., Johnstone, J. F., Kasischke, E. S., & Kielland, K. (2011). Persistent effects of fire severity on early successional forests in interior Alaska. *Forest Ecology and Management*, 261(3), 381–390. <https://doi.org/10.1016/j.foreco.2010.10.021>

Siljanen, H. M. P., Welti, N., Voigt, C., Heiskanen, J., Biasi, C., & Martikainen, P. J. (2020). Atmospheric impact of nitrous oxide uptake by boreal forest soils can be comparable to that of methane uptake. *Plant and Soil*, 454(1), 121–138. <https://doi.org/10.1007/s11104-020-04638-6>

Smith, D. M., Screen, J. A., Deser, C., Cohen, J., Fyfe, J. C., Garcia-Serrano, J., Jung, T., Kattsov, V., Matei, D., Msadek, R., Peings, Y., Sigmond, M., Ukita, J., Yoon, J.-H., & Zhang, X. (2019). The Polar Amplification Model Intercomparison Project (PAMIP) contribution to CMIP6: investigating the causes and consequences of polar amplification. *Geoscientific Model Development*, 12(3), 1139–1164. <https://doi.org/10.5194/gmd-12-1139-2019>

Sniderhan, A. E., Mamet, S. D., & Baltzer, J. L. (2020). Non-uniform growth dynamics of a dominant boreal tree species (*Picea mariana*) in the face of rapid climate change. *Canadian Journal of Forest Research*, 51(4), 565–572. <https://doi.org/10.1139/cjfr-2020-0188>

Sonnentag, O., Chen, J. M., Roulet, N. T., Ju, W., & Govind, A. (2008). Spatially explicit simulation of peatland hydrology and carbon dioxide exchange: Influence of mesoscale topography. *Journal of Geophysical Research: Biogeosciences*, 113(G2). <https://doi.org/10.1029/2007JG000605>

Sonnentag, O., Talbot, J., Chen, J. M., & Roulet, N. T. (2007). Using direct and indirect measurements of leaf area index to characterize the shrub canopy in an ombrotrophic peatland. *Agricultural and Forest Meteorology*, 144(3), 200–212. <https://doi.org/10.1016/j.agrformet.2007.03.001>

Soued, C., del Giorgio, P. A., & Maranger, R. (2016). Nitrous oxide sinks and emissions in boreal aquatic networks in Québec. *Nature Geoscience*, 9(2), 116–120. <https://doi.org/10.1038/ngeo2611>

Startsev, N., Bhatti, J., & Jassal, R. (2016). Surface CO₂ Exchange Dynamics across a Climatic Gradient in McKenzie Valley: Effect of Landforms, Climate and Permafrost. *Forests*, 7(12), 279. <https://doi.org/10.3390/f7110279>

Stocks, B. J., Mason, J. A., Todd, J. B., Bosch, E. M., Wotton, B. M., Amiro, B. D., Flannigan, M. D., Hirsch, K. G., Logan, K. A., Martell, D. L., & Skinner, W. R. (2002). Large forest fires in Canada, 1959–1997. *Journal of Geophysical Research: Atmospheres*, 107(D1), FFR 5-1-FFR 5-12. <https://doi.org/10.1029/2001JD000484>

Stoy, P. C., Mauder, M., Foken, T., Marcolla, B., Boegh, E., Ibrom, A., Arain, M. A., Arneth, A., Aurela, M., Bernhofer, C., Cescatti, A., Dellwik, E., Duce, P., Gianelle, D., van Gorsel, E., Kiely, G., Knohl, A., Margolis, H., McCaughey, H., ... Varlagin, A. (2013). A data-driven analysis of energy balance closure across FLUXNET research sites: The role of landscape scale heterogeneity. *Agricultural and Forest Meteorology*, 171–172, 137–152. <https://doi.org/10.1016/j.agrformet.2012.11.004>

Subke, J.-A., Kutzbach, L., & Risk, D. (2021). Soil Chamber Measurements. In T. Foken (Ed.), *Springer Handbook of Atmospheric Measurements*, 1603–1624. Springer International Publishing. https://doi.org/10.1007/978-3-030-52171-4_60

Sulman, B. N., Desai, A. R., Saliendra, N. Z., Lafleur, P. M., Flanagan, L. B., Sonnentag, O., Mackay, D. S., Barr, A. G., & van der Kamp, G. (2010). CO₂ fluxes at northern fens and bogs have opposite responses to inter-annual fluctuations in water table. *Geophysical Research Letters*, 37(19). <https://doi.org/10.1029/2010GL044018>

Sun, X., Wang, H., Song, C., Jin, X., Richardson, C. J., & Cai, T. (2021). Response of Methane and Nitrous Oxide Emissions from Peatlands to Permafrost Thawing in Xiaoxing'an Mountains, Northeast China. *Atmosphere*, 12(2). <https://doi.org/10.3390/atmos12020222>

Takatsu, Y., Miyamoto, T., Tahvanainen, T., & Hashidoko, Y. (2022). Nitrous Oxide Emission in Response to pH from Degrading Palsa Mire Peat Due to Permafrost Thawing. *Current Microbiology*, 79(2), 56. <https://doi.org/10.1007/s00284-021-02690-8>

Tarnocai, C., & Bockheim, J. (2011). Cryosolic soils of Canada: Genesis, distribution, and classification. *Canadian Journal of Soil Science*, 91(5), 749–762. <https://doi.org/10.4141/cjss10020>

Thompson, D. K., Baisley, A. S., & Waddington, J. M. (2015). Seasonal variation in albedo and radiation exchange between a burned and unburned forested peatland: implications for peatland evaporation. *Hydrological Processes*, 29(14), 3227–3235. <https://doi.org/10.1002/hyp.10436>

Thompson, L. M., Low, M., Shewan, R., Schulze, C., Simba, M., Sonnentag, O., Tank, S. E., & Olefeldt, D. (2023). Concentrations and Yields of Mercury, Methylmercury, and Dissolved Organic Carbon From Contrasting Catchments in the Discontinuous Permafrost Region, Western Canada. *Water Resources Research*, 59(11), e2023WR034848. <https://doi.org/10.1029/2023WR034848>

Thompson, L. M., Olefeldt, D., Mangal, V., & Knorr, K. H. (2022). Soil and porewater chemistry from peatlands of the Interior Plains, Northwestern Canada (dataset). University of Alberta Education & Research Archive. <https://doi.org/10.7939/r3-vp5e-aj53>

Torre Jorgenson, M., Harden, J., Kanevskiy, M., & Donnell, J. O. (2013). Reorganization of vegetation, hydrology and soil carbon after permafrost degradation across heterogeneous boreal landscapes. *Environmental Research Letters*, 8(3), 035017. <https://doi.org/10.1088/1748-9326/8/3/035017>

Treat, C. C., & Jones, M. C. (2018). Near-surface permafrost aggradation in Northern Hemisphere peatlands shows regional and global trends during the past 6000 years. *The Holocene*, 28(6), 998-1010. <https://doi.org/10.1177/0959683617752858>

Treat, C. C., Jones, M. C., Brosius, L., Grosse, G., Walter Anthony, K., & Frohling, S. (2021). The role of wetland expansion and successional processes in methane emissions from northern wetlands during the Holocene. *Quaternary Science Reviews*, 257, 106864. <https://doi.org/10.1016/j.quascirev.2021.106864>

Treat, C. C., Jones, M. C., Camill, P., Gallego-Sala, A., Garneau, M., Harden, J. W., Hugelius, G., Klein, E. S., Kokfelt, U., Kuhry, P., Loisel, J., Mathijssen, P. J. H., O'Donnell, J. A., Oksanen, P. O., Ronkainen, T. M., Sannel, A. B. K., Talbot, J., Tarnocai, C., & Väiliranta, M. (2016). Effects of permafrost aggradation on peat properties as determined from a pan-Arctic synthesis of plant macrofossils. *Journal of Geophysical Research: Biogeosciences*, 121(1), 78–94. <https://doi.org/10.1002/2015JG003061>

Turetsky, M. R. (2004). Decomposition and Organic Matter Quality in Continental Peatlands: The Ghost of Permafrost Past. *Ecosystems*, 7(7), 740–750. <https://doi.org/10.1007/s10021-004-0247-z>

Turetsky, M. R., Abbott, B. W., Jones, M. C., Anthony, K. W., Olefeldt, D., Schuur, E. A. G., Grosse, G., Kuhry, P., Hugelius, G., Koven, C., Lawrence, D. M., Gibson, C., Sannel, A. B. K., & McGuire, A. D. (2020). Carbon release through abrupt permafrost thaw. *Nature Geoscience*, 13(2), 138–143. <https://doi.org/10.1038/s41561-019-0526-0>

Turetsky, M. R., Benscoter, B., Page, S., Rein, G., van der Werf, G. R., & Watts, A. (2015). Global vulnerability of peatlands to fire and carbon loss. *Nature Geoscience*, 8(1), 11–14. <https://doi.org/10.1038/ngeo2325>

Turetsky, M. R., Kane, E. S., Harden, J. W., Ottmar, R. D., Manies, K. L., Hoy, E., & Kasischke, E. S. (2011). Recent acceleration of biomass burning and carbon losses in Alaskan forests and peatlands. *Nature Geoscience*, 4(1), 27–31. <https://doi.org/10.1038/ngeo1027>

Turetsky, M. R., Mack, M. C., Hollingsworth, T. N., & Harden, J. W. (2010). The role of mosses in ecosystem succession and function in Alaska's boreal forest. *Canadian Journal of Forest Research*, 40(7), 1237–1264. <https://doi.org/10.1139/X10-072>

Turetsky, M. R., Wieder, R. K., Vitt, D. H., Evans, R. J., & Scott, K. D. (2007). The disappearance of relict permafrost in boreal north America: Effects on peatland carbon storage and fluxes. *Global Change Biology*, 13(9), 1922–1934. <https://doi.org/10.1111/j.1365-2486.2007.01381.x>

Ueyama, M., Harazono, Y., Ohtaki, E., & Miyata, A. (2006). Controlling factors on the interannual CO₂ budget at a subarctic black spruce forest in interior Alaska. *Tellus B: Chemical and Physical Meteorology*, 58(5), 491–501. <https://doi.org/10.1111/j.1600-0889.2006.00205.x>

Ueyama, M., Iwata, H., Endo, R., & Harazono, Y. (2023). Methane and carbon dioxide emissions from the forest floor of a black spruce forest on permafrost in interior Alaska. *Polar Science*, 35, 100921. <https://doi.org/10.1016/j.polar.2022.100921>

Ueyama, M., Iwata, H., & Harazono, Y. (2014). Autumn warming reduces the CO₂ sink of a black spruce forest in interior Alaska based on a nine-year eddy covariance measurement. *Global Change Biology*, 20(4), 1161–1173. <https://doi.org/10.1111/gcb.12434>

United Nations Environment Programme. (2022). *Global Peatlands Assessment: The State of the World's Peatlands - Evidence for Action toward the Conservation, Restoration, and Sustainable Management of Peatlands*. <https://wedocs.unep.org/20.500.11822/41222>

van Beest, C., Petrone, R., Nwaishi, F., Waddington, J. M., & Macrae, M. (2019). Increased Peatland Nutrient Availability Following the Fort McMurray Horse River Wildfire. *Diversity*, 11(9). <https://doi.org/10.3390/d11090142>

Van Dijk, A., Moene, A. F., & De Bruin, H. A. R. (2004). The principles of surface flux physics: theory, practice and description of the ECPACK library. In *Meteorology and Air Quality Group*

(Internal Report; No. 2004/1), 99-100. Wageningen University. Retrieved from <https://edepot.wur.nl/44341>

Vekuri, H., Tuovinen, J.-P., Kulmala, L., Papale, D., Kolari, P., Aurela, M., Laurila, T., Liski, J., & Lohila, A. (2023). A widely-used eddy covariance gap-filling method creates systematic bias in carbon balance estimates. *Scientific Reports*, 13(1), 1720. <https://doi.org/10.1038/s41598-023-28827-2>

Veraverbeke, S., Rogers, B. M., & Randerson, J. T. (2015). Daily burned area and carbon emissions from boreal fires in Alaska. *Biogeosciences*, 12(11), 3579–3601. <https://doi.org/10.5194/bg-12-3579-2015>

Vickers, D., & Mahrt, L. (1997). Quality Control and Flux Sampling Problems for Tower and Aircraft Data. *Journal of Atmospheric and Oceanic Technology*, 14(3), 512–526. [https://doi.org/10.1175/1520-0426\(1997\)014<0512:QCAFSP>2.0.CO;2](https://doi.org/10.1175/1520-0426(1997)014<0512:QCAFSP>2.0.CO;2)

Vincent, L. A., Wang, X. L., Milewska, E. J., Wan, H., Yang, F., & Swail, V. (2012). A second generation of homogenized Canadian monthly surface air temperature for climate trend analysis. *Journal of Geophysical Research: Atmospheres*, 117(D18). <https://doi.org/10.1029/2012JD017859>

Voigt, C., Lamprecht, R. E., Marushchak, M. E., Lind, S. E., Novakovskiy, A., Aurela, M., Martikainen, P. J., & Biasi, C. (2017). Warming of subarctic tundra increases emissions of all three important greenhouse gases – carbon dioxide, methane, and nitrous oxide. *Global Change Biology*, 23(8), 2929–3432. <https://doi.org/10.1111/gcb.13563>

Voigt, C., Marushchak, M. E., Abbott, B. W., Biasi, C., Elberling, B., Siciliano, S. D., Sonnentag, O., Stewart, K. J., Yang, Y., & Martikainen, P. J. (2020). Nitrous oxide emissions from permafrost-affected soils. *Nature Reviews Earth and Environment*, 1(8), 420–434. <https://doi.org/10.1038/s43017-020-0063-9>

Voigt, C., Marushchak, M. E., Lamprecht, R. E., Jackowicz-Korczyński, M., Lindgren, A., Mastepanov, M., Granlund, L., Christensen, T. R., Tahvanainen, T., Martikainen, P. J., & Biasi, C. (2017). Increased nitrous oxide emissions from Arctic peatlands after permafrost thaw.

Proceedings of the National Academy of Sciences of the United States of America, 114(24), 6238–6243. <https://doi.org/10.1073/pnas.1702902114>

Voigt, C., Marushchak, M. E., Mastepanov, M., Lamprecht, R. E., Christensen, T. R., Dorodnikov, M., Jackowicz-Korczyński, M., Lindgren, A., Lohila, A., Nykänen, H., Oinonen, M., Oksanen, T., Palonen, V., Treat, C. C., Martikainen, P. J., & Biasi, C. (2019). Ecosystem carbon response of an Arctic peatland to simulated permafrost thaw. *Global Change Biology*, 25(5), 1746–1764. <https://doi.org/10.1111/gcb.14574>

Walker, X. J., Baltzer, J. L., Cumming, S. G., Day, N. J., Ebert, C., Goetz, S., Johnstone, J. F., Potter, S., Rogers, B. M., Schuur, E. A. G., Turetsky, M. R., & Mack, M. C. (2019). Increasing wildfires threaten historic carbon sink of boreal forest soils. *Nature*, 572(7770), 520–523. <https://doi.org/10.1038/s41586-019-1474-y>

Walker, X. J., Rogers, B. M., Baltzer, J. L., Cumming, S. G., Day, N. J., Goetz, S. J., Johnstone, J. F., Schuur, E. A. G., Turetsky, M. R., & Mack, M. C. (2018). Cross-scale controls on carbon emissions from boreal forest megafires. *Global Change Biology*, 24(9), 4251–4265. <https://doi.org/10.1111/gcb.14287>

Walker, X. J., Rogers, B. M., Veraverbeke, S., Johnstone, J. F., Baltzer, J. L., Barrett, K., Bourgeau-Chavez, L., Day, N. J., de Groot, W. J., Dieleman, C. M., Goetz, S., Hoy, E., Jenkins, L. K., Kane, E. S., Parisien, M.-A., Potter, S., Schuur, E. A. G., Turetsky, M., Whitman, E., & Mack, M. C. (2020). Fuel availability not fire weather controls boreal wildfire severity and carbon emissions. *Nature Climate Change*, 10(12), 1130–1136. <https://doi.org/10.1038/s41558-020-00920-8>

Walter Anthony, K., Schneider von Deimling, T., Nitze, I., Frohking, S., Emond, A., Daanen, R., Anthony, P., Lindgren, P., Jones, B., & Grosse, G. (2018). 21st-century modeled permafrost carbon emissions accelerated by abrupt thaw beneath lakes. *Nature Communications*. <https://doi.org/10.1038/s41467-018-05738-9>

Wang, F., Li, J., Wang, X., Zhang, W., Zou, B., Neher, D. A., & Li, Z. (2014). Nitrogen and phosphorus addition impact soil N₂O emission in a secondary tropical forest of South China. *Scientific Reports*, 4(1), 5615. <https://doi.org/10.1038/srep05615>

Wang, J. A., Baccini, A., Farina, M., Randerson, J. T., & Friedl, M. A. (2021). Disturbance suppresses the aboveground carbon sink in North American boreal forests. *Nature Climate Change*, 11(5), 435–441. <https://doi.org/10.1038/s41558-021-01027-4>

Wang, J. A., Sulla-Menashe, D., Woodcock, C. E., Sonnentag, O., Keeling, R. F., & Friedl, M. A. (2020). Extensive land cover change across Arctic–Boreal Northwestern North America from disturbance and climate forcing. *Global Change Biology*, 26(2), 807–822. <https://doi.org/10.1111/gcb.14804>

Wang, M., Talbot, J., & Moore, T. R. (2018). Drainage and fertilization effects on nutrient availability in an ombrotrophic peatland. *Science of The Total Environment*, 621, 1255–1263. <https://doi.org/10.1016/j.scitotenv.2017.10.103>

Wang, T., Hamann, A., Spittlehouse, D., & Carroll, C. (2016). Locally Downscaled and Spatially Customizable Climate Data for Historical and Future Periods for North America. *PLOS ONE*, 11(6), e0156720-. <https://doi.org/10.1371/journal.pone.0156720>

Watts, J. D., Farina, M., Kimball, J. S., Schiferl, L. D., Liu, Z., Arndt, K. A., Zona, D., Ballantyne, A., Euskirchen, E. S., Parmentier, F.-J. W., Helbig, M., Sonnentag, O., Tagesson, T., Rinne, J., Ikawa, H., Ueyama, M., Kobayashi, H., Sachs, T., Nadeau, D. F., ... Oechel, W. C. (2023). Carbon uptake in Eurasian boreal forests dominates the high-latitude net ecosystem carbon budget. *Global Change Biology*, 29(7), 1870–1889. <https://doi.org/10.1111/gcb.16553>

Watts, J. D., Natali, S. M., Minions, C., Risk, D., Arndt, K., Zona, D., Euskirchen, E. S., Rocha, A. V, Sonnentag, O., Helbig, M., Kalthori, A., Oechel, W., Ikawa, H., Ueyama, M., Suzuki, R., Kobayashi, H., Celis, G., Schuur, E. A. G., Humphreys, E., ... Edgar, C. (2021). Soil respiration strongly offsets carbon uptake in Alaska and Northwest Canada. *Environmental Research Letters*, 16(8), 084051. <https://doi.org/10.1088/1748-9326/ac1222>

Webb, E. K., Pearman, G. I., & Leuning, R. (1980). Correction of flux measurements for density effects due to heat and water vapour transfer. *Quarterly Journal of the Royal Meteorological Society*, 106(447), 85–100. <https://doi.org/10.1002/qj.49710644707>

Wessa, P. (2015). Kernel Density Estimation (v1.0.12) in Free Statistics Software (v1.2.1), Office for Research Development and Education. https://www.wessa.net/rwasp_density.wasp

Western Ag Innovations. (2000). Plant Root Simulator™ (PRS) probes are an effective tool for measuring nutrient supplies to plant roots. Retrieved from <https://www.westernag.ca/innovations/publications/techupdates?view=tu&id=3>

Wickland, K. P., Waldrop, M. P., Aiken, G. R., Koch, J. C., Jorgenson, M. T., & Striegl, R. G. (2018). Dissolved organic carbon and nitrogen release from boreal Holocene permafrost and seasonally frozen soils of Alaska. *Environmental Research Letters*, 13(6), 065011. <https://doi.org/10.1088/1748-9326/aac4ad>

Wieder, R. K., Scott, K. D., Kamminga, K., Vile, M. A., Vitt, D. H., Bone, T., Xu, B. I. N., Benscoter, B. W., & Bhatti, J. S. (2009). Postfire carbon balance in boreal bogs of Alberta, Canada. *Global Change Biology*, 15(1), 63–81. <https://doi.org/10.1111/j.1365-2486.2008.01756.x>

Wilczak, J. M., Oncley, S. P., & Stage, S. A. (2001). Sonic Anemometer Tilt Correction Algorithms. *Boundary-Layer Meteorology*, 99(1), 127–150. <https://doi.org/10.1023/A:1018966204465>

Wilkinson, S. L., Andersen, R., Moore, P. A., Davidson, S. J., Granath, G., & Waddington, J. M. (2023). Wildfire and degradation accelerate northern peatland carbon release. *Nature Climate Change*. <https://doi.org/10.1038/s41558-023-01657-w>

Wilson, R. M., Hopple, A. M., Tfaily, M. M., Sebestyen, S. D., Schadt, C. W., Pfeifer-Meister, L., Medvedeff, C., McFarlane, K. J., Kostka, J. E., Kolton, M., Kolka, R. K., Kluber, L. A., Keller, J. K., Guilderson, T. P., Griffiths, N. A., Chanton, J. P., Bridgham, S. D., & Hanson, P. J. (2016). Stability of peatland carbon to rising temperatures. *Nature Communications*, 7(1), 13723. <https://doi.org/10.1038/ncomms13723>

Wright, S. N., Thompson, L. M., Olefeldt, D., Connon, R. F., Carpino, O. A., Beel, C. R., & Quinton, W. L. (2022). Thaw-induced impacts on land and water in discontinuous permafrost: A

review of the Taiga Plains and Taiga Shield, northwestern Canada. *Earth-Science Reviews*, 232, 104104. <https://doi.org/10.1016/j.earscirev.2022.104104>

Xiang, X., Shi, Y., Yang, J., Kong, J., Lin, X., Zhang, H., Zeng, J., & Chu, H. (2014). Rapid recovery of soil bacterial communities after wildfire in a Chinese boreal forest. *Scientific Reports*, 4(1), 3829. <https://doi.org/10.1038/srep03829>

Yang, G., Peng, Y., Marushchak, M. E., Chen, Y., Wang, G., Li, F., Zhang, D., Wang, J., Yu, J., Liu, L., Qin, S., Kou, D., & Yang, Y. (2018). Magnitude and Pathways of Increased Nitrous Oxide Emissions from Uplands Following Permafrost Thaw. *Environmental Science & Technology*, 52(16), 9162–9169. <https://doi.org/10.1021/acs.est.8b02271>

Yu, Z., Loisel, J., Brosseau, D. P., Beilman, D. W., & Hunt, S. J. (2010). Global peatland dynamics since the Last Glacial Maximum. *Geophysical Research Letters*, 37(13). <https://doi.org/10.1029/2010GL043584>

Yuan, K., Li, F., McNicol, G., Chen, M., Hoyt, A., Knox, S., Riley, W. J., Jackson, R., & Zhu, Q. (2024). Boreal–Arctic wetland methane emissions modulated by warming and vegetation activity. *Nature Climate Change*. <https://doi.org/10.1038/s41558-024-01933-3>

Yue, C., Ciais, P., Luysaert, S., Cadule, P., Harden, J., Randerson, J., Bellassen, V., Wang, T., Piao, S. L., Poulter, B., & Viovy, N. (2013). Simulating boreal forest carbon dynamics after stand-replacing fire disturbance: insights from a global process-based vegetation model. *Biogeosciences*, 10(12), 8233–8252. <https://doi.org/10.5194/bg-10-8233-2013>

Zoltai, S. C. (1993). Cyclic Development of Permafrost in the Peatlands of Northwestern Alberta, Canada. *Arctic and Alpine Research*, 25(3), 240–246. <http://www.jstor.org/stable/1551820>

Zoltai, S. C., & Tarnocai, C. (1975). Perennially Frozen Peatlands in the Western Arctic and Subarctic of Canada. *Canadian Journal of Earth Sciences*, 12(1), 28–43. <https://doi.org/10.1139/e75-004>

Appendices

A.1. Supporting Information for Chapter 1

There is no need for supporting information for Chapter 1.

A.2. Supporting Information for Chapter 2

A.2.1. N₂O Flux Measurements at Scotty Creek by Carolina Voigt

The area within the PVC collars was 0.054 m² at Scotty Creek, where each peatland stage was represented by six collars. The chambers used at Scotty Creek had heights of 17 or 32 cm at Scotty Creek (9.2 L and 17.3 L, respectively). Gas samples from Scotty Creek were analyzed at the University of Eastern Finland using an Agilent 7890B GC (Agilent Technologies, Santa Clara, CA), with an autosampler (Gilson Inc., Middleton, WI), an electron capture detector for N₂O, a thermal conductivity detector for CO₂ and a flame ionization detector for CH₄. Two certified standards were used for samples from Scotty Creek as follows: CH₄ concentrations of 2.02 and 15 ppm, CO₂ concentrations of 398 and 3990 ppm, and N₂O concentrations of 0.84 and 5000 ppm. Flux calculations were done in the same way as described in the main document.

To measure soil moisture contents at Scotty Creek, we used a HydroSense II probe (CS-658 and HS2, Campbell Scientific, Logan, UT). Soil temperature at Scotty Creek was measured at 2, 5, 10, and 20 cm with a handheld thermometer (TM-80N with K-type thermocouple probe, Tenmars Electronics, Taipei City, Taiwan). The same handheld thermometer was used to measure air and chamber temperature at Scotty Creek. Regarding soil sampling at Scotty Creek, the methods and data have previously been reported (Pelletier et al., 2017).

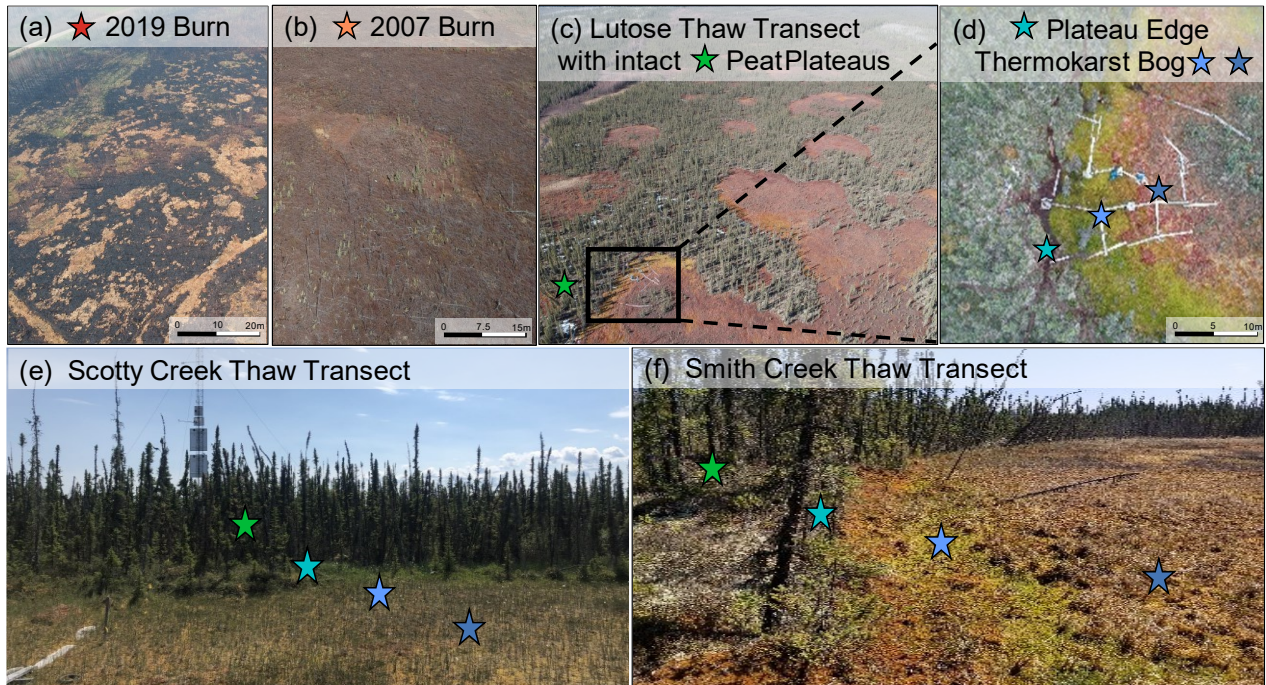


Figure A2.1: (a, b, c, d) Aerial and (e, f) ground photos of sampling locations at (a, b) wildfire-affected and (c, d, e, f) thermokarst-affected permafrost peatland complexes in the Taiga Plains ecozone, including all three permafrost thaws transect (peatland stages in the order left to right: Peat Plateau, Plateau Edge, Young Bog, and Mature Bog) at (c, d) Lutose, (e) Scotty Creek, and (f) Smith Creek

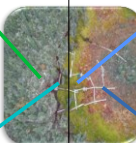
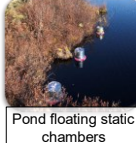
Disturbance	Wildfire	Intact	Thermokarst	Chamber Type
Peatland Stages	 2019 Burn  2007 Burn	 Peat Plateau  Plateau Edge	  Young Bog  Mature Bog	 Ground-mounted static chambers  Pond floating static chambers
Peatland Ponds	 Burned Edge*	 Intact Edge	 Thermokarst Edge	 Pond floating static chambers

Figure A2.2: Sampling scheme including peat landforms (=stages) and peatland ponds and chamber types used.
*The Peatland Pond L2 has situated in the middle of the 2007 Burn fire scar and had beaver activity as well

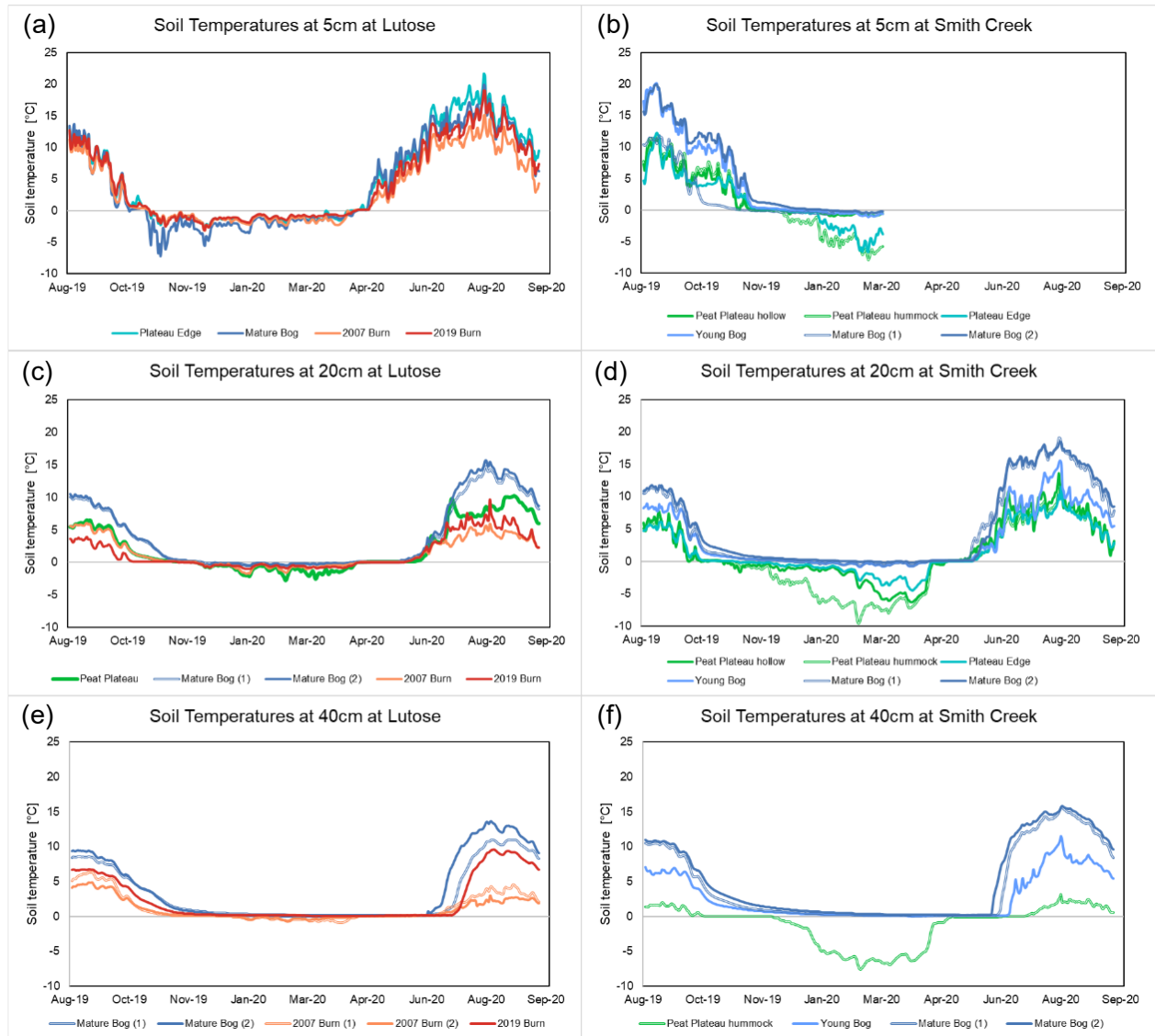


Figure A2.3: Soil temperature curves for one entire year at Lutose and Smith Creek at (a, b) 5 cm, (c, d) 20 cm, and (e, f) 40 cm depth

Table A2.1: Overview of sampling occasions, activities (marked with 'X', GHG = greenhouse gas, PRS = plant root simulators©) and locations including peatland stages: B19 = 2019 Burn, B07 = 2007 Burn, P = Peat Plateau, PE = Plateau Edge, YB = Young Bog, and MB = Mature Bog.

Date	Site	Peatland Stages/Ponds included	Activity			
			GHG Flux	Soil gas	Pore-water	PRS
2018-09-13	Scotty Creek	P, PE, YB, MB	X	X		
2019-04-13	Lutose	P, PE, YB, MB	X		X	
2019-04-14	Lutose	B07	X		X	
2019-05-12	Lutose	P, PE, YB, MB	X		X	
2019-05-13	Lutose	B07, L1, L4	X		X	
2019-05-28	Smith Creek	P, PE, YB, MB	X		X	
2019-05-30	Smith Creek	P, W1, W2	X		X	
2019-06-13	Lutose	MB, YB	X			
2019-06-14	Lutose	P, PE, YB, B07, L1, L4	X		X	
2019-06-17	Smith Creek	P, PE, YB, MB	X		X	
2019-06-17	Smith Creek	W1, W2	X		X	
2019-07-11	Lutose	L2	X		X	
2019-07-11	Lutose	B07, P, PE, YB, MB				In
2019-07-13	Smith Creek	P, PE, YB, MB	X		X	
2019-07-14	Smith Creek	W1, W2	X		X	
2019-07-15	Smith Creek	P, PE, YB, MB				In
2019-07-17	Lutose	B07	X		X	
2019-07-18	Lutose	B19, P, PE, YB, MB, L4	X		X	
2019-07-18	Lutose	B19				In
2019-07-19	Lutose	L1	X		X	
2019-08-18	Lutose	P, PE, YB, MB	X		X	
2019-08-19	Lutose	P, PE, YB, MB		X		
2019-08-20	Lutose	B07, L2	X		X	
2019-08-20	Lutose	B19, L1, L4	X		X	
2019-08-21	Lutose	P, PE, YB, MB				Out
2019-08-23	Smith Creek	P, PE, YB, MB	X		X	
2019-08-24	Smith Creek	W1, W2	X		X	
2019-08-25	Smith Creek	P, PE, YB, MB				Out
2019-08-26	Smith Creek	P, PE, YB, MB		X		
2019-07-18	Lutose	B19				Out
2019-09-27	Smith Creek	P, PE, YB, MB	X		X	
2019-09-28	Smith Creek	W1, W2	X		X	
2019-09-30	Lutose	P, PE, YB, MB	X		X	
2019-10-01	Lutose	L1, L2	X		X	
2019-10-02	Lutose	B19, B07, L4	X		X	

Table A2.2: Two-way ANOVA results, comparing porewater nutrient concentrations and supply rates among sites (Lutose, Smith Creek), and among peatland stages (Peat Plateau, Plateau Edge, Young Bog, Mature Bog).

	Df	Sum Sq	Mean Sq	F-Value	p-Value
<i>Porewater NO₃⁻</i>					
Site	1	1,950	1,950	7.02	0.012*
Stage	3	1,280	425	1.53	0.226
Site:Stage	3	1,630	542	1.94	0.142
Residuals	33	9,190	279		
Tukey HSD results	Smith Creek < Lutose: 0.012*				
<i>Porewater NH₄⁺</i>					
Site	1	182,000	182,000	3.37	0.075
Stage	3	70,400	23,500	0.434	0.730
Site:Stage	3	16,400	5,480	0.101	0.959
Residuals	33				
Tukey HSD results	n/a				
<i>Porewater PO₄³⁻</i>					
Site	1	6,280	6,280	2.01	0.166
Stage	3	47,800	15,900	5.09	0.005**
Site:Stage	3	11,500	3,840	1.26	0.316
Residuals	33	103,000	3,130		
Tukey HSD results	Plateau Edge > Mature Bog, p = 0.032				
<i>Supply rate NO₃⁻</i>					
Site	1	0.200	0.190	0.013	0.909
Stage	3	188	62.6	4.48	0.012*
Site:Stage	3	63.3	21.1	1.51	0.237
Residuals	24	335	14.0		
Tukey HSD results	Young Bog < Mature Bog, p = 0.017, Young Bog < Plateau Edge, p = 0.027				
<i>Supply Rate NH₄⁺</i>					
Site	1	6,140	6,140	0.233	0.634
Stage	3	87,900	29,300	1.11	0.364
Site:Stage	3	145,000	48,500	1.84	0.167
Residuals	24	633,000	26,400		
Tukey HSD results	n/a				
<i>Supply Rate P</i>					
Site	1	0.210	0.210	0.005	0.945
Stage	3	98.9	32.3	0.769	0.523
Site:Stage	3	175	58.3	0.136	0.279
Residuals	24	1,030	42.9		
Tukey HSD results	n/a				

Table A2.3: One-way ANOVA results, comparing porewater nutrient concentrations and supply rates among peatland stages (2019 Burn, 2007 Burn, Peat Plateau, Plateau Edge, Young Bog, Mature Bog), or among disturbances (Intact, Thermokarst, Wildfire).

	Df	Sum Sq	Mean Sq	F-Value	p-Value
<i>Porewater NO₃⁻</i>					
Stage	5	1,420	284	0.923	0.475
Residuals	44	13,500	308		
Tukey HSD	n/a				
<i>Porewater NH₄⁺</i>					
Stage	5	73,800	14,500	0.271	0.927
Residuals	44	2,400,000	54,500		
Tukey HSD	n/a				
<i>Porewater PO₄³⁻</i>					
Stage	5	7,840,000	1,570,000	6.05	<0.001***
Residuals	44	11,400,000	259,000		
Tukey HSD	2019 Burn > Peat Plateau, p < 0.001, 2019 Burn > Plateau Edge, p = 0.001 2019 Burn > Young Bog, p < 0.001, 2019 Burn > Mature Bog, p < 0.001				
Disturbance	2	5,990,000	2,990,000	10.6	<0.001***
Residuals	47	13,300,000	282,000		
Tukey HSD	Wildfire > Intact, p < 0.001, Wildfire > Thermokarst, p < 0.001				
<i>Supply Rate NO₃⁻</i>					
Stage	5	189	37.8	2.41	0.055
Residuals	36	564	15.6		
Tukey HSD	Young Bog < Mature Bog, p = 0.043				
<i>Supply Rate NH₄⁺</i>					
Stage	5	105,000	20,100	0.961	0.454
Residuals	36	806,000	21,800		
Tukey HSD	n/a				
<i>Supply Rate P</i>					
Stage	5	1930	386	2.32	0.063
Residuals	36	5980	166		
Tukey HSD	n/a				
Disturbance	3	1690	845	5.30	0.009***
Residuals	39	6220	160		
Tukey HSD	Wildfire > Intact, p = 0.011; Wildfire > Thermokarst, p = 0.023				

Table A2.4: Two-way ANOVA results, comparing collar average N₂O, CH₄ and CO₂ fluxes among sites (Lutose, Smith Creek), and among peatland stages (Peat Plateau, Plateau Edge, Young Bog, Mature Bog).

	Df	Sum Sq	Mean Sq	F-Value	p-Value
<i>N₂O Fluxes</i>					
Site	1	0.000456	0.000456	0.576	0.455
Stage	3	0.00824	0.00275	3.47	0.032*
Site:Stage	3	0.00199	0.000662	0.835	0.488
Residuals	24	0.0190	0.000792		
Tukey HSD results	Plateau Edge > Mature Bog, p = 0.040				
<i>CH₄ Fluxes</i>					
Site	1	10.0	9.90	0.0470	0.831
Stage	3	651	2,170	10.1	<0.001***
Site:Stage	3	460	1,530	7.17	0.001**
Residuals	24	513	214		
Tukey HSD results	Young Bog > Peat Plateau, p = 0.002; Young Bog > Plateau Edge, p = 0.044 Mature Bog > Plateau Edge, p < 0.001; Mature Bog > Plateau Edge, p = 0.016				
<i>CO₂ Fluxes</i>					
Site	1	2,590,000	2,590,000	0.628	0.436
Stage	3	14,100,000	4,700,000	1.14	0.352
Site:Stage	3	34,500,000	11,500,000	2.79	0.062
Residuals	24	98,800,000	4,110,000		
Tukey HSD results	n/a				

Table A2.5: One-way ANOVA results, comparing collar average N₂O, CH₄, and CO₂ fluxes among peatland stages (2019 Burn, 2007 Burn, Peat Plateau, Plateau Edge, Young Bog, Mature Bog), or among disturbances (Intact, Thermokarst, Wildfire).

	Df	Sum Sq	Mean Sq	F-Value	p-Value
<i>N₂O Fluxes</i>					
Stage	5	0.0237	0.00474	6.96	<0.001***
Residuals	42	0.0286	0.000681		
Tukey HSD results	Plateau Edge > Mature Bog, p = 0.039				
<i>CH₄ Fluxes</i>					
Disturbance	2	0.0210	0.0105	15.1	<0.001***
Residuals	45	0.0313	0.000695		
Tukey HSD results	Thermokarst < Intact, p = 0.010, Thermokarst < Wildfire, p < 0.001 Intact < Wildfire, p = 0.050				
<i>CO₂ Fluxes</i>					
Stage	5	9,830	1,970	8.35	<0.001***
Residuals	42	9,900	236		
Tukey HSD results	Mature Bog > Peat Plateau, p < 0.001, Mature Bog > Plateau Edge, p = 0.035 Young Bog > Peat Plateau, p < 0.001				
Disturbance	2	9,300	4,650	20.1	<0.001***
Residuals	45	10,400	232		
Tukey HSD results	Thermokarst > Intact, p < 0.001, Thermokarst > Wildfire, p < 0.001				
<i>CO₂ Fluxes</i>					
Stage	5	69,200,000	13,800,000	3.79	0.006**
Residuals	42	154,000,000	365,000		
Tukey HSD results	2019 Burn < Mature Bog, p = 0.002, 2019 Burn < Plateau Edge				
Disturbance	2	32,300,000	18,600,000	4.52	0.016*
Residuals	45	185,000,000	4,120,000		
Tukey HSD results	Wildfire < Intact, p = 0.050, Wildfire < Thermokarst, p = 0.022				

A.3. Supporting Information for Chapter 3

A.3.1. Energy balance

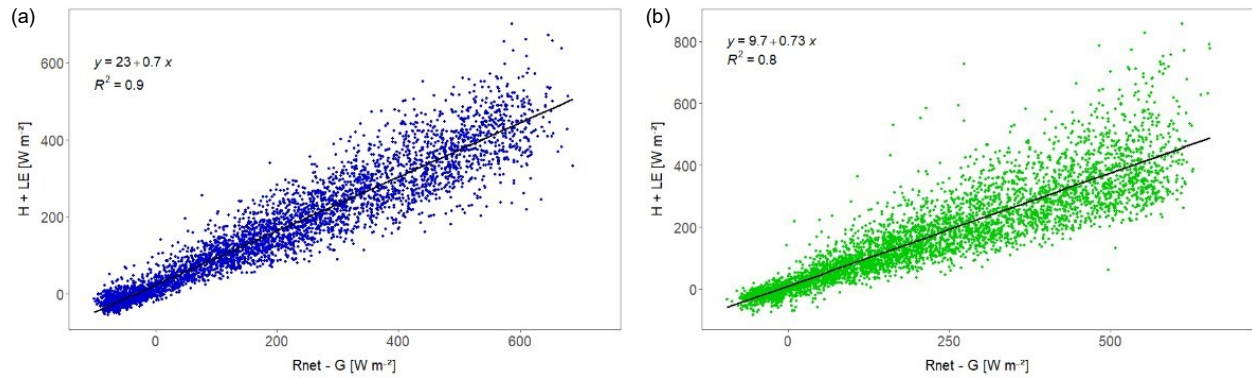


Figure A3.1: Energy balance closures of (a) CA-SCC (Scotty Creek, sporadic permafrost) and (b) CA-SMC (Smith Creek, discontinuous permafrost) over the measurement period from July 8, 2017, to September 21, 2022.

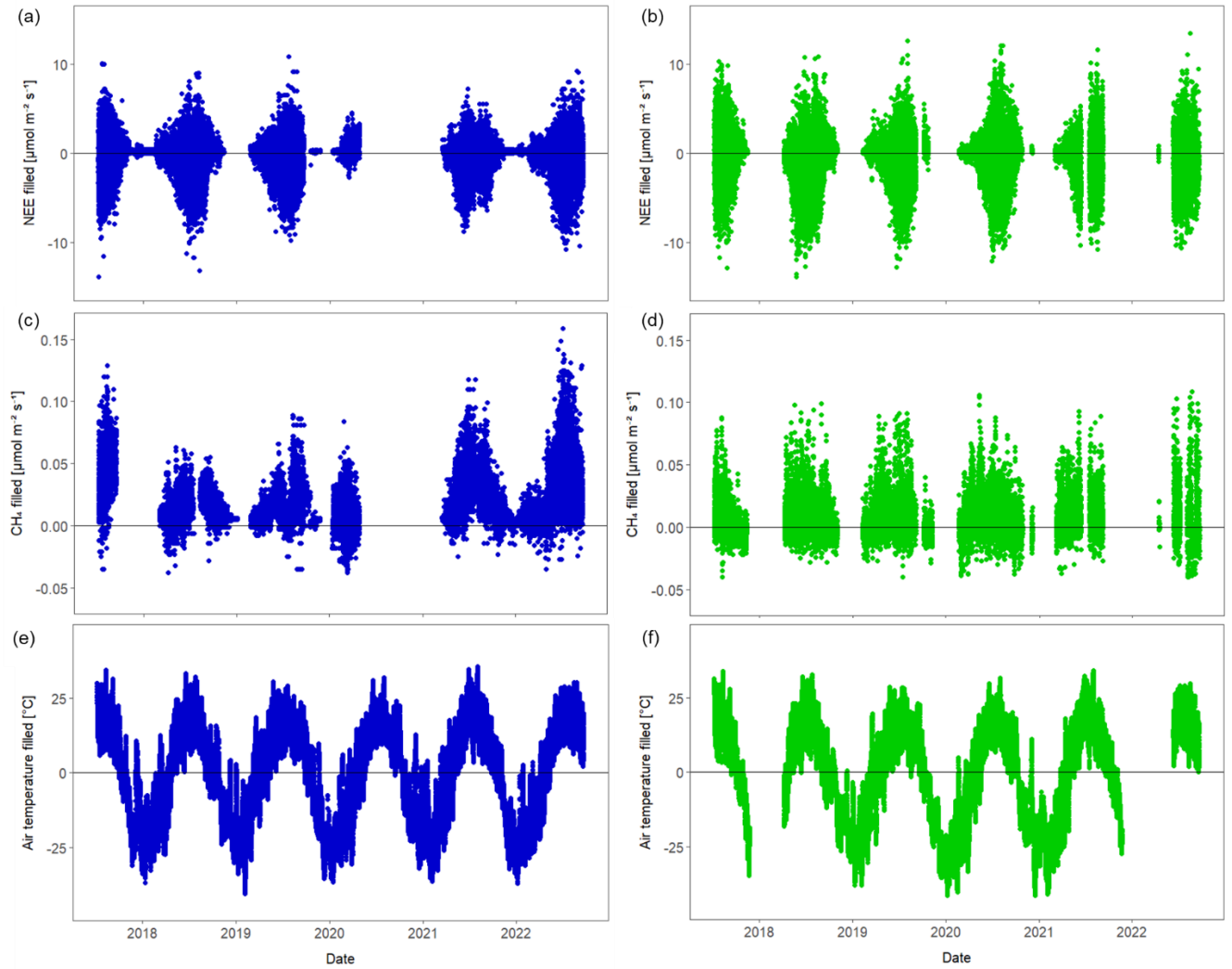


Figure A3.2: Time series over the measurement period from July 8, 2017, to September 21, 2022 of available gapfilled data for (a, c, e) CA-SCC (Scotty Creek, sporadic permafrost) and (b, d, f) CA-SMC (Smith Creek, discontinuous permafrost) regarding net ecosystem exchange (NEE), methane (CH₄), and air temperature representative of other environmental variables.

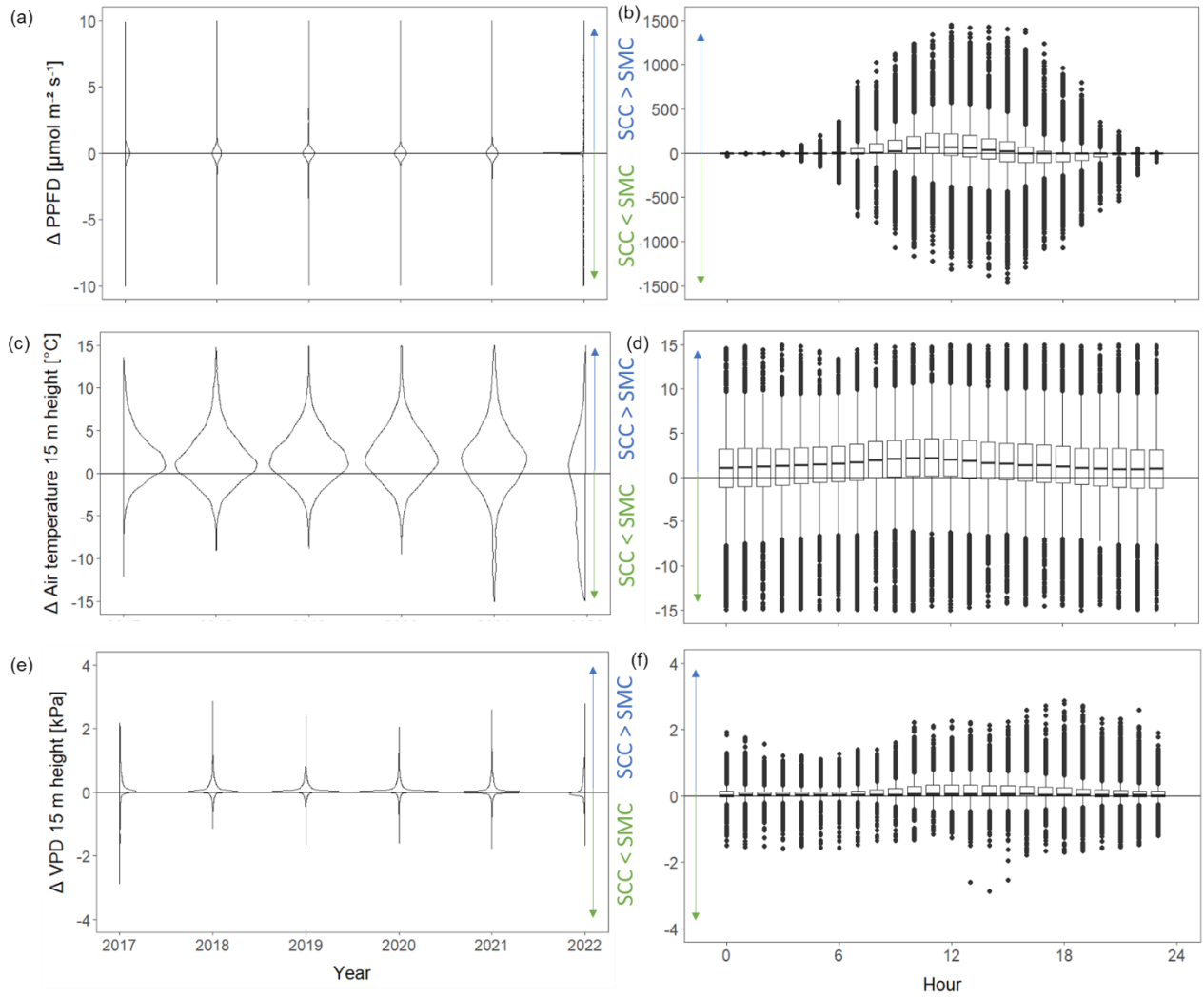


Figure A3.3: Yearly (a, c, e) and diurnal (b, d, f) differences in biometeorological variables between the eddy covariance tower sites, Scotty Creek (SCC, sporadic permafrost) and Smith Creek (SMC, discontinuous permafrost) across the study period (July 2017 - September 2022).

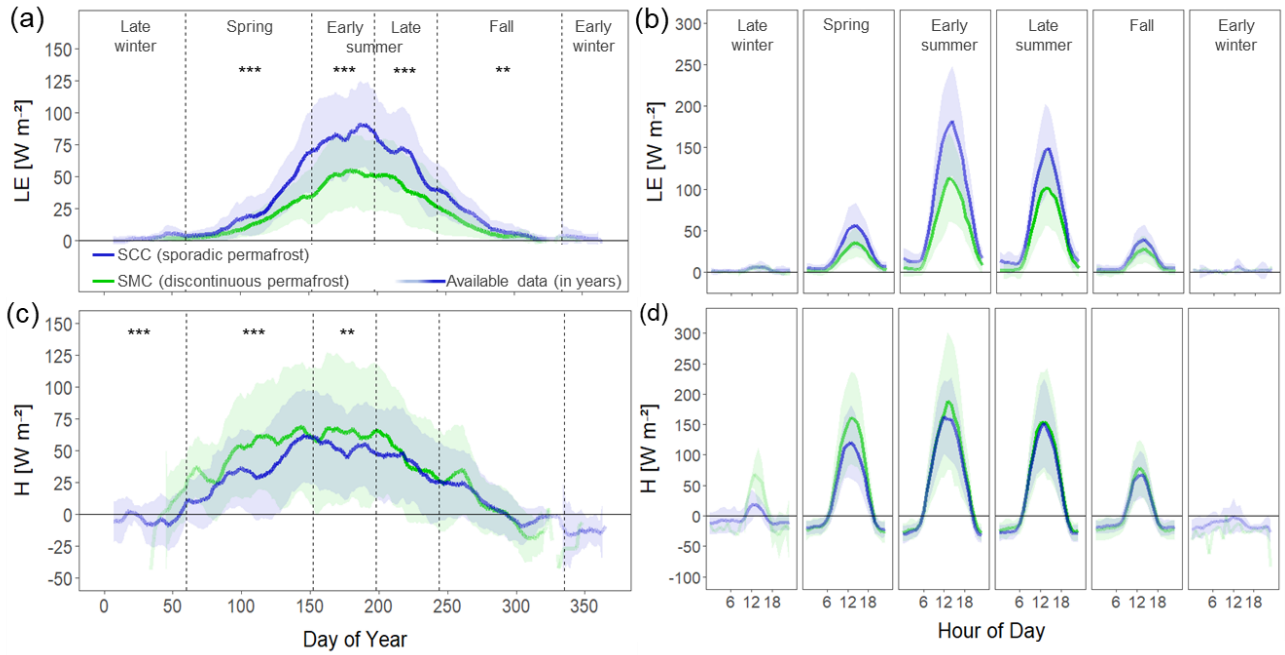


Figure A3.4: Seasonal (a, c) and diurnal (b, d) patterns of generalized annual energy fluxes \pm standard deviation of (a, b) latent heat (LE), (b) sensible heat (H) flux from the two eddy covariance tower sites, Scotty Creek (SCC, sporadic permafrost) and Smith Creek (SMC, discontinuous permafrost). Line intensity reflects data availability across all years (July 2017 - September 2022, $n=0-6$).

A.4. Supporting Information for Chapter 4

A.4.1.



Figure A4.1: Images of eddy covariance tower setup. Left: scaffolding structure at the 2019 Burn to bring high-frequency instrumentation above the tree canopy. Right: tripod structure at 2007 Burn where most burned tree remainders have fallen to the ground and regrowth of vegetation is still below 1 meter in height.



Figure A4.2: Drone images of sampled landscapes around the Lutose peatland complex, left: 2019 Burn with distinct burned (black ashy areas) and unburned area (brown and green areas), middle: 2007 Burn where the vegetation is still recovering more than a decade after the wildfire event, right: Unburn with intact black spruce (*Picea mariana*) canopy.

Table A4.1: Overview of installed instruments for meteorological and soil measurements at the two sites 2019 Burn and 2007 Burn.

Environmental variable	Manufacturer	Instrument	Replicates per site	Height/depth in cm
Wind speed and direction	Campbell Scientific	CSAT3	1	2007 Burn: 210 2019 Burn: 600
Precipitation	Campbell Scientific	TE525-M	1	2007 Burn: 240 2019 Burn: 600
Air temperature	Vaisala	HMP45C212	1	2007 Burn: 210 2019 Burn: 600
Air pressure	LI-COR Environmental	LI-7200 CO ₂ /H ₂ O gas analyzer	1	2007 Burn: 210 2019 Burn: 600
photosynthetically active radiation	Kipp & Zonen	PAR Lite	1	2007 Burn: 240 2019 Burn: 600
Net radiation	Kipp & Zonen	NR Lite	1	2007 Burn: 150 2019 Burn: 150
Soil temperature	Campbell Scientific	107	1	2007 Burn: -10 2019 Burn: -10
Soil moisture	Campbell Scientific	616-L	3	2007 Burn: -10 2019 Burn: -10
Soil heat flux	Hukseflux Thermal Sensors	HFT3	1	2007 Burn: -10 2019 Burn: -10
		HFP01	1	2007 Burn: -10 2019 Burn: -10